The role of sloughing on the pathophysiology of chytridiomycosis in amphibians

NICHOLAS C. WU

BSc (Tech) | BSc (Hons) 1st Class

A thesis submitted for the degree of Doctor of Philosophy at

The University of Queensland in 2019

School of Biological Sciences

"'An understanding of the natural world and what's in it is a source of not only a great curiosity but great fulfilment' ~ David Attenborough (2010)

In dedication to my family

© 2019 Nicholas C Wu

ABSTRACT

Amphibians periodically remove the dead skin layer through a process known as sloughing. Because of their thin semi-permeable skin, sloughing is important to maintain skin integrity and biological functions such as ionic and osmotic regulation. However, sloughing has been shown to affect cutaneous ion and water movements, temporarily disrupting osmotic homeostasis. Since sloughing occurs regularly in amphibians, every 1–14 days depending on the species and temperature, it is important to assess the potential magnitude of osmotic/ionic disturbances that may accompany normal sloughing regimes and the mechanisms underpinning the temporary loss of homeostasis. Thus, the first aim of this thesis (Chapter 2) was to investigate the effects of sloughing on the expression, abundance and activities of cutaneous ion transport proteins in cane toads (*Rhinella marina*). Sodium efflux and skin permeability significantly increased during sloughing. However, internal electrolyte balance remained stable after the sloughing period, via increase in epithelial transport protein abundance and activity in the skin, which lead to a commensurate increase in active sodium uptake back into the skin. This suggests amphibians actively maintain osmotic homeostasis despite having a 'leaky' skin.

Chytridiomycosis, caused by the fungal pathogen *Batrachochytrium dendrobatidis* (*Bd*), has been linked to worldwide amphibian population declines. *Bd* disrupts the skin's ionic and osmotic function, and blood electrolyte levels. Infected amphibians increase the rate of sloughing in an attempt to remove the fungus before the onset of chytridiomycosis. However, the cumulative impact of increased sloughing frequency and the disruption of skin function by *Bd* may interact to reduce the overall physiological health of the animal. Thus, the second aim examined how chytridiomycosis alters cutaneous ion transport properties of green tree frogs (*Litoria caerulea*) during sloughing (Chapter 3), by measuring the responses of associated epithelial transport proteins to *Bd* infection. While animals infected with *Bd* during the non-sloughing phase showed reduced skin resistance, and sodium influx, there was an increase in the rate of synthesis of new transport proteins. However, low sodium channel abundance in the skin of infected frogs suggests the synthesis of new proteins is disrupted by high zoospore loads. Interestingly, infected animals sloughing was associated with an increase in sodium transport activity and abundance. This may relate to the newly exposed, undisrupted skin layer, and to the temporary reduction of zoospore load following sloughing, allowing the transporters to function. However, skin permeability was the highest during sloughing and plasma ion levels remained low.

Smaller frogs are also more susceptible to *Bd*, with higher mortality rates observed in smaller individuals compared to larger individuals. Higher mortality rates may be due to greater relative surface-to-body volume in smaller individuals that results in a relatively greater diffusive loss of ions across the skin, and allow proportionally more zoospores to establish on the skin. Since the

combination of sloughing and chytrid is detrimental to susceptible species, this may exacerbate both osmoregulatory and energetic cost in smaller animals. Thus, the third aim (Chapter 4) examined how body size affects the energetic and osmoregulatory costs of sloughing in *Bd* infected animals. I examined whole-animal metabolic rate (MR) and ion loss rate in *L. caerulea* over a range of body sizes both with and without *Bd* during sloughing. I found that infected frogs had a greater rate of ion loss and higher MR during non-sloughing periods, but there were no additional effects of sloughing on either of these parameters. Importantly, there were significant interactions with body size and *Bd* load suggesting that smaller animals with higher *Bd* load have greater rates of ion loss and higher energetic demands.

Osmoregulation is also critical for amphibians living in freshwater environments. Chytridiomycosis and sloughing have been shown to affect cutaneous osmotic regulation. However, the mechanisms of this interaction has yet to be determine, especially on water transporters such as aquaporin's (AQPs). The fourth aim examined how chytridiomycosis alters water transport properties of *L. caerulea* during sloughing, by measuring the activities and expression of cutaneous AQPs (Chapter 5). *Bd* greatly reduced the expression of AQPs during sloughing, and may explain the high influx of water observed in this study leading to high muscle water content, and low blood osmolality. Why *Bd* affects the expression of cutaneous AQPs during sloughing, but not ion transporters remains uncertain, and future research is required to explore the role that various chemicals released by *Bd* has on these processes.

This body of work highlights the complex interaction between sloughing and chytridiomycosis, and explains why susceptible species do not benefit from an increased rate of sloughing. Non-infected sloughing amphibians are able to compensate a 'leaky' skin by regulating cutaneous ion transporters. However, when infected with *Bd*, the increased sloughing rate and the alterations to skin function associated with *Bd* infection, accelerate disease progression for susceptible species that cannot regulate their pathogen load. I also show why smaller *Bd*-infected anurans exhibit greater physiological disruption during chytridiomycosis than larger individuals. Taken together, these results demonstrate the importance of taking an integrative approach to gaining a more comprehensive understanding of the pathophysiology of chytridiomycosis.

Front cover image: Australian green tree frog (*Litoria caerulea*). Photo credit: C. Baker.

DECLARATION BY AUTHOR

This thesis is composed of my original work, and contains no material previously published or written by another person except where due reference has been made in the text. I have clearly stated the contribution by others to jointly-authored works that I have included in my thesis.

I have clearly stated the contribution of others to my thesis as a whole, including statistical assistance, survey design, data analysis, significant technical procedures, professional editorial advice, financial support and any other original research work used or reported in my thesis. The content of my thesis is the result of work I have carried out since the commencement of my higher degree by research candidature and does not include a substantial part of work that has been submitted *to qualify for the award of any* other degree or diploma in any university or other tertiary institution. I have clearly stated which parts of my thesis, if any, have been submitted to qualify for another award.

I acknowledge that an electronic copy of my thesis must be lodged with the University Library and, subject to the policy and procedures of The University of Queensland, the thesis be made available for research and study in accordance with the Copyright Act 1968 unless a period of embargo has been approved by the Dean of the Graduate School.

I acknowledge that copyright of all material contained in my thesis resides with the copyright holder(s) of that material. Where appropriate I have obtained copyright permission from the copyright holder to reproduce material in this thesis and have sought permission from co-authors for any jointly authored works included in the thesis.

Nicholas C. Wu
School of Biological Sciences,
The University of Queensland

Supervisor
Prof. Craig E. Franklin
Deputy Head of School,
School of Biological Sciences, The
University of Queensland

Co-supervisor
Dr. Rebecca L. Cramp
Postdoctoral Research Fellow,
School of Biological Sciences, The
University of Queensland

PUBLICATIONS DURING CANDIDATURE

Peer-reviewed publications

Wu N. C., Cramp R. L. & Franklin. C. E. (2017) Living with a leaky skin: upregulation of ion transport proteins during sloughing. *Journal of Experimental Biology*, **220**, 2026–2035

Wu N. C., Cramp R. L. & Franklin. C. E. (2018) Body size influences energetic and osmoregulatory costs in frogs infected with *Batrachochytrium dendrobatidis. Scientific Reports*, **8**, 3739

Wu N. C., Cramp R. L., Ohmer M. E., & Franklin. C. E. (2019) Epidermal epidemic: unravelling the pathogenesis of chytridiomycosis. *Journal of Experimental Biology*, **222**, jeb191817

Conference abstracts

Wu N. C., Cramp R. L., Ohmer M. E. B., & Franklin C. E. (2018) Unravelling the pathogenesis of chytridiomycosis. *Joint Meeting of the Australian Society of Herpetologists and the Society for Research on Amphibians and Reptiles in New Zealand*. Kindilan, Australia. *SRARNZ student presentation award.

Wu N. C., McKercher C., Cramp R. L., & Franklin C. E. (2018) Cutaneous disruption of water balance in frogs infected with a lethal pathogen. *Society for Experimental Biology Annual Meeting*. Florence, Italy.

Wu N. C., Cramp R. L., & Franklin C. E. (2017) Chytridiomycosis alters cutaneous electrolyte transport during sloughing. *34th Annual meeting of the Australian and New Zealand Society for Comparative Physiology and Biochemistry*. Cape Tribulation, Australia. *Best student oral Presentation Award.

Wu N. C., Gauberg J, Cramp R. L. & Franklin. C. E. (2017) Epidermal epidemic: effects of chytridiomycosis on amphibian epithelial transport during sloughing. *Society for Experimental Biology Annual Meeting*. Gothenburg, Sweden. *Special mention for Young Scientist Award Session (YSAS) in Animal-Cell section.

Wu N. C., Cramp R. L. & Franklin. C. E. (2016) Living with a leaky skin: upregulation of ion transport proteins during sloughing. *33rd Annual meeting of the Australian and New Zealand Society for Comparative Physiology and Biochemistry*. Sydney, Australia.

Wu N. C., Cramp R. L. & Franklin. C. E. (2016) Cutaneous electrolyte transport during sloughing in amphibians. *8th World Congress of Herpetology*. Hangzhou, China. *Best student oral presentation Award.

Publications included in this thesis

Wu N. C., Cramp R. L. & Franklin. C. E. (2017) Living with a leaky skin: upregulation of ion transport proteins during sloughing. *Journal of Experimental Biology*, **220**, 2026–2035. Incorporated as Chapter 2 with minor changes.

Contributor	Statement of contribution
Nicholas C. Wu (Candidate)	Concept and design (60 %), data collection (100 %), data analysis (100 %), writing and editing (80 %)
Rebecca L. Cramp	Concept and design (20 %), writing and editing (10 %)
Craig E. Franklin	Concept and design (20 %), writing and editing (10 %)

Wu N. C., Cramp R. L., Ohmer M. E., & Franklin. C. E. (2019) Epidermal epidemic: unravelling the pathogenesis of chytridiomycosis. *Journal of Experimental Biology*, **222**, jeb191817. Incorporated as Chapter 3 with minor changes.

Contributor	Statement of contribution
Nicholas C. Wu (Candidate)	Concept and design (65 %), data collection (95 %), data analysis (100 %), writing and editing (75 %)
Rebecca L. Cramp	Concept and design (15 %), writing and editing (15 %)
Michel M. E. Ohmer	Concept and design (5 %), data collection (5 %), writing and editing (5 %)
Craig E. Franklin	Concept and design (15 %), writing and editing (5 %)

Wu N. C., Cramp R. L. & Franklin. C. E. (2018) Body size influences energetic and osmoregulatory costs in frogs infected with *Batrachochytrium dendrobatidis*. *Scientific Reports*, **8**, 3739. Incorporated as Chapter 4 with minor changes.

Contributor	Statement of contribution
Nicholas C. Wu (Candidate)	Concept and design (80 %), data collection (100 %), data analysis (100 %), writing and editing (80 %)
Rebecca L. Cramp	Concept and design (10 %), writing and editing (15 %)
Craig E. Franklin	Concept and design (10 %), writing and editing (5 %)

Submitted manuscripts included in this thesis

Wu N. C., McKercher C., Cramp R. L. & Franklin. C. E. (In review) Mechanistic basis for the loss of water balance in green tree frogs infected with a fungal pathogen. *American Journal of Physiology-Regulatory, Integrative and Comparative Physiology*. Incorporated as Chapter 5 with minor changes.

Contributor	Statement of contribution
Nicholas C. Wu (Candidate)	Concept and design (70 %), data collection (85 %), data analysis (100 %), writing and editing (80 %)
Callum McKercher	Data collection (15 %)
Rebecca L. Cramp	Concept and design (15 %), writing and editing (15 %)
Craig E. Franklin	Concept and design (15 %), writing and editing (5 %)

Other publications during candidature

Peer-reviewed publications

Ohmer M. E. B., Cramp R. L., White C. R., Harlow P. S., McFadden M. S., Merino-Viteri A., Pessier A. P., **Wu N. C.**, Bishop P. J., & Franklin C. E. (2019) Phylogenetic investigation of skin sloughing rates in frogs: relationships with skin characteristics and disease-driven declines. *Proceedings of the Royal Society B*, **286**, 20182378

Gauberg J., **Wu N. C.**, Cramp R. L., Kelly S. P., & Franklin C. E. (2019) A lethal fungal pathogen directly alters tight junction proteins in the skin of a susceptible amphibian. *Journal of Experimental Biology*, **222**, jeb192245

Clemente C. J., & **Wu N. C.** (2018) Body and tail-assisted pitch control facilitates bipedal locomotion in Australian agamid lizards. *Journal of the Royal Society Interface*, **15**, 20180276

Shu G., Gong Y., Xie F., **Wu N. C.**, & Li C. (2017) Effects of long-term preservation on amphibian body conditions: implication on historical morphological research. *PeerJ*, **5**, e3805

Wu N. C., & Waas J. R. (2017) No evidence for across-population scent discrimination in tuatara (*Sphenodon*). *Journal of Herpetology*, **51**, 178–185

Rusli M. U., **Wu N. C.**, & Booth D. T. (2016) Tonic immobility in newly emerged sea turtle hatchlings. *Chelonian Conservation and Biology*, **15**, 143–147

Wu N. C., Alton L. A., Clemente C. J., Kearney M. R., & White C. R. (2015) Morphology and burrowing energetics of semi-fossorial skinks (*Liopholis spp.*). *Journal of Experimental Biology*, **218**, 2416–2426

Conference abstracts

Wu N. C., & Clemente C. J. (2018) Unravelling the mechanisms for the exploitation of bipedal locomotion among Australian agamid lizards. *Society for Experimental Biology Annual Meeting*. Florence, Italy.***Awarded Irene Manton Poster Prize in Animal Section, & the R McNeill Alexander Awards for Biomechanics.**

Grosell M., Heuer R M., Mager E. M., Wang Y., **Wu N. C.***, Cramp. R. L., & Franklin C. E. (2017) Role of the cloaca in salt and water balance in estuarine crocodiles. *Society for Experimental Biology Annual Meeting*. Gothenburg, Sweden.***Presenter; Runner up for Irene Manton Poster Prize in Animal Section.**

Wu N. C., & Waas, J. R. (2016) No evidence for across-population scent discrimination in tuatara (*Sphenodon*). *8ᵗʰ World Congress of Herpetology*. Hangzhou, China.

Contributions by others to the thesis

Craig Franklin and Rebecca Cramp, through discussion and feedback, contributed significantly to the conception and design of this research overall. Simon (Simone) Blomberg provided statistical assistance for Chapters 2, 3, and 4. Martin Grosell (University of Miami) and Craig Campbell (University of Sydney) provided technical advice for the Ussing chamber set-up for Chapter 2. The Evolutionary Physiology lab team (Monash University) provided significant technical advice for the open-flow respirometry experiment for Chapter 4. Callum McKercher assisted with data collection for Chapter 5. Craig Franklin and Rebecca Cramp critically reviewed the final draft of this thesis.

Statement of parts of the thesis submitted to qualify for the award of another degree
None.

Research Involving Human or Animal Subjects

Animal subjects for this research were collected with approval of the Queensland Department of Environment and Heritage Protection Scientific Purposes Permit (WISP15102214), and procedures were conducted in accordance with the University of Queensland's Animal Ethics Committee (SBS/316/14/URG, and SBS/340/17). Copies of the approval certificates were provided in the Appendices section (Appendix 2).

ACKNOWLEDGEMENTS

Academic acknowledgements

This thesis has been, for the most part, a pleasure to write, and I think it reflects one of the things in my life for which I am most grateful—that I take so much joy in the science that is both my vocation and avocation. I would first like to express my deepest gratitude to my supervisor **Prof. Craig E. Franklin** for providing me the opportunity to conduct this research, and for his invaluable discussion and support throughout my candidature. His extensive knowledge and wisdom in ecophysiology has been extremely influential, and thus convinced me to pursue further into academia. Craig, through his invaluable discussions and support, has not only helped me developed into a competent researcher, but also taught me to challenge myself and develop critical thinking skills to explore new ideas. He allowed me the freedom to explore areas of science that interested me and for being not only a great advisor, but a great human being too, showing me that one can do good scientific research without losing touch with one's humanity.

Another major influence for the successful completion of my PhD is **Dr. Rebecca L Cramp**. She is a brilliant multi-talented researcher in all aspects, from problem solving all my technical issues, giving much needed general advice, and keeping me sane from all the stress-induced hypertension during the worst periods of my PhD. She taught me that making mistakes is normal, but one should never give up and learn the value of patience. Thank you Beck.

I had the fortune to meet many great academics who helped me during my PhD including Craig R. White, David Booth, Robbie Wilson, Martin Grosell, Simone Blomberg, Vera Weisbecker, and Darryl Whitehead. I have much respect and admiration for their work, and feel privileged to be working among the giants of in their respective fields.
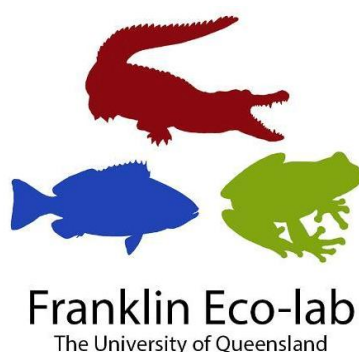
General acknowledgements

What would a lab be without the people who make it interesting? I gratefully thank the current and past Franklin lab members that made my PhD years enjoyable. It's more fun to be insane together! Thank you Ross, Jabin, Yulian, Pippa, Chrissy, Argelia, Alana, Callum, Ebony, Kathleen, Harriet, Samantha, Jess, Monique, Caroline, Lily, Kate, and Emma. Thank you Michel for training me in all chytrid-related protocols, providing excellent research ideas during the start of my PhD, and for invigorating my passion for frogs; Essie for being an wonderful senior by giving me valuable academic and life advice, setting a great example of a hard worker, and letting me help out with the Crocs; Daniel G and Nic for all the great research discussions and feedback, and enduring the suffering during our late night and weekend experiments; Cameron and Coen for fun herp-related discussions throughout my PhD; and Sam M for keeping the fun going in the lab (and distractions).

Of course, I can't forget my army of volunteers for helping me with the daily sloughing monitoring. It would have been impossible without you guys, so thank you for your help!

While it's been ages since I was part of the White lab, they still had a big influence on my academic life, so thank you Leslie, Jules, Piet, Hugh, Taryn, and Phil for making me feel like part of the family. I also thank all the wonderful people I met during my honours and PhD years at UQ, especially Juan, Uzair, Skye, Cara, Maddie, Carmen, Andrew, Brogen, Iva, Josh, Naomi, Laurie, Andréas, Ariel, Rebecca W, Judit, Mark, Karen, Hwee, Jiadai, Matt, Bianca, Chilli, Helen, James D, Daniel D, Christina, Jacinta, Melissa, Bob, and James B. To Chris Clemente, cheers for being the most chilled, down to earth academic I've met, and being an inspiration for a what a brilliant researcher and communicator should be.

Finally, above all else, I thank and love my whānau and hoa back home in New Zealand. To my father and mother for their moral support, and for understanding my busy and hectic life choices, and my brother for advice on my illustrations. My PhD journey has tested my limits physically, mentally, and emotionally, but allowed me to grow a bit stronger and wiser. This PhD dissertation is dedicated to my whole family, my loving wife, and the memory of my Grandmother 張鳳貞 (1936–2015), Grandfather 吳健行 (1925–2016), and uncles Wu Chen Pang 吳振邦 (1959–2015) and Wu Ting Pang 吳定邦 (1949–2016), who passed away during my candidature and whose funerals I could not attend.

Back cover illustration: Amy Cheu (Basiliskos)

Franklin Eco-lab
The University of Queensland

Financial support

KEYWORDS

anuran, chytridiomycosis, electrophysiology, energetics, gene expression, ionic and osmotic regulation, immunofluorescence, pathogen, skin sloughing, western blot.

Australian and New Zealand Standard Research Classifications (ANZSRC)

Australian and New Zealand Standard Research Classifications (ANZSRC)		
ANZSRC code	Divisions of Biological Sciences (06)	Percent weighting (%)
060806	Animal Physiological Ecology	60
060602	Animal Physiology - Cell	20
060203	Ecological Physiology	20
Fields of Research (FoR) Classification		
0606	Physiology	60
0608	Zoology	20
0602	Ecology	20

TABLE OF CONTENTS

LIST OF FIGURES

LIST OF TABLES

LIST OF ABBREVIATIONS

List of **general** abbreviations used in the thesis

AIC	akaike information criterion	M_b	body mass
AMP	antimicrobial peptide	MR	metabolic rate
ANOVA	analysis of variance	MRC	mitochondria-rich cell
ANCOVA	analysis of covariance	Na^+/K^+-ATPase	sodium-potassium pump (NKA)
AQP	aquaporin	NKCC	$Na^+/K^+/2Cl^-$ cotransporter
Av	ventral surface area	PBS	phosphate-buffered saline
β-actin	Beta-actin	PCR	polymerase chain reaction
Bd	*Batrachochytrium dendrobatidis*	PMSF	phenylmethylsulfonyl fluoride
Bs	*Batrachochytrium salamandrivorans*	qPCR	quantitative PCR
BSA	bovine serum albumin	RER	respiratory exchange ratio
cDNA	complementary deoxyribonucleic acid	RH	relative humidity
CSF	cutaneous surface fluid	RMR	resting metabolic rate
ECF	extracellular fluid	RNA	ribonucleic acid
ENaC	epithelial sodium channel	RO	reverse osmosis
EWL	evaporative water loss	s.e.	standard error
GAPDH	glyceraldehyde 3-phosphate dehydrogenase	SA	surface area
H_{CT}	haematocrit	SVL	snout-vent length
H&E	hematoxylin and eosin	TBST	tris-buffered saline with Tween-20
HRP	horseradish peroxide	TEP or V_T	transepithelial potential
IMI	intermoult interval	UV	ultraviolet radiation
IC_{50}	half maximal inhibitory concentration	$\dot{V}_{CO_2}$	rate of CO_2 production
I_{SC}	instantaneous short-circuit current	$\dot{V}_{O_2}$	rate of O_2 consumption
IUCN	International Union for Conservation of Nature	ZE	zoospore equivalent

List of **chemical** abbreviations used in the thesis

ATP	adenosine triphosphate	HCO_3^-	hydrogen carbonate (bicarbonate) ion
AVP or ADH	arginine vasopressin or antidiuretic hormone	HEPES	4-(2-Hydroxyethyl)piperazine-1-ethanesulfonic acid
AVT	arginine vasotocin	K^+	potassium ion
Ca^{2+}	calcium ion	KCl	potassium chloride
$CaCl_2$	calcium chloride	Mn^{+2}	manganese ion
cAMP	cyclic adenosine monophosphate	$MgCl_2$	magnesium chloride
Cl^-	chloride ion	Na^+	sodium ion
CO_2	carbon dioxide	Na_2HPO_4	disodium phosphate
DMSO	mimethyl sulfoxide	NaCl	sodium chloride
H^+	hydrogen ion	O_2	oxygen
H_2O	water	TMB	3,3′,5,5′-Tetramethylbenzidine

List of International System (SI) of units and non-SI units used in the thesis

Symbol	Unit name	Quantity (dimension symbol)
mm	millimetre	length (l)
cm	centimetre	length (l)
m	metre	length (l)
µg	microgram	mass (m)
mg	milligram	mass (m)
g	gram	mass (m)
kg	kilogram	mass (m)
s	second	time, duration (t)
min	minute	time, duration (t)
h	hour	time, duration (t)
d	day	time, duration (t)
°C	degree Celsius	temperature (T)
mm^2	square millimetre	area (A)
cm^2	square centimetre	area (A)
mm^3 (µl)	cubic millimetre (microlitre)	volume (V)
cm^3 (ml)	cubic centimetre (millilitre)	volume (V)
m^3 (l)	cubic meter (litre)	volume (V)
µmol	micromolar	molar concentration (c_i)
mmol	millimolar	molar concentration (c_i)
mol	molar	molar concentration (c_i)
mosmol	milliosmole	osmotic concentration
kDa	kilodaltons	molecular mass (M)
n	number, sample size	count, amount
%	percent sign	percentage
N	newton	force (F)
g	relative centrifugal force (RCF)	vector acceleration
J	joule	energy, work, heat (E)
W	watt	power (P)
Hz	hertz	frequency (f)
Δ	rate of change	time derivative

Electrical units

C	coulomb	charge (Q)
µA	microampere	electrical current (I)
mV	millivolt	voltage, potential difference (V)
Ω	ohm	resistance (R)
µS	microsiemens	conductance (G)
F	farad	capacitance (C)
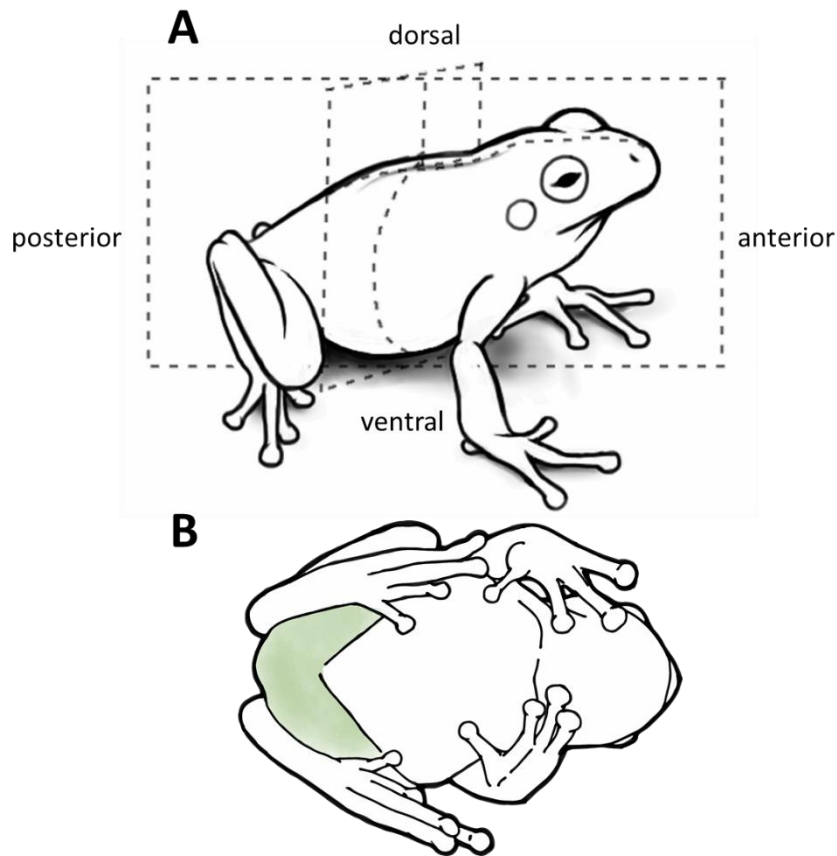
Terms for locating anatomical regions of a typical anuran. A) Lateral view with dash lines denote six polar points which consist of three axes that intersect at right angles; x-axis (anterior-posterior), y-axis (dorsal-ventral), z-axis (left and right). B) Ventral view with highlighted green area showing the ventral pelvic patch for water uptake.

General introduction

Amphibians are declining at an accelerated rate, contributing to mass global biodiversity loss, estimated to be as much as 200–1000 times higher than the normal background extinction rate (McCallum, 2007; Pimm et al., 2014). Globally, approximately 2030 amphibian species are currently threatened with extinction and a further 38 species are listed as extinct (IUCN, 2017). This comprises 32.4 % of all known amphibian species, making amphibians the most threatened vertebrate group (Stuart et al., 2004). While it is clear many amphibian populations are declining rapidly, the exact cause of these declines has been challenging to establish, and it is becoming increasingly clear that no single factor can explain these declines. The difficulty understanding amphibian declines lies in the large number of environmental factors acting on the organism (Collins and Crump, 2009), and the complexity and dynamics of interactions between them (Blaustein et al., 2011).

Declines associated with anthropogenic influences include habitat loss and degradation, introduction of invasive species, over-exportation, and pollution (Stuart et al., 2004; Beebee and Griffiths, 2005). However, many amphibian declines have also occurred in non-degraded habitats such as protected national parks. Around 27 % of threatened amphibians live in protected areas (Pimm et al., 2014), thus direct human disturbances are not the sole cause. As such, the emergence of global infectious diseases has come to attention in the past three decades (Daszak et al., 1999; Wake and Vredenburg, 2008) such as ranaviruses which causes gross lesions and chronic cell death in multiple organs of the host (Gray et al., 2009; Miller et al., 2011). However, the most wide-spread and devastating amphibian disease is caused by a group of chytridomycete fungal pathogens *Batrachochytrium dendrobatidis* (*Bd*) (Longcore et al., 1999; Fisher et al., 2009), and *B. salamandrivorans* (*Bs*) (Martel et al., 2013).

Batrachochytrium dendrobatidis is known to infect over 500 species of amphibian worldwide (Olson et al., 2013, http://www.bd-maps.net/surveillance/) and can result in the lethal skin disease chytridiomycosis. While *Bd* is found on a wide variety of amphibian hosts, not all hosts develop chytridiomycosis. Susceptibility to *Bd* can range from resistance (Ohmer et al., 2013; Eskew et al., 2015) or tolerance (Ramsey et al., 2010), to highly sensitive (La Marca et al., 2005; Bustamante et al., 2010; Hunter et al., 2010). *Bd* susceptibility depends on a number of factors, such as type of anti-microbial peptides on the skin (Woodhams et al., 2014), diversity of cutaneous microbiota (Burkart et al., 2017), *Bd* strain (Farrer et al., 2011), habitat preference (Lips et al., 2003), host immune defence, and ontogeny (Rollins-Smith, 2017). While most studies approach chytrid related declines from an ecological and epidemiological perspective, there is a lack of understanding in the underlying mechanisms influencing the relationship between *Bd* and its host, especially at the site of colonisation - the skin. The skin is an important organ for biological regulation in amphibians,

and disruption to the skin can lead to serious consequences for the animal's overall health (Emerson and Norris, 1905; Cunningham et al., 1996; Berger et al., 2005a).

The structure of the General Introduction chapter will introduce the amphibian skin and its function, the role of sloughing maintaining skin function, and the integration with the pathology of chytridiomycosis, emphasising our current understanding of this relationship, and signifying missing gaps that will be addressed in this Thesis. Lastly, specific aims were provided, along with an overview of the structure of subsequent chapters.

1.1 SKIN STRUCTURE & FUNCTION

Histologically, amphibian skin consists of an outer epidermis and an inner dermis (**Fig. 1.1**). The epidermis comprises 5–7 cell layers, predominantly keratinocytes or granular cells (Lindemann and Voute, 1976; Heatwole et al., 1994). The most basal layer of the epidermis is the *stratum germinativum*, attached to the dermis by a basement membrane (Hillyard et al., 2008). The *stratum germinativum* continually regenerates (via mitotic division), to replenish and maintain the rest of the epidermal cell population (Heatwole et al., 1994). Above the *stratum germinativum* is the *stratum spinosum* (spiny layer), where keratinisation begins forming polyhedral keratinocytes.

Next is the *stratum granulosum* (granular layer) where the keratinocytes become known as granular cells. These cells are connected by protein complexes including tight (*zonulae occludens*) and adherent junctions (Gumbiner et al., 1988) that separate the apical plasma membrane from the basolateral membrane (Farquhar and Palade, 1964; Niessen, 2007). The apical plasma membrane is the limiting barrier for trans-cellular solute and water transport across the epidermis, although evidence suggests that tight junctions are semi-permeable and paracellular transport occurs as well (Hillyard et al., 2004). The superficial layer of the epidermis is the *stratum corneum*, consisting of 1-2 thin layer/s of dead cells filled with keratin, called corneocytes. The *stratum corneum* acts as the first line of defence against the external environment (Baroni et al., 2012).
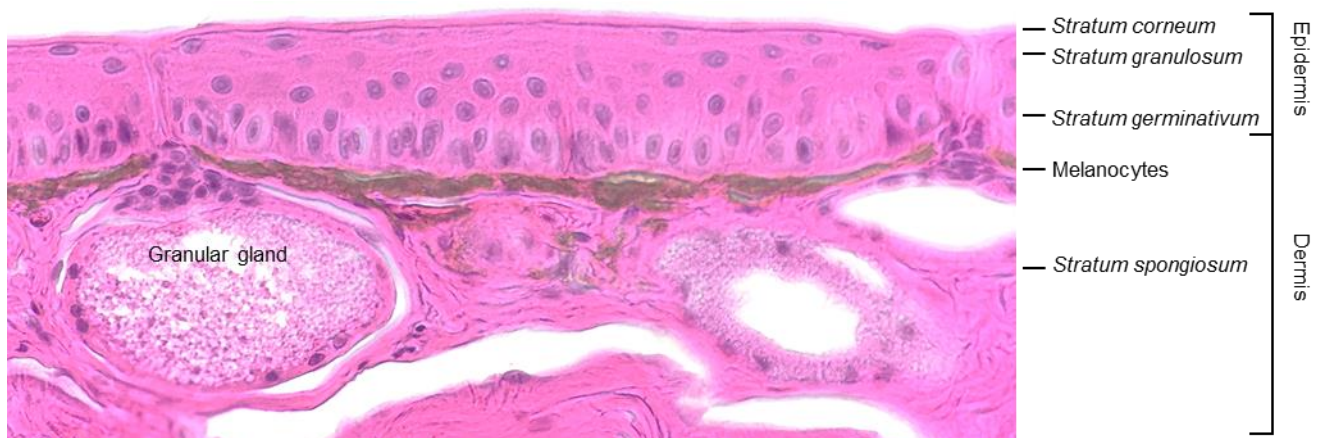
Fig. 1.1 │ Transverse section of haematoxylin and eosin (H&E) stained ventral skin (6 µm) from a non-infected *Litoria caerulea* revealing the epidermal and dermal layers of the skin. EXIF data: f/2.2, ISO-80, exposure time 1/33 s, focal length 4 mm.

Amphibian skin performs several important roles such as protecting the internal systems from the external environment (Baroni et al., 2012), while simultaneously sensing, interacting and exchanging materials with the surrounding environment. Due to their thin, semi-permeable skin (relative to other vertebrates), amphibian skin plays a large role in regulating physiological homeostasis and is directly involved in thermoregulation, ionic and osmotic regulation, respiratory gas exchange, acid-base balance, nitrogen excretion (Feder and Burggren, 1992), and immune defence (Rollins-Smith et al., 2005). Exchanges of heat, ions, water and respiratory gases in the amphibian skin are interdependently linked and this integration presents both benefits and challenges to maintaining physiological homeostasis (Feder and Burggren, 1992). The focus hereafter will be on cutaneous ion and water regulation.

1.2   CUTANEOUS ION & WATER REGULATION

Amphibians in freshwater environments lose ions/solutes to the environment via diffusion due to the ion gradient that exists between the animal (high salt concentration) and the environment (low salt concentration) (**Fig. 1.2**). To sustain a hyper-osmotic internal environment, the amphibian skin actively takes up large quantities of ions, in particular sodium (Na^+) and chloride (Cl^-), from the environment to counteract the passive diffusive loss of these ions to the environment (Hillyard et al., 2008). Maintaining a balanced internal electrolyte composition is essential, as inorganic solutes control many protein/enzyme functions and provide electrochemical gradients, such as those which drive all electrical transmission of information via the nervous system (Catterall, 2000; Pohl et al., 2013).
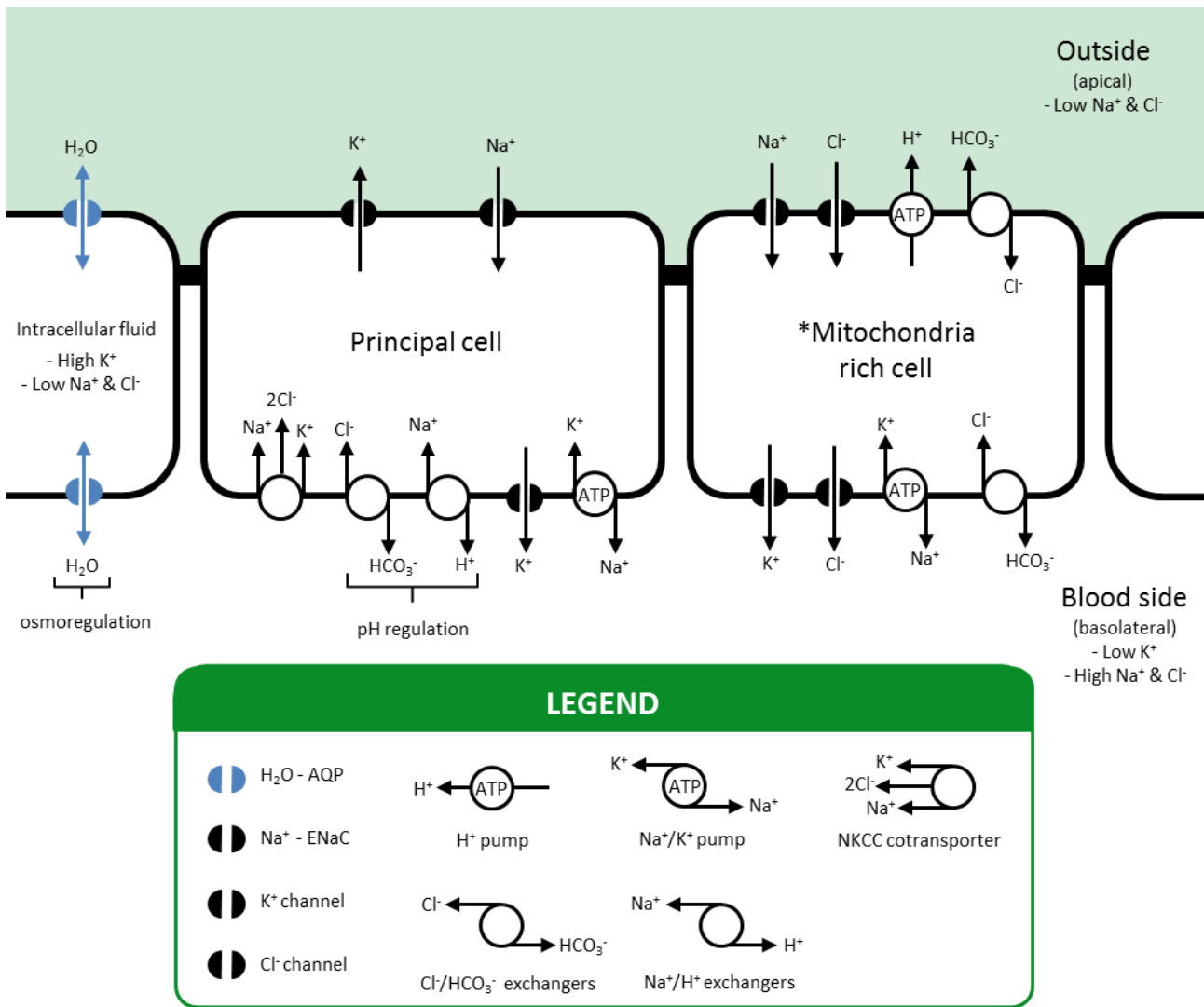
Fig. 1.2 │ Schematic description of principal cells and mitochondria-rich cells in the frog skin with their respective ion channels and pumps. Arrows indicate influx and efflux of ions and water molecules, mainly focusing on exchanges of Na^+, K^+ and Cl^- ions. Transcellular NaCl absorption generates an osmotic gradient that drives absorption of water via aquaporin channels (AQP). Illustration modified from (Ehrenfeld and Klein, 1997; Hillyard et al., 2008; Campbell et al., 2012). *represents typical MRC, as specialised subpopulations differ in transport proteins and abundance.

There are two cell types in the amphibian epithelium that contribute to ionic regulation: principal cells and mitochondria-rich cells. The principal cell compartment (granular cells) forms a functional syncytium between the *stratum granulosum*, *stratum spinosum* and the *stratum germinativum* (Shahin and Blankemeyer, 1989), with functions resembling the principal cells of the urinary bladder, and the collecting tubules and ducts of the kidney (Hillyard et al., 2008). Transcellular Na^+ enters across the apical cell membrane via epithelial sodium channels (ENaC) and in exchange for potassium ions (K^+), which move out of the cells against an electrochemical gradient via apical potassium channels (**Fig. 1.2**). These ion fluxes are driven by ATPase-dependent pathway, the sodium-potassium pump (Na^+/K^+-ATPase; NKA) in the basolateral membrane, which actively exchanges K^+ for Na^+ (Mills et al., 1977; Hillyard et al., 2008). The flask-shaped mitochondria-rich cells (MRC) also regulate Na^+ and K^+ fluxes (**Fig. 1.2**), but in addition, transport other ions such as chloride (Cl^-), hydrogen (H^+), bicarbonate (HCO_3^-) and organic molecules (Ehrenfeld et al., 1989;

Furuse et al., 1993). MRC represent less than 6 % of the total epithelial cell population (Ehrenfeld et al., 1976) but are estimated to contribute as much as 60 % of the exposed apical transporting area due to extensive apical membrane folding (Ehrenfeld et al., 1989). The MRC constitute a highly specialised pathway for transport of Cl$^-$ across the epithelium, with no contribution from principal cells (Larsen, 1991). To date, three types of MRC have been identified and each is specialised for different ion transport processes (reviewed in Hillyard et al., 2008).

Ionic- and osmoregulation are functionally linked to maintain internal ion and water balance. Osmoregulation is also crucial for maintaining intracellular osmotic pressure, volume and pH. The principal cell layer plays a key role in controlling water transport (MacRobbie and Ussing, 1961; Voûte and Ussing, 1968), where transcellular transport of water occurs through aquaporin transport proteins in the apical membrane (AQP) (**Fig. 1.2**). Aquaporins regulate water intake in aquatic environments and protect against evaporative water loss (EWL) in terrestrial environments (Larsen and Ramløv, 2013). There are also anuran-specific AQPs that might be involved in osmotic fluid secretion from the mucous glands and granular glands, possibly aiding maintenance of the moist skin, cutaneous gas exchange, and thermoregulation (Suzuki and Tanaka, 2009; Shibata et al., 2014). For aquatic amphibians, large water influxes can burden the kidneys, and so they have a lower rate of cutaneous water absorption than terrestrial amphibians (Schmid, 1965; Ogushi et al., 2010b). For terrestrial anurans, water uptake occurs primarily through the pelvic region of the ventral skin known as the 'pelvic patch' or the '*verrucae hydrophilicae'*, a highly vascularised region that is typically thinner than the dorsal skin (Drewes et al., 1977). It accounts for only 10 % of the ventral surface area but is responsible for up to 70 % of the water uptake in dehydrated *Bufo punctatus* (McClanahan Jr and Baldwin, 1969).

1.3   SLOUGHING

In order to maintain optimal skin function and integrity, the old *stratum corneum* is periodically removed, and replaced, through a process known as 'sloughing'. The term 'sloughing' is primarily applied to amphibians (Cramp et al., 2014; Ohmer et al., 2015), however, 'moulting', and 'shedding' have previously been used to describe the removal of the epidermis in amphibians. Sloughing may be a physiologically vulnerable period for amphibians due to the number of behavioural, morphological and physiological alterations that occur. These alterations will be discussed in brief:

1.3.1   Sloughing Behaviour

In frogs, sloughing behaviour is remarkably conserved across species (Larsen, 1976; Castanho and de Luca, 2001; Ohmer et al., 2017) and usually begins with the animal adopting a distinct posture, with the body hunched and front legs outstretched. Abdominal contractions and body wiping with the limbs removes the old *stratum corneum* where it is directed towards the mouth and consumed. The body is then raised above the substrate until the new skin dries (Ling, 1972; Larsen, 1976).

Consumption of the sloughed skin (auto-dermatophagy) may function to recycle nutrients such as free fats, bound phospholipids and calcium from the skin (Spearman, 1968), or to reduce reinfection of the skin by potential cutaneous pathogens (Weldon et al., 1993). Prior to the sloughing behaviour, various morphological changes take place to form the new skin layer.

1.3.2 Morphological changes during sloughing

Morphological changes to the epidermis, observed via light and electron microscopy, revealed five distinct sloughing phases in the toad, *Bufo bufo* (Budtz and Larsen, 1973, 1975): (a) intermoult phase, (b) preparation phase, (c) early shedding phase, (d) late shedding phase and (e) differentiation phase. During (a) and (b) no physical sloughing behaviour was observed and the *stratum corneum* seemed to be adhered to the underlying cell layers; during phase (c) the sloughing posture was adopted and the removal of the *stratum corneum* began. In phase (d) the *stratum corneum* was completely removed and the newly exposed skin became slimy, and lastly in phase (e) the new skin dries and loses its slimy appearance.

In the initial stages of epidermal cellular turnover, cells in the *stratum germinativum* lighten and swell (Budtz, 1977). The sloughing cycle involves a period of complex differentiation of the epidermal cells leading to the replacement of the outer most keratinised layer. In the early shedding stages, the old *stratum corneum* separates from the underlying cell layer (new *stratum corneum*) through the gradual dissolution of intercellular junctions (i.e. desmosomes) between these two layers (Budtz, 1977). The new *stratum corneum* (derived from the *stratum granulosum*) swells, flattens (Ernst, 1973) and becomes completely cornified prior to sloughing (Elias and Shapiro, 1957; Whitear, 1975). Mucus then appears beneath the separated *stratum corneum* (the 'slough') to facilitate its removal. The slough is then eaten. The whole process takes just a few minutes (Larsen, 1976). In the immediate post-shedding phase, the cells of the *stratum corneum* become flattened and more densely packed (Budtz and Larsen, 1973). Fusion of these layers and the formation of tight junctions (Budtz and Larsen, 1975), re-establishes the physical barrier function of the skin and prevents the loss of ions and water to the environment (Yokouchi et al., 2016).

1.3.3 Effect of sloughing on physiological homeostasis

Physiological alterations to skin function also occur as a result of a sloughing event. Jørgensen (1949) found that in sloughing *Bufo bufo, Rana temporaria* and *R. esculenta,* there was a 3–4 fold increase in water permeability of the skin. The rate of Na^+ efflux increased about 20 times when measured by placing the animals in distilled water and measuring the increase in electric conductivity of the bathing solution. Water and ion permeability returned to normal values within 3–4 h post-slough. While most changes coincided with the actual sloughing event, the osmotic uptake of water has been demonstrated as early as 12 hours before sloughing takes place (Ewer, 1951).

The disruption of the skin function during slough also alters the skin's electrophysiological parameters, where there is a decrease in the short-circuit current (indicative of active ion transport activity), transepithelial potential (potential difference between the two sides of the cell membrane), and skin resistance (permeability of the skin) (Larsen, 1970; Nielsen and Tomilson, 1970; Larsen, 1971a). These changes seem to result from the physical shedding of the slough, since they are initiated by the separation of the slough from the underlying skin layer (reviewed in Erlij and Ussing, 1978). However, most studies artificially induced sloughing via administration of hormones such as aldosterone (Nielsen, 1969; Larsen, 1971a) which could potentially provide unrealistic data (relative to natural sloughing) since aldosterone also acts to regulate ion and water reabsorption in the kidneys (Garty, 1986; Eaton et al., 2001). It becomes difficult to distinguish if the changes in ion and water permeability are due to the natural aspects of sloughing or the artificial effect of aldosterone. Nevertheless skin disruption does occur and may indicate a physiologically vulnerable period since disruptions to ionic and osmotic regulation directly affect electrolyte homeostasis.

Due to the behavioural aspects of removing the sloughed skin, the morphological and physiological alterations associated with epidermal cellular turnover, sloughing may potentially be energetically costly for the animal (Larsen, 1976; Houlihan, 1991). Although the energetic cost of sloughing has not been documented in amphibians; in snakes, skin shedding increases metabolic rate (MR) up to 146 % of standard MR in juvenile carpet pythons (*Morelia spilota imbricata*) (Thompson and Withers, 1999) and 126 % in death adders (*Acanthophis antarcticus*) (Pintor et al., 2010). However, the energetic cost of sloughing in amphibians remains to be established.

1.3.4   Regulation of sloughing

Amphibians shed periodically (Larsen, 1976), to the extent that under control laboratory conditions it is quite predictable (Cramp et al., 2014; Ohmer et al., 2015). The intermoult interval (IMI) is defined as the period from one sloughing event to the next and can vary from daily to weekly (Bouwer et al., 1953; Castanho and de Luca, 2001; Meyer et al., 2012). Differences in IMI depend on inter-specific (between species) and intra-specific (within species) factors, and also biotic and abiotic variables (Larsen, 1976; Ohmer et al., 2019). Temperature strongly influences IMI, where studies in the temperature range 12–30°C (Taylor and Ewer, 1956; Stefano and Donoso, 1964; Cramp et al., 2014) have demonstrated a decrease in IMI associated with increasing ambient air temperatures. Taylor and Ewer (1956) found that *Bufo regularis* kept in total darkness reduced their IMI compared to those kept in constant light, while Meyer et al. (2012) found no difference in *Rhinella marina* IMI when kept in constant darkness compared to 12:12 light:dark cycle. Intra-specific differences were observed in *R. marina*, showing ontogenetic differences in IMI, where juveniles (SVL <19 mm) have the lowest IMI compared to adults (SVL mean 80 mm; Triana et al.,

2013). Fittell et al. (unpublished) found that *R. marina* with higher average daily metabolic rate have shorter IMI, and sloughing more frequently, suggesting a relationship between rate of sloughing and rate of metabolic processes. Ultimately, sloughing is controlled by hormones, such as aldosterone which seems to be responsible for controlling the initiation of the sloughing behaviour in hypophysectomised toads, and skin shedding *in-vitro* skins (Jørgensen and Larsen, 1961; Nielsen, 1969). Other hormones that seem to initiate sloughing in frogs are cortisol and corticosterone (Stefano and Donoso, 1964). In urodeles, thyroid hormones are responsible for sloughing (Osborn, 1936).

1.3.5 Role of sloughing

Due to constant interactions with the external environment, over time the integrity of skin becomes compromised. The primary function of sloughing is to renew worn-out epidermal structures (Larsen, 1976), to maintain optimal functionality of the skin (Ling, 1972). Animals may increase the rate of skin shedding as a response to external stressors. For example, some snakes increase their skin shedding rate to remove heavy metals that are absorbed into the body (Jones and Holladay, 2006; Goiran et al., 2017). In amphibians, an increase in rate of sloughing has also been observed in response to harmful pathogens (Duneau and Ebert, 2012; Ohmer et al., 2017), and has been demonstrated to reduce the cultivatable cutaneous microbiome up to 100 % (Meyer et al., 2012). This can be both beneficial and detrimental for amphibians: sloughing can remove harmful pathogens, but also removes symbiotic microbes that can play a beneficial role (Brucker et al., 2008; Becker et al., 2009; Harris et al., 2009). The process of sloughing, therefore, could be of great importance for regulating cutaneous pathogen loads (Ohmer et al., 2015). Ohmer et al. (2017) showed species less susceptible to *Bd* were able to clear infection quicker through sloughing, while more susceptible species were not and eventually went on to develop chytridiomycosis. Conceivably, by decreasing the number of zoospores on the skin, sloughing could limit the physical and physiological damage to the skin caused by heavy *Bd* loads and therefore contribute to interspecific *Bd* susceptibility differences.

1.4 CHYTRIDIOMYCOSIS

Bd colonises the superficial epidermal layers of post-metamorphic amphibians (**Fig. 1.3**), specifically on the ventral abdomen, hindlimbs, axillae and toes (Berger et al., 1998; Berger et al., 2005b), and the keratinised mouthparts of tadpoles (Fellers et al., 2001). The life cycle of *Bd* starts with a free-flowing motile zoospore that attaches to the hosts outer epidermis (*stratum corneum* and *stratum granulosum*). The zoospore then develops into a thallus, which produces a single zoosporangium (**Fig. 1.3**). The zoosporangium then produces new zoospores that are released into the surrounding environment (Berger et al., 2005b; Van Rooij et al., 2012). Pathological symptoms include reddening of ventral skin, hyperkeratosis or hypokeratosis, erosions of the epidermis, and

irregular and accelerated sloughing rate (Nichols et al., 2001; Berger et al., 2005c). Physiological abnormalities include reduced blood plasma osmolality, Na^+, K^+, Cl^- and manganese (Mn^{+2}) concentrations (Voyles et al., 2007; Marcum et al., 2010; Voyles et al., 2012a). Full list of pathological symptoms is in **Table S1**.
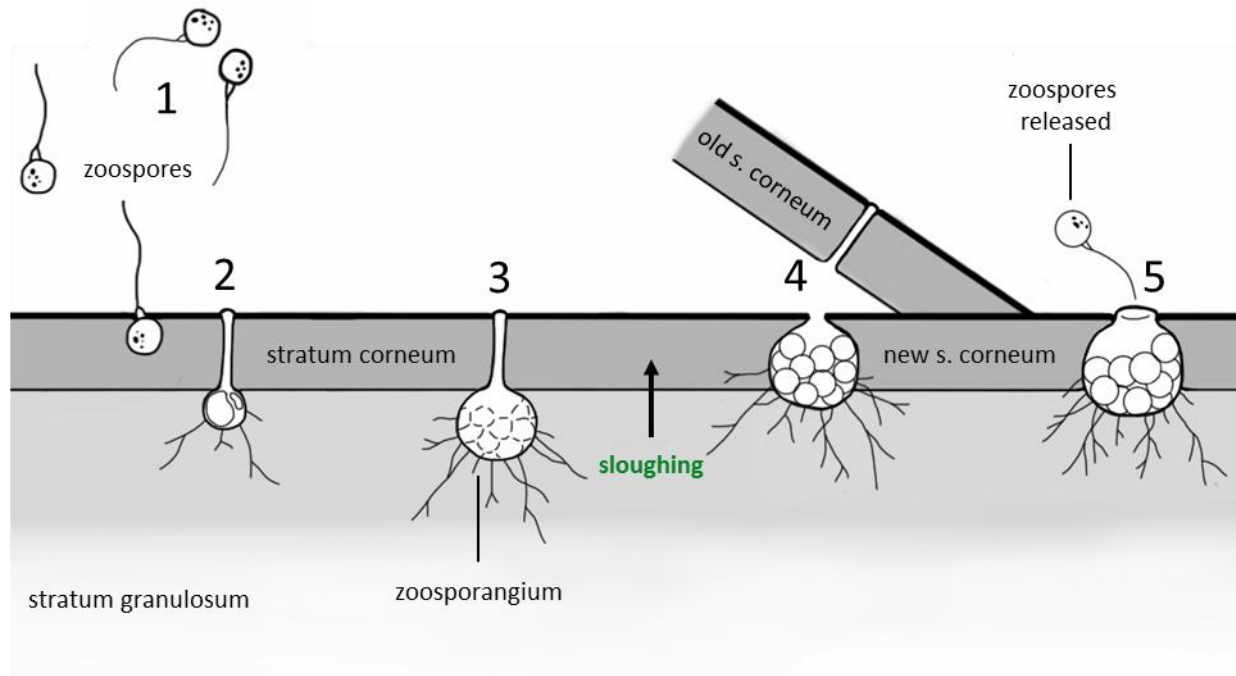
Fig. 1.3 │ **Life cycle of *Batrachochytrium dendrobatidis* in the amphibian skin.** 1) aquatic-motile zoospores (substrate-independent), 2) zoospore embeds in the hosts skin and develops into a thallus, 3) thallus matures and forms a zoosporangium in the *stratum granulosum* and becomes substrate-dependent, 4) host cells undergo epidermal turnover and the removal of the old *stratum corneum* (via sloughing) moves the mature zoosporangia towards the surface, and 5) new zoospores are released into the external environment. Modified from (Berger et al., 2005b; Greenspan et al., 2012).

Voyles et al. (2009) first demonstrated electrophysiological disruption of the epithelium, which coincided with the loss of electrolyte homeostasis, causing cardiac arrest in heavily infected *Litoria caerulea*. The cause of this disruption is yet to be determined, however Berger et al. (2005b) hypothesised its capacity to kill amphibians may be due to physical disruption of normal skin function, and/or the chemical release of a fungal toxin. For example, *Bd* produces a complex mixture of proteins (proteases, biofilm-associated proteins and a carotenoid ester lipase) that quickly disrupts epidermal intercellular junctions (Brutyn et al., 2012). Campbell et al. (2012) suggested that *Bd* may inhibit the activity of the ENaC but not NKA, based on the significant reduction in amiloride-sensitive short-circuit current (Voyles et al., 2009). Dysfunction of the ENaC has been associated with disorders of Na^+ and fluid homeostasis, blood pressure and lung fluid balance (Schild, 2004). Thus, examining the relative expression and activity levels of epithelial transport proteins between infected and non-infected animals may elucidate the mechanism behind the pathophysiology of *Bd*.

1.5   CHYTRID/SLOUGHING INTERACTION

Amphibians infected with *Bd* increase sloughing rate to reduce infection load (Davidson et al., 2003; Ohmer et al., 2015), and for some species, this removes up to 100 % *Bd* load leading to infection clearance (Ohmer et al., 2017). However, for susceptible species, an increase in sloughing frequency only provides a temporary relief from infection load and does not curb the progression of the disease (Ohmer et al., 2015). *Bd* seems to be well-adapted to live in amphibian skin as the timing of zoosporangium maturation and zoospore release syncs with the timing of epidermal turnover (**Fig. 1.3**), and maturation of zoospores occurs within the deeper layers of the epidermis (Berger et al., 2005b; Greenspan et al., 2012). Sloughing may therefore allow a mature zoosporangium to release zoospores external to the host, thereby encouraging self-reinfection of a newly keratinised epidermis that is free of potentially beneficial antifungal symbiotic bacteria (Meyer et al., 2012). Since sloughing does not significantly reduce zoospore numbers in susceptible species, Ohmer et al. (2015) suggested that the excessive sloughing of infected frogs can in fact contribute to the loss of physiological homeostasis seen in terminally ill frogs.

Once amphibians develop a high *Bd* load (>10,000 zoospore equivalent on the skin surface), they tend to slough abnormally in small fragments, cease the typical physical sloughing behaviour, and become lethargic (Berger et al., 1998; Nichols et al., 2001; Carver et al., 2010). Why amphibians cease the sloughing behaviour is unclear, however the lethargic aspect of heavily infected frogs may contribute, and also to reduce energy expenditure if sloughing itself is energetically expensive.

1.5.1   Energetic cost

The behavioural, physiological, and morphological changes associated with sloughing may translate into significant energetic consequences for infected amphibians. Physiological disruption caused by infection result in energetic consequences for the host, by increasing or decreasing metabolic rates (MR). Deviations in MR from parasitic infection can represent energetic disruption on the hosts physiology including maintenance costs, growth and activity (Lochmiller and Deerenberg, 2000). Depending on the energy allocation and strategy, the MR of parasitised hosts can either be significantly reduced (Kilgore et al., 1988; Arnold et al., 2013), increased (Booth et al., 1993; Giorgi et al., 2001), or unchanged (Orlofske et al., 2013). Varied responses in MR to parasitism may be due to the context-dependent nature of the energetic costs of parasitism and may reflect compensatory actions, such as changes in host behaviour and physiology, which may offset the effects of parasitism on growth and development instead (reviewed in Lochmiller and Deerenberg, 2000).

Bd has been shown to increase rates of O_2 consumption (a proxy for MR) in heavily infected frogs (Peterson et al., 2013), but not in sub-clinically infected frogs (Carver et al., 2010). This suggests low infection will not elicit substantial physiological consequences until levels reach a critical threshold (Voyles et al., 2007; Russo et al., 2018). Therefore, increasing the rate of sloughing may

act as an important immune defence to limit *Bd* growth, slowing the onset of physiological disruption (Ohmer et al., 2017). The metabolic costs required to remove the sloughed skin more frequently may increase the overall energy budget of infected frogs, and contribute to the negative health outcomes in susceptible species.

1.6   MISSING LINKS

Our understanding of *Bd* is quickly evolving; however, there is still much to investigate concerning the dynamic link between sloughing and the pathophysiology of chytridiomycosis, which will be the focus of this thesis.

1.6.1   Compensation response to sloughing?

To understand the physiological effects of sloughing and chytridiomycosis on the skin function, the responses of ion regulatory transporters to sloughing first needs to be addressed. Whole-animal to tissue level responses to sloughing have been examined (Larsen, 1970; Budtz, 1977; Erlij and Ussing, 1978). However, there is no direct link with the activities of the epithelial transport proteins and the changes in ion and osmotic transport during sloughing. There could be compensatory responses occurring when the skin becomes leaky, as observed in moulting crayfish (Zare and Greenaway, 1998). For example, ENaC on the apical side of the skin, may be upregulated in response to an increase in Na^+ efflux from sloughing. Alternatively, ENaC may be inhibited because the new skin layer may not be fully formed after the removal of the slough (Budtz and Larsen, 1973). This may in turn affect the animal's internal electrolyte balance. By understanding if sloughing temporarily disrupts an animal's homeostatic balance, it allows us to better understand how skin diseases may interact with this process.

1.6.2   Sloughing a double-edged sword?

Voyles et al. (2009) provided the first evidence for a physiological disruption of the skin function in *Bd*-infected animals, while Russo et al. (2018) showed a negative interactive effect between sloughing and chytridiomycosis on evaporative water loss. The mechanistic cause for cutaneous physiological disruption in susceptible species remains elusive, especially for ionic and osmotic regulation. Sloughing as an immune response may act as a 'double-edged sword' for susceptible species. On one hand an increase rate of sloughing may remove the fungus faster (Ohmer et al., 2017), but sloughing causes alterations in the skin function (Jørgensen, 1949). There may be a fine balance between the rate at which the fungus is removed from sloughing, and the rate at which animals are reinfected. If *Bd* quickly reinfects the skin, the skin function and integrity may be further damaged, ultimately accelerating the development of chytridiomycosis. The role and response of cutaneous ion and water regulators in compensating for the disrupted skin remains elusive, thus examining the underlying mechanisms behind the skin disruption is essential to understanding how much sloughing contributes to the disruption of the skin for infected susceptible animals.

1.6.3   Why is chytridiomycosis associated with size-dependent mortality?

Body size plays an important role in susceptibility to chytridiomycosis as smaller individuals are more susceptible to infection, and develop chytridiomycosis faster than their larger counterpart (Berger et al., 1999a; Carey et al., 2006; Bakar et al., 2016). This may be related to the differences in maturation of skin immune defence (Rollins-Smith, 1998), or immature systemic immune function (Bakar et al., 2016), differences in skin morphology (Chammas et al., 2014), diversity of microbiomes on the skin (Longo et al., 2015), relative surface area for colonisation, and/or the abundance of tissue damage in smaller individuals caused by chytridiomycosis. From a physiological perspective, smaller animals have larger surface area/volume ratio for ion loss to occur (Klein et al., 2016), and generally have higher mass-specific MR (White et al., 2006). The combination of increased ion loss, MR and relatively higher zoospore load may contribute to the greater susceptibility, and mortality in smaller frogs. There is also size dependency in the rate of sloughing, where smaller animals slough more often (Triana et al., 2013). Thus, smaller anurans may be more at risk of cutaneous and metabolic dysfunction relative to larger individuals due to the intrinsic differences in sloughing rate, surface area/volume ratio that favour the development of chytridiomycosis. Few studies, however, have directly examined the relationship between body size, *Bd* load and sloughing on the physiological consequences of *Bd* infection. By understanding this relationship, this may explain intraspecific differences in mortality relating to body size.

1.7   AIMS

Despite a growing amount of research exploring the role of sloughing in regulating amphibian skin pathogens, little information is provided on the physiological cost of sloughing alone, and how chytrid may further disrupt this process. Thus, the overall aim of this thesis was to understand the mechanistic basis, and the role of sloughing in the disruption of physiological homeostasis in animals with chytridiomycosis.

The first aim of this thesis was to investigate the effects of sloughing on cutaneous ion transport, and the underlying abundance, activities, distribution and expression of associated epithelial transport regulatory proteins in healthy amphibians (Chapter 2). Approaching this from an integrative perspective allows a more realistic interpretation of the animal's physiological response to sloughing.

The physiological cost of sloughing and chytridiomycosis may have interactive effects on cutaneous ion regulation, thus the second aim was to determine how chytridiomycosis alters cutaneous ion transport properties during sloughing (Chapter 3). This will help elucidate if the trade-off between decreased IMI from *Bd* infection is beneficial or detrimental to the host.

Body size plays an important role in disease susceptibility. However, the interaction of body size and physiological disruption has yet to be studied, thus the third aim examined the effects of body

size on the energetic and osmoregulatory costs of sloughing infected animals (Chapter 4). This may help clarify why smaller, younger individuals are more susceptible to *Bd*.

Lastly, the mechanisms underlying how *Bd* and sloughing interact to affect cutaneous water balance, especially through effects on cellular aquaporin proteins remains elusive. The fourth experimental aim determined how chytridiomycosis alters the activities and expression of cutaneous AQPs in the ventral skin during sloughing (Chapter 5).

1.8   STUDY SPECIES

Rhinella marina (prev. *Bufo marinus*) is a highly invasive species (native to South America) of the upper eastern and northern regions of Australia (Phillips et al., 2006; Shine, 2010). *R. marina* was used for the first experimental chapter to describe changes in skin morphology and physiology during sloughing (Chapter 2). *R. marina* were not used for chytrid-related research as adult *R. marina* are unaffected by *Bd* (Shine, 2010), but newly metamorphosed toads are susceptible (Berger et al., 1998). Sloughing frequency has also been documented in this species (Meyer et al., 2012).

Litoria caerulea (Anura: Hylidae) are a common endemic arboreal species widely distributed throughout the eastern and northern regions of Australia (Cogger, 2014). *L. caerulea* occupy a diverse range of habitats from humid forests to drier eucalypt woodlands, and urban areas (Reynolds, 2005). While they are listed as of least concern under the IUCN guidelines (IUCN, 2017), *L. caerulea* are susceptible to chytridiomycosis and have been considered a "model species" for Australian chytridiomycosis research (Berger et al., 2005a; Voyles et al., 2009; Peterson et al., 2013). Sloughing characteristics has also been documented in this species (Cramp et al., 2014; Ohmer et al., 2015). Therefore, *L. caerulea* was an appropriate choice for this study and was utilised in three remaining experimental chapters (Chapters 3–5).

Fig. 1.4 │ **Dorsal view of a cane toad (*Rhinella marina*) on the left and a green tree frog (*Litoria caerulea*) on the right side.** Photo credit: C. Baker.

1.9   STRUCTURE OF THESIS

This thesis comprises four experimental chapters (Chapters 2–5), written in the format of independent manuscripts (abstract, introduction, methods, results and a discussion) along with a general introduction (Chapter 1) and general discussion (Chapter 6). Chapter 2 was published in the *Journal of Experimental Biology* (Wu et al., 2017), and investigated changes in the skin function during sloughing of *R. marina*. The study examined skin function during sloughing from whole-animal responses down to expression of ion transport genes. The second experimental chapter (Chapter 3) published in the *Journal of Experimental Biology* (Wu et al., 2019) investigated the mechanisms behind how chytridiomycosis alters cutaneous ion transport, and if there was a synergistic effect during sloughing. The third experimental chapter (Chapter 4), published in *Scientific Reports* (Wu et al., 2018) examined the metabolic and osmoregulatory cost of sloughing in relation to body size and chytridiomycosis. The last experimental chapter (Chapter 5) examines how chytridiomycosis alters water balance during sloughing from an integrative perspective. The final chapter of this thesis (Chapter 6) forms the General Discussion and summarises the four experimental studies, discussing the implications of this work in a wider context, and suggests future research directions.

1.10 SUPPLEMENTARY INFORMATION

1.10.1 Supplementary table

Table S1.1 │ List of known biological responses to *Batrachochytrium dendrobatidis* infection.

Symptoms	Species	Response	Reference
Behavioural			
Lethargy	*Litoria caerulea*		Voyles et al 2009
Appetite	*L. caerulea*	Decrease	Voyles et al 2009; Peterson et al 2013
Sloughing frequency	Various	Increase	Ohmer et al 2017
Righting reflex	*L. caerulea*	Decrease	Voyles et al 2009
Abnormal posture	*L. caerulea*	Increase	Voyles et al 2009
Morphological, Anatomical & Histological			
Body mass	*L. caerulea*	Decrease	Peterson et al 2013
	Rana muscosa	Decrease	Volyes et al 2012
Heart ventricular & myofibril mass	*Lithobates catesbeianus* (tadpole)	Increase	Salla et al 2015
Hyperkeratosis	*L. caerulea*		Berger et al 1998, 1999 & 2005a
	L. chloris		Berger et al 1999
	Mixophyes fasciolatus		Berger et al 1999
	Dendrobates auratus		Nichols et al 2001
	Dendrobates tinctorius		Nichols et al 2001
	Xenopus tropicalis		Parker et al 2002
Hypokeratosis	*L. caerulea*		Berger et al 1998, 1999 & 2005a
Tight junctions and cell adherens	*L. caerulea*	Decrease	Appendix 1
Cellular apoptosis	*Pseudophryne corroboree*	Increase	Brannelly et al 2017
Cutaneous erythema	*L. caerulea*	Increase	Volyes et al 2009
Hematopoietic tissue	*P. corroboree*	Decrease	Brannelly et al 2016
Bone marrow	*P. corroboree*	Decrease	Brannelly et al 2016
	Rhinella marina	Increase	Brannelly et al 2016
Excess slough	*L. caerulea*		Ohmer et al 2015
	M. fasciolatus		Berger et al 1999
	D. auratus		Nichols et al 2001
	D. tinctorius		Nichols et al 2001
	Ambystoma tigrinum		Davidson et al 2003
Physiological			
Cutaneous ion loss	*L. caerulea*	Increase	Wu et al 2018
Cardiac stroke volume	*L. catesbeianus* (tadpole)	Increase	Salla et al 2015
Metabolic rate	*L. caerulea*	Increase	Wu et al 2018; Peterson et al 2013
Cutanous sodium transport	*L. caerulea*	Decrease	Volyes et al 2009
Skin resistance	*L. caerulea*	Decrease	Volyes et al 2009, Wu et al 2019
Electrolyte levels	*L. caerulea*	Decrease	Volyes et al 2007, 2009, & 2012
Evaporative water loss	*L. caerulea*	Increase	Russo et al 2018
	Dendropsophus minutus	Decrease	Bovo et al 2016
	Ishnocnema parva		
Testosterone	*L. wilcoxii*	Decrease	Kindermann et al 2017
Water uptake	Various	Decrease	Jørgensen 1949, Ewer 1951, Wardziak et al 2013, Chapter 5
Immunological			

Glucocorticoids	*L. caerula*	Increase	Peterson et al 2013
	Alytes obstetricans (tadpoles)	Increase	Gabor et al 2013
	L. wilcoxii	Increase	Kindermann et al 2017
Neutrophils	*L. caerulea*	Increase	Peterson et al 2013
Lymphocytes	*L. caerulea*	Decrease	Peterson et al 2013; Young et al 2014
	Xenopus laevis	Decrease	Fites et al 2013
White blood cell count	*L. caerulea*	Decrease	Peterson et al 2013; Young et al 2014
Immune function	*X. laevis*	Decrease	Fites et al 2014
	Lithobates yavapaiensis	Decrease	Savage et al 2016
Genetic			
Immune-related genes	*Atelopus zeteki*	Decrease	Ellison et al 2014
	Silurana tropicalis	Decrease	Ribas et al 2009
Skin integrity genes	*R. muscosa*	Decrease	Rosenblum et al 2012
	Rana sierrae	Decrease	Rosenblum et al 2012
	L. caerulea	Increase	Appendix 1

Living with a leaky skin:
upregulation of ion transport proteins during sloughing

2.1   ABSTRACT

Amphibian skin is a multifunctional organ providing protection from the external environment and facilitating the physiological exchange of gases, water and salts with the environment. In order to maintain these functions the outer layer of skin is regularly replaced in a process called sloughing. During sloughing, the outermost layer of the skin is removed in its entirety which has the potential to interfere with skin permeability and ion transport, disrupting homeostasis. In this study, we measured, *in vivo*, the effects of sloughing on the cutaneous efflux of ions in toads *Rhinella marina* kept in freshwater conditions. We also measured transepithelial potential, cutaneous resistance, active ion transport, and the distribution, abundance and gene expression of the key ion transport proteins sodium-potassium ATPase (NKA), and the epithelial sodium channel (ENaC) during sloughing. We hypothesised that during sloughing, the increase in transepithelial efflux of ions during sloughing is a consequence of increased permeability and/or a reduction in the abundance or expression of cutaneous ion transport proteins, resulting in disruption to of internal ion homeostasis. There was a significant increase in sodium and chloride efflux during sloughing in *R. marina*. However, although *in vitro* skin resistance decreased after sloughing, active sodium transport increased commensurate with an increase in NKA and ENaC protein abundance in the skin. These changes in skin function associated with sloughing did not affect the maintenance of internal electrolyte homeostasis. These results suggest that during sloughing, amphibians actively maintain internal homeostasis by increasing cutaneous rates of ion uptake.

2.2   INTRODUCTION

The skin, the largest vertebrate organ, has evolved into a complex, pluri-stratified, multi-membrane system (Lillywhite and Maderson, 1988) with vital, often contrasting, functions (reviewed in Chuong et al., 2002). It must act as an impermeable barrier to protect the organism from environmental stressors (abiotic and biotic) (Proksch et al., 2008) while simultaneously being able to sense, interact and exchange some solutes with the surrounding environment (Hillyard et al., 2007). For amphibians, this is especially important as their skin regulates the exchanges of electrolytes, water and respiratory gases with the environment to maintain internal homeostasis (Boutilier et al., 1992; Shoemaker et al., 1992).

Histologically, the skin of amphibians consists of an outer multilayered epidermis and an inner dermal layer (dermis). The most basal layer of the epidermis is the *stratum germinativum*, which is attached to the dermis by a basement membrane. The columnar cells of the *s. germinativum* continually regenerate (via mitotic division), to replenish and maintain the rest of the epidermal cell population (Heatwole et al., 1994). Above the *s. germinativum* is the *s. spinosum* ('spiny layer'), where cellular keratinisation begins. Above the *s. spinosum* is the *s. granulosum* (granular layer) where the keratinocytes become known as granular cells. These cells are connected by tight

junctions (*zonulae occludens*) that separate the apical plasma membrane from the basolateral membrane lining the lateral intercellular space (Farquhar and Palade, 1964). The apical plasma membrane of granular cells therefore forms the limiting barrier for transcellular solute and water transport across the epidermis, with connections between this layer and the underlying layers (*s. spinosum* and *s. germanitivum*) forming an electrical syncytium. The most superficial layer of the epidermis is the *s. corneum*, which consists of 1–2 thin layer/s of dead cells (reviewed in Heatwole et al., 1994).

Because of constant interactions with the external environment, the skin must be renewed in order to maintain functionality (Ling, 1972). All metamorphosed amphibians go through a physiological and behavioural phase known as 'ecdysis' or 'sloughing' (Ling, 1972; Larsen, 1976), where the old *s. corneum* is removed and replaced periodically with a new layer (derived from the underlying *s.granulosum*). In the early shedding stage, the old *s. corneum* becomes separated from the underlying cell layer via a gradual dissolution of the desmosomes between these two layers (Budtz, 1977). The new *s. corneum* (derived from the underlying *s. granulosum*) swells, flattens (Ernst, 1973), and becomes cornified (Elias and Shapiro, 1957; Whitear, 1975). Mucus also appears beneath the separated *s. corneum* (known as a 'slough') to facilitate removal (Larsen, 1976). During the post-shedding phase, the new *s. corneum* flattens and becomes denser in appearance (Budtz and Larsen, 1973). Fusion of the *s. granulosum* layer leads to the formation of tight junctions (Budtz and Larsen, 1975), which serve to limit the paracellular movement of salts and water (Tsukita et al., 2001; Niessen, 2007). While sloughing maintains the integrity of the skin, physiological changes have been observed to coincide with sloughing that may disturb homeostatic balance. Jørgensen (1949) first observed an increase in cutaneous permeability in sloughing *Bufo bufo*, *Rana temporaria* and *R. esculenta* which increased both water gain and sodium loss. These changes in skin permeability can start 12 h ahead of sloughing (Ewer, 1951), and continue 3–4 h post-sloughing (Jørgensen, 1949).

The temporary disruption of cutaneous integrity that occurs during sloughing corresponds with changes to the skin's electrophysiological properties. During sloughing there is a decrease in the short-circuit current (indicative of active ion transport activity), transepithelial potential (indicative of the electrical potential difference between the two sides of the cell membrane), and skin resistance (Larsen, 1970; Nielsen and Tomilson, 1970; Larsen, 1971a). These changes seem to result from the physical shedding of the slough, as they are initiated by the separation of the slough from the underlying skin layer (reviewed in Erlij and Ussing, 1978). However, these studies artificially induced sloughing through the administration of hormones such as aldosterone (Nielsen, 1969; Larsen, 1971a), which can potentially create unrealistic electrophysiological data (relative to natural or spontaneous sloughing), because aldosterone also acts to regulate ion and water

reabsorption in the kidneys (Garty, 1986; Eaton et al., 2001) and skin (Bentley, 2002), and increases protein synthesis in the bladder and skin (Crabbé and de Weer, 1964). Thus, many of these earlier sloughing studies are be difficult to interpret, as the observed electrophysiological changes of the skin observed may be an artefact of aldosterone administration instead of the natural physiological changes that occur during sloughing.

While earlier studies have suggested that the physical alterations that occur to amphibian skin during sloughing (e.g. removal of tight junctions) cause the increase skin permeability (Smith, 1975; Larsen, 1976), Katz (1978) suggested disruption of tight junctions was not solely responsible for the observed changes in specific permeability of the skin to sodium (Na^+) and potassium (K^+) during sloughing. A reduction in the abundance or activity of transepithelial ion transport proteins such as epithelial sodium channels (ENaC) or the sodium-potassium pump (Na^+/K^+-ATPase; NKA) during sloughing may also cause disruption to the transportation of ions. ENaC is a membrane-bound protein channel found in the apical membrane of epithelial cells that is responsible for the uptake of Na^+ from the environment, while NKA is an active membrane protein pump found in the basolateral layer of epithelial cells that establishes an electrochemical gradient for ion channels like ENaC to transport Na^+ against their concentration gradients (Hillyard et al., 2008). Thus, examining the relative expression of these proteins in sloughing amphibians relative to non-sloughing amphibians may clarify the mechanism through which this disruption of ion transport during sloughing occurs.

To date, there is no direct link with the activities of the epithelial transport proteins and the changes in ion and osmotic transport during sloughing. As there are physical and physiological changes in the skin associated with sloughing (Larsen, 1976; Erlij and Ussing, 1978), does the change in skin function cause temporary electrolyte disruption in the animal's homeostasis (e.g. blood biochemistry), or does the skin actively upregulate expression of epithelial ion transporters (e.g. ENaC and NKA) to maintain homeostasis? Taking an integrative approach, this study aimed to investigate the effects of sloughing on epidermal ion transport *in vivo* and *in vitro*, the distribution, abundance and expression of associated regulatory transport proteins, and blood plasma biochemistry in cane toads, *Rhinella marina* (Linnaeus, 1758). This study also avoided the influence of hormone-induced sloughing by investigating epithelial transport in spontaneously sloughing anurans.

We hypothesised that as a result of physical changes to the skin during spontaneous sloughing there would be disruption of cutaneous ion and water transport (Jørgensen, 1949), with a reduction in the abundance and expression of ion transport proteins (e.g. ENaC and NKA), resulting in a transient disruption to internal ion and water homeostasis.

2.3   MATERIALS AND METHODS

2.3.1   Animal collection maintenance

Rhinella marina ($n = 24$) were collected from The University of Queensland campus, Brisbane, Australia between November 2014 and January 2015, and housed in large black bins ($n = 5$ per bin) containing a thin layer of pine-bark mulch (Richgro, WA, Australia). Toads were checked daily, fed weekly on vitamin-dusted (Aristopet Pty Ltd, QLD, Australia) crickets (*Acheta domesticus*), and enclosures were cleaned weekly. After approximately 2 weeks, toads were housed individually in ventilated polypropylene plastic containers (130 x 140 x 325 mm) with a thin layer of pine-bark mulch saturated with tap water, which were tilted to allow a wet and dry gradient for the toads to move between. All toads were kept at 25 ± 0.3°C with a 12 h:12 h light:dark cycle.

2.3.2   Monitoring sloughing frequency

To determine sloughing events, *R. marina* ($n = 24$) were marked with a small amount of non-toxic waterproof zinc cream (Key-Sun Laboratories, NSW, Australia) on the dorsal surface following Meyer et al. (2012). Animals were checked twice daily to record the disappearance of the mark as an indication of sloughing. Once a mark disappeared, it was reapplied. The time (in days) between mark application and loss was recorded as the inter-moult interval (IMI). The sloughing behaviour for *R. marina* was divided into four stages: 1. *Intermoult*, the period in between each slough; 2. *Pre-sloughing*, when animals started to extend their limbs to lift the abdomen off the ground; 3. *Sloughing*, which begins with mouth gaping, followed by abdominal contractions, upper body wiping and removal of the old skin; and 4. *Post-sloughing*, up to 1 h after sloughing when normal behaviour resumes.

2.3.3   Ion loss measurements

To measure changes in *in vivo* ion efflux during sloughing, each animal was placed in an open-ended ventilated clear chamber (75 x 110 x 160 mm) containing 300 ml of reverse osmosis (RO) water with a magnetic stirrer to circulate the solution. The rate of ion efflux was measured as the change in conductivity (in μS h^{-1}) for toads in each of the following moult stages: 1) intermoult, 2) pre-sloughing, 3) sloughing, and 4) post-sloughing (**Fig. 2.1**) for nine animals. A conductivity electrode connected to a conductivity pod (ML307, ADInstruments, NSW, Australia) was placed at each end of the chamber. The output was digitised with a PowerLab 4/35 interface (ADInstruments) and recorded on Labchart software (ADInstruments). The baseline of the bathing solution was measured (average from the two electrodes) for roughly an hour before the animal was placed into the chamber (**Fig. 2.1**). A change in the conductivity of the bathing solution associated with sloughing was determined via video surveillance, and duration of the sloughing event (min) was recorded. The experiment was conducted at room temperature (22 ± 0.5°C). Animals were fed weekly, but because of the difficulty in determining when animals would slough (7 day variation),

animals were not fasted prior to measurements and may have been in different digestive states. Both fasted and recently fed animals were included in the analysis as there was no significant difference in the rate of conductivity (t_{50} = -0.76, P = 0.45) between fasted and recently fed animals.
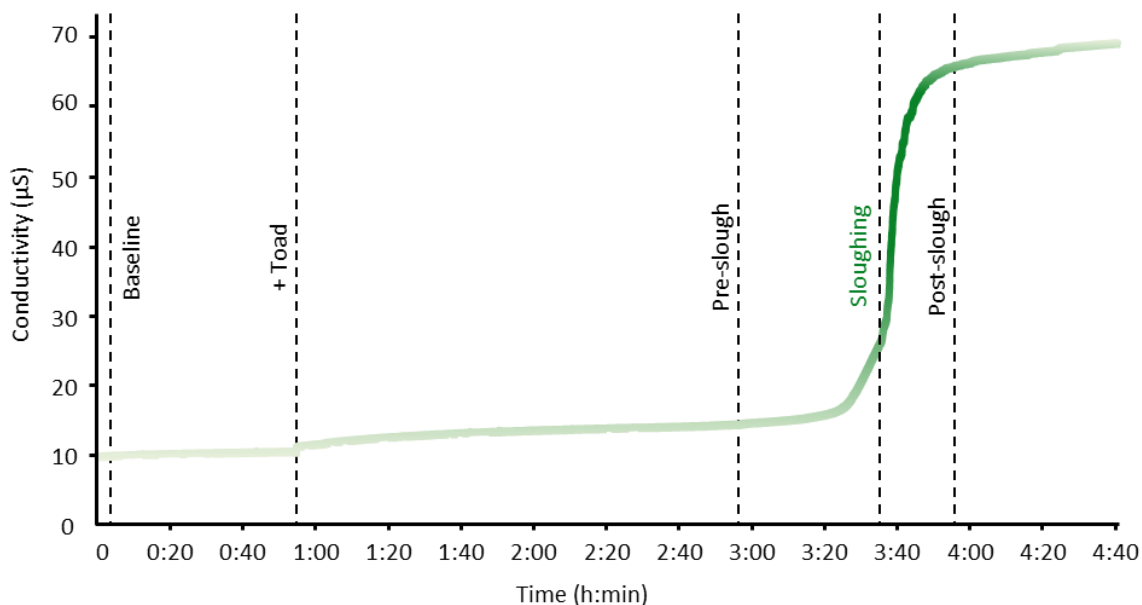
Fig. 2.1 │ **Example raw trace of changes in conductivity (µS) readings associated with sloughing for one cane toad (*Rhinella marina*).** Body mass (M_b) = 46.7 g, snout-vent length (SVL) = 86 mm). "Baseline" values were obtained from the chamber water in the absence of animals; '+ Toad' data were obtained with the animal inside the experimental chamber.

The net loss of Na$^+$ and K$^+$ into the bathing solution was measured using flame photometry (BWB-XP flame photometer; BWB Technologies Ltd, UK). The net loss of Cl$^-$ was determined spectrophotometrically (DTX 880 Multimode Detector; Beckman Coulter, IA, USA) using a commercially available chloride kit according to the manufacturer's instructions (MAK023; Sigma-Aldrich, MO, USA). The conductivity readings (µS h^{-1}) were converted to NaCl efflux (mmol l^{-1}) using known concentrations of NaCl solutions (0–1 mmol l^{-1}). The conductivity readings of the solution and known NaCl concentrations showed a predictable linear relationship (r^2 = 0.99, **Fig. S2.1**). To estimate the overall effect of sloughing on the total sodium content of the extracellular fluid (ECF), conductivity measures were converted to a rate of sodium loss (mmol h^{-1}) based on [Na$^+$] of bath water samples collected after sloughing and assuming that sodium was the primary ion contributing to solution conductivity and that there was an equal proportion of sodium lost relative to other ions. The net amount of Na$^+$ lost during sloughing was calculated assuming an ECF volume of approximately ~25 % of the body mass of the animal (Thorson, 1964). The actual Na$^+$ concentration of the ECF was measured from plasma samples (see below). The proportion of the total ECF Na$^+$ (as a percentage of ECF Na$^+$ h^{-1}) lost during sloughing was calculated by dividing the rate of ion loss (mmol l^{-1} h^{-1}) by the total amount of ECF Na$^+$ (mmol) multiplied by 100.

Before and after each conductivity trial, animals were voided of urine by gently applying pressure on the ventral side. Body masses (M_b; g) was then measured (Adam Equipment Co Ltd, CT, USA) to

calculate any change over the sloughing period as percentage change in M_b per hour. The change in M_b over the tested interval represents osmotic water flux. Animals that urinated or defecated during the experiment were taken out and re-weighed before being returned back to the chamber, with fresh bathing solution.

2.3.4   Blood plasma biochemistry

Toads ($n = 14$ intermoult, $n = 10$ post-sloughing) were euthanased via double pithing at one of two time points: 1) post-sloughing (no more than 1 h after sloughing had occurred), or 2) intermoult (at a point halfway through the IMI). Snout-vent length (SVL) and M_b were measured immediately. Blood was collected via cardiac puncture into a lithium heparinised syringe. Samples were then centrifuged at 5000 g for 5 min and the plasma collected and stored at -20°C for subsequent electrolyte analysis. Two heparinised capillary tubes of whole blood were also centrifuged at 5000 g for 3 min to determine haematocrit (H_{CT}). Plasma Na^+ and K^+ levels (mmol l^{-1}) were measured using a flame photometry, and plasma osmolality (mosmol l^{-1}) was measured using a Vapro 5520 vapour pressure osmometer (Wescor, Logan, UT, USA). Plasma Cl^- levels (mmol l^{-1}) were determined spectrophotometrically (DTX 880 Multimode Detector; Beckman Coulter, IA, USA) using a chloride kit according to the manufacturer's instructions (MAK023; Sigma-Aldrich, Missouri, USA).

2.3.5   Electrophysiology of the ventral skin

Ventral skin samples (<1 cm^2, intermoult $n = 8$, post-sloughing $n = 8$) were collected from the lower abdominal pelvic patch region of animals used for blood biochemistry analyses (see above), and mounted in a self-contained, single channel Ussing chamber apparatus (Model U-9926; Warner Instruments, Hamden, CT, USA) with a single-channel epithelial voltage-clamp amplifier (Model EC-800; Warner Instruments, Hamden, CT, USA). Apical and basolateral surfaces of the skin were perfused with an oxygenated (95 % O_2 and 5 % CO_2) frog Ringer solution (in mmol l^{-1}: NaCl (112), KCl (2.5), D-glucose (10), Na_2HPO_4 (2), $CaCl_2$ (1), $MgCl_2$ (1), HEPES salt (5), HEPES (5) at pH 7.4 with an osmolality of 230 ± 20 mosmol l^{-1}; Voyles et al. (2009)), and temperature was maintained via a water bath set at 25 ± 1°C. Electrophysiological parameters were measured as follows: (1) transepithelial potential (V_T) under open-circuit conditions by clamping the current to 0 µA and recording the resulting voltage (mV) with reference to the basolateral side, (2) active ion transport via clamping the voltage to 0 mV and recording the instantaneous short-circuit current (I_{SC}) response (µA cm^{-2}) and (3) transepithelial resistance per unit area (Ω cm^{-2}) by applying 3 s of 1 µA pulses across the epithelium every 60 s, or under voltage-clamp conditions by applying 3 s of 1 mV at 60 s intervals (Ruhr et al., 2014). The inflections from the resulting change in I_{SC} and V_T during pulsing were used to calculate resistance using Ohm's law. Sodium flux was calculated by dividing the I_{SC} by Faraday's constant using the following formula:

$$J_{\mathrm{Na^+}} = \frac{I_{\mathrm{SC}}}{F}$$

Where $J_{\mathrm{Na^+}}$ is the sodium flux (mol s^{-1}), I_{SC} is the short-circuit current (µA), and F is Faraday's constant (96 485 Coulomb mol^{-1}). The relationship between flux and current is the same as that between concentration and charge (Ussing and Zerahn, 1951). Thus, a current measured in µA corresponds to a net transport rate of 10^{-11} mol s^{-1}.

The transepithelial potential and resistance were also measured under more ecologically realistic conditions consistent with 'freshwater' on the apical skin side (26 mmol l^{-1} NaCl in distilled water), where the electrochemical gradient across the skin would favour a net efflux of ions during sloughing. The traditional approach of using Ringer solution on both surfaces of the membrane could potentially negate this condition.

2.3.6   Histological analysis of epithelial transport proteins

Epidermal thickness was compared between intermoult and post-sloughing toads. Ventral skin samples (<1 cm²) from the lower abdominal pelvic patch region were collected and placed into aqueous buffered zinc formalin fixative (Z-fix; Anatech, MI, USA) for 24 h, then transferred to 70 % ethanol, and stored at 4°C. Tissues samples (Intermoult $n = 6$; Post-sloughing $n = 6$) were then dehydrated through an ascending ethanol series, cleared in xylene and embedded in paraffin wax (Histoplast Paraffin; ThermoFisher Scientific, Sydney, Australia). Tissue samples were then transversely sectioned into approximately 6 µm-thick sections, (Leica RM2245; Leica Microsystems, NSW, Australia), stained with Mayer's hematoxylin and 1 % eosin in 70 % ethanol, and photographed with NIS-Elements software (v. 4.10, Nikon Instruments Inc., Tokyo, Japan) under a bright-field illumination (Nikon Eclipse E200 MV, Nikon Instruments Inc., Tokyo, Japan).

2.3.6.1   NKA distribution

Distribution of the NKA α-subunit in the ventral skin tissues was examined via immuno-fluorescence staining. Distribution of the ENaC α-subunit in skin sections was not examined as the antibody (Anti-SCNN1A antibody; HPA012939, Sigma-Aldrich) did not function well in our immunohistochemistry protocol. Sections were de-paraffinised then washed in washing buffer (0.01 mol l^{-1} PBS, 0.05 % Tween-20, pH 7.4; 2 x 3 min washes), and blocked at room temperature in normal goat serum (2 % goat serum, 1 % BSA, 0.1 % cold fish skin gelatin, 0.1 % Triton X-100, 0.05 % Tween-20, and 0.05 % thiomerosal in 0.01 mol l^{-1} PBS, pH 7.4). Sections were then incubated in a humidified chamber overnight at 4°C with the NKA primary antibody α5 (developed by the Developmental Studies Hybridoma Bank, created by the NICHD of the NIH, and maintained at The University of Iowa, Department of Biology), diluted 1:500 in 1 % BSA, 0.1 % cold fish skin gelatine, and 0.05 % thiomerosal in 0.01 mol l^{-1} PBS. Subsequently, sections were then incubated with a fluorophore-conjugated secondary antibody (Goat anti-Mouse IgG Dylight (ab96879; Abcam Inc,

Cambridge, UK)) diluted 1:500 in 0.01 mol l^{-1} PBS, and 0.05 % Tween-20 for 1 h in the dark at room temperature. They were then mounted with Fluroshield DAPI mounting medium (Sigma-Aldrich, Australia), and viewed using a Nikon Eclipse E200 MV series epi fluorescence microscope and photographed using NIS-Elements software.

2.3.7   Ion transporter abundance

Semi-quantitative Western blotting was performed to estimate the relative abundances of NKA α-subunit and ENaC α-subunit in the ventral skin tissues of intermoult ($n = 4$) and post-sloughing ($n = 4$) toads. Ventral skin samples (<1 cm^2) from the lower abdominal pelvic patch region were collected and stored at -80°C. Frozen tissues were then homogenised in ice-cold membrane extraction homogenisation buffer (250 mmol l^{-1} sucrose, 30 mmol l^{-1} Tris, 1 mmol l^{-1} EDTA, 100 μg ml^{-1} phenylmethylsulfonyl fluoride (PMSF) and 5 mg ml^{-1} protease inhibitor cocktail), and centrifuged at 1200 g for 15 min at 4°C. The supernatant was then removed and centrifuged at 23000 g for 25 min at 4°C. The resulting pellet was re-suspended in 50 μl of homogenisation buffer. An aliquot was used for Bradford protein quantification (Sigma-Aldrich).

A 5 μg sample of total membrane protein in NuPAGE LDS sample buffer (Invitrogen) was loaded in triplicate into Bolt 4-12 % Bis-Tris Plus gels (ThermoFisher Scientific) and electrophoresed at 140 V for 1 h. Gels were subsequently transferred onto 0.45 μm Westran PVDF blotting membranes (Sigma-Aldrich) at 20 V for 75 min. Membranes were then blocked in blocking buffer (5 % skim milk in TBST (20 mmol l^{-1} Tris, 150 mmol l^{-1} NaCl, and 1 % Tween-20, pH 7.6)) for 1 h at room temperature before incubation overnight at 4°C with their respective primary antibody (NKA primary antibody α5 (0.2 μg ml^{-1}), and ENaC α-subunit primary antibody (0.15 μg ml^{-1}; Anti-SCNN1A antibody; HPA012939, Sigma-Aldrich)) diluted in blocking buffer. Membranes were then incubated in secondary goat anti-mouse IgG Horseradish Peroxide (HRP)-conjugated antibody (1.2 μg ml^{-1}; C22P20, Antibodies Australia, Victoria, Australia) and goat anti-rabbit IgG HRP-conjugated antibody (0.6 μg ml^{-1}; C24P03, Antibodies Australia), respectively) antibody for 1 h at room temperature, and stained with 1-Step Ultra TMB-Blotting solution (ThermoFisher Scientific). The membranes were dried and digitised for densitometry analysis with Image J (https://imagej.nih.gov/ij/). The pixel densities were used to estimate protein abundance in the post-sloughing animals expressed relative to the intermoult group.

2.3.8   Ion transporter expression

2.3.8.1   RNA extraction and cDNA synthesis

Ventral skin samples (<1 cm^2) from the lower abdominal pelvic patch region were collected, and stored in RNA-later (Ambion Inc., Texas, USA) at -20°C. The skin samples were then homogenised with stainless steel beads using a TissueLyser II (Qiagen). Total RNA was isolated using an RNeasy Mini kit with on-column DNAse treatment as per the manufacturers' guidelines (RNeasy Mini kit;

Qiagen, Hilden, Germany). RNA purity was assayed by spectrometry, and yield measured using a Qubit fluorometer (ThermoFisher Scientific). RNA was then reversed transcribed into cDNA (SensiFAST™ cDNA synthesis kit, Bioline, NSW, Australia), with appropriate controls (no reverse transcriptase), followed by RNase H treatment.

2.3.8.2 *Primer design and quantification of mRNA by quantitative PCR (qPCR)*

Quantitative PCR (qPCR) primers against the target gene ENaC (*scnn1a* (Sodium Channel Epithelial 1 Alpha Subunit)) and the housekeeping gene, glyceraldehyde 3-phosphate dehydrogenase (*GAPDH*) were manufactured using previously published species specific primer sequences (Konno et al., 2007). Species specific primers against the targe gene NKA (*atp1a1* (ATPase Na$^+$/K$^+$ Transporting Subunit Alpha 1)) were designed from published *R. marina* NKA-α1 subunit sequence (GenBank: Z11798.2; Jaisser et al., 1992) using OligoPerfect™ Designer (ThermoFisher) with acceptance of the default parameters. qPCR was performed using the SensiFAST™ SYBR No-ROX kit (Bioline, NSW, Australia) in a thermal cycler (MiniOpticon™, Bio-Rad) using the cycling parameters recommended in the qPCR kit. Each assay (in triplicate) included a no-template control and a no-reverse transcriptase control. All PCR efficiencies were >90 % and all the assays produced unique dissociation curves. Bio-Rad CXF Manager software (version 3.1, Bio-Rad) results were exported as tab-delimited text files and imported into Microsoft Excel for further analysis. The expression of each gene was quantified relative to the expression of the housekeeping gene, *GAPDH* using the Pfaffl (2001) method.

2.3.9 Statistical analysis

All analyses were performed in R.3.0.1 (Pinheiro et al., 2013). Data were presented either as means $\pm$ s.e. or as individual data points depending on the nature of the data presented (Cumming et al., 2007; Krzywinski and Altman, 2013), and α was set at 0.05 for all statistical tests.

2.3.9.1 *Electrolyte conductivity*

Differences in the rate of conductivity (in µS h^{-1}) between each group were analysed using linear mixed effects (lme) models in the R 'nlme' package (Pinheiro et al., 2013) with groups (intermoult, pre-sloughing, sloughing, post-sloughing) as fixed effects, M_b (g) as covariate, and individual identity as a random effect to account for repeated measurements within individuals. Changes in M_b (M_b before – M_b after) following the *in vivo* ion loss experiment between intermoult and sloughing groups were analysed using linear mixed effects (lme) models with group (intermoult, post-sloughing) as fixed variables, duration in the experiment as covariate, and individual identity as a random effect to account for repeated measurements within individuals.

2.3.9.2 *Blood plasma biochemistry and electrophysiology of the skin*

Differences between the intermoult and post-sloughing group in plasma biochemistry (H$_{CT}$, Na$^+$, K$^+$, Cl$^-$ and osmolality), and the electrophysiological properties of the skin (transepithelial potential,

resistance and active transport) were analysed by analysis of covariance (ANCOVA) with time (h) of post-mortem blood and skin tissue collection as covariates.

2.3.9.3   ENaC and NKA abundance and gene expression

Differences in staining intensity of antibody bands representing NKA α-subunit and ENaC α-subunit relative abundance and relative expression of NKA and ENaC between intermoult and post-sloughing groups were compared using ANCOVA with group (intermoult and post-sloughing) as the fixed effect, and time (h) of post-mortem skin tissue sample collection as covariates.

2.4   RESULTS

2.4.1   Ion efflux and water influx during sloughing

The average rate of change in conductivity in the bathing water, representing ion efflux rate from toads, increased 160 times ($t_{48} = 27.7$, $P < 0.0001$; **Fig. 2.2A**) from 0.5 ± 0.1 $\mu S\,h^{-1}$ in intermoult animals to 90 ± 6.9 $\mu S\,h^{-1}$ during sloughing. An increase in conductivity was also recorded just prior to sloughing (11.5 ± 1.0 $\mu S\,h^{-1}$; $t_{48} = 3.2$, $P = 0.002$). The rate of efflux of ions returned to baseline levels rapidly (within 30 s, **Fig. 2.2**) after sloughing ($t_{48} = 0.67$, $P = 0.5$). The majority of the ions lost by the toads were sodium and chloride. The estimated net loss of Na^+ during the hour incorporating the sloughing event would represented $\sim 3.3 \pm 0.5$ % of the animal's total ECF Na^+ pool.

There was no significant difference in the net change in mass between those that sloughed (0.2 ± 0.3 % h^{-1}) and the intermoult group (-0.4 ± 0.6 % h^{-1}) during the conductivity measurements ($t_{22} = -0.01$, $P = 0.99$; **Fig. 2.2B**), and the duration of sloughing also had no effect on the change in M_b between treatments ($t_{30} = 1.16$, $P = 0.25$).
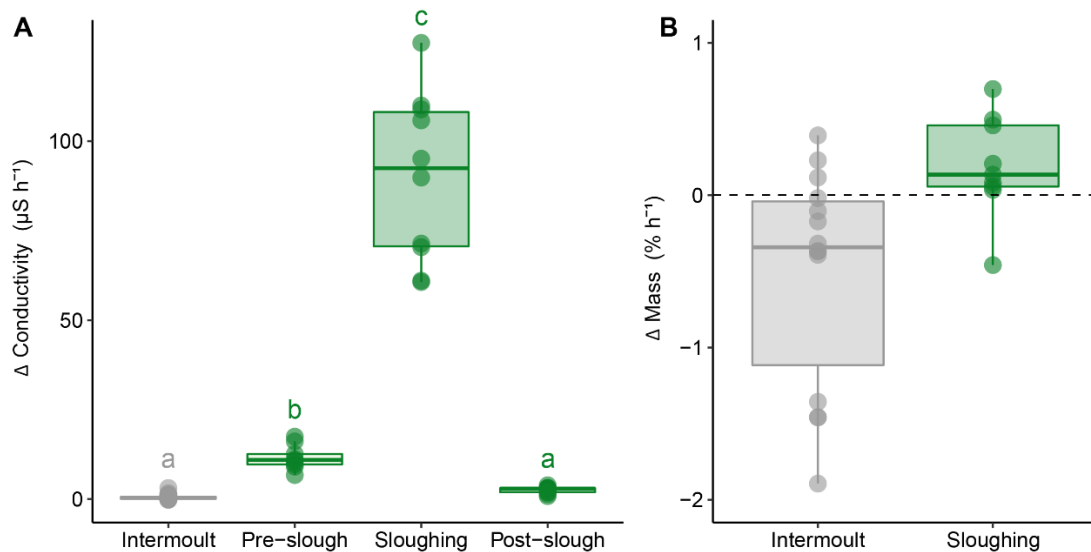
Fig. 2.2 │ **The rate of conductivity and M_b of *R. marina* during sloughing. A**) Rate of change in conductivity ($\mu S\,h^{-1}$) between intermoult, pre-sloughing, sloughing, and post-sloughing group. **B**) Change in M_b (% h^{-1}) in the conductivity experiment between intermoult and sloughing group. Data presented as individual data points for intermoult animals (●), and animals for the day of sloughing (●). Semi-transparent boxplots represent standard distribution of data, $n = 9$ for all groups, and lower-case letters represents significant differences between and groups ($P < 0.05$).

2.4.2 Electrophysiological properties of the skin

There was no significant difference in the transepithelial potential (mV) and resistance (Ω cm^{-2}) between the intermoult and post-sloughing groups when the toad skin was perfused with Ringer solution on both sides (**Table 2.1**). However, the post-sloughing group showed a significant increase in the I_{SC} (15.4 $\pm$ 2.7 µA cm^{-2}), compared to the intermoult group (8.0 $\pm$ 0.9 µA cm^{-2}; **Table 2.1**). This represents a rate of active Na$^+$ transport (influx) of $1.6 \times 10^{-10} \pm 3.2 \times 10^{-11}$ mol s^{-1} after sloughing.

When the skin was perfused with freshwater on the apical side of the chamber the transepithelial potential did not differ significantly between the intermoult and post-sloughing group (**Table 2.1**); however, there was a significant decrease in transepithelial resistance in the post-sloughing group compared to the intermoult group (**Table 2.1**).

2.4.3 Blood plasma biochemistry

H_{CT}, plasma osmolality, and sodium, chloride, and potassium concentrations were not significantly different between the intermoult and post-sloughing animals (**Table 2.2**).

Table 2.1 │ **Electrophysiological properties of cane toad (*Rhinella marina*) epidermis between the intermoult and post-sloughing group**. Apical freshwater treatment represents the apical side of the epidermis containing 26 mmol NaCl in distilled water. *n* = sample size, s.e. = standard error, and ANCOVA = data sets tested with one-way analysis of covariance.

		Epidermal Electrophysiological Parameters			
		Intermoult		**Post-sloughing**	
	n	**Mean ± s.e.**	***n***	**Mean ± s.e.**	**ANCOVA**
Transepithelial potential (mV)	8	-5.5 ± 0.6	8	-3.9 ± 0.7	$F_{1,13} = 1.9, P = 0.2$
Resistance (Ω cm^{-2})	8	3029 ± 433	6	2678 ±726	$F_{1,11} = 0.15, P = 0.7$
Short-circuit current (µA cm^{-2})	8	8 ± 0.9	8	15.4 ± 2.7	$F_{1,13} = 6.2, P = \mathbf{0.03}$
Sodium flux (mol s^{-1})	8	$8.3 \times 10^{-11} \pm 9.5 \times 10^{-12}$	8	$1.6 \times 10^{-10} \pm 3.2 \times 10^{-11}$	"
		Apical Freshwater Treatment			
Transepithelial potential (mV)	6	-13.2 ± 2.4	8	-19.6 ± 2	$F_{1,11} = 3.4, P = 0.09$
Resistance (Ω cm^{-2})	8	12 219 ± 1771	6	6349 ± 1955	$F_{1,11} = 5.4, P = \mathbf{0.04}$

Table 2.2 │ Comparison of cane toad (*Rhinella marina*) blood plasma biochemistry between the intermoult and post-sloughing group. *n* = sample size, s.e. = standard error, and ANCOVA = data sets tested with one-way analysis of covariance.

		Blood Biochemical Parameters			
		Intermoult		Post-sloughing	
	n	Mean ± s.e.	*n*	Mean ± s.e.	ANCOVA
Haematocrit (%)	14	19.8 ± 1.6	10	23.5 ± 3.7	$F_{1,21} = 0.9$, $P = 0.34$
Sodium (mmol l^{-1})	11	116 ± 3.3	10	113 ± 2.6	$F_{1,18} = 0.6$, $P = 0.45$
Chloride (mmol l^{-1})	10	92 ± 6.3	9	80 ± 4.8	$F_{1,16} = 1.8$, $P = 0.2$
Potassium (mmol l^{-1})	11	3.3 ± 0.1	10	3.4 ± 0.1	$F_{1,18} = 0.5$, $P = 0.47$
Osmolality (mosmol l^{-1})	11	236 ± 6.2	10	241 ± 8.4	$F_{1,18} = 0.2$, $P = 0.65$

2.4.4 Skin thickness

There were no significant differences in skin thickness between the intermoult and post sloughing groups ($t_8 = -0.99$, $P = 0.34$; **Fig. 2.3**). No morphological differences were observed between the groups.
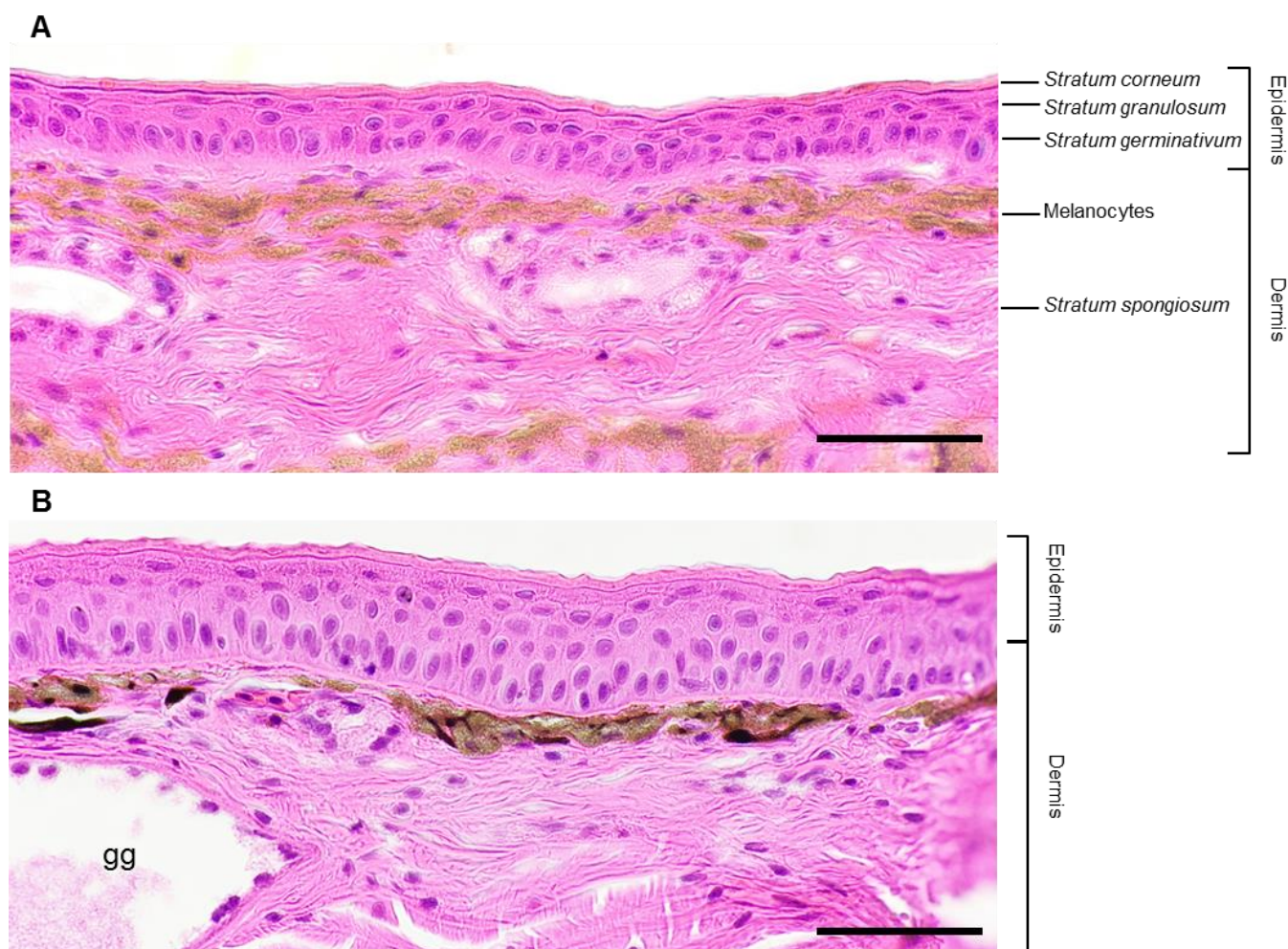
Fig. 2.3 │ Difference in the thickness of the epidermis between intermoult and post-sloughing *R. marina*. Transverse section (6 μm) of haematoxylin and eosin (H&E)-stained ventral skin. Average epidermal thickness of **A)** 27±5.83 μm

from an intermoult toad (SVL 106 mm), and **B**) 39.2±5.83 μm from a post-sloughing toad (SVL 107 mm). gg, granular gland. Scale bar: 50 μm. EXIF data: *f*2.2, ISO-32, exposure time 1/50 s.

2.4.5 ENaC α-subunit and NKA α-subunit protein distribution, abundance, and gene expression

The NKA α-subunit was mostly distributed in the epidermis, with little or no immunofluorescence staining in the dermis layer (**Fig. 2.4**). The submucosal glands within the skin also showed strong NKA α-subunit immunofluorescence in both intermoult and post-sloughing animals. Within the epidermal layer, the NKA α-subunit was concentrated around the basolateral membranes in the principal cell layer (excluding the *s. corneum*). NKA α-subunit distribution in the epidermis of all intermoult animals remained relatively uniform (**Fig. 2.4A**). In the post-sloughing group, however, NKA α-subunit distribution within the epidermis was less well defined. In some animals, NKA α-subunit distribution was concentrated in the most superficial layers of the epidermis, while in other animals the NKA α-subunit appeared to be restricted to cells in the basal layers of the epidermis (**Fig. 2.4B**).
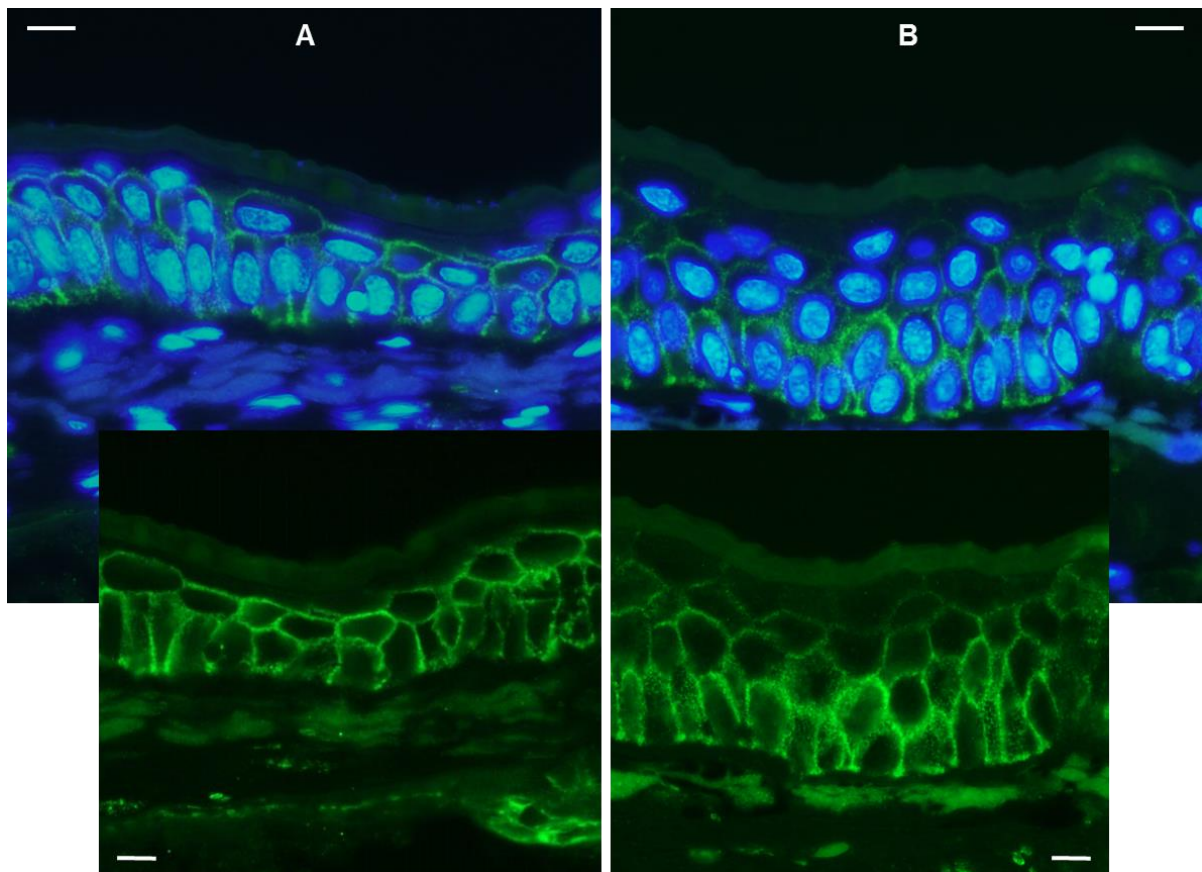
Fig. 2.4 │ Differences in Na⁺/K⁺-ATPase (NKA) distribution between intermoult and post-sloughing *R. marina*. Immunofluorescence staining of NKA α-subunit (green) in transverse sections (6 μm) of ventral skin. **A**) Bottom image: NKA distribution within the epidermis of an intermoult animal (SVL 106 mm) remains uniform throughout the epidermis. **B**) Bottom image: NKA distribution is concentrated in the basolateral area of the epidermis in a post-sloughing animal (SVL 107 mm). Cellular nuclear DNA was counterstained with DAPI (blue, top). Scale bar = 10 μm.

Semi-quantitative Western blotting for the NKA α-subunit (α5 antibody) identified a single band of approximately 100 kDa from membrane-enriched skin cell homogenates. NKA α-subunit abundance was significantly higher ($F_{1,12} = 9.5$, $P = 0.009$) in the post-sloughing group relative to

the intermoult group (**Fig. 2.5A**). The ENaC α-subunit antibody identified a single band of approximately 75 kDa. The relative ENaC α-subunit abundance was also significantly greater ($F_{1,12}$ = 8.8, P = 0.01) in the post-sloughing group compared to the intermoult group (**Fig. 2.5A**), with up to a 2.5-fold increase in abundance occurring in some animals (mean = 1.62 ± 0.16).

The relative expression of NKA (ATP1A1) and ENaC (SCNN1A) mRNA transcripts in the epidermis was not significantly different between the intermoult and post-sloughing group (Pfaffl ratio: 1.137, $F_{1,5}$ = 0.06, P = 0.8, and Pfaffl ratio: 2.14, $F_{1,5}$ = 2.5, P = 0.1 respectively; **Fig. 2.5B**).
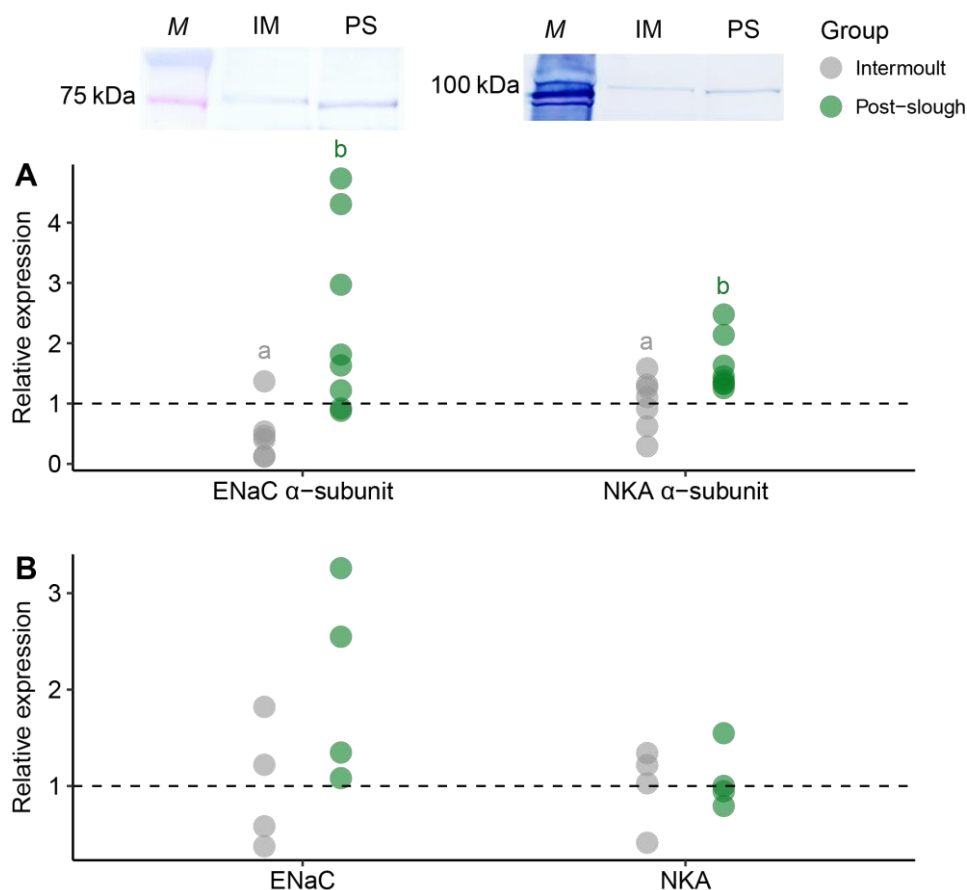
Fig. 2.5 │ Relative abundance and mRNA expression of epithelial sodium channel (ENaC) α-subunit and NKA α-subunit in ventral epidermal tissues of intermoult and post-sloughing *R. marina*. A) Relative abundance dataset with individual data points are presented as the mean of three technical replicates of ENaC α-subunit (intermoult *n* = 7, post-sloughing *n* = 8) and NKA α-subunit (intermoult *n* = 7, post-sloughing *n* = 8). Representative western blots associated with each transport protein (top) show the molecular mass (*M*), an intermoult animal (IM) and a post-slough animal (PS). **B**) Relative mRNA expression dataset with absolute gene expression (ΔCT) normalised to expression of the housekeeping gene GAPDH. Individual data points are presented as the mean of three technical replicates for each ion transporter (*n* = 4). Lower-case letters represents significant differences between and groups (*P* <0.05).

2.5 DISCUSSION

Amphibian skin is a complex multifunctional organ, with the ability to actively regulate the transcutaneous movement of ions and water necessary for maintaining physiological homeostasis (Feder and Burggren, 1992). Understanding the impact of sloughing on skin function is important to comprehend how amphibians maintain homeostatic balance in the face of frequent and significant perturbations. The present study demonstrates that during sloughing, amphibians in

freshwater environments are able to compensate for an increase in the rate of transcutaneous sodium loss by increasing the abundance of sodium transporters in the skin, which in turn allows amphibians to maintain their internal electrolyte homeostasis. These findings suggest that although sloughing causes an acute change in skin osmotic function, the effects are relatively transient and are offset by compensatory pathways. How sloughing may impact species with more frequent sloughing regimens or those with disease-related sloughing dysfunction, however, remains to be determined.

Sloughing-associated skin disturbances began ahead of the physical act of sloughing; indeed, there was a 10-fold increase in the rate of ion efflux in live toads prior to the initiation of sloughing. This finding is consistent with previous studies showing that also show changes in the electrophysiological properties of amphibian skin often precede the physical sloughing event. Specifically, a decrease in I_{SC} has been observed during the initiation of sloughing (*in vitro*) in *Bufo bufo* (Larsen, 1970, 1971a, b). In isolated amphibian skin, I_{SC} is predominately linked to active sodium uptake (Koefoed-Johnson and Ussing, 1958). A reduction in I_{SC} across the skin during sloughing therefore probably reflects a reduction in active transcutaneous sodium movement. The mechanistic basis for this pre-sloughing change in ion transport remains unclear; however, preparatory shifts in cellular differentiation within the epidermis have been hypothesised to contribute to the observed changes in electrical readings in pre-sloughing amphibians (Larsen, 1971b). Potentially, cellular apoptosis in the *s. granulosum* as a consequence of its transition to the *s. corneum* (Elias and Shapiro, 1957) may degrade the ion regulatory transporters responsible for maintaining the potential difference across the skin. This reduction in transporter abundance or activity would lower active sodium uptake rates and contribute to the net increase in sodium loss across the skin. Coincidentally, an increase in cutaneous granular secretions to form the mucus layer during sloughing may also contribute to ion loss (Larsen and Ramløv, 2013).

Although some physiological changes preceded sloughing, by far the greatest disruption to skin function in *R. marina* occurred during sloughing itself. Sloughing substantially increased the rate of cutaneous ion efflux in *R. marina,* indicating that skin function (specifically active ion transport) was temporarily disrupted during sloughing. In addition, contributing to this net increase in Na^+ efflux, the electrical resistance across the skin was significantly lower in post-sloughed toads, indicating that paracellular resistance to passive ion movements was substantially lower across newly sloughed skin. This reduction in cutaneous resistance following sloughing may be attributed to incompletely formed tight junctions in the new *s. granulosum* layer (Budtz and Larsen, 1975) that permits the passive paracellular movement of ions out of the animal along their concentration gradient (Larsen, 1970, 1971b, 1972). In *Bufo bufo*, the reduction in skin resistance can be observed a few hours before the initiation of sloughing (Larsen, 1970, 1971b), suggesting the process of

epidermal renewal and formation of the new *s. corneum* increases the skin's permeability before sloughing (Budtz and Larsen, 1975).

Despite the increased loss of Na^{+} preceding and during sloughing, toads were able to maintain osmoregulatory homeostasis with no changes in plasma solute concentration or osmolality detected post-sloughing. This indicates that either the transient nature of the sloughing-induced changes are not substantial enough to disrupt whole-animal ionic homeostasis or that active mechanisms are employed during or shortly after sloughing to counteract or compensate for ionic and osmotic fluxes. Jørgensen (1949), using *in vitro* measures of NaCl loss, estimated that the overall amount of Na^{+} lost during a sloughing cycle probably reflects a relatively small component of a healthy, normal animal's extracellular sodium pool, consistent with the small net sodium loss measured in this study. Compensatory changes to ion transport may include a change in the activity or abundance or ion transporters in the skin that allow sodium to be actively taken up across the skin from the environment. Consistent with this hypothesis, we observed a 2-fold increase in the I_{SC} across the skin of recently sloughed *R. marina*, suggestive of an increase in active sodium transport. Moreover, we observed a greater abundance of cutaneous ion transporter proteins (NKA α-subunit and ENaC α-subunit) in recently sloughed toads, suggesting that the increase in active sodium transport may, at least in part, be ascribed to an increase in the number of functional sodium transport proteins in the skin. However, the I_{SC} (the probability in number of opened channels of a transporter) alone cannot determine the functional activity of ENaC, as the open probability is highly variable depending on external factors (Anantharam et al., 2006; Kleyman et al., 2009), thus measuring amiloride-sensitive I_{SC} can quantify the functional activity of ENaC (Sariban-Sohraby and Benos, 1986). In addition, an increase in subunit abundance does not always indicate an increase in functional activity of the whole protein (Sardella and Kültz, 2009; Reilly et al., 2011). For example, the ENaC subunits (α, β and γ-subunits) alone cannot induce amiloride-sensitive currents (Canessa, Cecilia M et al., 1994), and in bullfrog (*Rana catesbeiana*) tadpoles, ENaC is expressed in the skin but not in a functional state (no amiloride-blockable Na^{+} transport present) until metamorphosis (Takada et al., 2006).

Combined with the increase in I_{SC}, indicating an increase in active ion transport, *R. marina* appears to increase NKA and ENaC protein abundance to compensate for Na^{+} losses incurred during sloughing. The changes in I_{SC} with spontaneous sloughing are also consistent in magnitude with those observed in toads following aldosterone-induced sloughing events (Nielsen, 1969; Larsen, 1971a; Denèfle et al., 1983), suggesting that the suite of physiological changes that accompany sloughing in amphibians is preserved regardless of whether the sloughing event is initiated naturally or via exogenous hormonal stimulation.

While the sloughing-induced disruption to skin ionoregulatory function in *R. marina* was relatively brief, amphibians display a wide range of sloughing frequencies (Ohmer et al., 2019) and the net impact of sloughing on physiological homeostasis may be greater in species that slough more frequently. For example, toads in this study sloughed about every 12 days, but some species of amphibians slough as often as every 24 h (Bouwer et al., 1953; Castanho and de Luca, 2001; Ohmer et al., 2019). In these frequently sloughing species, disruptions to ion and water exchanges during sloughing are likely to require a greater energetic investment to maintain ionic and osmotic homeostasis, which cumulatively may represent a significant cost to the animal. In addition, exogenous factors, both biotic and abiotic, that alter sloughing frequency may increase or decrease the overall impact of sloughing on physiological homeostasis. For example, increased sloughing frequency has been observed in amphibians suffering from the devastating disease, chytridiomycosis (Ohmer et al., 2015). Chytridiomycosis, a novel and often fatal cutaneous disease of amphibians caused by the fungus *Batrachochytrium dendrobatidis* (*Bd*), appears to disrupt electrolyte transport across the skin of infected frogs (Voyles et al., 2007; Voyles et al., 2012a). Green tree frogs (*Litoria caerulea*), infected with *Bd* slough as much as 25 % more frequently than uninfected frogs (Ohmer et al., 2015) and many other amphibian species are reported to slough more frequently when infected with *Bd*, though the evidence for this is largely anecdotal (Berger et al., 1998; Davidson et al., 2003; Meyer et al., 2012). While an increased sloughing rate may assist with removing pathogens from the skin of infected animals (Meyer et al., 2012; Cramp et al., 2014) sloughing also causes a temporary disruption of ionic and osmotic movements, which, if sloughing frequency is increased, may contribute to the fatal loss of internal ionic homeostasis in clinically infected frogs (Voyles et al., 2009). Thus, future studies that integrate the physiology of sloughing with *Bd* infection are required to more fully understand the mechanistic basis for the morbidity associated with cutaneous *Bd* infection.

2.6 SUPPLEMENTARY INFORMATION

2.6.1 S2.1 Intermoult interval in cane toads

The sloughing behaviour in toads resembled that described for other anurans (e.g. Larsen, 1976; Castanho and de Luca, 2001), on average lasting 16.6 ± 4.3 min. The intermoult interval (IMI) of *R. marina* was highly variable within and among individuals and ranged from 5 to 16 days. Mean IMI for *R. marina* was 10.5 ± 1.8 days ($n = 24$) at a constant 25°C, similar that reported by Meyer et al. (2012) for toads kept in a fluctuating temperature range of 20–30°C (mean = 25°C). Toads from this study, did not have a preference for sloughing either day or night, where on average toads tend to slough more at night (53.2 %) compared to during the day (46.7 %). These results were consistent with Triana et al. (2013) for adult *R. marina*. However, Triana et al. (2013) observed juveniles (SVL < 19 mm) mostly sloughed at night. The IMI of *R. marina* in the current study was borderline affected by body size ($t_{19} = -2$, $P = 0.051$) in *R. marina*. Taylor and Ewer (1956) found no correlation between IMI and the mass of *Amietophrynus regularis* (prev. *Bufo regularis*), and there was no difference between IMI and the sex of animals.

2.6.2 Supplementary figures
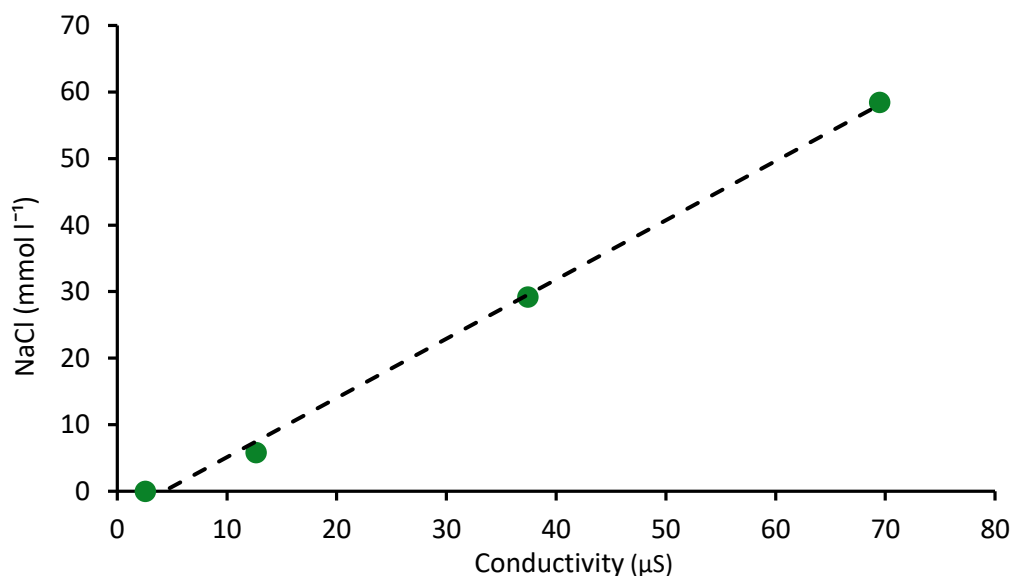
Fig. S2.1 │ Relationship between conductivity readings (G, μS) and known NaCl (c_i, mmol l⁻¹) concentrations show a predicable linear relationship (c_i = 0.015 x G - 0.064, r^2 = 0.99). The reverse osmosis (RO) only solution and solutions where the animal was in the intermoult phase did not have any detectable sodium or potassium.

Epidermal epidemic: unravelling the pathogenesis of chytridiomycosis

3.1 ABSTRACT

Chytridiomycosis, a fungal skin disease of amphibians, fatally disrupts ionic homeostasis. Infected amphibians increase their skin shedding rate (sloughing) to slow pathogen growth, but the process also increases skin permeability. Healthy amphibians increase active ion uptake during sloughing by increasing ion transporter abundance to offset the increased skin permeability. How chytridiomycosis affects skin function during and between sloughing events remains unknown. Here we show that non-sloughing frogs with chytridiomycosis have impaired cutaneous sodium uptake, in part because they have fewer sodium transporters in their skin. Interestingly, sloughing was associated with a transient increase in sodium transporter activity and abundance, suggesting that the newly exposed skin layer is initially fully functional until the skin is recolonised by the fungus. However, the temporary restoration of skin function during sloughing does not restore ionic homeostasis, and the underlying loss of ion uptake capacity is ultimately detrimental for amphibians with chytridiomycosis.

3.2 INTRODUCTION

Amphibians are the most threatened class of vertebrates, with approximately 30 % globally classified as threatened with extinction (IUCN, 2017). Although anthropogenic disturbances are the main cause of amphibian declines (Stuart et al., 2004), roughly 27 % of these declines have occurred in pristine habitats such as protected national parks (Pimm et al., 2014). Many of these non-anthropogenic declines have been attributed to a cutaneous pathogen, *Batrachochytrium dendrobatidis* (*Bd*) which infects the keratinised layers of amphibian skin and can cause the novel disease, chytridiomycosis (Berger et al., 1998; Pessier et al., 1999). Amphibian skin is unique amongst tetrapods given its high permeability, which allows it to serve a variety of physiological roles such as cutaneous gas exchange and osmotic and ionic regulation, but also renders amphibians more susceptible to evaporative water loss (Boutilier et al., 1992). Given the importance of physiological regulation via the skin, cutaneous disruption tends to have serious consequences for amphibian health (Pessier, 2002).

Amphibians with chytridiomycosis display altered behaviour (lethargy, lack of appetite) and suffer physical damage to the skin (cutaneous erythema, hyperkeratosis), leading to the loss of physiological homeostasis (low electrolyte levels) (Berger et al., 2005a; Voyles et al., 2012a; Peterson et al., 2013). In healthy frogs, electrolytes are exchanged through paracellular spaces or transcellularly via ion transport proteins (channels, co-transporters, exchangers, ATPase) in cutaneous epithelial cells (Hillyard et al., 2008). In frogs with chytridiomycosis, low levels of circulating electrolytes (hyponatremia and hypochloremia) correlate with a loss of cutaneous ion uptake capacity (Voyles et al., 2009). *Bd* produces a complex mixture of proteins (proteases, biofilm-associated proteins and a carotenoid ester lipase) that can disrupt epidermal intercellular

junctions (Brutyn et al., 2012) and suppress genes related to the production of keratin and collagen (Rosenblum et al., 2012). In addition to its effects on skin integrity, Campbell et al. (2012) suggested that cutaneous Bd infections may directly inhibit the epithelial sodium channels (ENaC) primarily responsible for the cutaneous uptake of Na^+ from the environment (Schild, 2010). This hypothesis was based on their observation that the amiloride-sensitive short-circuit current of the skin of infected frogs was lower than that of healthy frogs (Voyles et al., 2009). Amiloride is a non-specific Na^+-channel inhibitor (Kleyman and Cragoe, 1988). Dysfunction of ENaC transport is often associated with disorders of Na^+ and fluid homeostasis, and blood pressure (Schild, 2004). How Bd influences cutaneous ion uptake pathways, specifically those relating to Na^+ movement, including ENaC and Na^+/K^+-ATPase (NKA), which is responsible for creating electrochemical gradients in the epidermis (Lingrel and Kuntzweiler, 1994), remains unknown.

Given the vital role of the skin in sustaining amphibian homeostasis, maintaining skin integrity and function is of considerable importance. To this end, the outer keratinised layer is periodically removed and replaced through a process known as 'sloughing'. Sloughing also plays an important role in regulating cutaneous microbe abundances (Meyer et al., 2012; Cramp et al., 2014), and in frogs infected with Bd, sloughing helps remove Bd from the keratinised layer (Ohmer et al., 2017). Indeed, Ohmer et al. (2017) found that sloughing reduced Bd load in five anuran species, with less susceptible species eventually clearing infection. However, susceptible species continued to develop chytridiomycosis despite an increase in sloughing frequency, and in face of a temporary reduction in Bd load after sloughing (Ohmer et al., 2015). An increase in sloughing frequency might act as an immune response to remove the pathogen before the onset of disease (Ohmer et al., 2017). Importantly though, increased sloughing frequency may be a double-edged sword, as sloughing itself causes transient osmoregulatory disruption in amphibians (Jørgensen, 1949; Wu et al., 2017). We have shown that in healthy amphibians, sloughing is accompanied by an increase in cutaneous permeability (Wu et al., 2017). However, an increase in the expression and activity of epithelial Na^+ channels offsets the temporary increase in skin permeability such that animals suffer no loss of physiological homeostasis (Wu et al., 2017). Given that animals slough more frequently, the cumulative impact of sloughing and increased ion loss during non-sloughing periods leads to the loss of physiological homeostasis. Although it is clear that Bd affects cutaneous ion transport processes in infected frogs, the mechanistic basis for the disruption of ion transport, and the effects of sloughing on this, remains unclear.

Understanding how the disruption of skin function leads to the loss of physiological homeostasis in frogs with chytridiomycosis, and whether sloughing worsens cutaneous regulation, is important from a management standpoint. A greater understanding of the mechanistic basis for loss of homeostasis in infected frogs could lead to better treatment options, particularly for critically

endangered species and captive insurance populations. Thus, the aim of this study was to investigate the effects of *Bd* on cutaneous ion transport processes, focusing on the abundance, activity, and expression of ENaC and NKA in a susceptible species, the Australian green tree frog (*Litoria caerulea*). We hypothesised that both increased skin permeability and the reduction or inhibition of regulatory ion transporters resulting from *Bd* infection would contribute to the disruption of cutaneous ion flow, and sloughing would further exacerbate electrolyte permeability in infected frogs. The resulting disruption of both chytridiomycosis and sloughing could prolong electrolyte imbalance, causing conditions of low ion concentrations in the blood plasma such as hyponatremia.

3.3   MATERIALS AND METHODS

3.3.1   Animal collection and maintenance

Litoria caerulea spawn was collected from Bribie Island, southeast Queensland, Australia in March 2015, and raised in the laboratory until metamorphosis. The resulting 19 juveniles (10–20 g) were used for experimentation. An additional 17 *L. caerulea* (15-70 g) adults and subadults were collected from wet roads in non-protected areas near Fernvale, southeast Queensland, Australia in January 2015. Frogs were housed individually in either small (235 x 170 x 120 mm) or large (265 x 235 x 12 mm) ventilated clear plastic containers, with paper towels saturated with chemically aged water (dilution 1:4000; VitaPet, NSW, Australia) as substrate, and a half PVC pipe for shelter. The lighting conditions were set at a 12 h:12 h light-dark photoperiod cycle, and temperature was set at a constant $20.5 \pm 0.5°C$. Frogs were checked daily, fed once a week on vitamin-dusted crickets (*Acheta domesticus*), and enclosures were cleaned weekly. Prior to experiments, all frogs were swabbed to confirm the absence of *Bd* infection given its widespread distribution in natural *L. caerulea* populations (Berger et al., 1998). A quantitative polymerase chain reaction (qPCR; details below) assay was used to measure *Bd* loads following protocols by Ohmer et al. (2015) before experiments began.

3.3.2   Monitoring sloughing frequency

The intermoult interval (IMI; time between two successful sloughing events) was monitored continuously using infrared surveillance cameras (model EN-CI20B-65H, Eonboom Electronics Limited; and HW242C Security Camera, K Guard Security, New Taipei City, Taiwan), and a generic 16 channel H.264 Digital Video Recorder (DVR) system, mounted to a moveable metal frame in front of enclosures, with two cameras per row. Each camera monitored two frog enclosures at one time and at a sample rate of 1.56 frames s^{-1}.

3.3.3   *Bd* culture and experimental exposure

Bd strain EPS4 from Ohmer et al. (2015) was used for experimental infections. Cultures were maintained at 4°C until 4–5 days before exposure. Isolate EPS4 was passaged to sterile 1 % agar,

0.5 % tryptone, 0.5 % tryptone-soy plates and maintained at 20°C. After 4–5 days, zoospores were harvested by flooding plates with aged tap water for 30 min. The zoospore suspension was collected, and the concentration measured using a haemocytometer (Boyle et al., 2004). A randomised subset of frogs ($n = 21$) were exposed to ~500,000 zoospores. Frogs were exposed to *Bd* for 5 h in 300 ml plastic containers containing zoospores suspended in 100 ml aged water. Control animals were exposed to aged water only. After 14 days post-exposure, each frog was swabbed with a sterile fine-tipped cotton swab (MW100-100; Medical Wire & Equipment, Wiltshire, England) three times over the frog's ventral surface, thighs, armpit, forelimb feet, and hindlimb feet (Kriger et al., 2006; Ohmer et al., 2015) to assess infection status. To determine infection load as zoospore equivalents (ZE), swabs were extracted in 50µl PrepMan Ultra (Applied Biosystems, Foster City, CA, USA), and analysed in duplicate with qPCR in a thermal cycler (MiniOpticon™ Real-Time PCR Detection System, Bio-Rad Laboratories, Inc., CA, USA) with a modified 15 µl Taqman reaction following Ohmer et al. (2015). After one month, exposed frogs with no *Bd*-positive swabs was re-exposed with ~500,000 zoospores following the same procedure detailed above. The infection load or number of ZE was calculated from the mean value of each triplicate assay and log + 1 transformed (log(ZE+1)).

3.3.4   Measuring infection load and sampling

All frogs were checked daily for clinical signs of disease progression including a lack of appetite (monitoring food intake), abnormal posture, excessive or irregular sloughing, lethargy, cutaneous erythema and discolouration, and loss of righting reflex (Voyles et al., 2009). Once the IMI was determined for each frog (both uninfected and infected animals), frogs from the uninfected ($n = 8$ intermoult, $n = 8$ sloughing), and infected ($n = 11$ intermoult, $n = 7$ sloughing) groups were anaesthetised with an intracoelomic injection of 60 mg kg^{-1} body mass thiopentone sodium (Thiobarb Powder, Jurox Pty Limited, NSW, Australia), and then euthanased via double pithing. Animals were euthanased at one of two time points: 1) sloughing (no more than 1 h after sloughing had occurred), or 2) intermoult (at a point halfway through the IMI). Snout-vent length (SVL; mm) and body mass (g) were measured immediately. A final skin swab was also taken to determine *Bd* infection load. Prevalence of infection with *Bd* was high: in the first set of exposures resulted in 60.8 % of exposed frogs developed an infection, and after re-exposure 73.9 % of originally exposed frogs had developed an infection. The three frogs that did not develop infection after re-exposure were excluded from the analysis.

3.3.5   Blood plasma electrolytes

Whole blood was collected from euthanased animals via cardiac puncture into a lithium heparinised syringe. Samples were then centrifuged at 5000 g for 5 min and the plasma collected and stored at -20°C for subsequent electrolyte analysis. Plasma Na$^+$ and K$^+$ levels (mmol l^{-1}) were measured

using flame photometry (BWB, Berkshire, UK), and plasma Cl⁻ levels (mmol l⁻¹) were determined spectrophotometrically (DTX 880 Multimode Detector; Beckman Coulter, IN, USA) with a chloride kit (MAK023; Sigma-AldrIon).

3.3.6   Electrophysiology of the ventral skin

Following collection of blood samples, isolated ventral skin samples (<1 cm²) were collected from the lower abdominal pelvic patch region and mounted in a self-contained, single channel Ussing chamber apparatus (Model U-9926; Warner Instruments, Hamden, CT, USA) with a single channel epithelial voltage clamp amplifier (Model EC-800; Warner Instruments), and connected to a PowerLab 4/35 interface (Mod n: PL3504, ADInstruments, NSW, Australia). Apical and basolateral surfaces of the skin were perfused with an oxygenated (95 % O_2 and 5 % CO_2) modified frog Ringer's solution based on Voyles et al. (2009) [in mmol l⁻¹: NaCl (112), KCl (2.5), D-glucose (10), Na_2HPO_4 (2), $CaCl_2$ (1), $MgCl_2$ (1), sodium HEPES salt (5), HEPES (5) at pH 7.3-7.4 with osmolality of 230 $\pm$ 20 mosmol l⁻¹] maintained at 20.5 $\pm$ 0.5°C. Electrophysiological parameters were measured as followed: 1) transepithelial potential (TEP or V_T) under open-circuit conditions (clamp current to 0 µA) and the resulting voltage (mV) in reference to the basolateral side, 2) active ion transport via clamping voltage to 0 mV and the instantaneous short-circuit current (I_{SC}) response as µA cm⁻², and 3) transepithelial resistance per unit area (Ω cm⁻²) by applying 3 s of 1 µA pulses across the epithelium every 60 s, or under voltage clamp conditions by applying 3 s of 1 mV at 60 s intervals (Wu et al., 2017). The inflections from the resulting change in I_{SC} and V_T during pulsing were used to calculate resistance using Ohm's law. Sodium flux (mol s⁻¹) was calculated by dividing the I_{SC} (µA) by Faradays constant (96 000 Coulomb mol ⁻¹). I_{SC} and V_T readings were recorded in LabChart (ADInstruments).

3.3.6.1   *Pharmacological inhibitor experiments*

Amiloride hydrochloride hydrate (Sigma-Aldrich) was applied on the apical side of the chamber to calculate the amiloride-sensitive short circuit current (I_{SC}). Since amiloride is a non-specific Na⁺ channel inhibitor, ENaC is normally inhibited by very low (<1 µmol) concentrations of amiloride, compared with other transporters such as Na⁺/H⁺ exchanger (>100 µmol), Na⁺/Ca²⁺ exchanger (1000 µmol), and NKA (>3000 µmol)(Kleyman and Cragoe, 1988). Amiloride was dissolved in dimethyl sulfoxide (DMSO) and added to the chamber to achieve final concentrations of 0.1, 0.5, 1, 2, 5, 10, 20, and 50 µmol l⁻¹. I_{SC} readings at each concentration were obtained 5 min post-application. The half maximal inhibitory concentration (IC_{50}) of amiloride was calculated for each individual. Preliminary trials with DMSO only (vehicle control) did not significantly affect the overall voltage and current readings. After amiloride treatment, skin preparations were washed out with Ringers solution until readings returned to starting values (or close to it), and 100 µmol l⁻¹

ouabain octahydrate (Sigma-Aldrich) dissolved in distilled H_2O was applied to the basolateral skin side chamber, and measurements were recorded until 15 min post-application of ouabain.

3.3.7 Skin histology

Ventral skin samples ($<1\ cm^2$) from the lower abdominal pelvic patch region were collected and placed into aqueous buffered zinc formalin fixative (Z-fix; Anatech, MI, USA) for 24 h, then transferred to 70 % ethanol, and stored at 4°C. Tissues samples were then dehydrated through an ascending ethanol series, cleared in xylene and embedded in paraffin wax (Histoplast Paraffin; ThermoFisher Scientific, Sydney, Australia). Tissue samples were then transversely sectioned into approximately 6 μm thick sections, (Leica RM2245; Leica Microsystems, NSW, Australia). A sub-sample of sections was stained with Mayer's hematoxylin and 1 % eosin in 70 % ethanol, and photographed with an iPhone 6s (Apple Inc., CA, USA) and NIS-Elements software (v. 4.10, Nikon Instruments Inc., Tokyo, Japan) under a bright-field illumination microscope (Nikon Eclipse E200 MV, Nikon Instruments Inc.).

3.3.8 ENaC and NKA abundance

Ventral skin samples ($<1\ cm^2$) from the lower abdominal pelvic patch region were collected and stored at -80°C. Frozen tissues were then homogenised in RIPA buffer (150nM NaCl, 1 % Triton X-100, 0.5 % sodium deoxycholate, 0.1 % SDS and 50 nM Tris-HCL with general protease inhibitors (Sigma-Aldrich General protease inhibitor cocktail (P2714) with 1 mM PMSF)) using an IKA Ultra-Turrax. The protein content was quantified via a Qubit fluorometer (ThermoFisher Scientific, QLD, Australia). Protein (15 μg) was dissolved in NuPAGE LDS sample buffer (Invitrogen) and denatured at 70°C for 10 min, then loaded in duplicate into Bolt 4-12 % Bis-Tris Plus gels (ThermoFisher Scientific) and electrophoresed at 120 V for 30 min. Gels were subsequently transferred onto 0.45 μm Immobilon PVDF membranes (Merck Millipore, MA, USA) at 20 V for 1 h. Membranes were then blocked in blocking buffer (5 % skim milk in TBST (20 mmol l^{-1} Tris, 150 mmol l^{-1} NaCl, and 1 % Tween-20, pH 7.6)) for 1 h at room temperature before incubation overnight at 4°C with their respective primary antibody (NKA-α5 primary antibody α5 (1:1000 dilution), and ENaC-α primary antibody (1:1000 dilution; Anti-SCNN1A antibody; HPA012939, Sigma-Aldrich)) in blocking buffer. Membranes were then incubated in secondary goat anti-mouse IgG Horseradish Peroxide (HRP)-conjugated antibody (1:2000; C22P20, Antibodies Australia, VIC, Australia) and goat anti-rabbit IgG HRP-conjugated antibody (1:2000; C24P03, Antibodies Australia), respectively for 1 h at room temperature, and stained with 1-Step Ultra TMB-Blotting solution (ThermoFisher Scientific). Wells with no protein were used as negative controls. The membranes (in duplicates) were dried and digitised for densitometry analysis via Image J (https://imagej.nih.gov/ij/). The pixel densities were used to estimate protein abundance in the ventral skin and were expressed relative to uninfected intermoult group.

3.3.9 ENaC and NKA mRNA expression

3.3.9.1 RNA extraction and cDNA synthesis

Ventral skin samples ($<$1 cm^2) from the lower abdominal pelvic patch region were collected, and stored in RNA-later (Ambion Inc., TX, USA) at -20°C. The skin samples were then homogenised with stainless steel beads using a TissueLyser II (Qiagen). Total RNA was isolated (RNeasy Mini kit; Qiagen, Hilden, Germany), and the resulting RNA yield was measured using a Qubit fluorometer (ThermoFisher Scientific). Genomic DNA contamination in RNA samples was removed, then the RNA was then reversed transcribed into cDNA, with appropriate no reverse transcriptase controls (QuantiTech Reverse Transcription Kit; Qiagen).

3.3.9.2 Primer design and quantification of mRNA by qPCR

Transcripts for each gene of interest were located in an in-house *L. caerulea* larval and adult tissue transcriptome using homologous sequences from other amphibians as the reference query. Reference sequences were blasted against the transcriptome using the 'blastn' tool in Galaxy/GVL 4.0.1 (Afgan et al., 2016). Putative *L. caerulea* sequences were then compared against the entire National Centre for Biotechnology Information (NCBI) database (http://www.ncbi.nlm.nih.gov/) using 'blastn' with acceptance of the default parameters. qPCR primers against the target genes (**Table S3.6**) were designed using OligoPerfect™ Designer (Thermofisher Scientific) with acceptance of the default parameters. qPCR was performed using Power SYBR Green PCR Master Mix (ThermoFisher Scientific) using recommended cycling parameters. Each assay (in triplicate) included a no-template control and a no reverse transcriptase control. All PCR efficiencies were $>$90 % and all the assays produced unique dissociation curves. Bio-Rad CXF Manager software (version 3.1, Bio-Rad) results were exported and each gene was quantified relative to the expression of the housekeeping gene, β-actin. Changes in expression levels were presented as fold-change relative to the uninfected intermoult group.

3.3.10 Statistical analysis

All analyses were performed in R.3.4.1 (R Core Team, 2018). Data are either presented as means $\pm$ standard error (s.e.), or individual data points depending on the nature of the data (Cumming et al., 2007; Krzywinski and Altman, 2013), and α was set at 0.05 for all statistical tests. Data that were not normally distributed were log-transformed prior to analysis. Percentage data were logit transformed prior to analysis. All models used a Gaussian error structure, and the confidence intervals for each model are presented in the supplementary tables 3.6.2.

3.3.10.1 Blood plasma levels and electrophysiology

Blood plasma ion measurements (Na$^+$, Cl$^-$, K$^+$) and electrophysiological measurements of the skin [TEP, amiloride-sensitive I_{SC} (50 µmol l^{-1} concentration), skin resistance, and % ouabain inhibition of I_{SC}] between each group were initially analysed using linear models from the R default 'stats'

package, with Bd load as an interactive effect and body mass as an additive effect. To test the effects of body mass and exposure period (exposed once or twice), models with body mass and exposure as additive effects were compared with models with no additive effects. The final model was chosen based on Akaike's information criterion (AIC). To test for interactions between treatments within groups while adjusting for Bd slope, a 'holm'-adjusted F-test was performed (package 'phia', function 'testInteractions')(Rosario-Martinez et al., 2015).

The effect of amiloride dose and Bd load on the I_{SC} between intermoult and sloughing animals was analysed using a quadratic model (package 'nlme', function 'lme')(Pinheiro et al., 2013), with $\log(I_{SC})$ as the dependent variable, log(amiloride concentration) as a fixed effect, Bd load as an interactive effect, and frog ID as a random effect to account for repeated measurements on the same individuals at different dosages. The IC_{50} was calculated for each individual, and the differences between the uninfected and infected individuals for the intermoult and sloughing groups were analysed using a linear model (lm) with Bd load as an interactive effect.

3.3.10.2 ENaC and NKA subunit abundance and expression

Relative abundance of ENaC-α and NKA-α proteins in the ventral skin between each group were analysed using linear models (lm), with Bd load as interactive effect. To test the effects of body mass and exposure period (exposed once or twice), models with body mass, and exposure as additive effects were compared with models with no additive effects. The final model was chosen based on the AIC. To test for factor interactions between treatments within groups and adjusting for Bd slope, a 'holm'-adjusted F-test was performed (package 'phia', function 'testInteractions').

Relative mRNA expression of ENaC subunits (α, β, γ) and NKA subunits (α1, β1, β3) in the ventral skin between each treatment and sloughing group were analysed with the following equation:

$$E^{-C_T} = \beta_0 + \beta_{treatment} + \beta_{gene} + \beta_{group} + \beta_{treatment:gene} + \beta_{treatment:group} + \beta_{group:gene}$$
$$+ \beta_{treatment:gene:group} + b_{ID} + \epsilon$$

where E^{C_T} is the Δ threshold cycle (C_T), β is the fixed effects parameter where 0 is the intercept, b_{ID} is the random intercept for frog ID expressed as $b_{ID} \sim N(o - \delta^2)$, where δ^2 is the variance of random intercept, and ϵ is the Gaussian error term expressed as $\epsilon \sim N(o - \sigma^2)$, where σ^2 is the variance of residual (see supplementary file for lme function in R). The model examines relative C_T values of the target gene normalised to the C_T values of the reference gene β-actin, and the interaction between treatment:group and gene with respect to the reference gene gives the ΔΔ C_T, where uninfected intermoult frogs were set as the control. To test the effects of body mass and exposure period (exposed once or twice), models with body mass, and exposure as additive effects were compared with models with no additive effects. The final model was chosen based on the AIC. To

test for factor interactions between treatments within groups, controlling for gene, a 'holm'-adjusted Chi-square test was performed (package 'phia', function 'testInteractions').

3.4   RESULTS

3.4.1   Gross pathology and histopathology of the ventral skin

The pathology of the skin of infected *L. caerulea* after sloughing was the focus of this aspect of the study since infected intermoult (non-sloughing) animals have been thoroughly detailed in several past studies (Berger et al., 1999b; Pessier et al., 1999; Nichols et al., 2001). In general, heavily infected frogs displayed cutaneous erythema, histological lesions and thinning of the skin, as described previously (**Fig. 3.1B**). However, the skin of recently sloughed animals with low *Bd* zoospore loads (<10,000 ZE) was very similar to that of uninfected animals (**Fig. 3.1C, D**). In heavily infected animals (>10,000 ZE) after sloughing, some *Bd* sporangia were observed attached to the sloughed skin that had been fully removed (**Fig. 3.1G**), however some sporangia also remained within the deeper layers of the epidermis (*stratum granulosum*; **Fig. 3.1E, F**).
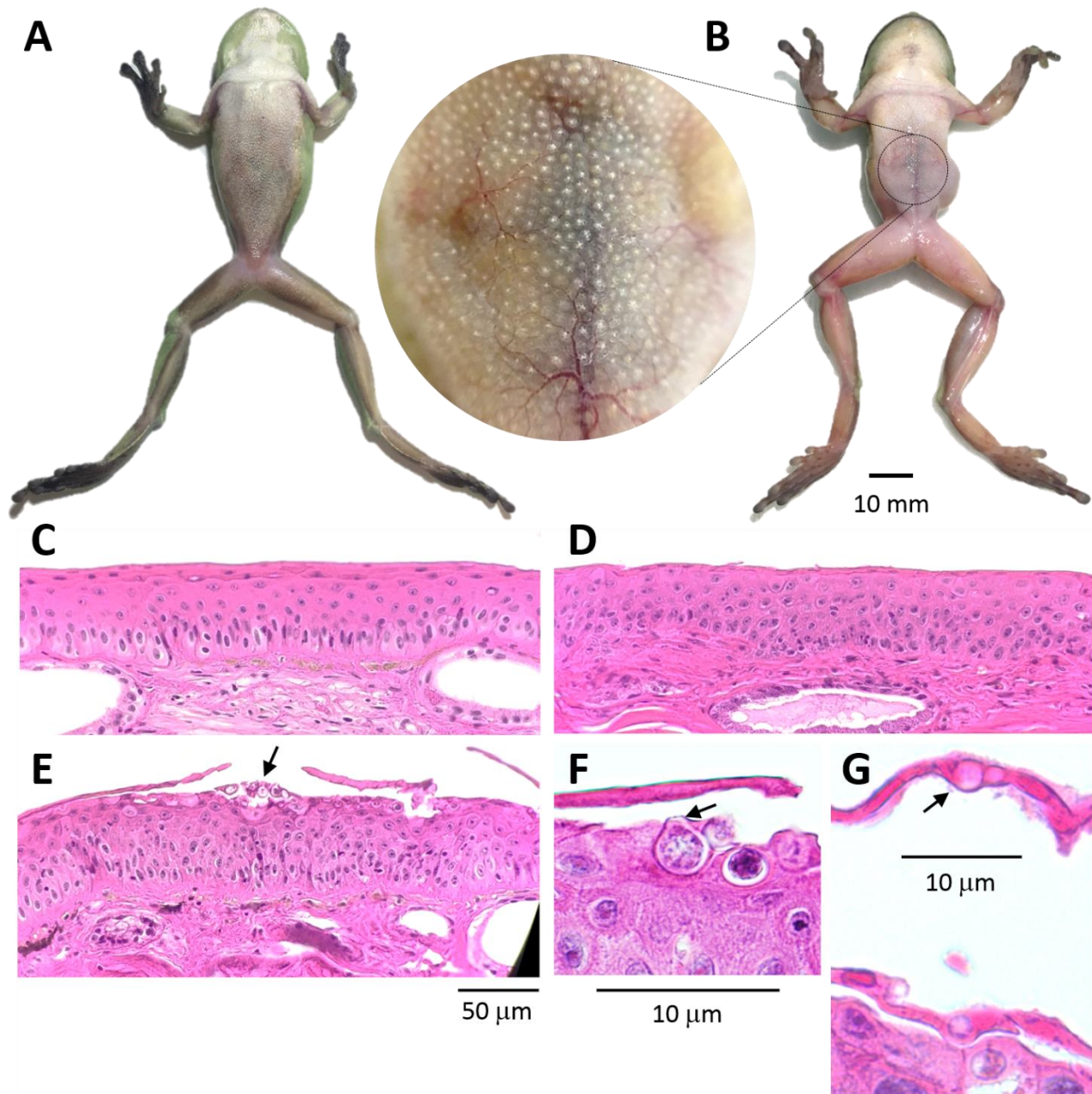
Fig. 3.1 │ Gross pathology and histopathology (transverse haematoxylin and eosin (H&E)-stained section 6µm) of *Litoria caerulea* **ventral skin with chytridiomycosis.** Ventral view of **A**) an uninfected (0 ZE) and **B**) an infected (~44,000 ZE) *L. caerulea* during the intermoult (non-sloughing) period. Infected individuals showed various gross morphological abnormalities such as cutaneous erythema with visible capillary vessels. Transverse section through the ventral skin of **C**) an uninfected (intermoult) animal with no visable abnormalities. **D**) Transverse section through the ventral skin of a lightly infected animal (~1,600 ZE) collected immediately after sloughing occurred. The newly exposed *stratum corneum* was similar to that of uninfected animals, and had no visable abnormalities. **E**) Transverse section through the ventral skin of a heavily infected, sloughing animal (20,000 ZE). *Bd* sproangia below the shed *s. coreneum* (arrow) are clearly visible. (**F-G**) High power views of the ventral skin from two infected sloughing animals showing *Bd* sporangia below and within (arrows) the old *s. corneum*. EXIF data: f/2.2, ISO-80, exposure time 1/33 s, focal length 4mm.

3.4.2 Blood plasma electrolytes

Frogs infected with *Bd* (both during the intermoult and sloughing periods) in general showed a significant decrease in plasma sodium [Na$^+$] and chloride [Cl$^-$] levels with increasing *Bd* load (t_{25} = -5.4, *P*<0.001, and t_{25} = -3, *P* = 0.004, respectively; **Table 3.1**); plasma potassium [K$^+$] did not differ significantly between infected and uninfected animals (t_{25} = -1, *P* = 0.3). Both plasma [Na$^+$] and [Cl$^-$] were lower in intermoult animals with significant *Bd* loads compared to uninfected frogs in the intermoult phase ($F_{1,25}$ = 29, *P*<0.001, and $F_{1,25}$ = 10, *P* = 0.007; Table 1). In sloughing animals, only plasma [Na$^+$] levels remained significantly lower in infected frogs relative to uninfected frogs ($F_{1,25}$ = 11, *P* = 0.003), while [Cl$^-$] levels were not significantly different between infected and uninfected treatments ($F_{1,25}$ = 1.6, *P* = 0.2).

Table 3.1 │ **Blood plasma ion levels of infected and uninfected (control)** *Litoria caerulea* **during the intermoult and sloughing periods.** *n* = sample size, s.e. = standard error. Summary statistics provided in Table. S3.1.

		Blood plasma ion levels						
		Intermoult				Sloughing		
		Uninfected		Infected		Uninfected		Infected
	n	mean ± s.e.	*n*	mean ± s.e.	*n*	mean ± s.e.	*n*	mean ± s.e.
Sodium (mmol l^{-1})	7	147.6 ± 3.9	9	84.5 ± 8	5	145 ± 8.7	4	90.5 ± 5.2
Chloride (mmol l^{-1})	7	57 ± 2.2	9	40 ± 5.3	5	58.9 ± 2	4	53.2 ± 9.6
Potassium (mmol l^{-1})	7	3.4 ± 0.3	9	2.6 ± 0.3	5	2.9 ± 0.4	4	3.3 ± 0.6

3.4.3 Electrophysiology of the ventral skin

The TEP of the ventral skin was significantly affected by an interaction between infection load and sloughing phase (t_{28} = 4.9, *P*<0.001; **Table S3.2**). As infection load increased in intermoult animals, the TEP decreased from –32.5 ± 5.2 mV to –10.8 ± 1.7 mV ($F_{1,28}$ = 16.9, *P*<0.001). However, in sloughing animals, the TEP increased from –8.8 ± 0.85 mV to –21 ± 5.5 mV as infection load increased ($F_{1,28}$ = 8.9, *P* = 0.006; **Fig. 3.2A**).

Similarly, skin resistance decreased with increasing *Bd* load (t_{28} = -2.3, *P* = 0.03; **Fig. 3.2B**; **Table S3.2**). In both infected and uninfected animals, skin resistance was the lowest after sloughing (301 ± 79 Ω cm^{-2}); there was no significant difference in resistance between infected and uninfected animals immediately after sloughing (**Fig. 3.2B**). There was also a borderline significant difference between the intermoult and sloughing animals ($F_{1,28}$ = 5.6, *P* = 0.05) with the sloughing animals showing lower skin resistance (321 ± 51 Ω cm^{-2}) compared with the intermoult animals (478 ± 82 Ω cm^{-2}; **Fig. 3.2B**).

Active sodium transport, represented by amiloride-sensitive instantaneous short-circuit current (Isc), showed a significant interaction between infection load and sloughing phase (**Table S3.2**). For intermoult animals, as infection load increased, the Isc decreased from 59.2 ± 9.8 µA cm^{-2} to 35.6 ± 4.5 µA cm^{-2} ($F_{1,27} = 7.3$, $P = 0.01$). When converted to sodium flux, the rate of sodium transport decreased from $6.1 \times 10^{-4} \pm 1 \times 10^{-4}$ mol s^{-1} in uninfected animals to $3.7 \times 10^{-4} \pm 4.6 \times 10^{-5}$ mol s^{-1} in infected animals. Recently sloughed animals showed the opposite response, with Isc increasing from 28.8 ± 4.2 µA cm^{-2} to 84.7 ± 14.3 µA cm^{-2} as infection load increased ($F_{1,27} = 27$, $P < 0.001$; **Fig. 3.2C**). This represents an increase in the rate of sodium transport during sloughing from $3 \times 10^{-4} \pm 4.4 \times 10^{-4}$ mol s^{-1} in uninfected animals to $8.8 \times 10^{-4} \pm 1.5 \times 10^{-4}$ mol s^{-1} in infected animals. For ouabain inhibition of I_{SC}, there was an overall significant difference between groups, where post-sloughing animals had greater inhibition from 100 µmol l^{-1} ouabain compared with intermoult animals ($t_{15} = 2.3$, $P = 0.04$; **Fig. 3.2D**). Treatments did not have a significant effect on the ISC inhibition (**Table. S3**).

There was a significant decrease in Isc as amiloride dose increased in both intermoult and sloughing groups, which was independent of infection load (**Table S3.3**). In the intermoult group there was a significant interaction between infection load and amiloride concentration ($t_{107} = 2.2$, $P = 0.02$) where at a high dosage the Isc slope decreases to a plateau with increasing infection load (**Fig. 3.2E**). This indicates the isolated ventral skin during the intermoult phase of infected animals was more sensitive to amiloride dosage, requiring 0.7 ± 0.14 µmol l^{-1} of amiloride to inhibit 50 % of the Isc, compared with uninfected frogs (IC$_{50}$ = 2.35 ± 0.6 µmol l^{-1}; $t_{12} = -2.6$, $P = 0.02$). For animals after sloughing, there was a significant effect of Bd infection alone ($t_{11} = 3.5$, $P = 0.004$) with a decrease in Isc as infection load increased. However, no interactions between infection load and amiloride concentration were observed (**Table S3.3**), suggesting no difference in the sensitivity to amiloride in the newly exposed skin between uninfected (IC$_{50}$ = 1.4 ± 0.26 µmol l^{-1}), and infected frogs (IC$_{50}$ = 0.84 ± 0.2 µmol l^{-1}; $t_{12} = -0.7$, $P = 0.5$; **Fig. 3.2F**).
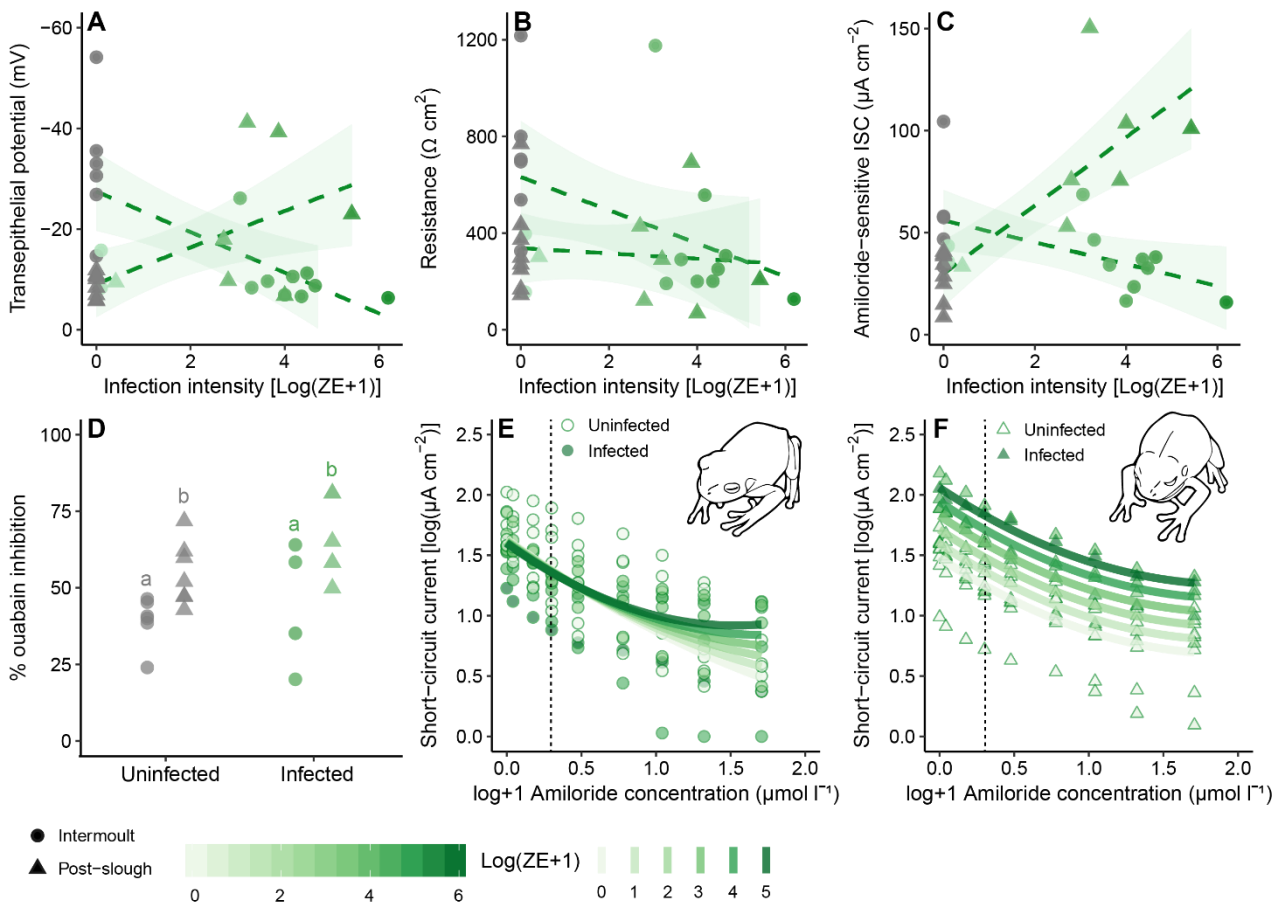
Fig. 3.2 | Electrophysiological parameters of isolated ventral skins of *Litoria caerulea*. A) Transepithelial potential (mV), **B)** transepithelial resistance (Ω cm^{-2}), and **C)** amiloride-sensitive short-circuit current (*Isc* (μA cm^{-2})) of isolated ventral skins, either during the intermoult period (solid line) or after sloughing (dashed line) in relation to infection intensity (Log(ZE+1)). Shaded area around regression lines represents 95 % confidence intervals, and all data are presented (intermoult: uninfected ● n = 6, infected ● n = 11, sloughing: uninfected ▲ n = 9, infected ▲ n = 7). **D)** The percentage inhibition of *Isc* (%) between infected and uninfected animals after application of 100 μmol l^{-1} ouabain. All data points are presented (Intermoult: uninfected ● n = 4, infected ● n = 4, sloughing: uninfected ▲ n = 9, infected ▲ n = 4). Lower-case letters represents significant differences between and groups (P <0.05). *Isc* (μA cm^{-2}) response of isolated ventral skin from **E)** Intermoult and **F)** sloughing *L. caerulea* to different amiloride concentrations (0.1–50 μmol l^{-1}) in the apical reservoir. All data points presented (intermoult:● uninfected n = 5, ● infected n = 10, sloughing:▲ uninfected n = 7, ▲ infected n = 7), and solid lines for each *Bd* load range [0-5 log(ZE+1)] represent model predictions. Summary statistics are provided in Table. S3.2 and S3.3.

3.4.4 ENaC and NKA protein abundance

There was an overall significant decrease in ENaC-α subunit (SCNN1A) protein abundance with increasing infection load (t_{19} = -2.4, P = 0.02; **Table S3.4**), however there were no significant difference in abundance between the intermoult and sloughing groups (t_{19} = -1.2, P = 0.2). Within the intermoult group, as infection load increased, the relative abundance of SCNN1A protein decreased ($F_{1,19}$ = 5.8, P = 0.05; **Fig. 3.3A**). For animals after sloughing, there was a marginally significant decrease in SCNN1A protein abundance as infection load increased ($F_{1,19}$ = 3.8, P = 0.06). The abundance of the NKA-α subunit (ATP1A1) was significantly greater in infected animals after sloughing compared to uninfected animals ($F_{1,20}$ = 9.7, P = 0.01; **Fig. 3.3B**), whereas there was no difference between infected and uninfected animals in the intermoult group ($F_{1,20}$ = 0.34, P = 0.56).
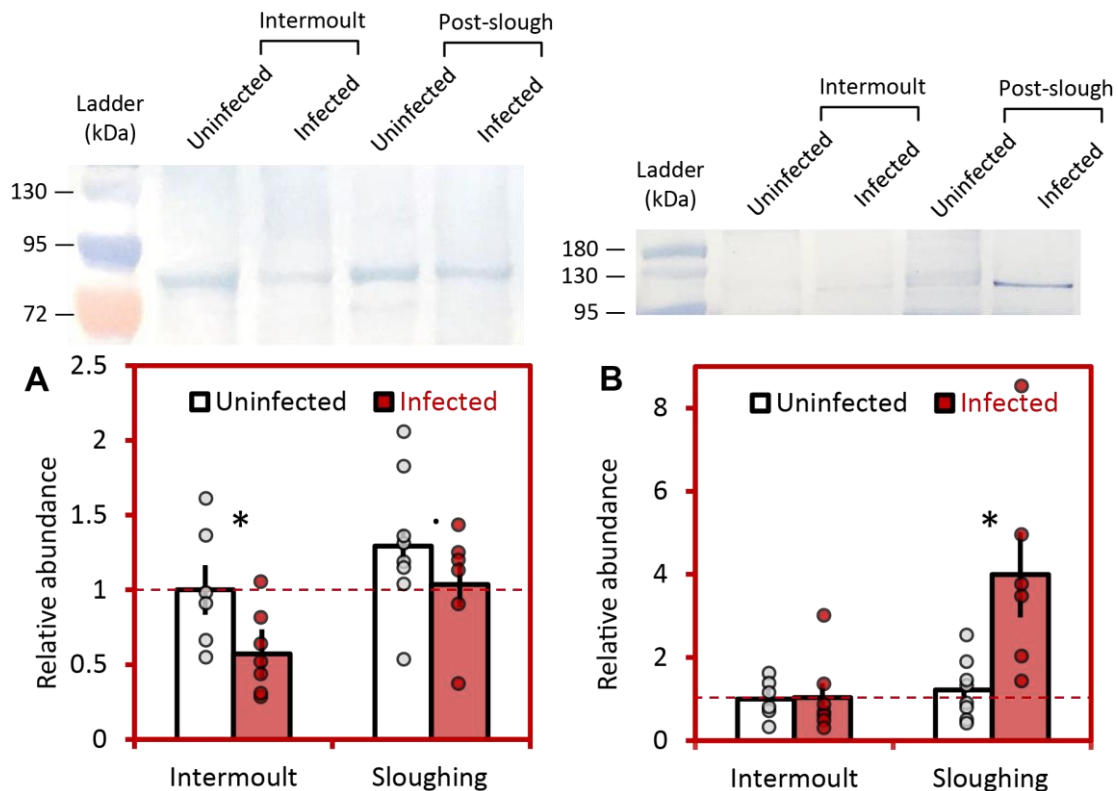
Fig. 3.3 │ Relative abundance of epithelial ion transporter proteins in the ventral skin of infected and uninfected *Litoria caerulea* during the intermoult and sloughing periods. Abundance of the **A**) ENaC-α subunit (SCNN1A) and **B**) NKA-α subunit (ATPA1A) expressed relative to the uninfected intermoult group (dashed line). Western blot analysis detected major bands at ~80 kDa for ENaC-α, and ~112 kDa for NKA-α. Representative western blots associated with each transport protein (top) show the molecular mass for the respective treatment groups. Bars represent mean ± s.e. with individual values overlain for intermoult (uninfected *n* = 6, infected *n* = 7) and sloughing (uninfected *n* = 8, infected *n* = 6) animals. '*', *P* < 0.05, '.': *P* <0.1. Summary statistics provided in Table. S3.4.

3.4.5   ENaC and NKA mRNA expression

Within the ENaC family, there were significant differences in α and β subunit mRNA expression between infected and uninfected frogs (**Fig. 3.4A, B**). For *ENaC-α* (*SCNN1A*) there was a significant increase in expression in the infected group compared with the uninfected group (t_{22} = -3.8, *P* = 0.001), whereas for *ENaC-β* (*SCNN1B*) there was a significant decrease in expression (t_{22} = 2.7, *P* = 0.01). No effect of sloughing phase was observed for either gene (**Fig. 3.4A**; **Table S3.5**). There was no effect of *Bd* infection or sloughing phase on the expression of the *ENaC-γ* (*SCNN1G*) subunit (**Fig. 3.4A**).

Within the NKA family, there were significant increases in expression of both α1 (*ATP1A1*) and β1 (*ATP1B1*) subunit mRNA in the infected group relative to the uninfected group (**Fig. 3.4B**; **Table S3.5**). *NKA-β3* (*ATP1B3*) subunit expression did not differ between infected and uninfected animals (t_{22} = -2, *P* = 0.06). However, there was a significant effect of sloughing phase on *ATP1B3* expression (t_{22} = -3.2, *P* = 0.003) with expression increasing in the sloughing group relative to the intermoult group (**Fig. 3.4B**).
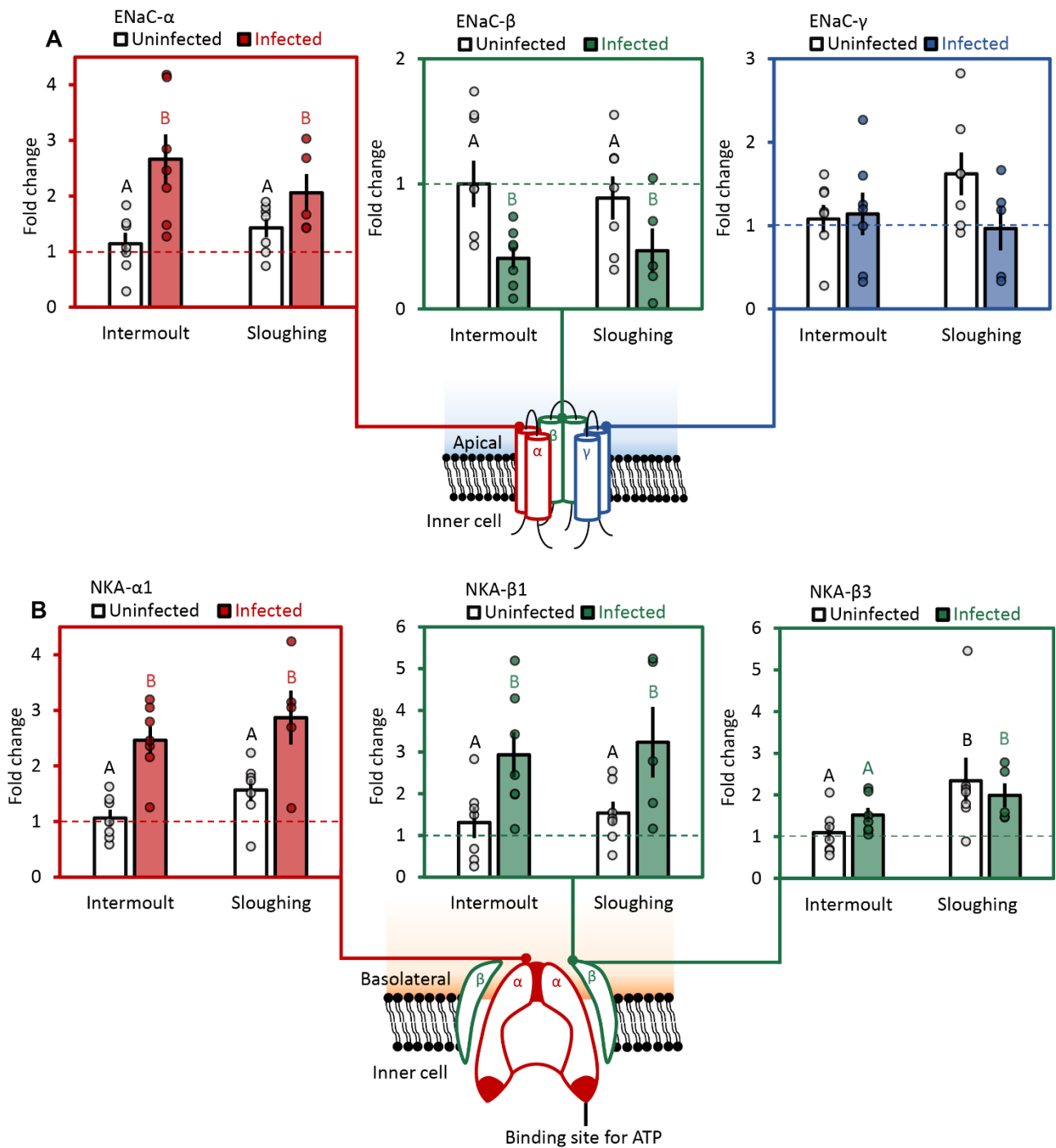
Fig. 3.4 │ Relative mRNA expression of epithelial ion transporters in the ventral skin of infected and uninfected *Litoria caerulea* during the intermoult and sloughing period. A) mRNA expression of epithelial sodium channel (ENaC) subunits (α, β, and γ). Absolute gene expression (ΔCT) was normalised to expression of the housekeeping gene β-actin, and is presented as fold change relative to uninfected intermoult groups (dashed line). Diagrammatic representation of the ENaC structure (based on Canessa, Cecilia M. et al., 1994) with the position of subunits on the cell surface of the epidermis. **B**) mRNA expression of Na⁺/K⁺-ATPase (NKA) subunits (α1, β1, and β3). Diagrammatic representation of the NKA structure (Suhail, 2010) with the position of subunits on the cell surface of the epidermis. All data points are presented with mean ± s.e. bar chart overlay for intermoult (uninfected $n = 7$, infected $n = 7$) and sloughing (uninfected $n = 7$, and infected animals $n = 5$) animals. Different letters represent significant differences between treatments and groups ($P < 0.05$). Summary statistics provided in Table S3.5.

3.5   DISCUSSION

With the recent discoveries that sloughing can regulate cutaneous *Bd* loads (Ohmer et al., 2017) and that increasing *Bd* loads contribute to the severity of clinical disease symptoms in infected animals (Voyles et al., 2009; Peterson et al., 2013), it is important to understand the mechanistic basis for these relationships. The present study confirms the hypothesis (Campbell et al., 2012) that a reduction in ENaC-associated cutaneous sodium transport contributed to the loss of ionic homeostasis in frogs with chytridiomycosis. We showed that elevated cutaneous sodium efflux in *Bd*-infected frogs is due in part to reduced Na^+ uptake capacity attributable to a reduced abundance of ENaC transporters, and to elevated (passive) ion leakage. Although ENaC mRNA expression was elevated in non-sloughing frogs with chytridiomycosis, the abundance of ENaC protein in the skin was lower than in uninfected frogs, suggesting that either protein synthesis was being inhibited or that newly synthesised proteins were being lost. Interestingly, sloughing stimulated a transient upregulation of Na^+ uptake in both infected an uninfected animals, and the newly exposed skin of infected frogs had a similar abundance of ENaC protein compared with uninfected frogs. This suggests the new skin layer initially possesses a full complement of functional Na^+-transport machinery that facilitates the temporary restoration normal physiological function. However, this restoration period is brief; it appears that ENaC proteins in the skin are destroyed by exposure to *Bd* during the intermoult period, contributing to the ongoing loss of ionic homeostasis.

Consistent with previous findings by Voyles et al. (2009), infected *L. caerulea* during the intermoult period had lower transcutaneous electrophysiological parameters (TEP, amiloride-sensitive I_{SC}, skin resistance) and lower levels of plasma Na^+ and Cl^- than uninfected frogs. Small changes in the electrical properties of transporting epithelia can have large consequences for the maintenance of physiological homeostais (Wood and Grosell, 2008); for example, a modest -10 mV change in the TEP can reduce plasma $[Na^+]$ from 140 mmol l^{-1} to 93 mmol l^{-1} in killifish (Wood and Grosell, 2015). Thus, the combination of a reduction in TEP, reduced active uptake, and increased skin permeability could explain the low plasma Na^+ and Cl^- levels seen in infected animals. The reduced TEP is likely the result of the reduction in both skin resistance and active transcutaneous Na^+ uptake (amiloride-sensitive I_{SC}) across the skin of non-sloughing infected frogs. Several lines of evidence suggest that secretion of proteolytic enzymes and toxins by *Bd* (Rosenblum et al., 2008; Symonds et al., 2008; Brutyn et al., 2012) can break down proteins and intercellular junctions leading to an increase in cellular apoptosis (Brannelly et al., 2017) and increased skin permeability (Voyles et al., 2009). The loss of skin resistance and reduced uptake capacity is consistent with the idea that *Bd* may directly damage local proteins in the skin. Further evidence for this hypothesis is that *Bd* had no effect on the activity or abundance of NKA in the skin. In frog skin, the multiple layers of the epithelium function as an interconnected syncytium (Heatwole et al., 1994); active ion uptake occurs in the

more apical skin layers, while the deeper skin layers contain the basolateral membrane-associated proteins (i.e. NKA) responsible for the generation of the electrochemical gradient that facilitates the apical transporter activities (Nielsen, 1979). The impairment of active Na^+ uptake is consistent with the hypothesis that *Bd* infection in the most apical layers of the skin (*stratum corneum* and upper *granulosum*) (Greenspan et al., 2012), directly affects the functional capacity of ENaC and the paracellular junctions, whereas ion transporters in the deeper layers of the epidermis (i.e. NKA) are largely unaffected by infection.

Bd infection appears to alter the functional capacity of Na^+ transport pathway by directly destroying these channels in the skin. *Bd* increased the sensitivity of the cutaneous active ion transport pathway to amiloride in intermoult frogs, reducing the IC_{50} by 70 % relative to the uninfected group. A reduction in amiloride-sensitive Na^+ transport indicates that there are fewer functional ENaC proteins in the skin of infected animals and so saturation of pumps is achieved at lower drug concentrations. This is consistent with our data showing that there was less ENaC-α protein in the skin of infected (intermoult) frogs compared with healthy frogs. ENaC exists as an obligate heterotrimer with α, β and γ subunits (or β, γ, δ subunits in some organisms (Hanukoglu and Hanukoglu, 2016)), and although we did not quantify the abundance of all ENaC subunits, it is likely that the reduction in ENaC-α reflects similar changes in the abundance of the functional heterotrimer. Interestingly, the skin of infected animals appears to compensate for the loss of functional proteins by increasing the expression of the ENaC-α gene. However, the gene expression of the other ENaC subunits did not follow the same pattern: *Bd* infection reduced the expression of ENaC-β and had no effect on the expression of ENaC-γ. Whether *Bd* differentially affects the abundance of ENaC subunit proteins is unknown. ENaC subunit expression is under tight control by hormones and extracellular factors (Butterworth et al., 2008), including stress hormones, so fluctuations in circulating hormone levels as a consequence of natural cycles or disease-related processes may contribute to the differential regulation of ENaC subunit expression. It is also possible that only ENaC-α protein is affected by *Bd* and, since ENaC-α is a requirement for ENaC channel activity, ENaC-β expression may be down-regulated to prevent an oversupply of the β-subunit in the absence of the corresponding α-subunit.

In infected animals, amiloride-sensitive Na^+ transport into the skin increased immediately after sloughing. The stark difference in Na^+ uptake rates between recently sloughed and intermoult animals, particularly in infected frogs, likely reflects the exposure of the new skin layer. Sloughing removes the most degraded outermost layer of skin, effectively 'resetting' the skin surface (Larsen, 1976). However, until the newly exposed *stratum corneum* layer becomes fully keratinised, the skin remains relatively permeable to ions (i.e. it has low resistance to ion loss). Therefore, the increase in *Isc*, therefore may serve to offset the transient increase in skin permeability that accompanies

sloughing. Indeed, we and others have observed a similar change in *Isc* across the skin immediately after sloughing in other amphibian species (Larsen, 1970; Nielsen and Tomilson, 1970; Wu et al., 2017). The increase in *Isc* post-sloughing in cane toads (Wu et al., 2017) commensurate with an increase in the abundance of ENaC-α and NKA proteins in the epithelium. This is consistent with the idea that the increase in *Isc* post sloughing is the result of more functional transporters present in the new skin, although isotope binding studies (Cramp et al., 2009) would be needed to quantify this. A similar increase in cutaneous Na^+ transport after moulting has been observed in crayfish (Zare and Greenaway, 1998).

Importantly, for frogs infected with *Bd*, the increase in transporter numbers in the skin post-sloughing was sufficient to restore active Na^+ uptake (*Isc*), albeit transiently. This finding supports the idea that *Bd* directly damages ion-transport proteins in the apical skin layers (Campbell et al., 2012), and that sloughing restores skin function by both exposing relatively undamaged cells and reducing the abundance of *Bd* on the skin which may reduce fungal toxins or secretions. However, the increased expression of ENaC-α, NKA-α and NKA-β mRNA in the tissues of recently sloughed frogs indicates that *Bd* infection does exert some influence over ion transporter systems even in the more basal skin layers. Although tissues were collected as soon after sloughing as possible, there was often a gap of up to one hour between sloughing and when tissues were collected, during which time the newly exposed skin would have been in direct contact with *Bd* in the surrounding environment. So, although increased mRNA expression in newly exposed skin of *Bd*-infected frogs might be a pre-sloughing compensatory response to elevated rates of protein degradation in the skin, contact between the newly exposed skin and *Bd* zoospores or toxins in the environment may have also stimulated ion transporter mRNA synthesis.

Compared with non-sloughing frogs, sloughing temporarily increased skin permeability. In healthy frogs, this increase in permeability following sloughing is relatively short-lived, however, which could be due to the combination of a leaky skin from the act of sloughing (Wu et al., 2017), structural disruption from infection with *Bd* (Nichols et al., 2001; Berger et al., 2005a), and reduction in the expression of skin integrity genes (Rosenblum et al., 2012; Ellison et al., 2015). To compensate for this high leakage demonstrated in this study, we found that NKA activity and abundance increased during sloughing. An increase in NKA activity is associated with maintaining osmotic balance when animals are subjected to osmotic stressors (Choi and An, 2008; Cramp et al., 2010). However, because NKA is a pump that actively exchanges ions against their concentration gradients via ATPase (Lingrel and Kuntzweiler, 1994), there may be an increase in cellular energy expenditure to uptake Na^+ into the cells (Harvey and Kernan, 1984). Susceptible species infected with *Bd* have greater expressions of cellular metabolic processes compared to non-susceptible species (Poorten and Rosenblum, 2016). Thus, the combination of increased skin permeability, cellular energy

expenditure, ionic disruption, and rate of sloughing may have additional cumulative consequences for maintaining electrolyte homeostasis in highly infected frogs.

Our results reveal a complex interaction between sloughing and chytridiomycosis. The cumulative effect of increased skin permeability during non-sloughing periods and increased sloughing frequency, effectively counteracted any benefit that might have be gained from the temporary, post-sloughing increase in electrolyte uptake capacity. Given that the magnitude of effects from *Bd* on skin function and sloughing frequency are proportional to *Bd* loads, animals that fail to regulate *Bd* loads effectively, are likely to suffer greater physiological disruption and for the disease to progress more rapidly than those species that can regulate their fungal loads (Ohmer et al., 2017). This work demonstrates the mechanisms underlying cutaneous disruption during *Bd* infection in susceptible amphibian species and highlights the intrinsic role of sloughing on this process. Importantly, this study explains why sloughing can be detrimental for susceptible species that develop high infection load, and may accelerate disease progression. Our results may also be important in light of another recently emerging fungal pathogen, *Batrachochytrium salamandrivorans* (*Bs*) which also causes the disease chytridiomycosis (Martel et al., 2013), and has been responsible for a number of amphibian population declines in Europe (Spitzen-van der Sluijs et al., 2016; Stegen et al., 2017). *Bs* may cause similar physiological disruption as *Bd*, however differences in host preferences and deeper skin penetration of *Bs* may indicate potential differences in the pathogenesis for species susceptible to *Bs* (Farrer et al., 2017). Further research on the pathophysiology of *Bs* is required to understand the similarities and differences in chytridiomycosis related deaths.

"The old-cited quote by Dhabzhansky reflects the importance of applying evolutionary approach to the study of biological questions. Although this almost certainly holds true for the study of ecoimmunology, an equally strong case can be made that **nothing makes sense in biology without an understanding of the underlying mechanisms** *as well"* ~ Demas et. al. (2011) The energetics of immunity: Mechanisms mediating trade-offs in ecoimmunology. Ecoimmunology, pp 259

3.6   SUPPLEMENTARY INFORMATION

3.6.1   Lme function for CT values

Relative mRNA expression of ENaC subunits (α, β, γ) and NKA subunits (α1, β1, β3) in the ventral skin between each treatment and slough group were analysed with the following 'lme' function from 'nlme' package (Pinheiro et al., 2013):

lme(log2(efficiency^-C$_T$) ~ treatment*gene*group, random=~1|ID, data=dataset)

where the base 2 logarithm of the efficiency (PCR amplification efficiency) and C$_T$ (threshold cycle) are the response variables, treatment (uninfected/infected), gene (reference gene (β-actin) and target gene of interest) and group (intermoult/post-slough) as interactive effects, and individual identity as random effect to account for repeated measurements between reference and target gene.

3.6.2   Supplementary tables

Table S3.1 │ Summary statistics from linear model and pairwise comparison for blood plasma ion (sodium, chloride, and potassium) levels between slough groups (intermoult, and post-slough) with zoospore equivalent (ZE) as an interactive effect. Df = degrees of freedom, s.e. = standard error, *P* = *P* value with α set at 0.05, CI = confidence interval set at 95 %, and Sum Sq = sum of squares. Significant codes: 0 '***' 0.001 '**' 0.01 '*' 0.05 '.' 0.1 ' ' 1.

						CI		
Plasma sodium ion level								
	Estimate	**Df**	**s.e.**	**t-value**	***P***			
Fixed effects						**2.5 %**	**97.5 %**	
Intercept	146.831	25	7.928	18.520	**<0.001**	130.503	163.159	***
Group	0.452	25	11.997	0.038	0.970	-24.257	25.160	
ZE	-14.489	25	2.680	-5.406	**<0.001**	-20.009	-8.969	***
Group:ZE	1.558	25	4.691	0.332	0.743	-8.104	11.220	
	Value	**Df**	**Sum of Sq**	**F-value**	***P***			
Intermoult	-14.489	1	15205.1	29.224	**<0.001**	***		
Post-slough	-12.932	1	5869.1	11.28	**0.003**	**		
Residuals		25	13007.5					
Plasma chloride ion level								
	Estimate	**Df**	**s.e.**	**t-value**	***P***			
Fixed effects						**2. 5%**	**97.5 %**	
Intercept	58.912	25	4.106	14.347	**<0.001**	50.455	67.369	***
Group	2.600	25	6.214	0.418	0.679	-10.197	15.398	
ZE	-4.456	25	1.388	-3.210	**0.004**	-7.316	-1.597	**
Group:ZE	1.899	25	2.430	0.781	0.442	-3.106	6.903	
	Value	**Df**	**Sum of Sq**	**F**	***P***			
Intermoult	-4.4564	1	1438.3	10.3044	**0.007**	**		
Post-slough	-2.5575	1	229.6	1.6447	0.211			
Residuals		25	3489.6					
Plasma potassium ion level								
	Estimate	**Df**	**s.e.**	**t-value**	***P***			
Fixed effects						**2.5 %**	**97.5 %**	
Intercept	3.325	25	0.346	9.618	**<0.001**	2.613	4.037	***

Group	-0.267	25	0.523	-0.510	0.615	-1.344	0.811
ZE	-0.119	25	0.117	-1.016	0.320	-0.359	0.122
Group:ZE	0.153	25	0.205	0.746	0.463	-0.269	0.574

Table S3.2 │ Summary statistics from linear model and pairwise comparison for electrophysiological parameters (transepithelial potential, skin resistance, and amiloride-sensitive short-circuit current) of the ventral skin between slough groups (intermoult, and post-slough) and zoospore equivalent (ZE) as an interactive effect. Df = degrees of freedom, s.e. = standard error, P = P value with α set at 0.05, CI = confidence interval set at 95 %, and Sum Sq = sum of squares. Significant codes: 0 '***' 0.001 '**' 0.01 '*' 0.05 '.' 0.1 ' ' 1.

Transepithelial potential								
Fixed effects	**Estimate**	**Df**	**s.e.**	**t-value**	**P**	**CI**		
						2.5 %	**97.5 %**	
Intercept	6.376	28	0.339	18.782	**<0.001**	5.680	7.071	***
Group	-2.036	28	0.468	-4.346	**<0.001**	-2.995	-1.076	***
ZE	-0.448	28	0.109	-4.118	**<0.001**	-0.670	-0.225	***
Group:ZE	0.851	28	0.173	4.912	**<0.001**	0.496	1.205	***
	Value	**Df**	**Sum of Sq**	**F-value**	**P**			
Intermoult	-0.448	1	16.173	16.959	**0.001**	***		
Post-slough	0.403	1	8.518	8.932	**0.006**	**		
Residuals		28	26.703					
Skin resistance								
Fixed effects	**Estimate**	**Df**	**s.e.**	**t-value**	**P**	**CI**		
						2.5 %	**97.5 %**	
Intercept	6.311	28	0.219	28.872	**<0.001**	5.863	6.759	***
Group	-0.607	28	0.302	-2.011	0.054	-1.224	0.011	.
ZE	-0.165	28	0.070	-2.360	**0.026**	-0.309	-0.022	*
Group:ZE	0.091	28	0.112	0.818	0.420	-0.137	0.320	
	Value	**Df**	**Sum of Sq**	**F-value**	**P**			
Intermoult	-0.165	1	2.202	5.568	**0.051**	.		
Post-slough	-0.074	1	0.287	0.725	0.402			
Residuals		28	11.073					
Amiloride-sensitive short-circuit current								
Fixed effects	**Estimate**	**Df**	**s.e.**	**t-value**	**P**	**CI**		
						2.5 %	**97.5 %**	
Intercept	3.979	27	0.161	24.761	**<0.001**	3.650	4.309	***
Group	-0.686	27	0.215	-3.184	**0.004**	-1.127	-0.244	**
ZE	-0.135	27	0.050	-2.710	**0.012**	-0.238	-0.033	*
Group:ZE	0.448	27	0.078	5.746	**<0.001**	0.288	0.608	***
	Value	**Df**	**Sum of Sq**	**F-value**	**P**			
Intermoult	-0.135	1	1.381	7.346	**0.012**	*		
Post-slough	0.312	1	5.125	27.270	**<0.001**	***		
Residuals		27	5.074					

Table S3.3 │ Summary statistics from linear model (and quadratic mixed effects model) and pairwise comparison for drug parameters on instantaneous short-circuit current (I_{SC}) (ouabain, amiloride dosage, IC$_{50}$ or amiloride) between

slough group (intermoult, and post-slough) and zoospore equivalent (ZE) as an interactive effect. Frog ID was account for as random effect. Df = degrees of freedom, s.e. = standard error, P = P value with α set at 0.05, CI = confidence interval set at 95 %, Sum Sq = sum of squares, and s.d. = standard deviation. Significant codes: 0 '***' 0.001 '**' 0.01 '*' 0.05 '.' 0.1 ' ' 1.

% Ouabain inhibition on I_{SC}							
Fixed effects	**Estimate**	**Df**	**s.e.**	**t-value**	**P**	**CI**	
						2.5 %	**97.5 %**
Intercept	-0.830	5	0.482	-1.723	0.105	-1.857	0.197	
Group	0.780	5	0.339	2.301	**0.036**	0.058	1.503	*
ZE	0.280	5	0.159	1.765	0.098	-0.058	0.618	.
Mass	0.008	5	0.009	0.844	0.412	-0.012	0.028	
Exposure	-0.626	5	0.432	-1.451	0.167	-1.546	0.294	
Group:ZE	0.112	15	0.144	0.778	0.449	-0.195	0.419	

Effect of amiloride concentration on I_{SC}							
	Intermoult					**CI**	
Fixed effects	**Value**	**Df**	**s.e.**	**t-value**	**P**	**2.5 %**	**97.5 %**
Intercept	1.139	107	0.095	11.936	**<0.001**	0.950	1.328	***
poly(dose, 2) 1	-4.307	107	0.595	-7.239	**<0.001**	-5.487	-3.128	***
poly(dose, 2) 2	0.380	107	0.140	2.714	**0.008**	0.102	0.658	**
ZE	0.017	107	0.023	0.760	0.449	-0.028	0.062	
poly(dose, 2) 1:ZE	0.328	107	0.179	1.838	0.069	-0.026	0.682	.
poly(dose, 2) 2:ZE	0.097	107	0.043	2.271	**0.025**	0.012	0.182	*
Random effect	**s.d.**				**Residual**		
dose │ Frog ID	0.233				0.093		
	Sloughing					**CI**	
Fixed effects	**Value**	**Df**	**s.e.**	**t-value**	**P**	**2.5 %**	**97.5 %**
Intercept	1.093	109	0.083	13.205	**<0.001**	0.950	1.328	***
poly(dose, 2) 1	-3.064	109	0.424	-7.220	**<0.001**	-5.487	-3.128	***
poly(dose, 2) 2	0.638	109	0.067	9.463	**<0.001**	0.102	0.658	***
ZE	0.115	11	0.032	3.581	**<0.001**	-0.028	0.062	**
poly(dose, 2) 1:ZE	-0.002	109	0.165	-0.014	0.989	-0.026	0.682	
poly(dose, 2) 2:ZE	-0.001	109	0.027	-0.044	0.965	0.012	0.182	
Random effect	**s.d.**				**Residual**		
dose │ Frog ID	0.176				0.051		

IC$_{50}$ of amiloride							
	Intermoult					**CI**	
Fixed effect	**Estimate**	**Df**	**s.e.**	**t value**	**P**	**2.5 %**	**97.5 %**
Intercept	1.8497	12	0.3423	5.403	**<0.001**	1.104	2.596	***
ZE	-0.2774	12	0.1047	-2.651	**0.021**	-0.505	-0.049	*
	Post-slough					**CI**	
Fixed effect	**Estimate**	**Df**	**s.e.**	**t value**	**P**	**2.5 %**	**97.5 %**
Intercept	1.22166	12	0.22519	5.425	**<0.001**	0.731	1.712	***
ZE	-0.06512	12	0.09087	-0.717	0.487	-0.263	0.133	

Table S3.4 │ Summary statistics from linear model and pairwise comparison for ENaC-α and NKA-α abundance of the ventral skin between slough group (intermoult, and post-slough) and zoospore equivalent (ZE) as an interactive effect. Body mass was a covariate. Df = degrees of freedom, s.e. = standard error, *P* = *P* value with α set at 0.05, CI = confidence interval set at 95 %, and Sum Sq = sum of squares. Significant codes: 0 '***' 0.001 '**' 0.01 '*' 0.05 '.' 0.1 ' ' 1.

ENaC-α abundance								
Fixed effect	**Estimate**	**Df**	**s.e.**	**t-value**	***P***	**CI**		
						2.5 %	**97.5 %**	
Intercept	1.236	19	0.235	5.259	**<0.001**	0.744	1.728	***
Group	0.237	19	0.188	1.262	0.222	-0.156	0.630	
ZE	-0.125	19	0.052	-2.421	**0.026**	-0.234	-0.017	*
Body mass	-0.007	19	0.006	-1.130	0.272	-0.019	0.006	
Group:ZE	0.034	19	0.069	0.493	0.628	-0.110	0.178	
	Value	**Df**	**Sum of Sq**	**F value**	***P***			
Intermoult	-0.125	1	0.791	5.859	**0.049**	*		
Post-slough	-0.091	1	0.516	3.826	0.065	.		
Residuals		19	2.564					
NKA-α abundance								
Fixed effect	**Estimate**	**Df**	**s.e.**	**t-value**	***P***	**CI**		
						2.5 %	**97.5 %**	
Intercept	0.660	20	0.149	4.420	**<0.001**	0.349	0.972	***
Group	0.201	20	0.199	1.008	0.326	-0.215	0.617	
ZE	0.030	20	0.051	0.586	0.564	-0.077	0.137	
Group:ZE	0.127	20	0.072	1.766	0.093	-0.023	0.276	.
	Value	**Df**	**Sum of Sq**	**F value**	***P***			
Intermoult	0.030	1	0.054	0.343	0.564			
Post-slough	0.157	1	1.522	9.716	**0.011**	*		
Residuals		20	3.133					

Table S3.5 │ Summary statistics from linear mixed effects model for ENaC and NKA subunit mRNA expression of the ventral skin between slough groups (intermoult, and post-slough) and treatments (uninfected, and infected). Gene is in reference to the reference gene (β- actin), and Frog ID was account for as random effect. Df = degrees of freedom, s.e. = standard error, *P* = *P* value with α set at 0.05, and CI = confidence interval set at 95 %. Significant codes: 0 '***' 0.001 '**' 0.01 '*' 0.05 '.' 0.1 ' ' 1.

ENaC-α expression								
Fixed effects	**Value**	**Df**	**s.e.**	**t-value**	***P***	**CI**		
						2.5 %	**97.5 %**	
Intercept	-25.869	22	0.288	-89.939	<0.001	-26.466	-25.273	
Treatment	1.306	22	0.407	3.211	0.004	0.462	2.150	
gene	5.310	22	0.247	21.523	<0.001	4.798	5.821	
Group	0.088	22	0.407	0.217	0.830	-0.755	0.932	
Treatment:Gene	-1.349	22	0.349	-3.867	**0.001**	-2.073	-0.626	**
Treatment:Group	-1.301	22	0.603	-2.156	0.042	-2.552	-0.050	
Gene:Group	-0.442	22	0.349	-1.268	0.218	-1.166	0.281	
Treatment:gene:Group	0.826	22	0.517	1.596	0.125	-0.247	1.899	
Random effect	**s.d.**				**Residual**			

							CI	
~1 | Frog ID	0.605				0.462			

ENaC-β expression

Fixed effects	Value	Df	s.e.		P	CI		
						2.5 %	97.5 %	
Intercept	-23.278	22	0.405	-57.490	<0.001	-24.118	-22.438	
Treatment	-0.369	22	0.135	-2.741	0.012	-0.648	-0.090	
gene	2.666	22	0.418	6.385	<0.001	1.800	3.532	
Group	-0.635	22	0.574	-1.106	0.281	-1.826	0.556	
Treatment:Gene	0.384	22	0.139	2.766	**0.011**	0.096	0.672	*
Treatment:Group	-0.135	22	0.200	-0.677	0.505	-0.550	0.279	
Gene:Group	0.360	22	0.592	0.609	0.549	-0.868	1.588	
Treatment:gene:Group	-0.020	22	0.206	-0.095	0.925	-0.447	0.408	
Random effect	**s.d.**				**Residual**			
~1 | Frog ID	0.750				0.799			

ENaC-γ expression

Fixed effects	Value	Df	s.e.	t-value	P	CI		
						2.5 %	97.5 %	
Intercept	-25.575	22	0.301446	-84.842	<0.001	-26.200	-24.950	
Treatment	-0.048	22	0.100196	-0.479	0.637	-0.256	0.160	
gene	4.963	22	0.328743	15.097	<0.001	4.281	5.645	
Group	0.116	22	0.427435	0.272	0.788	-0.770	1.003	
Treatment:Gene	0.063	22	0.109269	0.575	0.571	-0.164	0.289	
Treatment:Group	-0.267	22	0.148805	-1.798	0.086	-0.576	0.041	
Gene:Group	-0.391	22	0.466142	-0.839	0.410	-1.358	0.576	
Treatment:gene:Group	0.112	22	0.16228	0.693	0.496	-0.224	0.449	
Random effect	**s.d.**				**Residual**			
~1 | Frog ID	0.520				0.629			

NKA-α expression

Fixed effects	Value	Df	s.e.	t-value	P	CI		
						2.5 %	97.5 %	
Intercept	-22.108	22	0.287	-77.011	<0.001	-22.704	-21.513	
Treatment	0.287	22	0.095	3.010	0.006	0.089	0.485	
gene	1.496	22	0.243	6.156	<0.001	0.992	2.000	
Group	0.257	22	0.407	0.632	0.534	-0.587	1.102	
Treatment:Gene	-0.272	22	0.081	-3.371	**0.003**	-0.440	-0.105	**
Treatment:Group	-0.264	22	0.142	-1.863	0.076	-0.558	0.030	
Gene:Group	-0.532	22	0.345	-1.544	0.137	-1.247	0.183	
Treatment:gene:Group	0.109	22	0.120	0.909	0.373	-0.140	0.358	
Random effect	**s.d.**				**Residual**			
~1 | Frog ID	0.622				0.465			

NKA-β1 expression

Fixed effects	Value	Df	s.e.	t-value	P	CI		
						2.5 %	97.5 %	
Intercept	-21.671	22	0.332	-65.237	<0.001	-22.360	-20.982	
Treatment	0.295	22	0.110	2.675	0.014	0.066	0.524	
gene	1.059	22	0.383	2.768	0.011	0.266	1.853	

	Value	Df	s.e.	t-value	P	2.5 %	97.5 %	
Group	0.191	22	0.471	0.405	0.689	-0.786	1.168	
Treatment:Gene	-0.280	22	0.127	-2.205	**0.038**	-0.544	-0.017	*
Treatment:Group	-0.282	22	0.164	-1.721	0.099	-0.622	0.058	
Gene:Group	-0.466	22	0.543	-0.858	0.400	-1.591	0.660	
Treatment:gene:Group	0.127	22	0.189	0.673	0.508	-0.265	0.519	
Random effect	**s.d.**				**Residual**			
~1	Frog ID	0.522				0.732			

NKA-β3 expression								
Fixed effects	**Value**	**Df**	**s.e.**	**t-value**	**P**	**CI**		
						2.5 %	**97.5 %**	
Intercept	-27.331	22	0.269	-101.497	<0.001	-22.360	-20.982	
Treatment	0.162	22	0.090	1.807	0.085	0.066	0.524	
gene	6.719	22	0.222	30.322	<0.001	0.266	1.853	
Group	0.758	22	0.382	1.985	0.060	-0.786	1.168	
Treatment:Gene	-0.147	22	0.074	-1.993	0.059	-0.544	-0.017	.
Treatment:Group	-0.324	22	0.133	-2.434	0.024	-0.622	0.058	
Gene:Group	-1.033	22	0.314	-3.287	**0.003**	-1.591	0.660	**
Treatment:gene:Group	0.169	22	0.109	1.541	0.138	-0.265	0.519	
Random effect	**s.d.**				**Residual**			
~1	Frog ID	0.593				0.424			

Table S3.6 │ *Litoria caerulea*-specific designed primers for qPCR of target and reference genes.

Primer name	Orientation	Primer (5' to 3')	Amplicon size (bp)
ENaC-α	Forward	AAATGGGTGCTTCAAACACTG	213
	Reverse	CCAACTCTACCAACTCCACCA	
ENaC-β	Forward	AAGATCCAGACTGGGTGTCCT	225
	Reverse	TGATGATGCCATTTCTGTTCA	
ENaC-γ	Forward	TGTTTCCAAAAGGAGATGGTG	159
	Reverse	CTGACATCCAAGCTCTTCCTG	
NKA-α1	Forward	ACTGGAGATGGTGTGAACGAC	202
	Reverse	TGGTCAGGGTGTAGGCAATAG	
NKA-β1	Forward	GGATTTAAACCAAAGCCTCCA	237
	Reverse	GCACAGCAATAAGGGGTTGTA	
NKA-β3	Forward	CAATGAAGGGAGTCCATGTGT	345
	Reverse	ATACGTCTGATGTGCCGGTAG	
β-Actin	Forward	CTGGACGTACAACTGGTATTG	185
	Reverse	CCTCTCTGCTGTGGTAGTAA	

Body size influences energetic and osmoregulatory costs in frogs infected with Batrachochytrium dendrobatidis

4.1   ABSTRACT

Sloughing maintains the skins integrity and critical functionality in amphibians. Given the behavioural, morphological, and osmoregulatory changes that accompany sloughing, this process is likely to be physiologically costly. Chytridiomycosis, a cutaneous disease of amphibians caused by the fungus *Batrachochytrium dendrobatidis* (*Bd*), disrupts skin function and increases sloughing rates. Moreover, mortality rates from chytridiomycosis are significantly higher in juveniles, and so we hypothesised that smaller individuals maybe more susceptible to chytridiomycosis because of allometric scaling effects on the energetic and osmoregulatory costs of sloughing. We measured *in-vivo* cutaneous ion loss rates and whole animal metabolic rate (MR) of green tree frogs, *Litoria caerulea*, over a range of body sizes both infected and uninfected frogs during sloughing. Infected animals had a greater rate of ion loss and mass-specific MR during non-sloughing periods but there were no additional effects of sloughing on either of these parameters. There were also significant interactions with body size and *Bd* load indicating that smaller animals with higher *Bd* loads have greater rates of ion loss and higher energetic demands. Our results shed light on why smaller *Bd*-infected anurans often exhibit greater physiological disruption than larger individuals.

4.2   INTRODUCTION

Vertebrate skin is a multilayered, semi-permeable tissue providing physical protection from environmental damage, from pathogens and parasites and in some animals, allows the physiological regulation of cutaneous respiratory gases (O_2, CO_2), electrolytes (Na^+, Cl^-, K^+), and acid-base (H^+, HCO^-) and water balance (Boutilier et al., 1992). In order to maintain the integrity and proper physiological function of the skin, the most superficial layer (*stratum corneum*), is periodically removed and replaced with a new layer through a process known as 'moulting', 'shedding', or 'sloughing' (Ling, 1972; Larsen, 1976). Mammals shed skin cells continuously, while birds, snakes and amphibians undergo a cyclic regime of shedding (Ling, 1972) that may occur as frequently as daily to once or twice a year. For amphibians, sloughing is a physiologically complex process, requiring the integration and synchronisation of circulating hormones (Jørgensen, 1988) with control of cellular differentiation rates, and the dissolution and reformation of the impermeable skin layers (Budtz and Larsen, 1973). Skin sloughing has been hypothesised to be energetically costly due to both the physical aspect of removing the slough, and the cellular costs of skin regeneration (Houlihan, 1991). In amphibians, sloughing behaviour is largely consistent among species (Larsen, 1976; Ohmer et al., 2017) and involves a series of behaviours including hunching, abdominal contractions and limb wiping to remove and eat the old *stratum corneum* (Chapter 1; Larsen, 1976; Castanho and de Luca, 2001). Although the energetic cost of sloughing has not been documented in amphibians, it has in snakes. Shedding snakes can increase their metabolic rate

(MR) by up to 146 % of their standard metabolic rate (Thompson and Withers, 1999), and in some species, shedding can be more energetically expensive than digestion and venom production (Pintor et al., 2010). For endotherms such as penguins and northern elephant seals, a slight increase in energy expenditure over the moulting period does not markedly affect the animals average daily energetic expenditure (Adams et al., 1990; Worthy et al., 1992).

While sloughing allows the functionality of the skin to be maintained, there are significant osmoregulatory challenges associated with the removal of the slough for amphibians, such as increased leakage of cutaneous salts and influx of water into the body (Jørgensen, 1949; Wu et al., 2017). A substantial component of the energetic cost of sloughing in amphibians likely relates to the complex physiological processes occurring within the new epidermis (Budtz and Larsen, 1973, 1975). Specifically, cutaneous osmoregulatory disruptions such as sodium leakage, are compensated for by changing the electrophysiological properties of the skin (Erlij and Ussing, 1978), and increasing the expression of ion transporter proteins post removal of the slough (Wu et al., 2017). This leads to an increase in active transcellular ion transport which may also increase the cellular energy expenditure for the tissue (Dawson and Liu, 2008; Larsen et al., 2009). Under *in-vitro* conditions, cutaneous active sodium transport can account for ∼25 % of net O_2 cutaneous consumption (Zerahn, 1956). In addition, the biosynthesis of epidermal tissue also contributes to the cost of sloughing. Although there are no direct studies of the energetic cost of epidermal turnover in amphibians, in sparrows there was a 3.5 fold increase in protein synthesis associated with moulting (Murphy and Taruscio, 1995). The behavioural aspects of sloughing in combination with increased cellular differentiation, compensatory changes in ion transport, and the turnover of the cutaneous surface fluid (mucosal protective layer of the epidermis (Larsen et al., 2014)) are likely to contribute to the net energetic cost of sloughing and which may represent a considerable component of an amphibian's overall energy expenditure.

Sloughing may act as an innate immune defence against cutaneous pathogens by increasing the rate of epidermal turnover, and thereby reducing the opportunity for cutaneous pathogens to establish and cause infection (Meyer et al., 2012). Recently it was shown that in frogs infected with the pathogenic chytrid fungus, *Batrachochytrium dendrobatidis* (*Bd*), sloughing frequency increased significantly (Ohmer et al., 2015). Many anurans infected with *Bd* eventually develop chytridiomycosis, a fatal skin disease responsible for many amphibian declines around the world (Berger et al., 1998; Fisher et al., 2009). *Bd* infection also reduces cutaneous sodium uptake capacity and increases passive transcutaneous ion leakage (Voyles et al., 2009), which, combined with significant inappetence, contributes to the development of low plasma electrolyte levels (Voyles et al., 2007; Campbell et al., 2012; Peterson et al., 2013). These behavioural and physiological changes may translate into significant energetic consequences for the infected host. The energetic cost of

parasitic infections have been examined in other organisms and may be used a proxy for the impact of infection on overall host physiology including maintenance costs, growth and activity (Lochmiller and Deerenberg, 2000). However, this generalisation about the higher energetic cost of parasitism is not always consistent. In some cases, the MR of parasitised hosts is significantly reduced (Kilgore et al., 1988; Arnold et al., 2013), while in other cases host MR increases (Booth et al., 1993; Giorgi et al., 2001) or does not change (Orlofske et al., 2013). Such varied responses in MR to parasitism may be due to the context-dependent nature of the energetic costs of parasitism, and may reflect compensatory actions such as changes in host behaviour and physiology that may offset the effects of parasitism on growth and development instead.

Bd has been shown to increase the rate of O_2 consumption (a proxy for MR) in heavily infected frogs (Peterson et al., 2013) but not in sub-clinically infected frogs (Carver et al., 2010). This suggests that *Bd* may not elicit substantial physiological consequences in hosts until infection levels reach a critical threshold (Peterson et al., 2013). Sloughing, therefore, may be an important immune defence. By increasing the rate of sloughing, the host may constrain *Bd* growth, and thus slow the onset of physiological disruption (Ohmer et al., 2017). The additional effort required to remove the sloughed skin more frequently may increase the overall energy budget of infected frogs and may contribute to the negative health outcomes in susceptible species.

Adverse energetic and osmoregulatory consequences of chytridiomycosis have been observed in a few *Bd* infected anuran species (Campbell et al., 2012; Peterson et al., 2013; Bovo et al., 2016). These effects may be magnified in smaller frogs, especially juveniles, which often have greater *Bd*-associated mortality rates than larger individuals of the same species (Carey et al., 2006; Kriger et al., 2006; Langhammer et al., 2014; Bakar et al., 2016). Body size (e.g. body mass, snout-vent length, or surface area) dependent mortality rates have been attributed to differences in the maturation of skin immune defences (Rollins-Smith, 1998) or immature systemic immune function (Bakar et al., 2016), differences in skin morphology (Chammas et al., 2014), diversity of cutaneous microbiomes (Bates et al., 2018), and the relative surface area for colonisation. Few studies, however, have directly examined the relationship between body size, *Bd* load and the physiological consequences of *Bd* infection. Metabolic rate and cutaneous surface-area scale allometrically with body mass (exponents of 0.75 and 0.88-0.94, respectively (White et al., 2006; Klein et al., 2016)) such that smaller frogs have a greater cutaneous surface area and a higher metabolic rate than larger frogs. Therefore, smaller anurans may be more at risk of cutaneous and metabolic dysfunction relative to larger individuals, and this effect may be exacerbated by increased sloughing rates in infected animals. The present study investigated the effects of body size and *Bd* load on the energetic and osmoregulatory effects of sloughing in the Australian green tree frog (*Litoria caerulea*). We hypothesised that smaller individuals would experience greater osmoregulatory disturbances and

higher mass-specific MR during sloughing than larger individuals. We also predicted that in smaller individuals that develop symptomatic chytridiomycosis, sloughing would exacerbate the osmoregulatory and metabolic effects of *Bd* infection.

4.3 MATERIALS AND METHODS

4.3.1 Animal collection and maintenance

Litoria caerulea spawn was collected from Bribie Island, southeast Queensland in March 2015. Larvae were maintained in aged Brisbane tap water, changed weekly, and fed every second day with frozen spinach. Larvae were reared through to metamorphosis and 19 resulting juveniles (0.5–15 g) were used in subsequent experiments. In addition, 17 juvenile and adult *L. caerulea* (15–70 g) were collected from wet roads in non-protected areas near Fernvale, southeast Queensland in January 2015. All frogs were housed in individual ventilated clear plastic containers, either small (235 x 170 x 120 mm) or large containers (265 x 235 x 12 mm), with paper towels saturated with chemically aged water (dilution 1:4000; VitaPet, NSW, Australia) as substrate, and a half PVC pipe for shelter. Containers were also tilted at ~10° to allow a dry and moist gradient for the frogs to move between. The lighting conditions were set at a 12:12 h light-dark photoperiod cycle, and temperature maintained at a constant $20.5 \pm 0.5°C$. Frogs were checked daily, fed once a week on vitamin-dusted crickets (*Acheta domesticus*), and enclosures cleaned weekly. Prior to experiments, all frogs were swabbed to confirm the absence of *Bd* infection (see below).

4.3.2 Monitoring sloughing frequency

The intermoult interval (IMI), defined as the period between two successful sloughing events, was monitored continuously using infrared surveillance cameras (model EN-CI20B-65H, Eonboom Electronics Limited; and HW242C Security Camera, K Guard Security, New Taipei City, Taiwan), and a generic 16 channel H.264 Digital Video Recorder (DVR) system, mounted to a moveable metal frame in front of enclosures, with two cameras per row. Each camera monitored two frog enclosures at one time at a sample rate of 1.56 frames per second. The videos were extracted daily, and the intermoult interval (IMI) (h) and duration of the sloughing event (min), were calculated.

4.3.3 *Bd* culture and exposure

After one month of monitoring to establish IMI, *Bd* strain EPS4 detailed in Ohmer et al. (2015) was used for all experimental infections. Cultures were maintained at 4°C until 4–5 days before exposure. EPS4 isolate was passaged onto sterile 1 % agar, 0.5 % tryptone, 0.5 % tryptone-soy plates and incubated at 20°C. After 4–5 days, zoospores were harvested by flooding plates with aged tap water for 30 min. The zoospore suspension was collected, and the concentration calculated using a haemocytometer (Boyle et al., 2004). A randomised subset of frogs ($n = 23$) were exposed to ~500,000 zoospores. Frogs were exposed for 5 h in 300 ml plastic containers containing 100 ml aged water. Uninfected frogs were treated similarly, but with aged water only. At 2 weeks post-

exposure and fortnightly thereafter, each frog was swabbed with a sterile fine-tipped cotton swab (MW100-100; Medical Wire & Equipment, Wiltshire, England) three times over the frog's ventral surface, thighs, armpit, forelimb feet, and hindlimb feet (Kriger et al., 2006; Ohmer et al., 2015) to assess infection status. Samples were processed following Boyle et al. (2004). Swabs were extracted in 50 µl PrepMan Ultra (Applied Biosystems, Foster City, CA, USA), and analysed in duplicate with Taqman qPCR in a thermal cycler (MiniOpticon™ Real-Time PCR Detection System, Bio-Rad Laboratories, Inc.) in a modified 15 µl reaction following Ohmer et al. (2015). If after 1 month, exposed frogs had no detectable *Bd* infection, they were re-exposed as above. Infection load or number of zoospore equivalent (ZE) on the skin surface were log + 1 transformed (Log(ZE+1)). Prevalence of infection with *Bd* was high: in the first set of infection 65 % of exposed frogs developed infection, and one month re-exposure 87 % of exposed frogs developed an infection. The three frogs that did not develop infection after re-exposure were excluded from the analysis.

4.3.4   Experimental chronology

Once the IMI was determined for each animal (both uninfected and infected animals), ion loss and respirometry experiments were conducted concurrently (random order) during either the intermoult period or on the predicted day of slough. On the day of experiment, the frogs were swabbed to determine their infection load on that day.

4.3.5   Ion loss measurements

Changes in ion loss during sloughing were measured by placing animals into a ventilated clear chamber (50-1000 ml, depending on the frogs' mass) containing between 30 and 200 ml of distilled water with a magnetic stirrer to circulate the solution. The rate of ion efflux from the animal was measured as change in the conductivity of the bathing solution (microsiemens per hour; Δ µS h^{-1}). Conductivity was measured between two electrodes placed into the solution which were connected to a conductivity pod (ML307, ADInstruments, NSW, Australia). The output was digitised with PowerLab 4/35 interface (ADInstruments) and recorded onto Labchart software (ADInstruments). The baseline of the solution was measured for roughly an hour before the animal was placed into the chamber. Animals were at one of 5 points in their sloughing cycles when measurements were made: 1. intermoult (half way through slough cycle); 2. day of slough (3 h prior to slough, or day of predicted slough in infected frogs but did not slough); 3. pre-slough (10–20 min prior to slough); 4. mid-slough (during a slough); and 5. post slough (30 – 60 min post sloughing). Sloughing behaviour was monitored continuously via webcam (Microsoft VX-3000) and measurements for each group was defined: 1. intermoult and 2. day of slough, where the animals remain still; 3. pre-slough, when animals started to extend their limbs to lift the abdomen off the ground; 4. mid-slough which begins with mouth gaping, followed by abdominal contractions, upper body wiping and removal of the old skin; and 5. post-slough, up to 1 h after sloughing when normal behaviour resumes (**Fig. S4.1**). All

experiments were conducted at room temperature (20.5 $\pm$ 0.5°C), and animals were swabbed for *Bd* load prior to the introduction to the chamber.

Three dimensional (3D) agar models of 4 different sizes (20, 40, 60, and 80 % of adult size) were made to examine the effect of surface area on the rate of cutaneous ion loss across a free-flowing permeable surface. To make the agar replicas, a life size adult green tree frog plastic model was scanned using a HDI surface scanner on FlexScan3D software (LMI technologies Inc. BC, Canada), then cleaned, refined and filled using Autodesk Meshmixer (Autodesk Inc. CA, USA). The 3D images were then scaled to the appropriate body size by Autodesk 123D Design, and 3D printed via Makerbot Replicator (MakerBot Industries, NY, USA) in Polylactic acid (PLA) filament material. Molds of the models were made using Kromopan dental alginate. A 3 % agar solution in Ringers solution (in mmol l^{-1}: NaCl (112), KCl (2.5), Na$_2$HPO$_4$ (2), CaCl$_2$ (1), MgCl$_2$ (1), HEPES salt (5), HEPES (5), pH 7.4, osmolarity 270 $\pm$ 20 mOsmol l^{-1}) was poured into the molds and allowed to solidify. The agar replicas were placed into the ion loss water baths and subjected to the same conditions as the living frogs. Ion loss into the water bath was recorded for 1 h.

To estimate the overall effect of sloughing on the animals sodium budget, conductivity measures were converted to a rate of sodium loss (mmol h^{-1}) based on the [Na$^+$] of bath water samples collected after sloughing (measured via flame photometry (BWB-XP flame photometer; BWB Technologies Ltd, UK)), and assuming that (1) sodium was the primary ion contributing to solution conductivity, and (2) that the proportion of sodium lost relative to other ions was equal (Wu et al., 2017). The net amount of Na$^+$ lost during sloughing was approximated assuming an extracellular fluid (ECF) volume of approximately ~25 % of the body mass of the animal (Hillman et al., 2009). The actual Na$^+$ concentration of the ECF was measured from plasma samples collected from green tree frogs in a separate experiment following Wu et al. (2017). The proportion of the total extracellular fluid Na$^+$ (as % of ECF Na$^+$ h^{-1}) lost during sloughing was calculated by dividing the rate of ion loss (mmol l^{-1} h^{-1}) by the total amount of ECF Na$^+$ (mmol) and multiplied by 100.

The effective ventral surface area (A_v; cm^2) across which ion exchanges would occur was calculated by photographing the ventral side of the animal in contact with a glass surface and calculating the surface area (excluding surface area of limbs and head; **Fig. S4.2**). Images were analysed using Image J (http://imagej.nih.gov/ij/). For surface area-specific ion loss, data was presented as µS cm^{-2} h^{-1}.

4.3.6 Respirometry set-up

Positive pressure flow-through respirometry (**Fig. 4.1**) was used to measure whole animal rates of oxygen consumption ($\dot{V}_{O_2}$, ml O$_2$ h^{-1}) and carbon dioxide production ($\dot{V}_{CO_2}$, ml CO$_2$ h^{-1}), as a proxy for whole animal metabolism (the sum of both respiratory and cutaneous respiration). Atmospheric air scrubbed of CO$_2$ (using soda lime, Chem-Supply, Adelaide, Australia) and water

vapour (using Drierite, W. A. Hammond Drierite Co. Ltd, USA) was drawn in to the respirometry system via a sub-sampler pump (SS-3, Sable Systems International, Las Vegas, NV, USA), at a controlled flow rate of either 30 ml min^{-1} (for small frogs <10 g), 50 ml min^{-1} (for medium frogs 10–25 g) or 80 ml min^{-1} (for large frogs >25 g) by a mass flow controller (GFC17, Aalborg Instruments & Controls Inc., Orangeburg, NY, USA). The dry, CO_2–free air passed through the metabolic chamber (50 ml, 300 ml or 500 ml glass air-tight container (ClipFresh, Hong Kong)), before passing through a relative humidity (RH) analyser (RH-100; Sable Systems, Las Vegas, NE, USA). The air was then re-scrubbed of water vapour before passing through an infrared CO_2 gas analyser (LI-820, LI-COR® Biosciences Inc., Lincoln, NE, USA) and an O_2 analyser (Oxzilla II; Sable Systems, Las Vegas, NE, USA). The fractional concentrations of the CO_2 and O_2 in the excurrent air ($F_e co_2$ and $F_e o_2$) were recorded in a PowerLab 4/35 interface and imported into Labchart software (ADinstruments).

The mass flow controller was calibrated using a NIST-traceable bubble film flow meter (1-10-500 ml, Bubble-O-Meter, Dublin, Ohio, USA). The CO_2 analyser was calibrated with dry CO_2-free air and a certified gas mix (0.386 $\pm$ 0.008 % CO_2 in N_2, BOC Gases, Wetherill Park, Australia), and the O_2 analyser was calibrated with dry compressed air (20.5 $\pm$ 0.5 % O_2, BOC Gases, Wetherill Park, Australia).
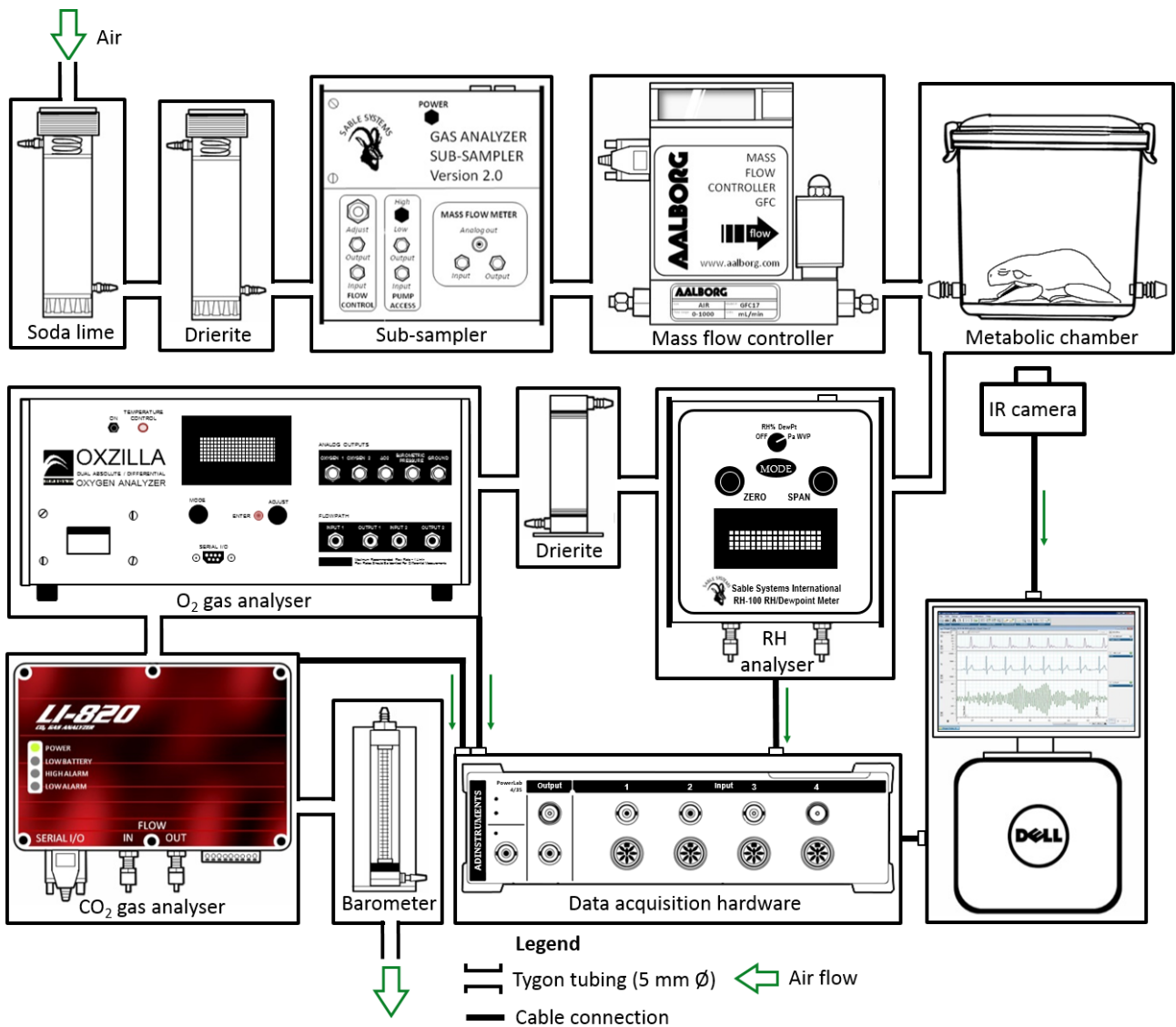
Fig. 4.1 │ **Schematic diagram representation of the positive pressure flow-through respirometry setup used to measure CO₂ and O₂ of *Litoria caerulea* during rest and sloughing.**

4.3.7   Resting and sloughing metabolic measurements

Each frog was fasted for at least four days prior to measurement to ensure a post-absorptive state (Secor et al., 2007). The background fractional CO_2 and O_2 concentration of the ex-current air from the respirometry chamber was recorded overnight prior to the introduction of the animal. Body mass (M_b, g) was recorded before and after the experiment, and animals were swabbed prior to the introduction of the chamber. The resting metabolic rate (RMR) was taken over the period when the animal was in a water conserving posture and behaviourally inactive which corresponded to the lowest O_2 and CO_2 readings observed. Metabolic rate during the day of slough, pre-slough, mid-slough, and post-slough stages were also recorded. Active metabolic rate, defined as the rate of CO_2 production during a period of continuous movement in the chamber was also measured to compare with the relative energetic cost of sloughing. All activities and behaviours were monitored remotely with a webcam (Microsoft VX-3000) and recorded in Labchart. The temperature of the

experimental room was maintained at $20.75 \pm 0.4°C$. The mean $\dot{V}_{O_2}$ and $\dot{V}_{CO_2}$ for all activities were calculated following Lighton (2008):

$$\dot{V}_{O_2} = \text{FR}_i[(F_iO_2 - F_eO_2) - F_eO_2(F_eCO_2 - F_iCO_2)]/(1 - F_eO_2)$$

and

$$\dot{V}_{CO_2} = \text{FR}_i[(F_eCO_2 - F_iCO_2) - F_eCO_2(F_iO_2 - F_eO_2)]/(1 - F_eCO_2)$$

Where FR_i = incurrent flow rate (ml min), F_iO_2 = incurrent O_2 concentration, F_eO_2 = excurrent O_2 concentration, F_iCO_2 = incurrent CO_2 concentration, and F_eCO_2 = excurrent CO_2 concentration. Instantaneous correction following Seymour et al. (1998) was applied to $\dot{V}_{CO_2}$ and $\dot{V}_{O_2}$ to correct for wash-out characteristics:

$$\text{Inst. } \dot{V}_{O_2} \text{ or } \dot{V}_{CO_2} = \left[\dot{V}_1 - \dot{V}_2 \times e^{k(t2-t1)}\right]/\left[1 - e^{k(t2-t1)}\right]$$

Where e is the natural logarithm constant (2.71828), k is the washout constant (absolute value of the slope between $\ln(F_eO_2 - F_iO_2)$ over time), $\dot{V}_1$ is the $\dot{V}_{O_2}$ or $\dot{V}_{CO_2}$ at time $t1$, $\dot{V}_2$ is the $\dot{V}_{O_2}$ or $\dot{V}_{CO_2}$ at time $t2$. The respiratory exchange ratio (RER) was also calculated by dividing $\dot{V}_{CO_2}$ by $\dot{V}_{O_2}$. The energy expenditure of sloughing and activity ($J\ h^{-1}$) was calculated by subtracting resting $\dot{V}_{CO_2}$ from sloughing/activity $\dot{V}_{CO_2}$, and multiplying by the energy equivalent of 1 ml CO_2 production ((1 ml CO_2 = 25.6 J Withers, 1992)).

Due to inconsistent drifts in the O_2 analyser for some experiments, overall sample size for $\dot{V}_{O_2}$ was low, thus $\dot{V}_{O_2}$ data were not used for further statistical analyses. Successful $\dot{V}_{O_2}$ were used to calculate RER and converted to energy expenditure. The estimated cost of sloughing ($J\ g^{-1}$) for an average 5 min sloughing duration relative to their minimal (assuming no activity during the surrounding 24 h period) daily energy expenditure ($J\ g^{-1}$ day) was calculated as percentage (%) sloughing expenditure per day.

4.3.8   Statistical analysis Statistical analysis

All analyses were performed in R.3.4.1 (R Core Team, 2018). Data were presented as means $\pm$ standard error (s.e.), and α was set at 0.05 for all statistical tests. For the allometric scaling of ion loss and MR, data were log10-transformed and grouped into uninfected and infected. Both ion loss and MR data were first log-transformed to meet the assumptions of normality. All models used a Gaussian error structure.

4.3.8.1   Ion loss

The scaling exponent for ion loss (Ci; $\Delta\ \mu S\ h^{-1}$) relative to surface area (A_v; cm^2) was calculated by linear regression. Differences in $\Delta\ Ci$ between each slough group were analysed using linear mixed effects (lme) models in the R 'lme4' package (Bates et al., 2014) with $\Delta\ Ci$ as the response variable,

slough cycle as a fixed effect. A_v (cm^2) was used as an additive covariate, and individual identity and number of exposure was included as a random effect to account for repeated measurements on the same individual, and the possible effect of exposure. A general linear hypothesis with Tukey contrasts was performed for multiple comparisons of means for both uninfected and infected treatments separately using the R 'multcomp' package (Hothorn et al., 2008). To examine interactions between slough groups and Bd load (log(ZE +1), a linear mixed effects (lmer) model using the R 'lmerTest' package (Kuznetsova et al., 2015) was performed. A summary ANOVA using type 2 Kenward-Roger approximation was performed, and post-hoc interactions analysed with Chi squared tests using the R 'phia' package (De Rosario-Martinez, 2013). For Δ Ci in the intermoult and mid-slough group, with the interaction between Bd load and A_v, a lme model was performed with A_v and Bd load as interactive covariate, and individual identity as a random effect to account for repeated measurements within individuals.

4.3.8.2   *Metabolic rate*

The scaling exponents of $\dot{V}_{CO_2}$ (ml h^{-1}) with body mass (M_b; g) were calculated by linear regression. Differences in $\dot{V}_{CO_2}$ between each slough group were analysed using linear mixed effects (lme) models in the R 'lme4' package with $\dot{V}_{CO_2}$ as the response variable, slough cycle and active MR as fixed effects. Body mass was included as an additive covariate, and individual identity and number of exposure as a random effect to account for repeated measurements on the same individual, and the possible effect of exposure. A general linear hypothesis with Tukey contrasts was performed for multiple comparisons of means for both uninfected and infected treatment separately using the R 'multcomp' package. To examine interactions between slough groups and Bd load (log(ZE +1)), a linear mixed effects (lmer) model using the R 'lmerTest' package (Kuznetsova et al., 2015) was performed. A summary ANOVA using type 2 Kenward-Roger approximation was performed. Model simplification was then performed using maximum likelihood in 'lmerTest' package to eliminate non-significant factors. Due to the non-significant interactive effect of slough groups and Bd load in the lmer model (log-likelihood ratio test; $\chi2 = 1.8$, df $= 1$, $P = 0.18$), it was removed, and the data were refitted to a simplified linear model removing the interactive effects. For $\dot{V}_{CO_2}$ in the intermoult and mid-slough group, and the interaction between Bd load and M_b, a lme model was performed with M_b and Bd load as interactive covariate, and individual identity as a random effect to account for repeated measurements within individuals.

4.4   RESULTS

4.4.1   Intermoult interval (IMI) and number of exposed animals

Intermoult interval (IMI) length was positively correlated with body mass ($t_{146} = 8$, $P = <0.001$), while Bd load was negatively correlated with IMI ($t_{146} = -2.3$, $P = 0.02$). There was an interactive effect between body mass, IMI and Bd load ($t_{146} = -2.3$, $P = 0.02$), with smaller individuals with high

Bd loads having the shortest IMI (**Fig. 4.2**). Animals with high *Bd* loads (>10,000 ZE) generally stopped performing the characteristic sloughing behaviour, but instead sloughed the *stratum corneum* in small fragments almost continuously. All animals infected (including re-exposure) either development chytridiomycosis or slowly increased infection load, with the exception of three animals that decreased infection load and recovered in the study.
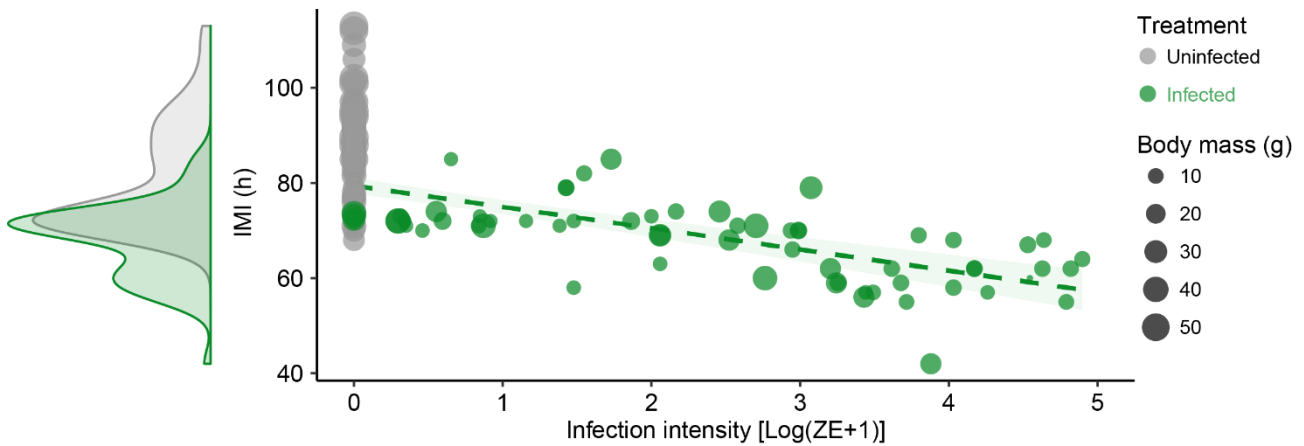
Fig. 4.2 │ Relationship between intermoult interval (IMI; h⁻¹), body size (g) and *Bd* infection intensity (Log (ZE +1)) in *Litoria caerulea*. Grey circles (●) represent uninfected animals, and infected circles (●) represent infected animals. Correlation between IMI and *Bd* load is 0.4 with a regression line of *IMI = -3.26(ZE +1) + 75.4*. Green shading represents 95 % confidence interval. The density plot represents distribution of IMI for uninfected and infected animals. Data were presented as individual points from uninfected (*n* = 21) and infected (*n* = 18) animals.

4.4.2   Ion loss

The rate of transcutaneous ion loss into the surrounding bath (as evidenced by an increase in conductivity; Δ Ci) was indistinguishable between the intermoult and day of slough groups and post slough groups within uninfected and infected treatments (**Table S4.1 and S4.2**). Sloughing however, had a significant effect on Δ Ci increasing by 70 times from 0.14 ± 0.02 μS cm² h⁻¹ in intermoult animals to 10.3 ± 0.6 μS cm² h⁻¹ during sloughing in uninfected animals ($z = 10.2$, s.e $= 0.04$, $P<0.001$; **Fig. 4.3**). For uninfected frogs during the intermoult phase, there was no significant correlation between rates of ion loss and ventral surface area (allometric exponent of 0.1; $t_{40} = 0.4$, $P = 0.7$; **Fig. 4.4A**). During sloughing, however, ventral surface area had a positive effect on rates of ion loss ($t_8 = 6.3$, $P = 0.0002$), with an allometric exponent of 0.86 (**Fig. 4.4B**).
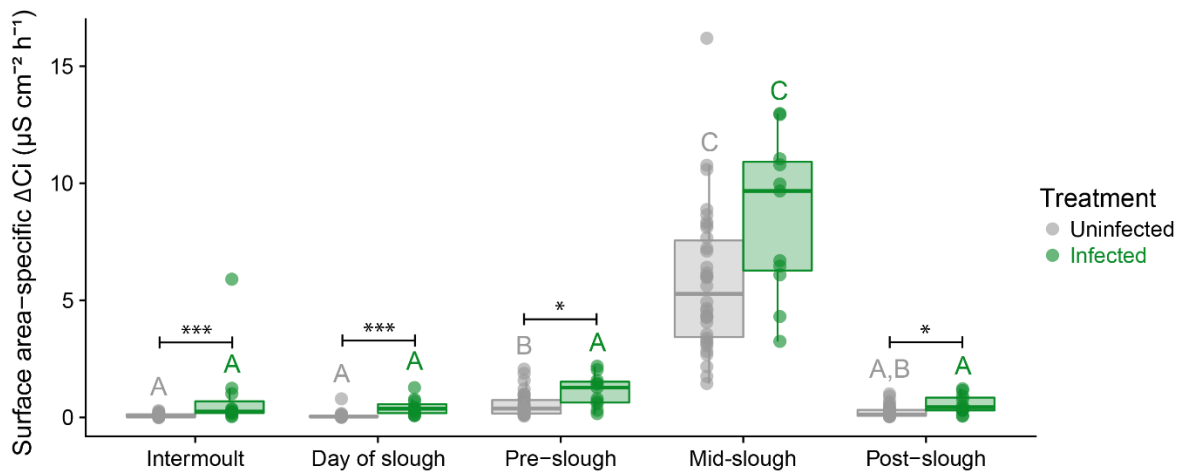
Fig. 4.3 │ Surface area-specific rate of change in conductivity (Δ Ci; μS cm² h⁻¹) between uninfected, and infected *L. caerulea* **through the sloughing cycle.** Data are presented as individual data points for uninfected (●, *n* = 33) and infected (●, *n* = 15) animals. Semi-transparent boxplots represent standard distribution of data. Within each treatment (infected or uninfected), slough groups with different letters above them are significantly different from one another. Significant differences between treatments for each slough group are indicated by asterisks. Summary statistics are presented in Tables S4.1, S4.2, & S4.3.
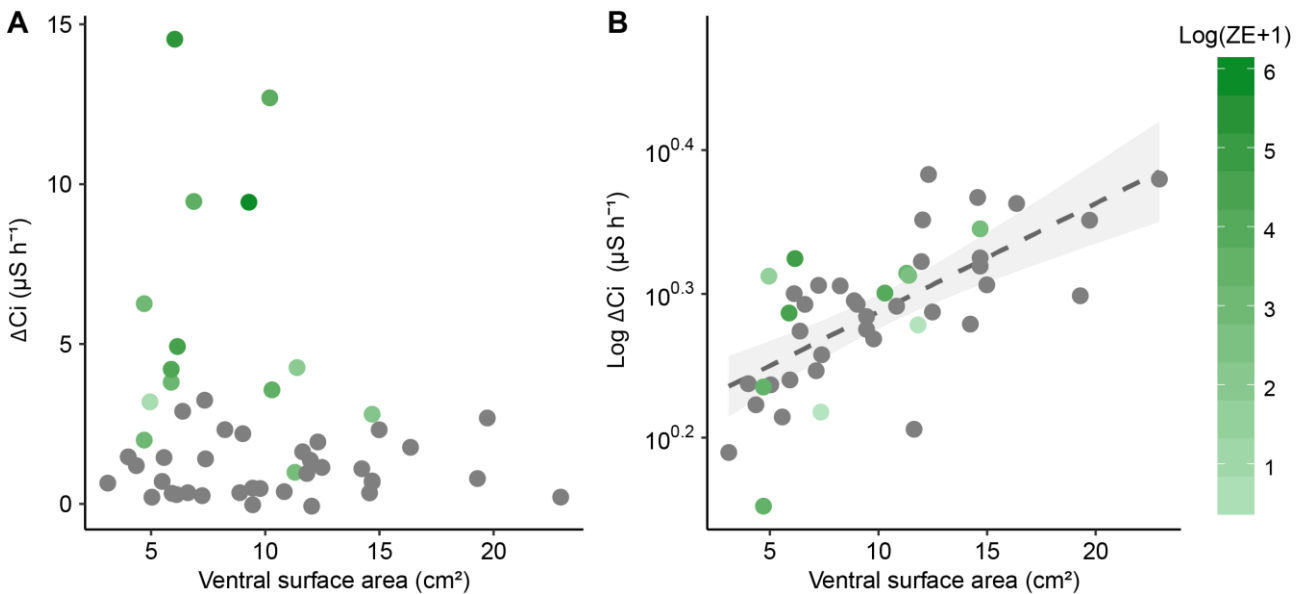
Fig. 4.4 │ Relationship between rate of change in conductivity (Δ *C*i; μS h⁻¹) and ventral surface area (*A*v; cm²) in *L. caerulea* **during A) intermoult and B) mid-slough periods.** Grey circles (●) represent uninfected animals, and gradient green circles (●) represent infected animals. Regression line for mid-slough represents an allometric scaling relationship of 0.87 ($Ci = 13A_v^{0.87}$, $r^2 = 0.72$) between surface area and rate of ion loss; grey shading represents 95 % confidence interval. Data presented as individual points from *n* = 33 uninfected frogs, *n* = 15 (intermoult) or 10 (mid-slough) *Bd* infected frogs.

During the intermoult period, there was a significant effect of *Bd* load on rates of ion loss, with ion efflux rates increasing with increasing *Bd* load ($t_{40} = 4.1$, $P = 0.002$; **Fig. 4.4A**). However, rates of ion loss during sloughing in infected and uninfected animals were not significantly different (**Fig. 4.4B**). Correcting for body mass, the increase in ion efflux rates with increasing *Bd* load accounted for 39 % of the variation during in both intermoult and day of slough stages (**Fig. 4.5A**). Like uninfected frogs, frogs infected with *Bd* had a higher rate of ion loss during sloughing ($z = 8.5$, s.e = 0.05, $P < 0.001$), compared to intermoult, day of sloughing and post-sloughing animals (**Fig. 4.3**).

There was no difference in the rate of ion loss between intermoult, day of sloughing, pre-sloughing and post-sloughing frogs infected with *Bd* (**Table S4.2**). When comparing with uninfected animals and accounting for *Bd* infection intensity (*Bd* load in zoospore equivalents, ZE) however, there was a significant interaction between all slough groups ($F_{1,4} = 4.14$, $P = 0.003$), with higher ion loss rates occurring in animals with higher infection loads (**Fig. 4.3**; **Table S4.3**). Ventral skin surface area did not affect ion loss rates during the non-sloughing phases of the moult cycle of infected animals ($t_{40} = -0.5$, $P = 0.6$), but like uninfected frogs, did significantly affect ion loss rates during the sloughing phase (**Fig. 4.3**). However, *Bd* infection did not alter the effect of sloughing on surface area-specific ion loss rates in frogs (**Fig. 4.4B**).
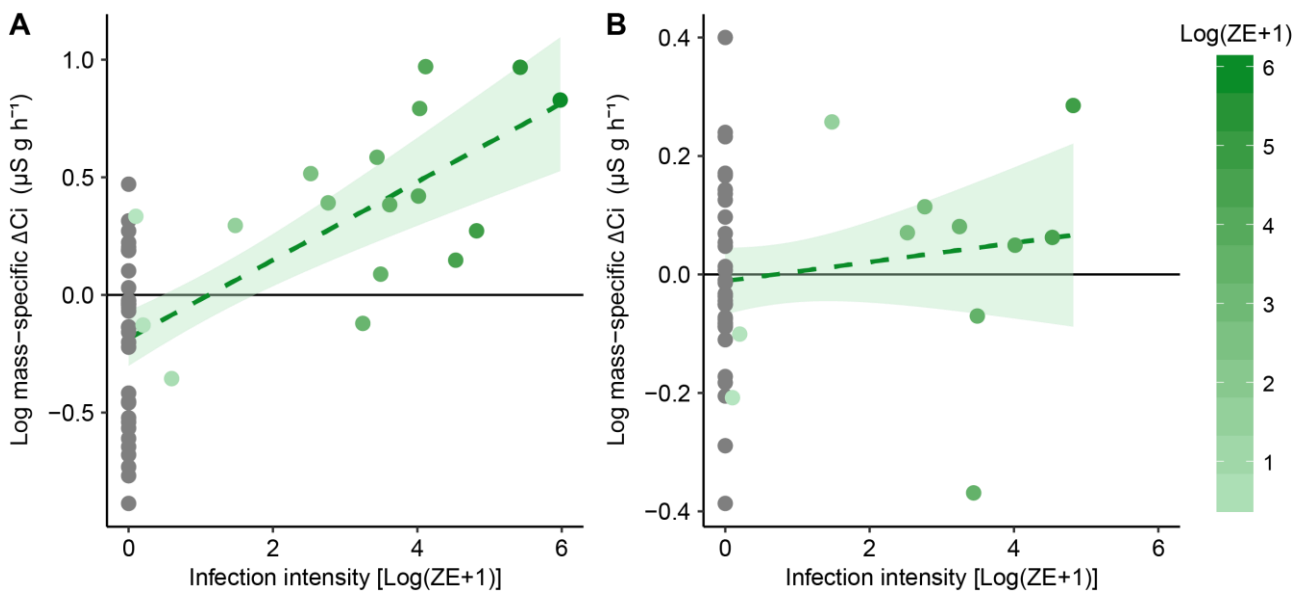
Fig. 4.5 │ Relationship between mass-specific residuals of rate of change in conductivity (Δ *C*i; µS g h⁻¹) and infection intensity (Log (ZE +1)) of *L. caerulea* during A) the intermoult, and B) mid-slough periods. Grey circles (●) represent uninfected animals, and green gradient circles (●) represent infected animals. Horizontal line denotes mean residual. Correlation between mass-specific Δ *C*i and infection intensity is 0.38 with a regression line of *Ci* = 0.14 *(ZE + 1)* − 0.06 for the intermoult group, and 0.09 with a regression line of *Ci* = 0.03 *(ZE + 1)* − 0.08 for mid-slough group. Green area shading around regression line represents 95 % confidence interval, and data presented as individual points from *n* = 33 uninfected frogs, *n* = 15 (intermoult) or 10 (mid-slough) *Bd* infected frogs.

Both uninfected and infected animals during sloughing had lower mass-specific ion loss rates compared to the fully permeable agar replica (uninfected $t_6 = -13$, $P < 0.001$, infected $t_6 = -7.8$, $P < 0.001$) indicating that ion loss rates were controlled and not unregulated during all phases of the sloughing cycle in both infected and uninfected frogs. The estimated net loss of Na⁺ (mmol h⁻¹) over the hour surrounding the sloughing event would represent ∼ 1.2 ± 0.26 % (uninfected) and ∼ 0.9 ± 0.4 % (infected) of the animals' total ECF Na⁺ pool. Body size had a significant effect on total Na⁺ loss ($t_{12} = 4.4$, $P = 0.001$), where the rate of Na⁺ loss was greater in smaller animals. The Na⁺ loss between uninfected and infected animals was not significantly different ($t_{12} = -0.9$, $P = 0.3$), and body size did not affect differences in Na⁺ loss between treatments ($t_{12} = 1.4$, $P = 0.1$).

4.4.3   Energetic cost of sloughing

During the intermoult phase, body mass had a highly significant effect on resting $\dot{V}_{CO_2}$ ($t_{16} = 10.6$, P <0.001; **Fig. 4.6**) with an allometric slope of 0.95 ($\dot{V}_{CO_2} = 0.025 M_b^{0.95}$; $r^2 = 0.95$). During sloughing, $\dot{V}_{CO_2}$ was also significantly affected by body mass ($t_2 = 13$, $P = 0.005$) with a scaling exponent of 0.98 ($\dot{V}_{CO_2} = 0.13 M_b^{0.98}$; $r^2 = 0.91$), as body mass increased, $\dot{V}_{CO_2}$ increased proportionally. Both uninfected and infected animals during sloughing had significantly higher $\dot{V}_{CO_2}$ than during all other stages of the sloughing cycle (**Table. S4.4 & 4.5**). For uninfected animals, the average rate of CO_2 production during sloughing was seven times higher than in non-sloughing animals, increasing from 0.02 ± 0.003 ml g^{-1} h^{-1} during the intermoult period to 0.14 ± 0.01 ml g^{-1} h^{-1} mid-slough ($z = 7.2$, s.e = 0.006, P <0.001; **Fig. 4.7**). This equates to an average energetic cost of 3.0 ± 0.5 J g^{-1} h^{-1} (**Table. 4.1**).
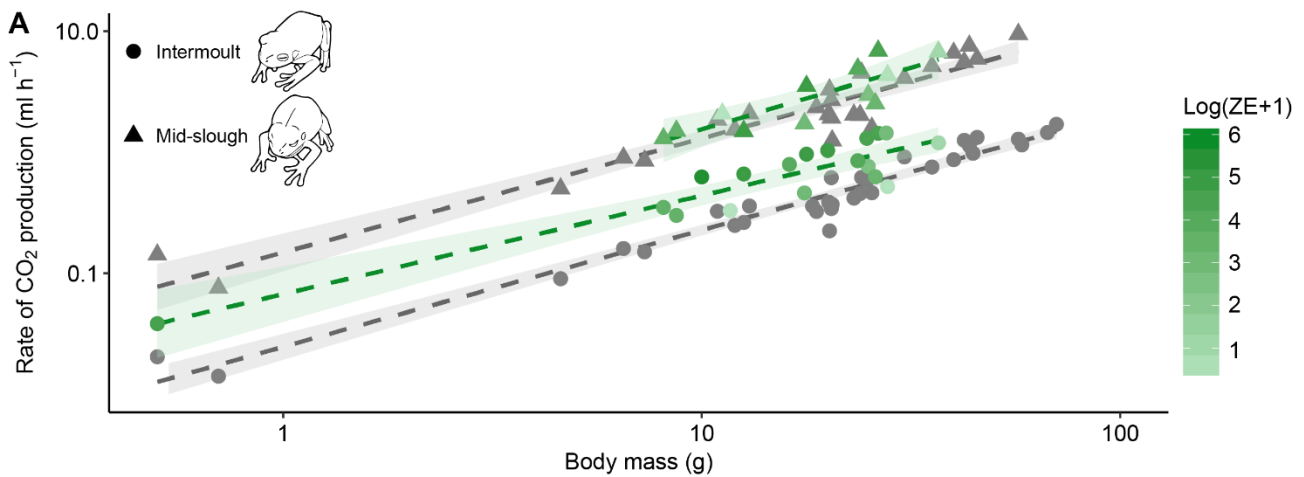
Fig. 4.6 │ The relationship between rate of CO₂ production ($\dot{V}_{CO_2}$; ml h⁻¹) and body mass (M_b; g) of *L. caerulea* during the intermoult and mid-slough periods. Grey circles (●) represent uninfected animals during intermoult period, grey triangles (▲) represent uninfected animals during mid-slough, green gradient circles (●) represent infected animals during the intermoult period, and green gradient triangles (▲) represent infected animals during mid-slough. Grey dashed regression lines (---) represents the relationship between mass and $\dot{V}_{CO_2}$ of uninfected animals (intermoult $\dot{V}_{CO_2} = 0.025 M_b^{0.95}$, $r^2 = 0.95$; Mid-slough $\dot{V}_{CO_2} = 0.13 M_b^{0.98}$, $r^2 = 0.91$), while green dashed regression lines (---) represents the relationship between mass and $\dot{V}_{CO_2}$ of infected animals (intermoult $\dot{V}_{CO_2} = 0.06 M_b^{0.8}$, $r^2 = 0.85$; Mid-slough $\dot{V}_{CO_2} = 0.15 M_b^1$, $r^2 = 0.7$). Shaded areas around regression lines represents 95 % confidence intervals. Data are presented as individual results from $n = 29$ uninfected and $n = 15$ infected intermoult animals, and $n = 28$ uninfected and $n = 10$ infected mid-slough animals.
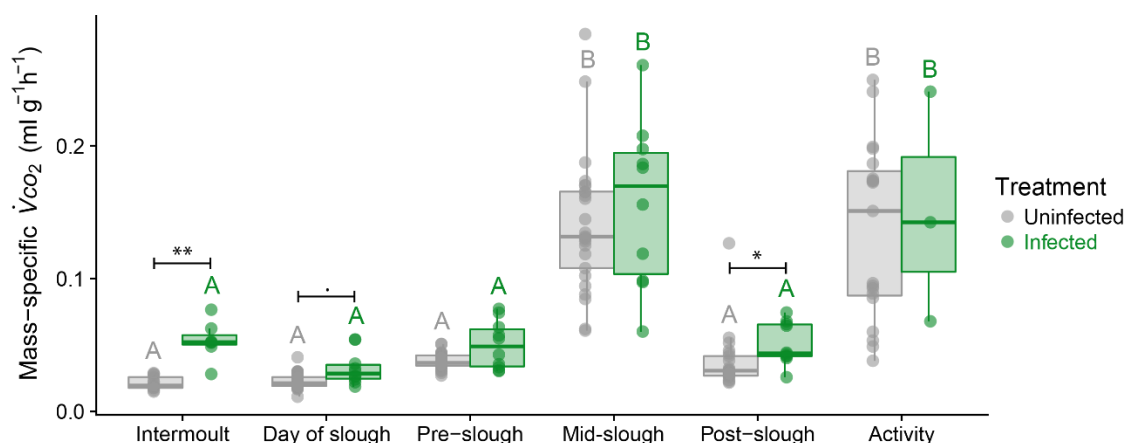
Fig. 4.7 │ Mass-specific rate of CO₂ production ($\dot{V}_{CO_2}$; ml g⁻¹ h⁻¹) between uninfected and infected *L. caerulea* during each recorded behaviour. Data presented as individual data points for uninfected (●, *n* = 29) and infected (●, *n* = 15) animals. Semi-transparent boxplots represent standard distribution of data. Within each treatment (infected or uninfected), slough groups with different letters above them are significantly different from one another. Significant differences between treatments for each slough group were indicated as asterisks. Summary statistics are presented in Tables S4.4, S4.5, & S4.6.

Table 4.1 │ Whole-animal metabolic parameters of infected and uninfected *Litoria caerulea* during the intermoult, mid-slough and active period. $\dot{V}_{O_2}$ = rate of oxygen consumption (ml g⁻¹ h⁻¹), $\dot{V}_{CO_2}$ = rate of carbon dioxide production (ml g⁻¹ h⁻¹), RER = respiratory exchange ratio, MR = equivalent metabolic rate (J g⁻¹ h⁻¹), *n* = sample size. Data presented as mean ± s.e.

			Metabolic parameters				
			$\dot{V}_{O_2}$		$\dot{V}_{CO_2}$	**RER**	**MR**
Treatment	**Group**	*n*	ml g⁻¹ h⁻¹	*n*	ml g⁻¹ h⁻¹	$\dot{V}_{CO_2}/\dot{V}_{O_2}$	J g⁻¹ h⁻¹
	Intermoult	8	0.03 ± 0.007	29	0.02 ± 0.001	0.79	0.5 ± 0.02
Control	Mid-slough	9	0.15 ± 0.03	29	0.14 ± 0.01	1.04	3.07 ± 0.5
	Active	7	0.17 ± 0.02	16	0.13 ± 0.01	0.81	2.8 ± 0.5
	Intermoult	3	0.04 ± 0.01	15	0.03 ± 0.004	1.07	0.70
Infected	Mid-slough	3	0.21 ± 0.05	10	0.16 ± 0.02	0.96	3.58
	Active	0		4	0.14 ± 0.04		

While there was a significant main effect of *Bd* load on $\dot{V}_{CO_2}$ ($F_{1,5}$ = 17, *P*<0.001; **Table S4.6**), post-hoc analysis revealed that the intermoult and day of slough group showed greatest differences in $\dot{V}_{CO_2}$ between infected and uninfected animals (**Fig. 4.7**; **Table S4.6**). During the intermoult phase, body mass significantly interacted with *Bd* load (allometric slope 0.8; t_{16} = 6.2, *P*<0.001) such that smaller infected animals had higher resting $\dot{V}_{CO_2}$ than larger infected animals (**Fig. 4.6**). Moreover, when accounting for body mass, increasing *Bd* load accounted for 65 % of the variation in $\dot{V}_{CO_2}$ during the intermoult phase of sloughing (**Fig. 4.8A**). However, during sloughing itself, there was no significant effect of *Bd* load on mass-corrected $\dot{V}_{CO_2}$ with increasing *Bd* load accounting for ~3 % of body-mass corrected $\dot{V}_{CO_2}$ (**Fig. 4.8B**). In both infected and non-infected frogs, a typical sloughing

event lasting for 5 min would account for <2 % of the frog's total daily (24 h) expenditure (non-infected ~1.38 %; infected ~1.46 %).
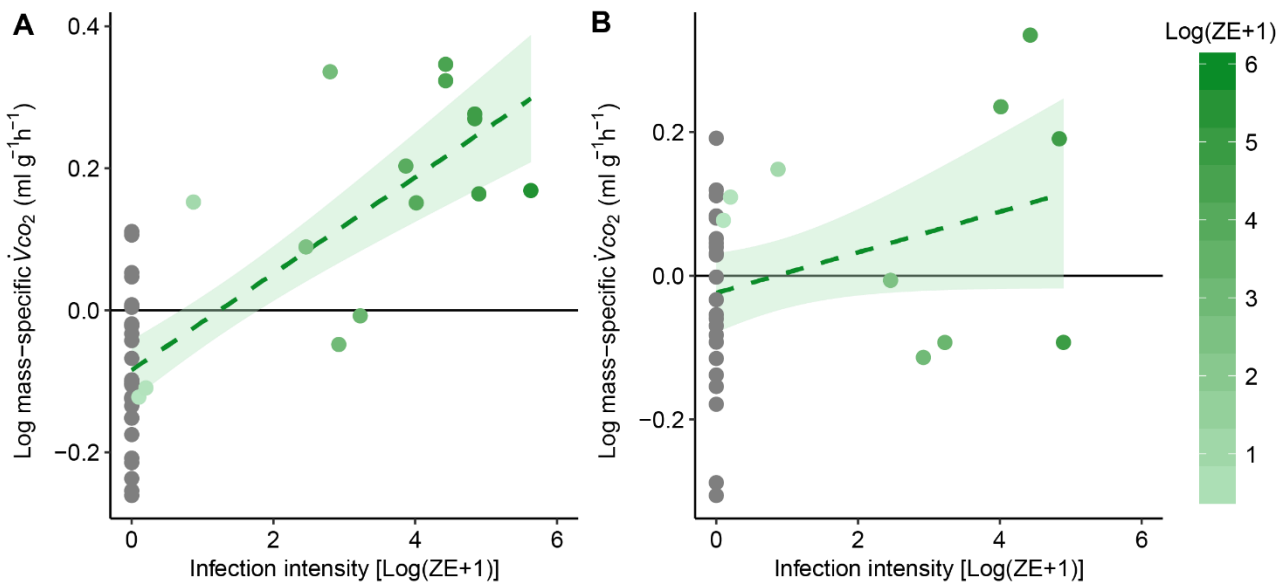
Fig. 4.8 │ Relationship between mass-specific residuals of rate of carbon dioxide production ($\dot{V}_{CO_2}$; ml g⁻¹ h⁻¹) and infection intensity (Log(ZE +1)) of *L. caerulea* during A) the intermoult, and B) mid-slough periods. Grey circles (●) represent uninfected animals, and green gradient circles (●) represent infected animals. Horizontal line denotes mean residual. Correlation between mass-specific $\dot{V}_{CO_2}$ and infection intensity is 0.46 with a regression line of $\dot{V}_{CO_2}$ = 0.06*(ZE + 1)* − 0.05 for the intermoult group, and 0.006 with a regression line of $\dot{V}_{CO_2}$= 0.006*(ZE + 1)* − 0.06 for the mid-slough group. Green area around regression line represents 95 % confidence interval, and data are presented as individual points of intermoult (uninfected *n* = 29, infected *n* = 15) and mid-slough (uninfected *n* = 28, infected *n* = 10).

4.5   DISCUSSION

Chytridiomycosis is an epidemic fungal disease affecting around 400 amphibian species worldwide (Bellard et al., 2016). Understanding its impact on host physiology is important to comprehend both inter- and intra-specific variation in disease susceptibility and morbidity. While sloughing has been shown to contribute to the clearing of *Bd* infections over time in some resistant species, more susceptible species continue to develop chytridiomycosis independent of changes in sloughing frequency (Ohmer et al., 2017). How sloughing and chytridiomycosis may interact in susceptible species to influence the loss of physiological homeostasis in susceptible species, still remains unknown. In the present study, we demonstrated that smaller frogs have shorter IMI than larger individuals, and IMI was further shortened when infected with *Bd*. We also found that frogs infected with *Bd* had a greater rate of cutaneous ion loss and higher resting metabolic rate (RMR) than uninfected individuals. Importantly, this effect was significantly exacerbated by body size, with smaller *L. caerulea* suffering much greater osmotic and metabolic imbalances than larger frogs. Interestingly, the rate of ion loss and metabolic rate (MR) during the actual sloughing event did not differ significantly between infected and uninfected individuals, suggesting that despite significant physical and physiological disruption, *Bd*-infected frogs were able to manage ion efflux to a certain degree during sloughing. However, the degree of physiological disruption from *Bd* increased as

animals become more heavily infected, which increases the likelihood that frogs would go onto develop clinical chytridiomycosis.

Body size did not affect rates of net transcutaneous ion loss in uninfected frogs during the intermoult phase, suggesting that healthy amphibians actively regulate cutaneous ion exchange rates to limit excessive ion loss during most of the sloughing cycle (Greenwald, 1972; Mullen and Alvarado, 1976). By contrast, small *L. caerulea* infected with *Bd* had a greater rate of cutaneous ion loss during the intermoult phase than larger individuals, and the rate of ion loss was exacerbated by increasing *Bd* load. The interaction between body size and *Bd* load may be due to greater surface area (relative to body volume) for *Bd* colonisation in smaller individuals (Klein et al., 2016), which is consistent with findings in wild *Mixophyes iteratus* showing that smaller individuals carried higher *Bd* loads than larger frogs (Kriger et al., 2006). Since *Bd* infects the skin, greater rates of ion loss with higher *Bd* loads might result from direct disruption of skin structure (Berger et al., 1998; Berger et al., 2005b) and/or through inhibition of skin ion transport proteins (Campbell et al., 2012). Similar disruption of other biological processes (reduced body mass, higher RMR and plasma corticosterone, and lower lymphocytes) have also be related to *Bd* load (Peterson et al., 2013), where the greater the *Bd* load, the greater the disruption of homeostatic balance.

The act of sloughing itself increased cutaneous ion-loss rates by 10-fold compared to frogs in the intermoult phase of the slough cycle. Moreover, smaller individuals had disproportionally greater rates of ion loss during sloughing than larger individuals. The relationship between body size and ion loss during sloughing in green tree frogs (exponent of 0.87) is similar to that observed in molting crayfish (*Procambarus clarkii*) (scaling exponent of 0.9)(Zanotto et al., 2004). Although *Bd* load affected rates of ion loss during the non-sloughing phases of the moult cycle, *Bd* infection did not exacerbate ion loss rates, relative to uninfected animals, during sloughing. Under low to moderate infections (<10,000 ZE), animals tend to perform normal sloughing behaviour. However, at high *Bd* loads (>10,000 ZE), animals cease the characteristic sloughing behaviours (Ohmer et al., 2015), and instead the slough detaches almost continuously in fragments (Nichols et al., 2001; Berger et al., 2005b; Peterson et al., 2013). The increase in ion loss that accompanies sloughing, to some extent, reflects the increase in activity associated with the physical removal of the slough itself. Conceivably then, frogs with heavy *Bd* loads and clinical chytridiomycosis may behaviourally avoid additional ion losses incurred during sloughing by stopping the behavioural process completely. Whether this reflects a deliberate avoidance of ion loss by heavily infected frogs or simply reflects the overall lethargy characteristic of frogs with severe chytridiomycosis (Nichols et al., 2001; Voyles et al., 2009), remains unclear.

While the skin becomes increasingly 'leaky' to ions during sloughing, it does not become fully permeable to ions like in the agar frog replica in this study, suggesting that both infected and

uninfected frogs maintain the ability to regulate their rate of ion loss during sloughing. This suggests that even in *Bd* infected frogs, the underlying skin layers maintain a degree of resistance to passive ion loss during sloughing despite the changes that are occurring in the more superficial layers. In addition, sloughing toads increased their cutaneous ion uptake activity and increased skin resistance to control ion losses during sloughing (Wu et al., 2017). This increase in cutaneous ion regulatory expression may also come at a physiological cost in the longer term as increasing *Bd* loads stimulate sloughing in *L. caerulea* (Ohmer et al., 2015). Once *Bd* loads reach a threshold intensity, however, control of cutaneous ion loss rates becomes more difficult and animals may stop sloughing altogether to reduce the physiological and energetic costs of sloughing.

Although sloughing only contributed to <2 % of their daily expenditure, *Bd*-infected animals slough up to 25 % more frequently than uninfected animals (Ohmer et al., 2017). Increased sloughing frequency in *Bd*-infected frogs likely has a cumulative, and ultimately detrimental, effect on the physiological balance of frogs infected with *Bd* (Carver et al., 2010; Peterson et al., 2013). Increases in both MR and rates of ion loss during sloughing appear to be largely due to the behavioural action of removing the slough. However, the changes in the cellular physiology that accompany sloughing including epidermal cellular proliferation (Vander Heiden et al., 2009), formation of tight junctions and desmosomes (Budtz and Larsen, 1975), and upregulating ion and water transport activity to account for leakage of skin (Civan et al., 1983; Wu et al., 2017) also contribute to the increased sloughing-associated energy expenditure.

Non-sloughing green tree frogs infected with *Bd* had a significantly higher RMR compared to uninfected animals, consistent with earlier observations (Peterson et al., 2013). However, our data show that there was a strong interaction with body size and *Bd* load on RMR, with smaller infected animals having a higher RMR and higher *Bd* loads than large ones. Our data suggest that not only the $\dot{V}_{CO_2}$ intercept increases with *Bd* load, but the slope shifts from 0.96 to 0.8 suggesting smaller infected animals have greater mass-specific metabolic costs. While interpretations of scaling exponents should be taken with caution (Packard and Birchard, 2008), our results suggest the greater RMR in smaller infected frogs is due to increased energy expenditure for biological maintenance. For example, changes in whole-animal MR in response to a pathogen could indicate the additional costs associated with mounting an immune response (Demas et al., 2011; Rollins-Smith and Woodhams, 2012). *Bd* stimulates a suite of immune responses in infected frogs (Van Rooij et al., 2015; Rollins-Smith, 2017), and the increased immune investment by infected animals may contribute to the increased RMR observed here. Ontological differences in immune responses to *Bd* may also contribute to the differences in mass-specific MR observed (Rollins-Smith, 1998; Rollins-Smith, 2017). The juvenile period is a vulnerable period for infection (Rollins-Smith, 1998),

and the demand to fight off infection may require that juvenile frogs allocate more energy to the immune responses than older frogs.

Frogs with heavy *Bd* loads have higher rates of ion loss and energy expenditure during non-sloughing periods. Increased rates of ion loss necessitate higher rates of compensatory cutaneous uptake. Under *in-vitro* conditions, the active uptake of 18 Na^+ ions by healthy amphibian skin costs approximately one mole of O_2 (Zerahn, 1956; Leaf and Dempsey, 1960), so an increase in cutaneous ion efflux would require a higher cellular respiration rate to maintain salt balance (Civan et al., 1983). Since chytridiomycosis also disrupts cutaneous ion uptake capacity (Voyles et al., 2009), frogs with heavy *Bd* loads may need to invest even more energy in ion uptake to compensate for higher rates of ion efflux and reduced uptake capabilities. In smaller frogs with a large surface area to volume ratio, this effect is likely to be magnified and probably contributes to the higher rates of fatal chytridiomycosis in juvenile frogs.

Our data explain, in part at least, why *Bd*-associated mortality rates are often much higher in juvenile frogs. Smaller (and therefore, younger) anurans carry higher infection loads, and are at greater risk of osmoregulatory and metabolic disruptions when infected with *Bd* on account of the allometric scaling of both MR and cutaneous ion loss rates. Although sloughing only transiently increased MR and ion loss rates in frogs, increasing *Bd* load did not exacerbate these changes further. However, the increase in sloughing frequency in small frogs and those with heavy *Bd* infections, may have long-term cumulative effects on the capacity of frogs to maintain homeostatic balance. Further work is needed to determine if the effects observed in the current study are consistent across *Bd* susceptible species and if body size predicts morbidity in *Bd* susceptible species, independent of age.

4.6   SUPPLEMENTARY INFORMATION

4.6.1   Supplementary figures
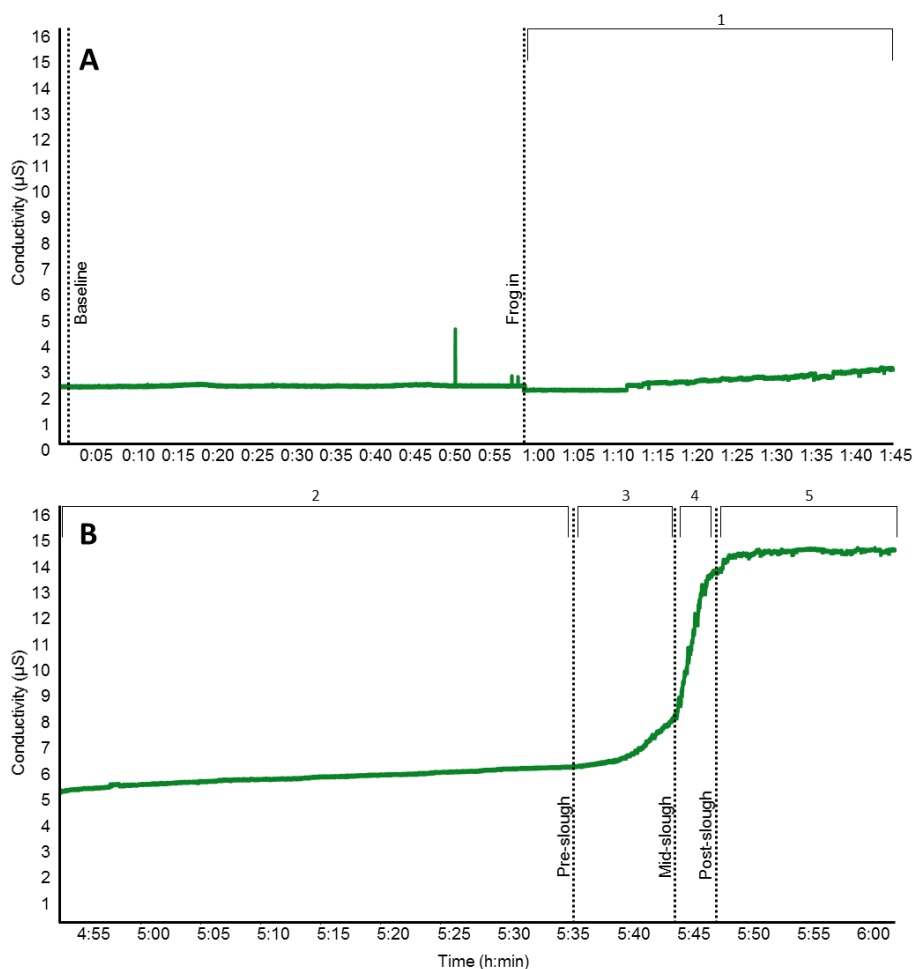
Fig. S4.1 │ Example raw trace from Labchart of change in conductivity readings for one uninfected *Litoria caerulea* during A) the intermoult period, and B) the sloughing period. Body mass (M_b) = 27.7 g, snout-vent length (SVL) = 75.4 cm. 'Baseline' values were obtained from the chamber water in absence of animals; 'Frog in' data was when the (1) Intermoult data was obtained with the animal inside the experimental chamber. (2) Indicates 'day of sloughing', (3) indicates 'pre-slough', (4) indicates 'mid-slough', and (5) indicates 'post-slough' period of measurements.
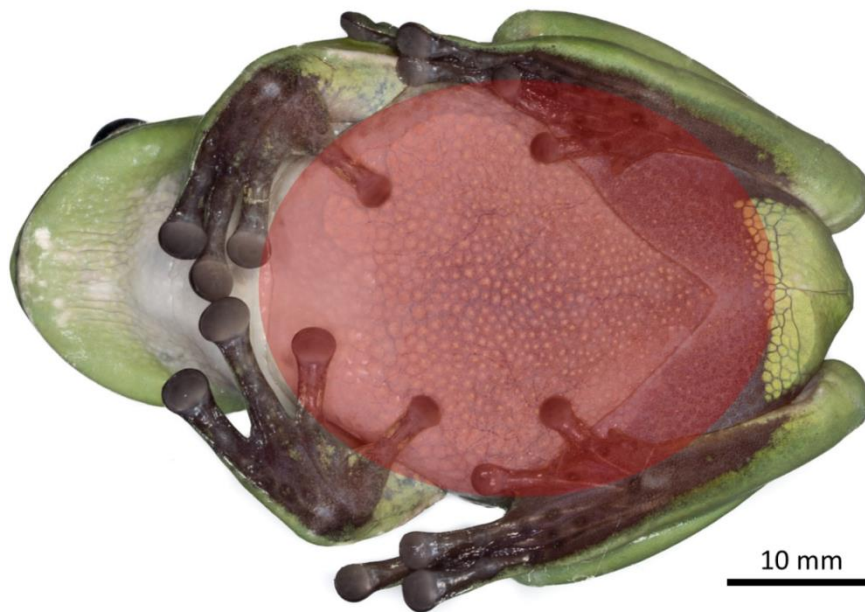
Fig. S4.2 │ Photograph of a green tree frogs' (*Litoria caerulea*) ventral side in its resting posture. The red semi-transparent circle represents the surface area (cm²) calculated in Image J. Photo credit: C. Baker.
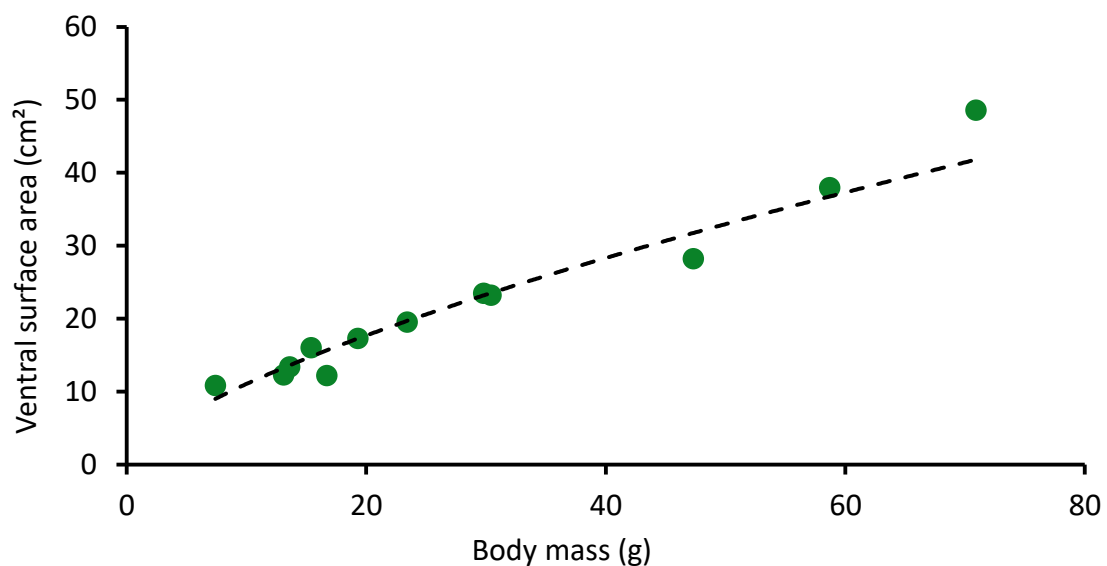
Fig. S4.3 │ Relationship between ventral surface area (A_v, cm²) and body mass (M_b, g) of various sized *Litoria caerulea*. Regression line represents an allometric slope of 0.68 ($A_v = 2.3 M_b^{0.68}$, $r^2 = 0.94$).
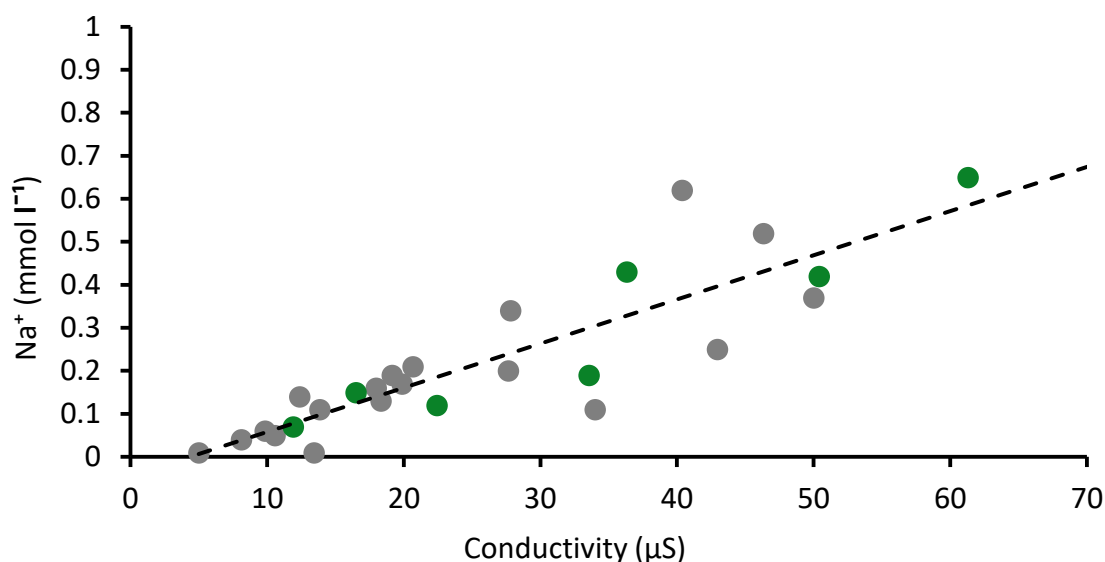
Fig. S4.4 │ Relationship between sodium (Na⁺) levels (mmol I⁻¹) and conductivity (µS) of sloughed water solutions between uninfected (●), and infected (●) *Litoria caerulea*. Correlation between conductivity and Na⁺ levels is 0.75 with a regression line of Na⁺ = 0.01(conductivity) – 0.04.

4.6.2   Supplementary tables

Table S4.1 │ Summary factor interactions from linear mixed effects model for the rate of conductivity between sloughing groups (intermoult, day of slough, pre-slough, mid-slough, and post-slough) for uninfected animals. Covariates were ventral surface area, and frog ID as random variable to correct for repeated measurements**.** *z* value = regression coefficient divided by standard error, s.e. = standard error of mean, and *P* = *P* value with α set at 0.05. Significant codes: 0 '***' 0.001 '**' 0.01 '*' 0.05 '.' 0.1 ' ' 1.

Groups – Uninfected					
Fixed Effects	**Estimate**	**s.e.**	**z value**	***P***	
Post-slough - Intermoult	0.05748	0.04789	1.2	0.751	
Pre-slough - Intermoult	0.15283	0.04746	3.22	**0.0113**	*
Day of slough - Intermoult	-0.03306	0.05002	-0.661	0.9645	
Mid-slough - Intermoult	0.48375	0.04746	10.194	**<0.001**	***
Pre-slough - Post-slough	0.09535	0.0451	2.114	0.2136	
Day of slough - Post-slough	-0.09054	0.04741	-1.91	0.3117	
Mid-slough - Post-slough	0.42628	0.0451	9.452	**<0.001**	***
Day of slough - Pre-slough	-0.18589	0.04717	-3.941	**<0.001**	***
Mid-slough - Pre-slough	0.33092	0.04468	7.406	**<0.001**	***
Mid-slough - Day of slough	0.51682	0.04717	10.957	**<0.001**	***

Table S4.2 │ Summary factor interactions from linear mixed effects model for the rate of conductivity between sloughing groups (intermoult, day of slough, pre-slough, mid-slough, and post-slough) for infected animals. Covariates were ventral surface area, and frog ID and number of exposure as random variable to correct for repeated measurements and influence of exposure. *z* value = regression coefficient divided by standard error, s.e. = standard error of mean, and *P* = P value with α set at 0.05. Significant codes: 0 '***' 0.001 '**' 0.01 '*' 0.05 '.' 0.1 ' ' 1.

Groups – Infected					
Fixed Effects	**Estimate**	**s.e.**	**z value**	**P**	
Post-slough - Intermoult	0.042014	0.048814	0.861	0.9108	
Pre-slough - Intermoult	0.128043	0.048814	2.623	0.0658	.
Day of slough - Intermoult	0.033768	0.049267	0.685	0.9595	
Mid-slough - Intermoult	0.416905	0.048814	8.541	**<0.001**	***
Pre-slough - Post-slough	0.086029	0.043196	1.992	0.2691	
Day of slough - Post-slough	-0.008425	0.045215	-0.182	0.9998	
Mid-slough - Post-slough	0.374891	0.043196	8.679	**<0.001**	***
Day of slough - Pre-slough	-0.094275	0.045215	-2.085	0.2257	
Mid-slough - Pre-slough	0.288862	0.043196	6.687	**<0.001**	***
Mid-slough - Day of slough	0.383137	0.045215	8.474	**<0.001**	***

Table S4.3 │ Summary statistics for rate of conductivity between sloughing groups (intermoult, day of slough, pre-slough, mid-slough, and post-slough) with ZE as interactive effects, and ventral surface area (A_v) as additive effect. Top: Type 2 ANOVA with Kenward-Roger approximation for degrees of freedom between groups, with ZE as interactive effects, and ventral surface area (A_v) as additive effect. Bottom: Post-hoc Chi-square test with Holm-Bonerroni method for the interactions between groups, and treatment accounting for ZE. Sum Sq = sum of squares, Mean Sq = mean squared error, Df = degrees of freedom, NumDF = numerator degrees of freedom, DenDF = denominator degrees of freedom, Chisq = Chi square test, and *P* = P value with α set at 0.05. Significant codes: 0 '***' 0.001 '**' 0.01 '*' 0.05 '.' 0.1 ' ' 1.

Analysis of Variance Table of type II with Kenward-Roger approximation for degrees of freedom							
	Sum Sq	**Mean Sq**	**NumDF**	**DenDF**	**F value**	**P**	
Group	338.54	84.635	4	176.8	324.78	**<0.001**	***
Bd	15.09	15.088	1	158.574	57.9	**<0.001**	***
A_v	8.02	8.02	1	38.367	30.78	**<0.001**	***
Group:*Bd*	4.31	1.078	4	181.878	4.14	**0.003126**	**
Chisq Test:							
P-value adjustment method: holm							
	Value	**Df**	**Chisq**	**P**			
Control-Infected : Intermoult	0.246840	1	25.7964	**<0.001**	***		
Control-Infected : Day of slough	0.306983	1	39.4300	**<0.001**	***		
Control-Infected : Pre-slough	0.159511	1	8.5481	**0.01038**	*		
Control-Infected : Mid-slough	0.033617	1	0.3797	0.53778			
Control-Infected : Post-slough	0.140524	1	6.6133	**0.02024**	*		

Table S4.4 │ Summary factor interactions from linear mixed effects model for the rate of CO₂ production between sloughing groups (intermoult, day of slough, pre-slough, mid-slough, post-slough, and active) for uninfected animals. Covariates were body mass, and frog ID as random variable to correct for repeated measurements. *z* value = regression coefficient divided by standard error, s.e. = standard error of mean, and *P* = *P* value with α set at 0.05. Significant codes: 0 '***' 0.001 '**' 0.01 '*' 0.05 '.' 0.1 ' ' 1.

Groups – Uninfected					
Fixed Effects	**Estimate**	**s.e.**	**z value**	***P***	
Intermoult – Active	-0.03383	0.0066	-5.126	**<0.001**	***
Post-slough – Active	-0.026	0.005901	-4.407	**<0.001**	***
Pre-slough – Active	-0.02764	0.005647	-4.894	**<0.001**	***
Day of slough – Active	-0.03612	0.005616	-6.431	**<0.001**	***
Mid-slough – Active	0.01168	0.005616	2.08	0.296	
Post-slough - Intermoult	0.007827	0.006403	1.222	0.824	
Pre-slough - Intermoult	0.006189	0.006275	0.986	0.922	
Day of slough - Intermoult	-0.00229	0.006247	-0.366	0.999	
Mid-slough - Intermoult	0.04551	0.006247	7.285	**<0.001**	***
Pre-slough - Post-slough	-0.00164	0.005387	-0.304	1	
Day of slough - Post-slough	-0.01011	0.005354	-1.889	0.406	
Mid-slough - Post-slough	0.037682	0.005354	7.039	**<0.001**	***
Day of slough - Pre-slough	-0.00848	0.005131	-1.652	0.561	
Mid-slough - Pre-slough	0.039321	0.005131	7.664	**<0.001**	***
Mid-slough – Day of slough	0.047797	0.005059	9.448	**<0.001**	***

Table S4.5 │ Summary factor interactions from linear mixed effects model for the rate of CO₂ production between sloughing groups (intermoult, day of slough, pre-slough, mid-slough, post-slough, and active) for infected animals. Covariates were body mass, and frog ID and number of exposure as random variable to correct for repeated measurements and influence of exposure. *z* value = regression coefficient divided by standard error, s.e. = standard error of mean, and *P* = *P* value with α set at 0.05. Significant codes: 0 '***' 0.001 '**' 0.01 '*' 0.05 '.' 0.1 ' ' 1.

Groups – Infected					
Fixed Effects	**Estimate**	**s.e.**	**z value**	***P***	
Intermoult – Active	-0.03567	0.009451	-3.774	**0.00217**	**
Post-slough – Active	-0.03636	0.008595	-4.231	**< 0.001**	***
Pre-slough – Active	-0.03652	0.008601	-4.245	**< 0.001**	***
Day of slough – Active	-0.04557	0.008595	-5.302	**< 0.001**	***
Mid-slough – Active	-0.00361	0.008595	-0.42	0.998261	
Post-slough - Intermoult	-0.0007	0.006881	-0.101	0.999998	
Pre-slough - Intermoult	-0.00085	0.00691	-0.123	0.999996	
Day of slough - Intermoult	-0.0099	0.006881	-1.439	0.694956	
Mid-slough - Intermoult	0.032058	0.006881	4.659	**< 0.001**	***
Pre-slough - Post-slough	-0.00015	0.005659	-0.027	1	
Day of slough - Post-slough	-0.0092	0.005689	-1.618	0.57716	

Mid-slough - Post-slough	0.032756	0.005689	5.758	**< 0.001**	***
Day of slough - Pre-slough	-0.00905	0.005659	-1.6	0.58946	
Mid-slough - Pre-slough	0.032907	0.005659	5.815	**< 0.001**	***
Mid-slough – Day of slough	0.041959	0.005689	7.376	**< 0.001**	***

Table S4.6│Summary statistics rate of conductivity between sloughing groups (intermoult, day of slough, pre-slough, mid-slough, post-slough, and activity) with ZE as interactive effects, and body mass as additive effect. Top: Type 2 ANOVA with Kenward-Roger approximation for degrees of freedom between groups with ZE as interactive effects, and body mass as additive effect. Bottom: Post-hoc Chi-square test with Holm-Bonerroni method for the interactions between groups, and treatment, accounting for ZE. Sum Sq = sum of squares, Mean Sq = mean squared error, Df = degrees of freedom, NumDF = numerator degrees of freedom, DenDF = denominator degrees of freedom, Chisq = Chi square test, and P = P value with α set at 0.05. Significant codes: 0 '***' 0.001 '**' 0.01 '*' 0.05 '.' 0.1 ' ' 1.

Analysis of Variance Table of type II with Kenward-Roger approximation for degrees of freedom						
	Sum Sq	Mean Sq	NumDF	DenDF	F value	P
Group	23.524	4.7048	5	139.178	90.803	**< 0.001**	***
Bd	0.8827	0.8827	1	96.776	17.036	**< 0.001**	***
Body mass	11.326	11.326	1	40.268	218.593	**< 0.001**	***
Group:*Bd*	0.3212	0.0642	5	147.549	1.24	0.2934	

Chisq Test:				
P-value adjustment method: holm				
	Value	Df	Chisq	P
Control-Infected : Intermoult	0.08487	1	10.1497	**0.008659**	**
Control-Infected : Day of slough	0.06179	1	5.7992	0.064134	.
Control-Infected : Pre-slough	0.03486	1	1.8047	0.420224	
Control-Infected : Mid-slough	0.03012	1	1.3905	0.420224	
Control-Infected : Post-slough	0.07094	1	7.3608	**0.033331**	*
Control-Infected : Activity	- 0.40750	1	2.1771	0.420224	

Mechanistic basis for the loss of water balance in green tree frogs infected with a fungal pathogen

5.1   ABSTRACT

Chytridiomycosis, a lethal skin disease caused by the fungal pathogen *Batrachochytrium dendrobatidis* (*Bd*) disrupts skin function of amphibians, interfering with ionic and osmotic regulation. To regulate infection load, amphibians can increase their rate of skin shedding (sloughing). However, sloughing also causes a temporary loss of ionic and osmotic homeostasis, due to disruption to the skin, a key osmoregulatory organ. Consequently, the combined disruption from increased sloughing frequency and chytridiomycosis may contribute to the high rates of mortality from *Bd* infections. However, the mechanisms behind the interaction on osmotic homeostasis and regulation remains unknown. We measured the changes in whole-animal water uptake rates, in-vitro trans-cutaneous water fluxes across the ventral skin and the expression of epithelial water transport proteins (aquaporins, AQPs) in *Bd*-infected and uninfected *Litoria caerulea* skin. We hypothesised that infected frogs would show a reduction/inhibition in cutaneous water transporters responsible for regulating water balance, and that in infected animals, sloughing would further exacerbate cutaneous water fluxes and compromise water imbalance. We found that infected, non-sloughing frogs had an impaired capacity to take up water, and had an increased rate of in-vitro water efflux across the ventral skin. Immediately after sloughing, the expression of AQPs genes in the skin of uninfected animals was significantly higher than that of non-sloughing frogs, which may assist in regulating cutaneous water movements in the newly exposed skin. In contrast, infected frogs did not show this post-sloughing increase in AQP gene expression. The combination of increased sloughing frequency, impaired water uptake and increased rate of water loss contributes to the loss of osmotic homeostasis in frogs infected with *Bd*. Our findings provide insights into the mechanisms underlying disruption of the barrier function associated with chytridiomycosis under different environmental contexts.

5.2   INTRODUCTION

Terrestrial amphibians are prone to dehydration due to their highly permeable skin which, while serving as protection from the external environment, also allows the active exchange of respiratory gases, ions and water with the environment (Boutilier et al., 1992). In aquatic environments, however, amphibians are prone to gaining water (influx) as water moves passively via osmosis, across the skin from the low-salt, freshwater environment (external environment) to the high-salt, internal environment (Evans, 2008). Amphibians employ a number of strategies to regulate the cutaneous influx/efflux of water. For example, some terrestrial amphibians produce a cutaneous surface fluid (Larsen et al 2013), or a waxy water-proof secretion (cutaneous layer of lipids) to generate an extremely low permeability to evaporative water loss (EWL) (McClanahan Jr et al., 1978; Lillywhite, 2006), while at the cellular level, the movement of ions and water across the skin is tightly regulated. Water can move between cells (paracellular pathway) or through cells (transcellular). The paracellular pathway comprises a network of intercellular linking junctions that form a selective barrier to ion and water movement (Farquhar and Palade, 1965; Niessen,

2007). These paracellular junctions have been shown to regulate water movement across epithelia in mammals (Furuse et al., 2002; Kawedia et al., 2007; Rosenthal et al., 2010) and fish (Kwong et al., 2013). The movement of water across the skin via the transcellular pathway is facilitated by a family of highly conserved transmembrane proteins called 'aquaporins' (AQPs) (Hillyard et al., 2008; Finn et al., 2014).

In amphibians, AQPs are expressed in the skin, liver, kidney, gastrointestinal tract, and skeletal muscles (Pandey et al., 2010). Furthermore, a distinct subset predominate in the ventral (pelvic and hindlimb) skin of semi-terrestrial anurans (Willumsen et al., 2007; Ogushi et al., 2010a). AQPs exhibit rapid plasticity by either increasing or decreasing in abundance and/or activity in response to environmental conditions to regulate water resorption or secretion across the skin. For example, the expression of several AQP (AQP5 (formally AQP-xt5a) and AQP5-like (formally AQP-xt5b)) genes increased in both the ventral and dorsal skin of dehydrated *Xenopus tropicalis* (Shibata et al., 2014). For terrestrial and arboreal frogs, there are amphibian–specific AQPs found only in the ventral pelvic patch of the epidermis like AQP6ub (formally AQP-h2; Hasegawa et al., 2003) and AQP6vs (formally AQP-h3; Tanii et al., 2002), which are responsible for 70-80 % of the animals' total water uptake (McClanahan Jr and Baldwin, 1969; Christensen, 1974).

To maintain the skins' integrity and ensure proper osmoregulatory function, amphibians go through a process known as 'sloughing' to regularly replace the outer-most layer of the epidermis, the *stratum corneum* (Larsen, 1976). Sloughing has been shown to significantly increase the permeability of the skin leading to increased ion efflux (Wu et al., 2017), an increase in water uptake rates in aquatic environments (Jørgensen, 1949; Ewer, 1951), and increased water loss rates in dry environments (Russo et al., 2018). Although the ionic and osmotic disruption to skin during sloughing can be substantial, we have shown that in healthy amphibians, there is no evidence for a loss of internal ion homeostasis (Wu et al., 2017). We hypothesised that sloughing frogs may upregulate the transcellular and/or paracellular movement of water to compensate for the increase in skin permeability from sloughing. The same response may occur with water transport proteins, however this remains to be tested.

Sloughing has also been shown play an important role in immune defence, aiding in the removal of potential cutaneous pathogens before they can establish an infection (Ohmer et al., 2017). One particularly important cutaneous pathogen of amphibians is the fungus *Batrachochytrium dendrobatidis* (*Bd*). *Bd* is the causative agent of the fatal skin disease chytridiomycosis, and is responsible for a number of significant amphibian declines around the world (Olson et al., 2013, http://www.bd-maps.net/surveillance/). Chytridiomycosis affects the osmoregulatory functions of amphibian skin by disrupting skin structure (Berger et al., 2005c) and by supressing cutaneous ion transport (Voyles et al., 2009). Importantly, some frog species increase their rate of sloughing

following infection with *Bd*, which in turn reduces their *Bd* load and prevents them from developing clinical chytridiomycosis (Ohmer et al., 2017). However, increased sloughing frequency can be detrimental for some frog species that are unable to remove the fungus completely or quickly enough (Ohmer et al., 2017). In these frogs, the combined effect of increased sloughing frequency and damage from *Bd* further exacerbates the loss of cutaneous function (Wu et al., 2018).

Bd infection had been shown to disrupt water balance in amphibians. Frogs infected with *Bd*, display evidence of dehydration (increased haematocrit and increase plasma protein levels; Voyles et al., 2012a). Under laboratory conditions, *Bd* infection increases the rate of evaporative water loss (EWL) in some (but not all) species (Carver et al., 2010; Russo et al., 2018), and also impedes water uptake in some species (Carver et al., 2010; Wardziak et al., 2013). The underlying mechanism behind these disruptions not well understood. However, there are some evidence for integument dysfunction that may increase osmotic leakage (Berger et al., 2005a; Brutyn et al., 2012). Water transport may also be disrupted indirectly with cutaneous ion transport disruption (Wu et al., 2019), or directly at the AQPs. For example, viral infection in mouse lungs have shown to reduce gene expression of APQ1 and AQP5 that maintain mucus formation in the lungs (Towne et al., 2000). The consequential effects for the loss of control of cutaneous water flux can eventually lead to hyponatremia (Voyles et al., 2007) for aquatic frogs. Symptoms of hyponatremia including fatigue, muscle weakness, spasm, and death, which have been observed in frogs with chytridiomycosis (Voyles et al., 2009). While for terrestrial frogs, cutaneous disruption may increase dehydration through increased EWL, and reduced water uptake (Voyles et al., 2012a; Russo et al., 2018). Amphibians may be susceptible under both wet and dry conditions because field observations have shown that during the rainfall season, *Bd* prevalence in the environment is higher (increasing likelihood of infection), while in drier seasons, amphibians tend to have higher infection burden (Ruggeri et al., 2018).

Understanding the interaction between *Bd* infection and sloughing is especially important, because of the potential additive or synergistic effects of water disruption. The overall aim of this study was to examine the interactions between sloughing and chytridiomycosis on the control of cutaneous water uptake in the Australian green tree frog (*Litoria caerulea*). Although there is evidence to show that rates of water loss are elevated in this species when severely infected with *Bd* (Russo et al., 2018), its unknown if water uptake pathways are similarly affected. We hypothesised that the disruption of cutaneous water flux is caused by a reduction or inhibition cutaneous water uptake proteins (AQPs) in the ventral pelvic patch region. Understanding the pathophysiology behind host-pathogen relationships, especially how *Bd* affects the core biological functions of the skin, such as water movement, is critical for understanding causal links to recent extirpation events and global amphibian declines.

5.3   MATERIALS AND METHODS

5.3.1   Animal maintenance

Litoria caerulea spawn were collected from Bribie Island, southeast Queensland in March 2015, raised under laboratory conditions until metamorphosed. Resulting juveniles ($n = 38$) were reared for 2 years in the laboratory before being used in experiments (body mass range: 12–35 g). Frogs were housed individually in either small (235 x 170 x 120 mm) or large (265 x 235 x 12 mm) ventilated clear plastic containers, with paper towels saturated with chemically aged water (dilution 1:4000; VitaPet, NSW, Australia) as substrate, and a half PVC pipe for shelter. The lighting and thermal conditions were maintained at a constant 12:12 h light-dark photoperiod and 20.5 $\pm$ 0.5°C, respectively. Frogs were checked daily, fed once a week on vitamin-dusted crickets (*Acheta domesticus*), and enclosures cleaned weekly. Prior to experiments, all frogs were swabbed to confirm the absence of *Bd* infection.

5.3.2   *Bd* culture and experimental exposures

Bd strain EPS4 (Ohmer et al., 2015) was used for experimental infections. Cultures were maintained at 4°C in 0.5 % tryptone, 0.5 % tryptone-soy broth. To harvest zoospores, EPS4 isolate was passaged to sterile 1 % agar, 0.5 % tryptone, 0.5 % tryptone-soy plates and maintained at 20°C for 4–5 days. Zoospores were harvested by flooding plates with aged tap water. After 30 min, the zoospore suspension was collected, and the concentration calculated using a haemocytometer (Boyle et al., 2004). A randomised subset of frogs ($n = 18$) were exposed to ~500,000 zoospores following Wu et al. (2018). Frogs were exposed to *Bd* zoospores for 5 h in 300 ml ventilated plastic containers containing 100 ml aged water. Uninfected frogs were sham 'exposed' in containers with aged water only. Fourteen days post-exposure, all frogs were swabbed with a sterile fine-tipped cotton swab (MW100-100; Medical Wire & Equipment, Wiltshire, England) three times each over the frog's ventral surface, thighs, armpit, forelimb feet, and hindlimb feet (Kriger et al., 2006; Ohmer et al., 2015) to assess infection status. To determine infection load, swabs were homogenised in 50 μl PrepMan Ultra (Applied Biosystems, Foster City, CA, USA), and analysed in duplicate with quantitative polymerase chain reaction (qPCR) in a thermal cycler (MiniOpticon™ Real-Time PCR Detection System, Bio-Rad Laboratories, Inc., CA, USA) using a modified 15 μl reaction (Taqman Universal Master Mix, Applied Bioscience) following Ohmer et al. (2015). Infection loads (zoospore equivalents) was calculated from the mean value of triplicate qPCR assays, and $\log_{10} + 1$ transformed (Log(ZE+1)) to normalise. All frogs were checked daily for clinical signs of disease progression including a lack of appetite (monitoring food intake), abnormal posture, excessive or irregular sloughing, lethargy, cutaneous erythema and discolouration, and loss of righting reflex (Voyles et al., 2009).

5.3.3   Monitoring sloughing frequency

The intermoult interval (IMI; time between two successful sloughing events in hours) was monitored continuously using infrared surveillance cameras (model EN-CI20B-65H, Eonboom Electronics Limited; and HW242C Security Camera, K Guard Security, New Taipei City, Taiwan), and a generic 16 channel H.264 Digital Video Recorder (DVR) system. Cameras were mounted to a moveable metal frame, positioned in front of enclosures, with two cameras per row. Each camera monitored two frog enclosures at one time and sampled at a rate of 1.56 frames per second.

5.3.4   Experimental chronology and measuring infection load

Once the IMI was determined for each animal (both uninfected and infected animals), water uptake experiments (see *'In-vivo* water uptake' below) were conducted during either the intermoult period or on the predicted day of sloughing. On the day of experiment, the frogs were swabbed to determine their infection load.

5.3.5   *In-vivo* water uptake

Seven infected and seven uninfected animals were used to measure *in-vivo* water uptake rates. All frogs were swabbed, voided of urine by gently squeezing their abdomen, blotted dry, and the snout-vent-length (SVL) and initial body mass (g) measured prior to water uptake measurements. Animals were then placed into a clear, ventilated chamber (135 x 100 x 56 mm) following Russo et al. (2018). Dry air was pumped through the box using an air pump (HP40 Air pump, Techno Takatsuki, Osaka, Japan) to induce evaporative water loss. The chamber was positioned on top of a balance scale (EJ-303 Compact Precision Balance, A&D Weighing, VIC, Australia) to measure body mass continually during the water loss period. Animals were maintained in this setup until they had lost approximately 10 % of their initial body mass. At this point, animals were immediately transferred to a container (170 x 105 x 77 mm) with sufficient aged water to cover the frog's ventral abdominal surface. Animals were removed, carefully blotted with paper towels and body mass recorded every 2 min during the first hour of rehydration, then every 5 min thereafter. Experiments were ended once the animals' body mass had returned to within 0.5 % of their the initial body mass. Rates of water uptake were calculated as grams of water per hour (g h^{-1}). For sloughing animals, water loss procedures commenced immediately following a sloughing event. Data was excluded if animals urinated or defecated during experimentation. Experiments was conducted at 20.5 $\pm$ 0.5°C.

5.3.6   Skin sampling

Frogs from the uninfected ($n = 10$ intermoult, $n = 10$ post-slough), and infected ($n = 12$ intermoult, $n = 6$ post-slough) group were first anesthetised with an intracoelomic injection of 60 mg kg^{-1} body mass thiopentone sodium (Thiobarb Powder, Jurox Pty Limited, NSW, Australia), then euthanased by double pithing at one of two time points in their sloughing cycle: 1) post-slough (no more than 1 h after sloughing had occurred), or 2) intermoult (at a point halfway through the IMI). Snout-vent

length (SVL) in mm and body mass in g were measured immediately. A final skin swab was taken to determine *Bd* infection load.

5.3.7 Muscle hydration and blood osmolality

White muscle from the thigh region (sartorius and gracilis major muscles) from both sides of the body were collected. The wet muscle mass (g) was recorded, then dried at 60°C until a constant mass (~ 24 h). The difference between wet and dry mass is presented as muscle water content (%). Whole blood was collected via cardiac puncture into a lithium heparinised syringe. Samples were then centrifuged at 5000 g for 5 min and the plasma collected and stored at -20°C. Plasma osmolality (mosmol l^{-1}) was measured using a Vapro 5520 vapour pressure osmometer (Wescor, Logan, UT, USA).

5.3.8 *In-vitro* permeability of ventral skin

Following water uptake experiments, animals were euthanased as detailed above and ventral skin samples (~ 1 cm^2) were collected from the lower abdominal pelvic patch region. Data were only collected from intermoult animals (infected and uninfected) due to time and animal number constraints. Tissues were mount in two modified Franz cells. Each vertical glass diffusion (Franz) cell consisted of a water-jacketed, 5 ml capacity bottom chamber with a 0.5 cm orifice, and a 1 ml capacity top chamber with a 0.5 ml orifice. Skin samples were sandwiched between the top and bottom chambers and secured in place with a stainless steel clamp. In the first Franz cell, the skin was placed apical surface up (influx direction), while in the second cell, skin was positioned apical surface down (efflux direction). In both preparations, freshwater (26 mmol l^{-1} NaCl in distilled water) was placed into the chamber adjacent to the apical skin surface, while a modified frog Ringer's solution (in mmol l^{-1}: NaCl (112), KCl (2.5), D-glucose (10), Na$_2$HPO$_4$ (2), CaCl$_2$ (1), MgCl$_2$ (1), HEPES salt (5), HEPES (5) at pH 7.3-7.4 with osmolality of 230 ± 20 mosmol l^{-1}) was placed into the chamber adjacent to the basolateral skin surface. 200 µCi of ^{3}H$_2$O (1mCi ml^{-1}; PerkinElmer, Melbourne, Vic, Australia) was added to solution in the top chamber of both preparations and mixed well. The bottom chambers contained 5 ml of solution and a magnetic stirrer set at 600 RPM. Duplicate 25 µl aliquots were taken immediately from both the top and bottom chambers and placed into polyethylene scintillation vials containing 4 ml of Ultima Gold scintillant (PerkinElmer). Vials were mixed by repeated inversion and then counted for 60 s in a Triathler Multilabel Tester (Hidex, Finland). Sample collection was repeated at 30 min intervals for 1 h. Solutions removed from the chambers for counting purposes were not replaced, and volume changes were accounted for in the analysis. After 1 h of baseline water flux rate measurements, fluids in the top chambers were drained and completely replaced with the appropriate solution (Ringer or FW) containing 200 µCi of ^{3}H$_2$O and 0.3 mmol l^{-1} HgCl$_2$ (Ogushi et al., 2010b) to block aquaporin activity. Preparations were left to stabilise for 30 min and then one hour of water flux measurements were

conducted as described above. Water flux (influx or efflux) was calculated using the following formula;

$$\Delta\Phi = \frac{\Delta C}{(SA \times t \times A)}$$

Where, $\Delta\Phi$ is the rate of isotope flux (µl cm⁻² h⁻¹), ΔC is the change in isotope abundance in the bottom chamber, SA is the specific activity of the isotope in the top chamber (mean CPS of isotope per µl water over the experimental period), t is the time (h) and A is the skin area exposed (cm²). Experiments were conducted at 25 ± 0.5°C.

5.3.9   AQP mRNA expression

5.3.9.1   *RNA extraction and cDNA synthesis*

Ventral skin samples ($\sim$1 cm²) from the lower abdominal pelvic patch region were collected, and stored in RNA-later (Ambion Inc., TX, USA) at -20°C. The skin samples were then homogenised with stainless steel beads using a TissueLyser II (Qiagen). Total RNA was isolated using an RNeasy Mini kit (Qiagen, Hilden, Germany) following the manufacturers guidelines. RNA was eluted into ultrapure water and the resulting yield was quantified using a Qubit fluorimeter (ThermoFisher Scientific). One µg of RNA was reversed transcribed into cDNA following a genomic DNA elimination step using a QuantiTech Reverse Transcription Kit (Qiagen) according the to manufacturer's protocols. Primer design and quantification of mRNA by quantitative PCR (qPCR).

5.3.9.2   *Primer design and quantification of mRNA by quantitative PCR (qPCR)*

Quantitative PCR (qPCR) primers against the target genes (**Table S5.1**) were manufactured using PrimerQuest (Integrated DNA Technologies, IA, USA) and OligoPerfect™ Designer (Thermofisher Scientific) with acceptance of the default parameters. Known amino acid sequences from an in-house *L. caerulea* transcriptome were identified using Galaxy/GVL 4.0.1 (Afgan et al., 2015). Homologous peptide sequences from other amphibians were used to probe the *L. caerulea* transcriptome using the integrated basic local alignment search tool (BLAST) from the National Centre for Biotechnology Information (NCBI) database (Camacho et al., 2009; Cock et al., 2015). qPCR was performed using the Power SYBR Green PCR Master Mix (ThermoFisher Scientific) and the machine-specific cycling parameters recommended by the manufacturer. Each assay (in triplicate) included a no-template control and a no reverse transcriptase control. All PCR efficiencies were >90 % and all assays produced unique dissociation curves. Bio-Rad CXF Manager software (version 3.1, Bio-Rad) was used to collect data and results were exported to Microsoft Excel. Each gene was quantified relative to the expression of the housekeeping gene, β-actin, using the Pfaffl (2001) method. Changes in expression levels are presented as fold-change relative to the uninfected intermoult group.

5.3.10 Statistical analysis

All analyses were performed in R.3.4.1 (R Core Team, 2018). Data are either presented as means $\pm$ standard error (s.e.), or individual data points depending on the nature of the data (Cumming et al., 2007; Krzywinski and Altman, 2013), and α was set at 0.05 for all statistical tests. Data that were not normally distributed were log or square-root transformed prior to appropriate analysis. Data for muscle hydration was power transformed using Tukey's Ladder of Powers to fit normal distribution.

5.3.10.1 Water uptake and permeability

The rate of water uptake between groups were analysed using a linear mixed-effects model 'lme' function from 'nlme' package (Pinheiro et al., 2013). Water uptake was the response variable, while slough cycle (sloughing or non-sloughing), and *Bd* load were fixed interactive effects. SVL did not show a significant effect on water uptake rate, thus it was removed from the analysis.

The rate of *in-vitro* water flux across the skin were analysed using linear mixed-effects model 'lme' function, where water flux rate was the response variable, treatment (infected or uninfected), condition (baseline or AQP-inhibited), and flux direction (influx or efflux) as interactive effects. Individual identity was incorporated as a random effect to account for the effect of individual on flux direction and response to $HgCl_2$ Comparisons between the three interaction terms were analysed with the 'lsmeans' function adjusting with 'Tukey' from the 'lsmeans' package (Lenth, 2016). In addition, water flux rate as a function of *Bd* load was analysed via 'lm', with *Bd* load and flux as interactive effects. Under AQP-inhibited conditions, there was a significant interactive effect between the two factors, thus a 'holm'-adjusted F test was performed using the 'testinteractions' function in the 'phia' package (Rosario-Martinez et al., 2015), where flux direction was the fixed factor, and adjusting for *Bd* slope.

5.3.10.2 Muscle hydration and plasma osmolality

The effect of *Bd* infection on muscle hydration status between intermoult and sloughing groups were analysed using linear mixed effects model, 'lme' function from 'nlme' package. Muscle water content was the response variable, slough cycle and *Bd* load as fixed interactive effects. Body mass was included as an additive covariate, and individual identity as a random effect to account for repeated measurements on both leg muscles for each animal. To test for interactions between treatments within groups and adjusting for *Bd* slope, a Chi square test adjusting with 'holm' was performed with the 'testinteractions' function in 'phia' package.

The effect of infection on blood plasma osmolality between intermoult and sloughing groups were analysed using linear model (lm) from R default stats package with osmolality as the response variable, slough cycle and *Bd* load as fixed interactive effects, and body mass as interactive effects.

To test for interactions between treatments within groups and adjusting for *Bd* slope, an F test adjusting with 'holm' was performed with the 'testinteractions' function in 'phia' package.

5.3.10.3 AQP expression

Relative expression of AQPs in the ventral skin across treatment and slough cycle were analysed following Yuan et al. (2006):

$$E^{-\Delta\Delta C_T} = \beta_0 + \beta_{treatment} + \beta_{gene} + \beta_{group} + \beta_{treatment}X_{gene} + \beta_{treatment}X_{group} + \beta_{group}X_{gene}$$
$$+ \beta_{treatment}X_{gene}X_{group} + b_{ID} + \epsilon$$

where $E^{-\Delta\Delta C_T}$ is the $\Delta\Delta$ threshold cycle (C_T), β is the fixed effects parameters where 0 is the intercept, X is the interaction term, b_{ID} is the random intercept for frog ID expressed as $b_{ID} \sim N(o, \delta^2)$, δ^2 is the variance of random intercept, and ϵ is the Gaussian error term expressed as $\epsilon \sim N(o, \sigma^2)$, with σ^2 being the variance of the residual. The model examines relative C_T values of the target gene normalised to the C_T values of the reference gene, β-actin. The interaction between treatment (infected and uninfected) and group (intermoult and sloughing) with respect to the reference gene gives the $\Delta\Delta C_T$, where uninfected intermoult frogs were set as the control. To test the effects of body mass and exposure period (exposed once or twice), models with body mass as an additive effect were compared to models with no additive effects. The final model was chosen based on Akaike information criterion (AIC). To test for factor interactions between treatments within groups, controlling for gene, a 'holm'-adjusted Chi-square test was performed (package 'phia', function 'testInteractions').

5.4 RESULTS

5.4.1 Whole animal water uptake rate

The rate of water uptake was not significantly different between sloughing and non-sloughing animals groups (**Table S5.2**). There was, however, a significant effect of *Bd* load on water uptake rate ($t_3 = -3.2$, $P = 0.05$), with uptake decreasing as *Bd* load increased (**Fig. 5.1**).
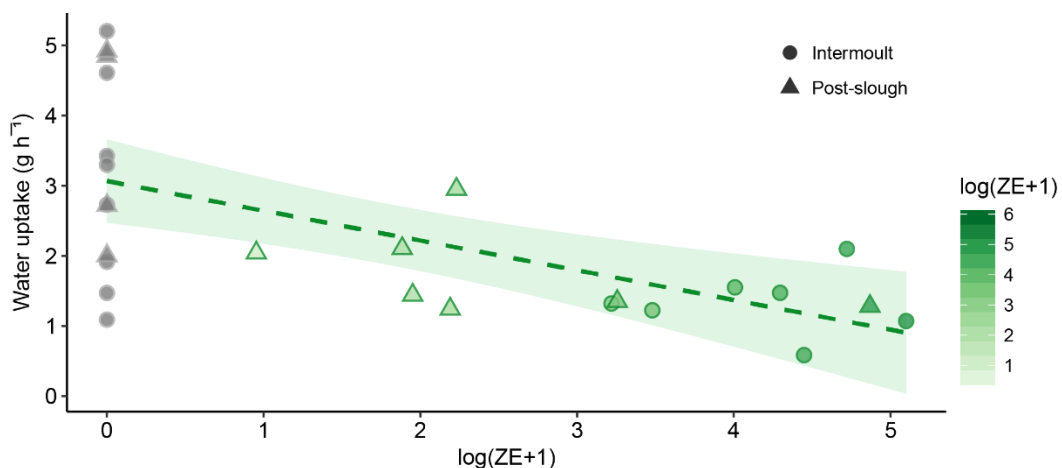
Fig. 5.1 │ Rate of water uptake (g h⁻¹) of the ventral skin of *Litoria caerulea* throughout infection load. Data are presented as individual data points during the intermoult phase (● uninfected *n* = 7, ● infected *n* = 7), and during post-

slough (▲ uninfected $n = 4$, ▲ infected $n = 7$). Correlation between water uptake and *Bd* load is 38 % with a regression line of $y = 3.1 - 0.42(x)$. Green shading represents 95 % confidence interval. Summary statistics are presented in Tables S5.2.

5.4.2 *In-vitro* Water fluxes

In both infected and uninfected animals, water efflux rates were almost 2.5 times higher than water influx rates (169 ± 17.5 and 68 ± 5.7 μl cm^{-2} h $^{-1}$, respectively; **Fig. 5.2A**). There was also a three way interaction with treatment (infected and uninfected), experimental condition (control/inhibited), and flux (influx/efflux). There was no significant effect infection status or AQP inhibition by HgCl$_2$ on the rate of water influx (**Table S5.3**). By contrast the inhibition of AQPs from HgCl$_2$ significantly increased the rate of water efflux across infected skin ($t_{27} = -3.3$, $P = 0.04$) but did not affect the rate of water efflux in uninfected skin ($t_{27} = -0.57$, $P = 0.99$).

When accounting for *Bd* load, there was an increase in water flux as *Bd* load increased under baseline conditions (non-inhibited) for both influx and efflux pathways (**Fig. 5.2B; Table S5.4**). When AQPs were inhibited by HgCl$_2$, there was an interactive effect with *Bd* load and flux direction, where there was a significant increase in water efflux as *Bd* load increased ($F_{1,18} = 11.8$, $P = 0.006$; **Fig. 5.2C**). This accounted for 76 % of the total variation in water efflux. The rate of water influx was independent of *Bd* load, accounting for 3 % of the variation in water influx ($F_{1,18} = 0.027$, $P = 0.87$).
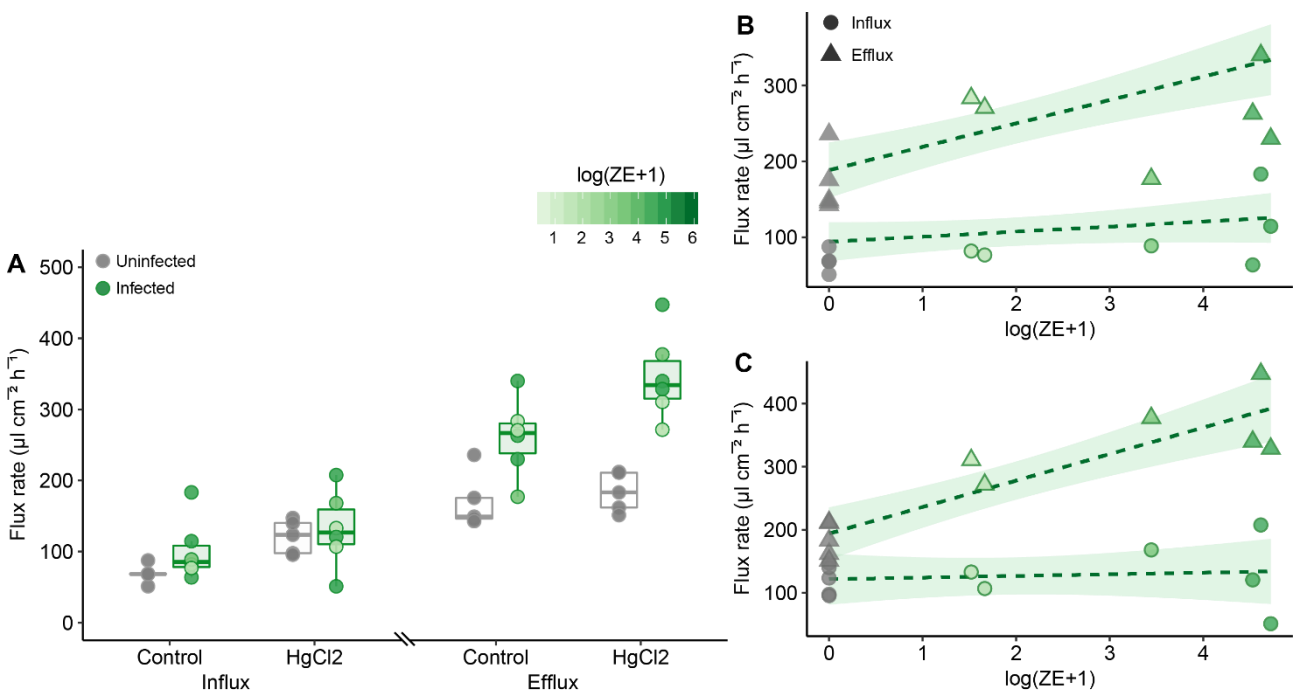
Fig. 5.2 │ The rate of water influx and efflux (μl cm⁻² h⁻¹) in the pelvic-patch region of the ventral skin of uninfected and infected *L. caerulea*. A) Comparison of the rate of *in-vitro* water influx and efflux, and the effect of non-competitive AQP inhibitor (HgCl₂) across the ventral skin of uninfected and infected animals. Semi-transparent boxplots represent standard distribution of data. B) rate of water influx and efflux across *Bd* load (log(ZE+1)) under normal conditions. C). rate of water influx and efflux across *Bd* load (log(ZE+1)) after HgCl₂ inhibition. Data presented as individual data points with regression line. Summary statistics presented in Table S5.3 & S5.4.

5.4.3   Muscle hydration and plasma osmolality

There was no significant effect of sloughing on muscle water content, however, *Bd* infection did influence muscle water content, with muscle water content increasing with increasing *Bd* load (t_{26} = 5.6, $P<0.001$; **Fig. 5.3A**). There was also a significant interaction between sloughing stage and *Bd* load on tissue water content (t_{26} = -3.77, $P<0.001$), with muscle water content increasing with *Bd* load in intermoult animals (X^2_1 = 31.3, $P<0.001$; **Fig. 5.3A**) but not in sloughing animals (X^2_1 = 1.5, $P= 0.2$).

There was a significant decrease in plasma osmolality as *Bd* load increased (t_{24} = -4.7, $P<0.001$; **Fig. 5.3B).** There was no main effect of sloughing stage on plasma osmolality but there was a significant interaction between sloughing stage and *Bd* load (t_{24} = 2.3, $P= 0.03$), with osmolality decreasing with increasing *Bd* load in intermoult ($F_{1,24}$ = 21.7, $P<0.001$), but not in sloughing ($F_{1,24}$ = 0.3, $P= 0.6$), animals.
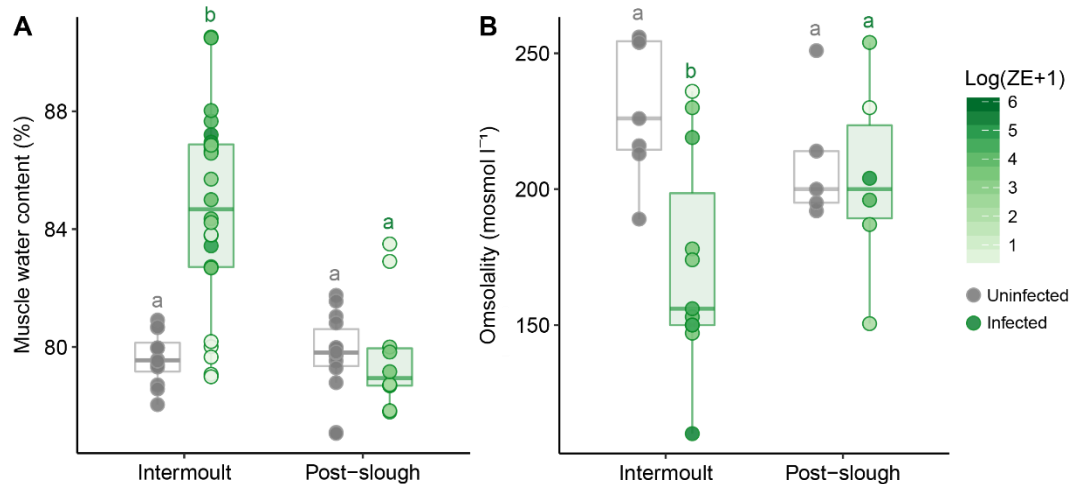
Fig. 5.3 │ **(A) Water content as percentage of the wet thigh muscle mass (%) and (B) blood plasma osmolality of infected (●) and uninfected (●)** *L. caerulea* **during the intermoult or post-slough period**. Data for muscle water content are presented as individual data points for intermoult (uninfected *n* = 6, infected *n* = 12) and post-slough (uninfected n = 7, infected *n* = 5). For plasma osmolality**,** data are presented as individual data points for intermoult (uninfected *n* = 7, infected *n* = 11) and post-slough (uninfected *n* = 5, infected *n* = 6) animals. Semi-transparent boxplots represent standard distribution of data. Lower-case letters represent significant differences between and groups (*P* <0.05). Summary statistics are presented in Tables S5.5.

5.4.4   AQP expression

Expression of all AQP6 genes (*AQP6ub*, *AQP6vs1*, *AQP6vs2*) was higher in the ventral skin of uninfected, recently sloughed animals compared to uninfected, intermoult animals (**Table. S5.6**). In particular, *AQP6vs1* was approximately 45 times more highly expressed in the skin of recently sloughed uninfected frogs compared with intermoult animals (**Fig. 5.4C**). In contrast, the expression of all ventral skin AQP6 genes was significantly reduced in infected, recently sloughed frogs (relative to uninfected intermoult animals (**Fig. 5.4A,B,C**)). *AQP3*, *AQP5* and *AQP1* expression patterns were not significantly affected by either infection status or sloughing stage treatment (**Table S5.6; Fig. 5.4D,E,F**). Although non-significant, there was trend towards a slight increase in

AQP1 expression in the skin of infected frogs compared to uninfected frogs (**Fig. 5.4D**), while *AQP5* showed a slight decrease in expression compared to uninfected frogs (**Fig. 5.4F**).
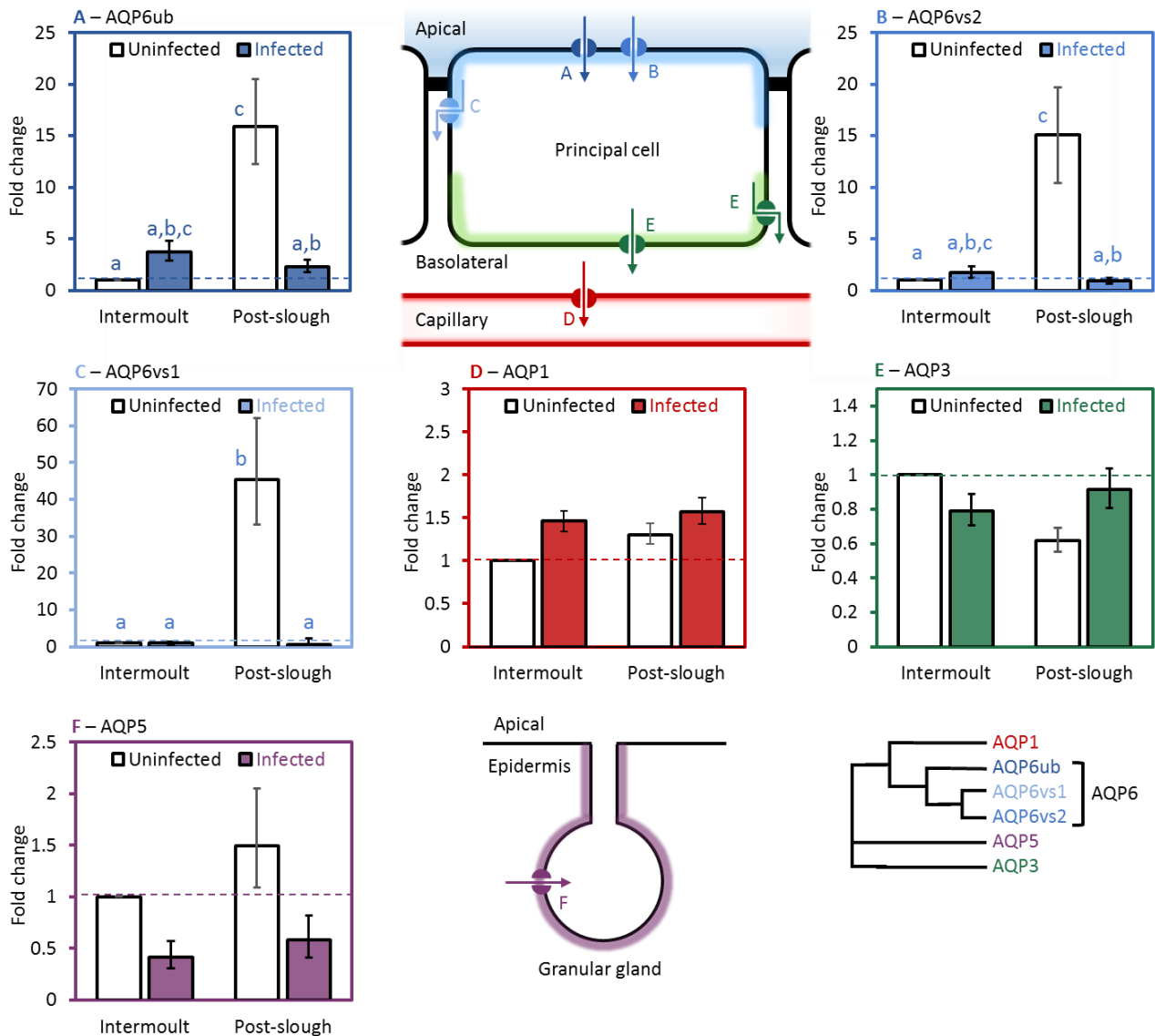
Fig. 5.4 │ Relative mRNA expression of epithelial aquaporin's (AQP) in the ventral skin of infected and uninfected Litoria caerulea during the intermoult and post-slough period. Absolute gene expression was normalised to expression of the housekeeping gene *β*-actin. Diagram of the ventral skin with the positions and distributions of each AQPs (blue = AQP6, green = AQP3, purple = AQP5, and red = AQP1) from Suzuki and Tanaka (2009). Arrows denote direction of water movement through the epithelia. Cladogram in the bottom right of the figure shows the evolutionary relationship amphibian cutaneous AQPs (Suzuki et al., 2007; Hillyard et al., 2008). Data are presented as mean ± s.e. for uninfected intermoult *n* = 7, infected intermoult *n* = 7, uninfected post-slough *n* = 7, and infected post-slough animals *n* = 5. Lower-case letters represent significant differences between all treatment groups. Treatments with different letters are significantly different (P <0.05). Summary statistics are provided in Table S5.6.

5.5   DISCUSSION

Batrachochytrium dendrobatidis causes substantial health effects for its host, with global consequences, particularly the decline and extinction of numerous frog species (Lips, 2016; Wu et al., 2019). However, the mechanistic basis for many of these negative health consequences remains largely unresolved, especially involving osmotic disruption. In line with our hypothesis, we found that whole animal water uptake rate was impaired, and that *in vitro* transcutaneous water flux rates

were higher across the ventral skin region of *Bd*-infected frogs. We also identified a significant reduction in mRNA expression levels for the major water uptake AQPs post-sloughing, suggesting that impaired net water uptake may be the result of reduced aquaporin activity in the ventral skin. Elevated rates of transcutaneous water loss in *Bd* infected animals likely reflects the loss of tight junction integrity. Plasma osmolality and muscle water contents mirrored these patterns, with *Bd* infection loads being negatively correlated with increasing tissue and blood water content.

5.5.1 Mechanistic basis for impaired transcutaneous water movements

For both infected and uninfected frogs, there was a significant increase in the rate of water flux post-AQP inhibition. However, the increase in water flux was not substantially greater after AQP inhibition, suggesting $HgCl_2$-sensitive AQPs do not have a large role in maintaining water flux under hydrated conditions. Similar conclusions were made by Ogushi et al. (2010b) where they found that $HgCl_2$-sensitive AQPs are not constitutively expressed in any great number in 'at-rest' skin, and Shibata et al. (2014) found AQPs were only upregulated under dehydrated conditions. The small increase in water flux after inhibition by $HgCl_2$ may indicate greater paracellular water flux. While there was no significant difference in water flux between infected and uninfected frogs, on average the increased water flux in infected frogs (especially post-AQP inhibition) may suggest osmotic disruption occurring through the physical damage of the skin (Berger et al., 2005a; Gauberg et al., 2019) resulting in increased permeability of the skin (Wu et al., 2019).

The greater *in-vitro* water efflux, especially in infected animals observed in this study may be a consequence of solvent drag, where water can be pulled across a membrane against its concentration gradient due to coupling with the movement of solutes such as NaCl (Whittembury et al., 1980; Fischbarg, 2010). Evidence for solvent drag can be seen in toad skin (Benedictis and Lacaz-Vieira, 1982; Aboulafia and Lacaz-Vieira, 1985). Given that *Bd*-infected frogs lose large amounts of salt via leakage across the ventral skin surface (Wu et al., 2018), solute-linked water movements may explain why infected frogs also have greater rates of water efflux despite an osmotic gradient that should promote net water uptake.

A greater expression of several genes coding for apical AQPs (*AQP6ub, AQP6vs1, AQP6vs2*) in the ventral skin immediately post-slough was observed in this study, suggesting that an increase in the production of AQPs may be needed to counteract the increased permeability of the skin (Voyles et al., 2009; Wu et al., 2017). We have previously shown that epithelial ion transporters in the ventral skin of frogs were similarly upregulated immediately after slough in response to increased salt loss (Wu et al., 2017). AQPs may be highly expressed under conditions requiring large flux of water, such as in terrestrial frogs or when animals are dehydrated where water uptake is essential to maintain proper osmotic balance (Shibata et al., 2014). In the context of chytridiomycosis, the reduction of AQP expression post-slough in the infected group may suggest *Bd* is specifically or

directly inhibiting the production of apical AQPs. Additionally, the basolateral AQPs (*AQP1, AQP3, AQP5*) were not affected by *Bd*, suggesting inhibition is restricted to the outer layer of the skin where *Bd* is normally found (Berger et al., 2005b; Greenspan et al., 2012). *Bd* secretes a range of proteases that affect the integrity of the skin (Rosenblum et al., 2008; Symonds et al., 2008; Brutyn et al., 2012). However, it is not clear which types of proteases may be responsible for inhibiting AQP production.

5.5.2   Whole animal water uptake capacity

The molecular and cellular changes in AQPs expression and water flux when infected with *Bd* may affect the animal's ability to regulate cutaneous water flow. Consistent with Carver et al. (2010), the rate of whole-animal water uptake decreased in green tree frogs as infection intensity increased. However, not all amphibian species infected with *Bd* show decreased water uptake rates. Less susceptible species to *Bd* infection showed no difference in the rate of water uptake (Bovo et al., 2016). This is consistent with the *Bd* threshold hypothesis, where a certain threshold of zoospore load needs to be reached before pathological symptoms begin to occur (Kinney et al., 2011). In fact, frogs with low zoospore abundance show compensatory responses such as increased skin resistance and lower EWL (Bovo et al., 2016). For *Bd*-susceptible species such as *L. caerulea*, the consequences of increased EWL (Russo et al., 2018), and reduction of water uptake (this study) from chytridiomycosis may lead to dehydration, as has been observed in the field with infected frogs (Voyles et al., 2012a). The mechanisms underpinning this disruption may include increased skin permeability, and inhibited AQP-dependent water uptake activity. Because rate of water uptake correlates with level of dehydration (Anderson et al., 2017), AQPs may play a greater role in water balance under dry conditions compared to freshwater (Shibata et al., 2014). Thus, future studies should examine the underlying mechanisms responsible for reduced water uptake in infected frogs, especially comparing the role of AQPs under dehydrating and overhydrating conditions.

An important factor for water disruption and *Bd* infection is ambient temperature. Frogs infected with *Bd* modify thermoregulatory behaviour to raise their core body temperature in order to reduce and clear infection (Richards-Zawacki, 2009; Rowley and Alford, 2013). By moving to areas outside their preferred thermal niche, frogs may be subjected to greater osmotic disruption where at higher temperatures, frogs may be more prone to EWL (Buttemer, 1990; Tracy et al., 2008), and they may increase their sloughing frequency (Cramp et al., 2014). Frogs can show thermal plasticity when introduced to new thermal environments, however water loss does not show the same extent of plasticity (no reduction in water loss) (Davies et al., 2015), which suggests frogs rely on high cutaneous resistance and behavioural means to reduce EWL. Infected frogs may therefore be able to thermoregulate by moving to warmer areas to remove *Bd*, but may not be able to compensate

for temperature-induced increases in rates of water loss. Infected newts have been shown to spend less time in water (Daversa et al., 2018), and infected frogs spend less time sloughing in direct contact with water (Doody et al., In review). Potentially this may be a behavioural avoidance strategy to avoid losing salts when the skin becomes temporarily leaky (Wu et al., 2019). However, infected frogs sloughing will then be more susceptible to EWL (Russo et al., 2018) and reduced water uptake found this study. More studies are required to examine the relationship between behavioural responses to *Bd* infection and their physiological trade-offs.

In the current study, infected frogs housed with unlimited access to both freshwater and dry environments showed an increase in water muscle content and a decrease in plasma osmolality, consistent with hyperhydration and/or excessive salt loss. Water normally enters into the cutaneous capillaries in the pelvic patch region (Word and Hillman, 2005) and is retained in the vasculature. The water retention results in osmotic dilution in the surrounding cavity system, which in excess can cause an increase in water muscle content and a decrease in plasma osmolality, as observed in infected frogs in this study. Impairment of skin function in relation to water balance can therefore lead to disruption of the blood volume, capillary filtration, lymphatic function (Hillman et al., 2004), and ultimately cardiovascular homeostasis as seen *Bd*-infected animals (Voyles et al., 2009; Salla et al., 2018).

5.5.3   Conclusion

Our results reveal a not only a complex interaction between sloughing and chytridiomycosis, but also that the environmental context of water disruption leads to different osmotic consequences. This has large impacts on both physiological and behavioural consequences for osmotic balance in infected amphibians. This work also demonstrates the mechanisms underlying cutaneous disruption of water movement during *Bd* infection, where we showed inhibition of AQPs post-slough, correlating with an increase in cutaneous water flux, and disrupting osmotic balance. The cumulative effect of increased water flux, skin permeability during non-sloughing periods and increased sloughing frequency (Wu et al., 2018), may further accelerate disease progression. Importantly, these results help us understand the dynamic interplay between the host's compensatory responses, and costs associated with disease progression, in the context of disease associated mass extinctions. Further studies should examine the role of AQPs in fully terrestrial species to investigate the underlying mechanisms of for increased EWL, and integrate the role of osmoregulatory hormones relating to *Bd* infection.

5.6   SUPPLEMENTARY INFORMATION

5.6.1   Supplementary tables

Table S5.1 │ *Litoria caerulea*-**specific designed primers for qPCR of target and reference genes.**

Primer name	Orientation	Primer (5' to 3')	Amplicon size (bp)
AQP1	Forward	AATTGCGATCGATTACACTGG	216
	Reverse	TACTCTTCCACCTGTCCGTTG	
AQP3	Forward	AATCCTGCTAGGGACTTTGGA	214
	Reverse	CATTGGCCAACTTGACATTCT	
AQP6ub	Forward	CCAAAGGTCCAATCCAGAAG	155
	Reverse	CTGACATCCAAGCTCTTCCTG	
AQP6vs1	Forward	AATCCAGCAAGGTCTTTTGGT	203
	Reverse	TCCTCTCGCTCTTGTTCATGT	
AQP6vs2	Forward	GCGCTGATTACAGGAAACT	148
	Reverse	TGTTGCCACGTAGGATTTC	
AQP5	Forward	ACGGTAGACGAAATGACAACG	204
	Reverse	TGAGTGAAGCCAAAATTCCAC	
β-Actin	Forward	CTGGACGTACAACTGGTATTG	185
	Reverse	CCTCTCTGCTGTGGTAGTAA	

Table S5.2 │ **Summary statistics from linear mixed-effects model for water uptake between slough groups (intermoult, and post-slough), and zoospore equivalent (ZE).** s.e. = standard error, Df = degrees of freedom, *P* = *P* value with α set at 0.05, and CI = confidence interval set at 95 %. Significant codes: 0 '***' 0.001 '**' 0.01 '*' 0.05 '.' 0.1 ' ' 1.

	Water uptake							
Fixed effects	**Value**	**s.e.**	**Df**	**t value**	***P***		**CI**	
						2.5 %	**97.5 %**	
Intercept	0.956	0.155	19	6.168	**<0.001**	0.658	1.255	*
ZE	-0.172	0.054	3	-3.202	**0.049**	-0.329	-0.015	*
Group	0.171	0.248	3	0.693	0.538	-0.553	0.896	
ZE:Group	-0.051	0.103	3	-0.494	0.655	-0.354	0.252	
Random effect	**s.d.**				**Residual**			
~1 │ Frog ID	0.000				0.443	1.15E-294	7.67E+283	

Table S5.3 │ **Summary statistics from linear mixed-effects model and Least-square means comparison for the rate of influx and efflux, with the effect of non-competitive AQP inhibitor (HgCl₂) between uninfected and infected *Litoria caerulea*.** Frog ID was account for as random effect. s.e. = standard error, Df = degrees of freedom, *P* = *P* value with α set at 0.05 (adjustment method: holm), and Significant codes: 0 '***' 0.001 '**' 0.01 '*' 0.05 '.' 0.1 ' ' 1.

Fixed effects	Estimate	s.e.	Df	t value	*P*	
Intercept	8.347	0.707	27	11.811	**<0.001**	***
Treatment (Uninfected - Infected)	1.792	1.048	9	1.709	0.122	.
Condition (control - HgCl2)	2.499	0.820	27	3.047	**0.005**	**
Flux (Influx - efflux)	5.204	0.820	27	6.345	**<0.001**	***
Treatment:Condition	-1.233	1.217	27	-1.013	0.320	
Treatment:Flux	0.650	1.217	27	0.535	0.597	

Condition:Flux	-2.031	1.160	27	-1.751	0.091	
Treatment:Condition:Flux	3.724	1.720	27	2.165	**0.039**	*
Random effect	**s.d.**				**Residual**	
~1 | Frog ID	0.989				1.421	

Least-sqaure means with P value adjustment: Tukey method						
	Estimate	**s.e.**	**Df**	**t.ratio**	***P***	
Control,baseline,Influx - Infected,baseline,Influx	-1.792	1.048	9	-1.709	0.684	
Control,baseline,Influx - Control,inhibited,Influx	-2.499	0.820	27	-3.047	0.083	.
Control,baseline,Influx - Infected,inhibited,Influx	-3.058	1.048	9	-2.918	0.177	
Control,baseline,Influx - Control,baseline,Efflux	-5.204	0.820	27	-6.345	**<.0001**	***
Control,baseline,Influx - Infected,baseline,Efflux	-7.647	1.048	9	-7.295	**0.001**	***
Control,baseline,Influx - Control,inhibited,Efflux	-5.673	0.820	27	-6.916	**<.0001**	***
Control,baseline,Influx - Infected,inhibited,Efflux	-10.606	1.048	9	-10.119	**0.000**	***
Infected,baseline,Influx - Control,inhibited,Influx	-0.707	1.048	9	-0.675	0.996	
Infected,baseline,Influx - Infected,inhibited,Influx	-1.266	0.898	27	-1.410	0.845	
Infected,baseline,Influx - Control,baseline,Efflux	-3.413	1.048	9	-3.256	0.112	
Infected,baseline,Influx - Infected,baseline,Efflux	-5.855	0.898	27	-6.516	**<.0001**	***
Infected,baseline,Influx - Control,inhibited,Efflux	-3.881	1.048	9	-3.702	0.061	.
Infected,baseline,Influx - Infected,inhibited,Efflux	-8.814	0.898	27	-9.810	**<.0001**	***
Control,inhibited,Influx - Infected,inhibited,Influx	-0.559	1.048	9	-0.533	0.999	
Control,inhibited,Influx - Control,baseline,Efflux	-2.705	0.820	27	-3.298	**0.048**	*
Control,inhibited,Influx - Infected,baseline,Efflux	-5.147	1.048	9	-4.911	**0.012**	*
Control,inhibited,Influx - Control,inhibited,Efflux	-3.174	0.820	27	-3.869	**0.013**	*
Control,inhibited,Influx - Infected,inhibited,Efflux	-8.107	1.048	9	-7.734	**0.001**	***
Infected,inhibited,Influx - Control,baseline,Efflux	-2.146	1.048	9	-2.048	0.503	
Infected,inhibited,Influx - Infected,baseline,Efflux	-4.588	0.898	27	-5.107	**0.001**	***
Infected,inhibited,Influx - Control,inhibited,Efflux	-2.614	1.048	9	-2.494	0.304	
Infected,inhibited,Influx - Infected,inhibited,Efflux	-7.548	0.898	27	-8.401	**<.0001**	***
Control,baseline,Efflux - Infected,baseline,Efflux	-2.442	1.048	9	-2.330	0.370	
Control,baseline,Efflux - Control,inhibited,Efflux	-0.468	0.820	27	-0.571	0.999	
Control,baseline,Efflux - Infected,inhibited,Efflux	-5.402	1.048	9	-5.153	**0.009**	**
Infected,baseline,Efflux - Control,inhibited,Efflux	1.974	1.048	9	1.883	0.590	
Infected,baseline,Efflux - Infected,inhibited,Efflux	-2.959	0.898	27	-3.294	**0.048**	*
Control,inhibited,Efflux - Infected,inhibited,Efflux	-4.933	1.048	9	-4.707	**0.016**	*

Table S5.4 │ Summary statistics from linear mixed-effects model and pairwise comparison for comparison for the rate of influx and efflux over Bd load (log(ZE+1)), under control and AQP inhibited conditions. Frog ID was account for as random effect. s.e. = standard error, Df = degrees of freedom, *P* = *P* value with α set at 0.05 (adjustment method: holm), CI = confidence interval set at 95 %, s.d. = standard deviation, and Chisq = Chi square value. Significant codes: 0 '***' 0.001 '**' 0.01 '*' 0.05 '.' 0.1 ' ' 1.

Control condition

Fixed effects	Estimate	s.e.	Df	t value	P	CI		
						2.5 %	97.5 %	
Intercept	4.210	0.110	9	38.279	<0.001	3.962	4.459	***
ZE	0.103	0.041	9	2.537	0.032	0.011	0.194	*
Flux	0.969	0.118	9	8.242	<0.001	0.703	1.235	***
ZE:Flux	-0.012	0.043	9	-0.266	0.796	-0.110	0.086	
Random effect	**s.d.**				**Residual**			
~1	Frog ID	0.174				0.201	0.076	0.398	

AQP inhibited condition								
Fixed effects	**Estimate**	**s.e.**	**Df**	**t value**	**P**	**CI**		
						2.5 %	97.5 %	
Intercept	4.799	0.123	9	38.892	<0.001	4.520	5.078	***
ZE	-0.007	0.045	9	-0.163	0.874	-0.110	0.095	
Flux	0.457	0.136	9	3.355	0.009	0.149	0.765	**
ZE:Flux	0.164	0.050	9	3.266	0.010	0.050	0.278	*
Random effect	**s.d.**				**Residual**			
~1	Frog ID	0.186				0.232	0.076	0.457	
Chisq test	**Value**		**Df**	**Chisq**	**P**			
Influx	-0.007		1	0.027	0.871			
Efflux	0.157		1	11.863	0.001	**		

Table S5.5 │ Summary statistics from linear mixed-effects model and pairwise comparison for muscle water content and blood plasma osmolality between slough groups (intermoult, and post-slough) and zoospore equivalent (ZE) as an interactive effect. Frog ID was account for as random effect. s.e. = standard error, Df = degrees of freedom, P = P value with α set at 0.05 (adjustment method: holm), CI = confidence interval set at 95 %, s.d. = standard deviation, and Chisq = Chi square value. Significant codes: 0 '***' 0.001 '**' 0.01 '*' 0.05 '.' 0.1 ' ' 1.

Muscle hydration								
Fixed effects	**Value**	**s.e.**	**Df**	**t value**	**P**	**CI**		
						2.5 %	97.5 %	
Intercept	-8.32E-20	8.98E-21	29	-9.260	<0.001	-1.01E-19	-6.48E-20	***
Group	-1.47E-22	7.42E-21	26	-0.019	0.9844	-1.54E-20	1.51E-20	
ZE	9.11E-21	1.63E-21	26	5.582	<0.001	5.75E-21	1.24E-20	***
Mass	-4.36E-22	2.72E-22	29	-1.603	0.1197	-9.91E-22	1.20E-22	
Group:ZE	-1.28E-20	3.38E-21	26	-3.776	<0.001	-1.97E-20	-5.81E-21	***
Random effect	**s.d.**				**Residual**			
~1	Frog ID	1.44E-20				6.97E-21	1.056E-20	1.968E-20	
	Value	**Df**		**Chisq**	**P**			
Intermoult	9.11E-21	1		31.1677	<0.001	***		
Post-slough	-3.66E-21	1		1.5253	0.216			

Plasma osmolality								
Fixed effects	**Estimate**	**s.e.**	**Df**	**t value**	**P**	**CI**		
						2.5 %	97.5 %	
Intercept	234.239	17.926	24	13.067	<0.001	197.242	271.236	***
Group	-21.731	15.541	24	-1.398	0.175	-53.805	10.344	
ZE	-17.313	3.712	24	-4.664	<0.001	-24.974	-9.652	***
Mass	-0.065	0.513	24	-0.126	0.901	-1.124	0.995	

Group:ZE	14.773	6.481	24	2.279	**0.032**	1.396	28.150	*
	Value	**Df**	**Sum of Sq**	**F value**	***P***			
Intermoult	-17.313	1	18985.8	21.755	**<0.001**	***		
Post-slough	-2.540	1	218.6	0.250	0.621			
Residuals		24	20945.4					

Table S5.6 │ Summary statistics from linear mixed effects model for AQP mRNA expressions of the ventral skin between slough groups (intermoult, and post-slough) and treatments (uninfected, and infected). Gene is in reference to the reference gene (β- actin), and Frog ID was account for as random effect. Df = degrees of freedom, s.e. = standard error, *P* = *P* value with α set at 0.05, and CI = confidence interval set at 95 %. Significant codes: 0 '***' 0.001 '**' 0.01 '*' 0.05 '.' 0.1 ' ' 1.

AQP6ub expression								
Fixed effects	**Value**	**s.e.**	**Df**	**t value**	***P***	**CI**		
						2.5 %	**97.5 %**	
Intercept	-29.789	0.570	22	-52.263	**<0.001**	-30.971	-28.607	***
Treatment	1.920	0.806	22	2.382	**0.026**	0.248	3.592	*
Gene	9.229	0.673	21	13.709	**<0.001**	7.829	10.629	***
Group	3.634	0.836	22	4.346	**<0.001**	1.900	5.368	***
Treatment:gene	-1.899	0.952	21	-1.994	0.059	-3.879	0.081	
Treatment:group	-5.244	1.216	22	-4.313	**<0.001**	-7.766	-2.723	***
Group:gene	-3.988	0.978	21	-4.079	**<0.001**	-6.021	-1.955	***
Treatment:gene:group	4.705	1.430	21	3.291	**0.004**	1.732	7.678	**
Random effect	**s.d.**				**Residual**			
~1	Frog ID	0.829				1.260	0.401	1.714	

AQP6vs2 expression								
Fixed effects	**Value**	**s.e.**	**Df**	**t value**	***P***	**CI**		
						2.5 %	**97.5 %**	
Intercept	-28.076	0.800	22	-35.093	**<0.001**	-29.736	-29.736	***
Treatment	0.836	1.131	22	0.739	0.468	-1.510	-1.510	
Gene	7.517	0.995	22	7.552	**<0.001**	5.453	5.453	***
Group	3.558	1.131	22	3.144	**0.005**	1.211	1.211	**
Treatment:gene	-0.814	1.408	22	-0.579	0.569	-3.734	-3.734	
Treatment:group	-5.410	1.678	22	-3.223	**0.004**	-8.890	-8.890	**
Group:gene	-3.912	1.408	22	-2.779	**0.011**	-6.831	-6.831	*
Treatment:gene:group	4.870	2.088	22	2.332	**0.029**	0.540	0.540	*
Random effect	**s.d.**				**Residual**			
~1	Frog ID	1.006				1.862	0.393	2.576	

AQP6vs1 expression								
Fixed effects	**Value**	**s.e.**	**Df**	**t value**	***P***	**CI**		
						2.5 %	**97.5 %**	
Intercept	-29.631	0.673	22	-44.047	**<0.001**	-31.026	-28.236	***
Treatment	-0.005	0.951	22	-0.005	0.996	-1.978	1.968	
Gene	9.072	0.845	22	10.737	**<0.001**	7.319	10.824	***
Group	5.148	0.951	22	5.411	**<0.001**	3.175	7.121	***
Treatment:gene	0.026	1.195	22	0.022	0.983	-2.452	2.504	
Treatment:group	-6.600	1.411	22	-4.678	**<0.001**	-9.527	-3.674	***

	Value	s.e.	Df	t value	P	2.5 %	97.5 %	
Group:gene	-5.502	1.195	22	-4.605	**<0.001**	-7.980	-3.024	***
Treatment:gene:group	6.061	1.772	22	3.420	**0.003**	2.385	9.736	**
Random effect	**s.d.**				**Residual**			
~1	Frog ID	0.818				1.581	0.298	2.246	

AQP1 expression

Fixed effects	Value	s.e.	Df	t value	P	CI 2.5 %	97.5 %	
Intercept	-24.409	0.345	22	-70.742	**0.000**	-25.125	-23.694	***
Treatment	0.405	0.488	22	0.831	0.415	-0.607	1.417	
Gene	3.850	0.238	22	16.204	**0.000**	3.357	4.342	***
Group	0.194	0.488	22	0.398	0.695	-0.818	1.206	
Treatment:gene	-0.384	0.336	22	-1.142	0.266	-1.081	0.313	
Treatment:group	-0.819	0.724	22	-1.132	0.270	-2.320	0.682	
Group:gene	-0.548	0.336	22	-1.631	0.117	-1.245	0.149	
Treatment:gene:group	0.280	0.498	22	0.561	0.580	-0.754	1.313	
Random effect	**s.d.**				**Residual**			
~1	Frog ID	0.797				0.444	0.565	1.125	

AQP3 expression

Fixed effects	Value	s.e.	Df	t value	P	CI 2.5 %	97.5 %	
Intercept	-22.033	0.329	22	-67.039	**<0.001**	-22.714	-21.351	***
Treatment	-0.316	0.465	22	-0.681	0.503	-1.280	0.648	
Gene	1.473	0.309	22	4.771	**<0.001**	0.833	2.114	***
Group	-1.048	0.465	22	-2.256	**0.034**	-2.012	-0.085	*
Treatment:gene	0.338	0.437	22	0.774	0.447	-0.568	1.244	
Treatment:group	0.363	0.689	22	0.527	0.604	-1.066	1.793	
Group:gene	0.694	0.437	22	1.590	0.126	-0.211	1.600	
Treatment:gene:group	-0.903	0.648	22	-1.394	0.177	-2.246	0.440	
Random effect	**s.d.**				**Residual**			
~1	Frog ID	0.650				0.578	0.423	0.998	

AQP5 expression

Fixed effects	Value	s.e.	Df	t value	P	CI 2.5 %	97.5 %	
Intercept	-24.065	0.643	22	-37.415	**0.000**	-25.399	-22.731	***
Treatment	-1.251	0.910	22	-1.375	0.183	-3.137	0.635	
Gene	3.505	0.850	22	4.122	**0.000**	1.742	5.269	***
Group	0.227	0.910	22	0.249	0.806	-1.660	2.113	
Treatment:gene	1.273	1.203	22	1.058	0.301	-1.221	3.767	
Treatment:group	-0.639	1.349	22	-0.473	0.641	-3.437	2.159	
Group:gene	-0.581	1.203	22	-0.483	0.634	-3.075	1.913	
Treatment:gene:group	0.099	1.784	22	0.056	0.956	-3.600	3.798	
Random effect	**s.d.**				**Residual**			
~1	Frog ID	0.604				1.591	0.113	3.229	

6

General discussion
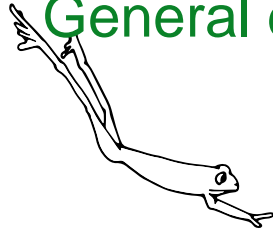
6.1 OVERVIEW

The lethal skin disease chytridiomycosis has been detected in around 400 amphibian species worldwide (Bellard et al., 2016), with host responses varying from tolerance/resistance to being highly susceptible. Amphibians that develop chytridiomycosis exhibit similar pathological symptoms, thus it is important to understand the mechanisms of how chytridiomycosis causes mortality, and why there are variations in disease susceptibility and morbidity. While most studies have focused on the differences in immune function (McMahon et al., 2014; Ellison et al., 2015), cutaneous microbiota (Woodhams et al., 2014; Bates et al., 2018), life history (Rachowicz and Vredenburg, 2004; Greenberg et al., 2017), environment (Berger et al., 2004; Voyles et al., 2012b), and pathogen virulence strain (Farrer et al 2011, Jenkinson et al 2016), only a few studies have examined the physiological consequences of chytridiomycosis (Voyles et al., 2009; Carver et al., 2010; Peterson et al., 2013). With the recent progress on how sloughing regulates cutaneous *Bd* loads and how it relates to interspecific differences in susceptibility to chytridiomycosis (Ohmer et al., 2017), it has become increasingly clear that sloughing plays an important role in mitigating disease progression. Since both sloughing and chytridiomycosis alter cutaneous physiological function, understanding the underlying disruptions is important to establish causal links to recent extirpation events and global amphibian declines. This thesis explored the physiological costs (energetic, ionoregulatory and osmoregulatory) of chytridiomycosis, and how the costs are influenced by sloughing, providing new insight into the mechanisms underpinning the often fatal ionic and osmotic disruptions in *Bd*-susceptible species. Key findings from Chapters 2–5 are discussed within a comparative framework relating to existing literature, and future directions focusing on chytridiomycosis are presented.

6.1.1 Physiology and control of sloughing

Since the 1980s, there has been a 40 year literature gap on the physiology of amphibian sloughing (Larsen, 1976). With the development of powerful, modern laboratory techniques, it is now possible to examine the molecular and genetic responses of specific proteins during sloughing. Chapter 2 focused on the mechanisms of cutaneous ion regulation during sloughing, integrating classical epithelial physiology techniques with molecular biology (western blotting, qPCR) to provide an integrative understanding of sloughing, from whole animal to molecular level responses. Due to the extensive morphological and physiological changes that occur prior, during and after sloughing (Jørgensen, 1949; Larsen, 1970; Budtz and Larsen, 1973, 1975), I hypothesised that sloughing would disrupt internal ionic and osmotic balance, as proposed by Ewer (1951) and Larsen (1976). I found that sloughing in uninfected frogs had minimal impact on blood plasma electrolyte and osmotic levels due to compensatory increases in the abundance and activity of epithelial sodium channels (ENaC) and sodium-potassium pumps (NKA) abundance and activity,

and expression of aquaporin's (AQPs) in the skin (Chapter 2 & 5). While this was the first study to reveal a physiological feedback response to maintain homeostatic balance in sloughing amphibians, other shedding freshwater animals also show similar responses. For example, in moulting crustaceans, increases in NKA and V-ATPase activity occur prior to moulting in order to reuptake essential electrolytes (Zare and Greenaway, 1998) in response to large increases in water influx during ecdysis (Dall and Smith, 1978).

In Chapter 5, I found that during sloughing there was a large increase (~20-fold) in AQPs expression on the apical surface of the skin. The upregulation of cutaneous AQPs during sloughing suggests that they play an important role in minimising osmotic disruption when the skin becomes more permeable (Chapter 2; Larsen, 1970). AQPs have been shown to be responsible for increases in water flux pre- and post-moulting in freshwater decapods (Foguesatto et al., 2017). Similar responses in upregulation were observed in cutaneous Na^+ transporters, however not to the same extent (Chapter 2). Because the transport of ions and water are often linked (Whittembury et al., 1980; Benedictis and Lacaz-Vieira, 1982), the differences in mRNA responses may reflect the timing of ionic and osmotic regulation throughout the sloughing cycles, as observed in toads (Budtz, 1977) and aquatic arthropods (Bliss et al., 1966). For example, in moulting lobsters, the haemolymph ionic composition and osmolality increase pre-moult suggesting that influx of salts precede the uptake of water at ecdysis (Mykles, 1980). However, Zare and Greenaway (1997) found that the osmolality of the haemolymph of freshwater crayfish declined by 11 % post-moult compared to lobsters, thus species-specific responses need to be accounted for. For aquatic amphibians, large osmotic influxes can burden the kidneys which must produce an equivalent volume of dilute urine, and hence have a lower rate of cutaneous water absorption compared to terrestrial amphibians (Schmid, 1965; Ogushi et al., 2010b). AQPs may not play an important role during sloughing for aquatic amphibians compared to semi-aquatic amphibians (Ogushi et al., 2010b) as observed in Chapter 5 and instead, epithelial tight and adherens junctions may play a more significant role in maintaining water balance for aquatic amphibians (Farquhar and Palade, 1965; Meyer et al., 2010).

6.1.2   Chytrid-sloughing relationship

Chapters 3-5 focused on the interaction between physiological alterations during sloughing, and disruption from chytridiomycosis. Chytridiomycosis is a deadly fungal disease affecting a broad range of amphibians (Bellard et al., 2016). It is therefore important to understanding the impacts of chytridiomycosis on the host's physiology in order to make predictions about inter- and intra-specific variation to disease susceptibility and morbidity. While sloughing has been shown to contribute to the clearing of *Bd* infections over time in resistant species, more susceptible species continue to develop chytridiomycosis independent of changes in sloughing frequency (Ohmer et al., 2017). In Chapter 4, I found that cutaneous ion loss was greater in infected intermoult animals and

was influenced by body size, showing that smaller infected individuals suffered greater ionic and metabolic costs than larger sized individuals. Sloughing alone increased ion loss (Chapter 2 & 4); however, contrary to my hypothesis, the effects were not enhanced in infected animals. Chapter 3 revealed the mechanisms for why there was no difference in ion loss between infected and uninfected animals during sloughing. This was due to upregulation in the activity and abundance of cutaneous ion transporters (ENaC and NKA). These changes in skin function during sloughing appear to provide a temporary relief from cutaneous ionic disruption by reducing *Bd* load in a susceptible species (Chapter 3). For cutaneous water transport, *Bd* greatly reduced the mRNA expression of AQPs in the ventral skin during sloughing. This correlated with an increase in water influx leading to greater water-muscle content, and low osmolality in the blood (Chapter 5). It remains unclear why *Bd* affected the expression of cutaneous AQPs but not the expression of ion transporters (ENaC and NKA; Chapter 3). Potentially, the AQPs are directly inhibited by the chemical toxins and proteases released by the fungus (Rosenblum et al., 2008; Symonds et al., 2008; Brutyn et al., 2012), however experimental studies are needed to determine this.

I also hypothesised that sloughing would further exacerbate internal ionic and osmotic homeostatic disruptions in infected frogs (Chapter 3 & 5). I found differences in plasma ion and osmolality levels in infected frogs during sloughing. Infected frogs had similarly low plasma ion (Na^+ and Cl^-) levels during the intermoult and post-slough period (relative to uninfected intermoult), indicating no recovery from electrolyte imbalance (Chapter 3). However, osmolality and muscle water content levels in the infected post-slough group were the same as the uninfected group, suggesting temporary recovery of water balance (Chapter 5). The differences may lie in other osmoregulatory organs (e.g. kidney, urinary bladder (Uchiyama and Konno, 2006)) that may be upregulated during skin disruption in order to maintain water balance. Potentially, during the sloughing period, there may be an increase in osmoregulatory hormones such as aldosterone and cortisol (Lang et al., 1975; Larsen, 1976; Jørgensen, 1988) to up-regulate water transport and maintain osmolality when frogs are not infected (Uchiyama and Konno, 2006). Because osmoregulatory hormones influence water regulation in the skin, kidney, and urinary bladder equivocally, the plasma osmolality and muscle water content may be maintained not because of the skin alone, but due to action of other osmoregulatory organs in infected animals. Nevertheless, sloughing only provides a temporary recovery of water balance, and once in the intermoult phase, infected animals exhibit signs of hyponatraemia (Chapter 3 & 5), a result which is consistent with Voyles et al. (2007).

An increase in metabolic cost in infected animals observed in Chapter 4 correlated with cutaneous ionic and osmotic disruption (Chapter 3 & 5). Evidence for energetic cost of ion transport can be seen in Zerahn (1956) and Leaf and Dempsey (1960), where under *in-vitro* conditions, the active uptake of 18 Na^+ ions by healthy amphibian skin costs approximately one mole of O_2. Thus, an

increase in cutaneous ion and water flux may partly explain the increase in metabolic cost with infected animals, along with energetic costs of increased immunity (Rollins-Smith and Woodhams, 2012; Van Rooij et al., 2015), epidermal cellular repair (Vander Heiden et al., 2009), and physiological regulation (Peterson et al., 2013).

6.2 FUTURE DIRECTIONS

Overall, the research in this thesis has advanced our understanding of cutaneous physiological regulation during sloughing and how the fatal chytrid disrupts key functions of the skin, resulting in irreversible loss of ionic and osmotic homeostasis. While this body of work addressed important topics relating to the pathophysiology of chytridiomycosis and the influence of sloughing, due to the complex dynamics of sloughing and chytridiomycosis on skin function, many more questions arise.

6.2.1 What is the ultimate cause of death in frogs with chytridiomycosis?

To date, the main consensus for the expiration of frogs with chytridiomycosis is the disruption of cutaneous ion transport caused by *Bd* damage to the skin, and the subsequent electrolyte imbalance in the blood results in cardiac arrest (Voyles et al., 2007; Voyles et al., 2009). Chapter 3 and 5 revealed the mechanisms behind how ion and water transporters are disrupted in infected frogs, resulting in low plasma osmolality and electrolyte concentrations; it raises the question of whether or not skin disruption alone is the main cause of death? Voyles et al. (2009) found that electrolyte supplementation in infected frogs resulted in prolonged survival, however the frogs ultimately died from infection. Potentially, fungal toxins produced by *Bd* and the disruption of the skin function itself initiate a cascade of physiological disruptions such as impaired kidney function (Brannelly et al., 2016), and the interruption of biosynthetic and degradation pathways (Grogan et al., 2018). However, these aforementioned disruptions remain untested.

Amphibians have been shown to survive fluctuations in plasma electrolyte concentrations (Mullen and Alvarado, 1976; Balinsky, 1981), and osmotic disruptions such as severe dehydration. For example under experimental dehydration, *L. caerulea* can survive losing 45 % of its body water content (Bentley, 1966). In the current study, I showed that infected frogs had around half the plasma Na^+ levels (Chapter 3), and ~27 % reductions in plasma osmolality (Chapter 5) compared to uninfected frogs. While amphibians can tolerate fluctuating internal salt and water levels (Hillman, 1980; Hillman et al., 2009; Anderson et al., 2017), functioning under suboptimal osmotic balance for long periods can have negative consequences on the animal's health (Voyles et al., 2012a; Peterson et al., 2013), and reduce animal fitness and long term survival. If low ion levels alone were the causative reason for cardiac arrest, a simple *in-vitro* experiment could be conducted by isolating healthy anuran hearts, manipulating the electrolyte levels (e.g. lower levels of Na^+, or Cl^-) of the surrounding saline, and measuring the cardiac responses associated with electrolyte

depletion. Alternatively, examining maximal oxygen consumption ($\dot{V}_{O_2\,\text{max}}$) in infected animals can also provide insight on how *Bd* affects oxygen transporting system relating to cardiovascular homeostasis (Hillman et al., 2013). Under dehydration (often seen with *Bd*-infected individuals), species with slower decline in $\dot{V}_{O_2\,\text{max}}$ are able to better maintain cardiovascular homeostasis, and mobilize lymph to replace lost plasma volume (Hillman et al., 2009). Thus, if $\dot{V}_{O_2\,\text{max}}$ was affected by *Bd* infection, there would be higher cardiovascular consequences for infected animals.

In frogs with chytridiomycosis, internal lesions have been documented, including focal or diffuse acute necrosis in renal tubules, as well as oedema (swelling) and vacuolation (development of vacuoles) in the brain (Berger, 2001). Further, Brannelly et al. (2016) found evidence of depleted hematopoietic tissue in the kidney of infected amphibian. Since the kidney is another major osmoregulatory organ, the combined disruption of internal osmoregulatory organs with the skin may alter ionic and osmotic balance observed in Chapter 3 and 5. The disruption of kidney function may also alter blood pressure and flow that may in turn affect cardiac output causing arrhythmia (Guyton, 1991; Sarnak et al., 2003). There is evidence of decreased contractile force and increased cardiac relaxation from frogs infected with *Bd* (Salla et al., 2018). How *Bd* causes this internal damage remains to be tested. It is possible that *Bd* releases chemicals or toxins that damage internal organs as observed with freshwater crayfish infected with *Bd* (McMahon et al., 2013). In addition, the kidneys or urinary bladder may also have similar compensation responses to that of the skin (Chapter 3), where there is an upregulation of ion transport (e.g. ENaC) activity to filter ions back into the body, and regulate circulation as observed with amphibians in osmotically challenging environments (Konno et al., 2007; Wu et al., 2014). Instead of focusing on a single aspect of ionic disruption (through the skin), the integration of whole animal water and ion budgets (Hillyard et al., 2008) in response to *Bd* are required, taking into account the inflow (food, cutaneous, gills where present), outflow (faeces, urine, glands, cutaneous) and storage (bladder, intracellular, extracellular) of ions and water. For example, heavily infected animals that become lethargic, reducing food intake (a large source of ions) and activity levels (Voyles et al., 2009), may suffer from accelerated ionic disruption.

6.2.2 Does *Bs* cause similar cutaneous disruption in amphibians as *Bd*?

The recent discovery of *Batrachochytrium salamandrivorans* (*Bs*), a sister-species to *Bd*, has been brought to attention as the next potential emerging global infectious disease (Martel et al., 2013). Current evidence suggests that *Bs* originated from Asia (Martel et al., 2014; Laking et al., 2017), and has since spread across regions of Europe, where rapid collapses of salamander populations have been recorded (Spitzen-van der Sluijs et al., 2016; Stegen et al., 2017). The introduction of *Bs* to the United States (USA) is of growing concern because the US has the highest diversity of salamanders

with 10 families and 675 species (Petranka, 1998), may greatly decimate a large proportion of Urodele diversity.

Bd and *Bs* have noticeable differences in thermal and host preferences, with *Bs* growing optimally at 10–15°C under lab conditions. Salamanders are more susceptible to *Bs* than anurans, suggesting different host niche occupation (Martel et al., 2013; Martel et al., 2014). In terms of pathophysiology, it is unknown if *Bs* also causes similar changes to skin function as seen in amphibians infected with–*Bd* (Chapter 3; Voyles et al., 2009). Farrer et al. (2017) showed that within the same host species, *Bs* and *Bd* elicited different immune responses, and different gene expression profiles involving epidermal cornification, electrolyte and fluid homeostasis and immunity. Histologically, *Bs* thalli are abundantly present across the entire thickness of the epidermis resulting in extensive loss of keratinocytes, whereas *Bd* thalli are associated with the superficial epidermal layers and hyperkeratotic foci (Farrer et al., 2017). From a sloughing perspective, this may suggest an increase in sloughing rate as an immune defence may not lower infection load in animals infected with *Bs,* since *Bs* thalli can be found throughout the entire epidermis, and may inhibit water and ion transporter proteins or junction proteins in the deeper layers of the skin (Chapter 3, and 5). Shedding the outer layer (*stratum corneum*) in response to infection may not be beneficial in removing *Bs* as compared to *Bd* infection (Ohmer et al., 2017). Salamanders have been shown to increase sloughing frequency in response to *Bd* (Davidson et al., 2003), but the sloughing response, or the physiological alterations of the skin in response to *Bs* have yet to be examined.

Many salamanders do not have lungs and solely rely on cutaneous gas exchange to meet their respiratory quota (Spotila, 1972; Feder, 1976). Thus, skin disruption from *Bs* may not only alter ion and water regulation (Chapter 3, and 5), but also reduce or inhibit cutaneous exchanges of respiratory gases (O_2 and CO_2). The cause of death for lungless salamanders may include: 1) reduced regulation of salts and water transport through the skin, low electrolyte levels in the blood leading to arrhythmic cardiac cycles as observed with anurans infected with *Bd* (Voyles et al., 2009; Voyles et al., 2012a); and/or 2) reduced cutaneous O_2 uptake resulting in anoxia and suffocation. The build-up of CO_2 in the blood may also cause acidosis leading to death. I would hypothesis that lungless amphibians would be more susceptible to hypoxemia or blood acidosis from *Bs* infection, compared to low electrolyte levels. Examining the metabolic responses, *in-vitro* cutaneous O_2 uptake, and blood gases (O_2, CO_2) and pH levels may help elucidate the promixate mechanisms of death in lungless salamanders.

6.2.3   How does sloughing influence with commensal microbial communities in animals with and without *Bd* infections?

Sloughing has a large influence on the abundance and diversity of cutaneous microbiota, where sloughing can clear up to 100 % of the microbiota on the new skin (Meyer et al., 2012). The diversity of some cutaneous microbes have been shown to reduce *Bd* load (Harris et al., 2009), by secreting antifungal metabolites that prevent the establishment of *Bd* (Brucker et al., 2008; Becker et al., 2009). Thus, maintaining a diverse skin microbiota is a key predictor of a host's resistance to *Bd* infection (Rebollar et al., 2016). This may indicate that an increase in sloughing frequency can be both beneficial and detrimental to amphibians as it can remove harmful pathogens, but also potentially remove commensal microbes that can play a beneficial role (Meyer et al., 2012; Cramp et al., 2014). Increasing the rate of sloughing may interfere with the establishment of beneficial microbiota (Walke et al., 2014) that in turn can affect the susceptibility of frogs to *Bd* infection. Potential experiments to elucidate this include examining changes in beneficial cutaneous microbes in response to increased sloughing between *Bd*-susceptible and *Bd*-resilient species, and correlating to levels of *Bd* infection.

An additional complexity is the interaction with fluctuating environmental temperatures that both increase the rate of sloughing alone (Cramp et al., 2014), and alters microbiota communities (Longo and Zamudio, 2017). The consequence of increased sloughing frequency and disrupted microbiome may influence the susceptibility of the host to *Bd* infection. For example, an increase in ambient temperature will not only increase the rate of sloughing (removing microbes more often), but also change the profile of the skins microbial diversity (less beneficial microbes). It is clear that species living in extremely fluctuating environments are more susceptible to *Bd* (Greenberg et al., 2017). In the context of climate change, changes in environmental temperature may alter the balance between regulating beneficial microbiota and removing harmful pathogen like *Bd*, potentially increasing the likelihood that a *Bd* infection progresses to clinical chytridiomycosis. Examining how increasing temperature affects beneficial microbiome communities on amphibians may elucidate how abiotic and biotic variables interact to increase *Bd* susceptibility.

6.2.4   How do extreme thermal fluctuations affect sloughing and susceptibility to chytridiomycosis?

Recent research has shown that amphibians outside of their thermal preferences range are more susceptible to infection than those within their thermal preferences (Cohen et al., 2017b). This is of increasing concern because extreme thermal events akin with climate changes may affect the virulence of the fungus and susceptibility of the frogs (Raffel et al., 2006; Raffel et al., 2013). The *thermal mismatch hypothesis* suggests that the hosts are more susceptible to parasitic infection when environmental conditions shift away from the host's thermal optima. This in turn reduces the performance (e.g. immune response) of the host, and increases susceptibility to pathogens (**Fig. 6.1**; Cohen et al., 2017b). In fact, species from highly seasonal environments (e.g. UV, rainfall and

temperature) are at greater risk of infection and experience greater zoospore loads (Greenberg et al., 2017).

The degree of mismatch between critical thermal tolerances of hosts and parasites may drive disease outbreaks (Rosenzweig et al., 2001). Similarly, the mismatch in temperature optima can occur within host–parasite interactions when cold-adapted hosts and parasites experience warm spells, and vice versa (Cohen et al., 2017b). Infected amphibians (*Osteopilus septentrionalis* and *Anaxyrus terrestris*) acclimated to colder temperatures had higher *Bd* loads compared to warm-acclimated groups, even though the temperatures were greater than the optimal growing conditions of *Bd* in cultures (17-25°C) (Piotrowski et al., 2004; Cohen et al., 2017b). Amphibians at colder temperatures were shown to have reduced DNA repair rates (Morison, pers. Comm.), and reduced immune function (Maniero and Carey, 1997; Rollins-Smith and Woodhams, 2012) that may allow infection to occur, furthering skin disruption (Chapter 3).

In relation to sloughing as part of the immune defence, the rate of sloughing has been shown to be influenced by temperature (Meyer et al., 2012; Cramp et al., 2014); as temperature decreases, the rate of sloughing also decreases (longer IMI; **Fig. 6.1**). Sloughing frequency does not seem to show thermal compensation, suggesting that a longer IMI at lower temperatures may allow cutaneous pathogens to establish on the skin and continuously develop before the next sloughing cycle begins (Cramp et al., 2014). A longer IMI also means that sloughing could potentially be less effective at removing *Bd*, and may contribute to increased susceptibility to the fungus at lower temperature (**Fig. 6.1**; Ohmer et al., 2017). The longer that *Bd* remains on the skin, the more likely that cutaneous damage will occur, increasing the risk of ion loss and water regulation (Chapter 3 & 5) and furthering disease progression. This may partially explain seasonal variation in mortality observed in the wild (Kriger and Hero, 2007; Rohr and Raffel, 2010).

Conversely, there is evidence of increased susceptibility at temperatures that exceed the host's thermal optima. *Atelopus zeteki*, a cool adapted, montane species that prefers cooler temperatures (17.8°C), experienced rapid *Bd* growth at warmer temperatures (>20°C) compared to those within their thermal preferences (Cohen et al., 2017a). Increasing the ambient temperature causes an increase in the metabolic rate (MR) of ectotherms, including amphibians (Clarke and Johnston, 1999; Clarke and Fraser, 2004; Wu et al., 2015). Sloughing itself increases MR (Chapter 4), thus the combination of both increasing ambient temperature and sloughing rate may disrupt the overall energy expenditure of the host. Elevated temperatures on top of increased metabolism from *Bd* infection (Peterson et al., 2013) may synergistically disrupt the host's energy balance, resulting in lower body mass and lethargy (**Fig. 6.1**; Nichols et al., 2001; Peterson et al., 2013). Future work should focus on the efficiency of sloughing in removing *Bd* at a range of different temperatures and linking to physiological trade-offs in a susceptible species to confirm this.
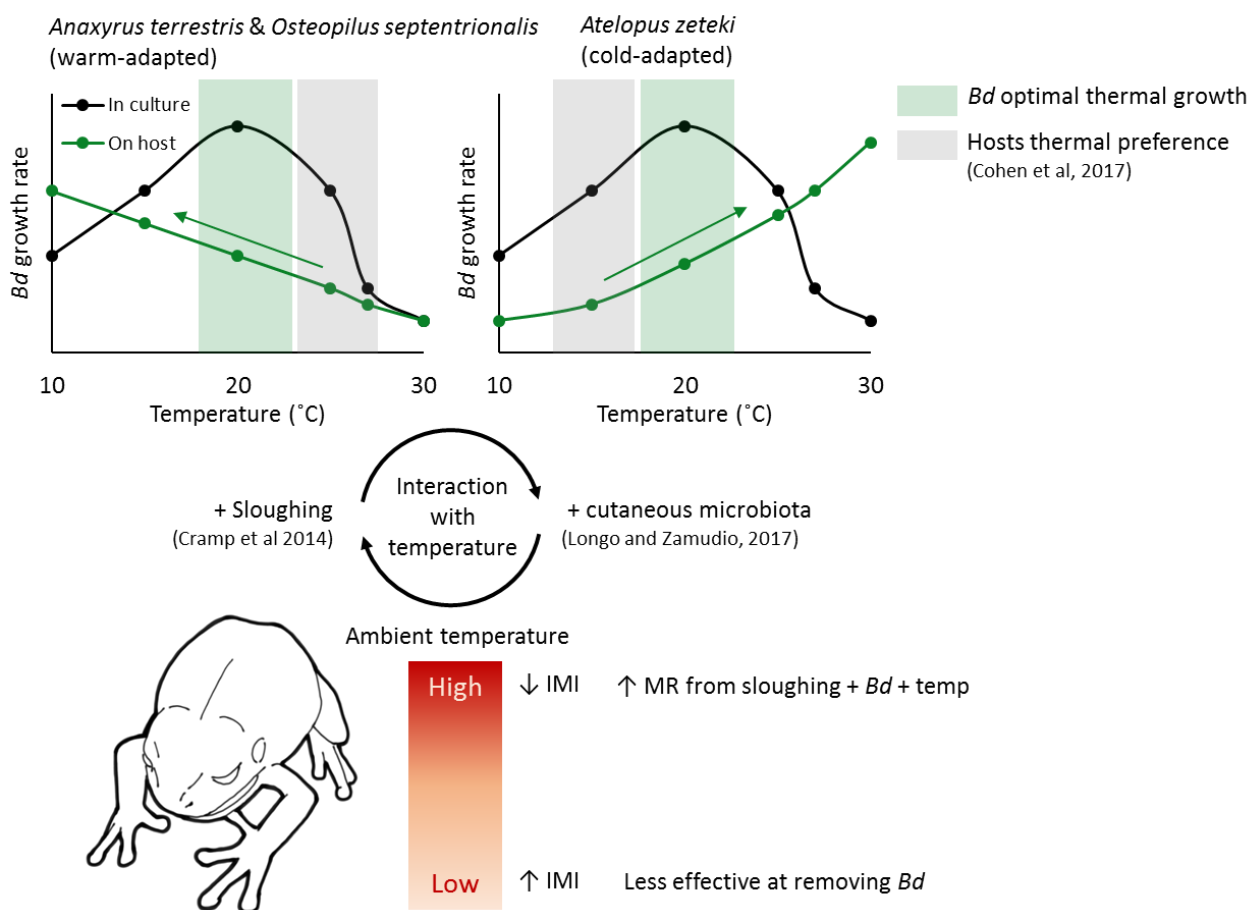
Fig. 6.1 │ Hypothetical scenario of how temperature fluctuations could interact with sloughing to influence the susceptibility of the host to infection. Top left graph shows warm-adapted species acclimated to colder temperatures, and top right graph shows cold-adapted species acclimated to warmer temperatures (modified from Cohen et al. (2017b)). Arrows represent an increase in *Bd* growth (independent of *Bd* optimal thermal growth (red box) as the hosts acclimated temperature moves away from the hosts' preferred temperate (grey box). Bottom images show how changes in the rate of sloughing and cutaneous microbiome with temperature may interact to affect either the host's physiology or clearing cutaneous pathogens. Higher temperatures, increased rate of sloughing, and infection can interact to greatly increase the animal's metabolic rate (MR). Lower temperatures and decreased rate of sloughing may interact to be less effective at removing *Bd*.

6.3   CONCLUSION

Amphibian susceptibility varies substantially among individuals, populations and species across various biotic and abiotic contexts, therefore understanding the mechanistic causes that contribute to these variations is important. This thesis aimed to understand the role of sloughing on regulating disease susceptibility and the physiological cost by investigating the metabolic and osmoregulatory alterations during sloughing in amphibians, as well as examining the effects of *Bd* on the sloughing process, with a focus on the capacity of individuals to maintain physiological homeostasis. This research contributes to an extensive literature on chytridiomycosis that provides links between mechanistic responses, pathophysiology of disease progression, and intraspecific susceptibility to the disease. The major findings of this work are the molecular compensatory responses during sloughing when infected with *Bd*, highlighting the role of sloughing on cutaneous ionic (Chapter 3) and osmoregulation (Chapter 5) when infected with *Bd*, and how smaller body size greatly

amplifies these physiological disruptions (Chapter 4). Overall, the findings presented in this thesis demonstrate the important role of sloughing in regulating disease progression and susceptibility, while also explaining the risks of increasing sloughing frequency for susceptible species. New directions for research emerge as new information about amphibian diseases unfolds. What is the ultimate cause of death from frogs with chytridiomycosis? Does the newly emergent pathogen *Bs* disrupt the host in the same way as *Bd*, and does sloughing contribute to the physiological costs of infection with *Bs*? How is the functional role of sloughing for susceptible species affected by increasing extremes in climate fluctuations? It will be exciting to see how our knowledge of amphibian declines progresses in the next decade.

"The same thrill, the same awe and mystery, comes again and again when we look at any question deeply enough. With more knowledge comes a deeper, more wonderful mystery, luring one on to penetrate deeper still. Never concerned that the answer may prove disappointing, with pleasure and confidence we turn over each new stone to find unimagined strangeness leading on to more wonderful questions and mysteries - certainly a grand adventure!" ~ Richard Feynman (1955) The Value of Science.

REFERENCES

Aboulafia, J. and Lacaz-Vieira, F. (1985). Hydrosmotic salt effect in toad skin: urea permeability and glutaraldehyde fixation of water channels. *J. Membr. Biol.* **87**, 249-252.

Adams, N. J., Brown, C. R., Davis, L. S. and Darby, J. T. (1990). Energetics of molt in penguins. In *Penguin Biology*, eds. L. S. Davis and J. T. Darby), pp. 297-315. California, USA: Academic Press Inc. .

Afgan, E., Sloggett, C., Goonasekera, N., Makunin, I., Benson, D., Crowe, M., Gladman, S., Kowsar, Y., Pheasant, M. and Horst, R. (2015). Genomics virtual laboratory: a practical bioinformatics workbench for the cloud. *PLOS ONE* **10**, e0140829.

Afgan, E., Baker, D., Van den Beek, M., Blankenberg, D., Bouvier, D., Čech, M., Chilton, J., Clements, D., Coraor, N. and Eberhard, C. (2016). The Galaxy platform for accessible, reproducible and collaborative biomedical analyses: 2016 update. *Nucleic Acids Res.* **44**, W3-W10.

Anantharam, A., Tian, Y. and Palmer, L. G. (2006). Open probability of the epithelial sodium channel is regulated by intracellular sodium. *J. Physiol.* **574**, 333-347.

Anderson, R. C. O., Bovo, R. P., Eismann, C. E., Menegario, A. A. and Andrade, D. V. (2017). Not good, but not all bad: dehydration effects on body fluids, organ masses, and water flux through the skin of *Rhinella schneideri* (Amphibia, Bufonidae). *Physiol. Biochem. Zool.* **90**, 313-320.

Arnold, P. A., Johnson, K. N. and White, C. R. (2013). Physiological and metabolic consequences of viral infection in *Drosophila melanogaster*. *J. Exp. Biol.* **216**, 3350-3357.

Bakar, A. A., Bower, D. S., Stockwell, M. P., Clulow, S., Clulow, J. and Mahony, M. J. (2016). Susceptibility to disease varies with ontogeny and immunocompetence in a threatened amphibian. *Oecologia* **181**, 997-1009.

Balinsky, J. B. (1981). Adaptation of nitrogen metabolism to hyperosmotic environment in Amphibia. *J. Exp. Zool. Part A* **215**, 335-350.

Baroni, A., Buommino, E., De Gregorio, V., Ruocco, E., Ruocco, V. and Wolf, R. (2012). Structure and function of the epidermis related to barrier properties. *Clin. Dermatol.* **30**, 257-262.

Bates, D., Mächler, M., Bolker, B. and Walker, S. (2014). Fitting linear mixed-effects models using lme4. *J. Stat. Softw.* **67**, 1-48.

Bates, K. A., Clare, F. C., O'Hanlon, S., Bosch, J., Brookes, L., Hopkins, K., McLaughlin, E. J., Daniel, O., Garner, T. W. J., Fisher, M. C. et al. (2018). Amphibian chytridiomycosis outbreak dynamics are linked with host skin bacterial community structure. *Nat. Commun.* **9**, 693.

Becker, M. H., Brucker, R. M., Schwantes, C. R., Harris, R. N. and Minbiole, K. P. (2009). The bacterially produced metabolite violacein is associated with survival of amphibians infected with a lethal fungus. *Appl. Environ. Microbiol.* **75**, 6635-6638.

Beebee, T. J. and Griffiths, R. A. (2005). The amphibian decline crisis: a watershed for conservation biology? *Biol. Conserv.* **125**, 271-285.

Bellard, C., Genovesi, P. and Jeschke, J. (2016). Global patterns in threats to vertebrates by biological invasions. *Proc. R. Soc. B.* **283**, 1-9.

Benedictis, E. and Lacaz-Vieira, F. (1982). Electrolytes control flows of water across the apical barrier in toad skin: the hydrosmotic salt effect. *J. Membr. Biol.* **67**, 125-135.

Bentley, P. (1966). Adaptations of amphibia to arid environments. *Science* **152**, 619-623.

Bentley, P. J. (2002). The Amphibia. In *Endocrines and osmoregulation: a comparative account in vertebrates*, vol. 39, pp. 155-186: Springer-Verlag, Berlin. Heidelberg.

Berger, L. (2001). Diseases in Australian frogs. In *School of Public Health and Tropical Medicine*, vol. PhD Thesis: James Cook University.

Berger, L., Speare, R. and Hyatt, A. (1999a). Chytrid fungi and amphibian declines: Overview, implications and future directions. In *Declines and disappearances of Australian frogs*, (ed. A. Campbell). Canberra, Australia: Environment Australia.

Berger, L., Speare, R. and Kent, A. (1999b). Diagnosis of chytridiomycosis in amphibians by histologic examination. *Zoo. Print J.* **15**, 184-190.

Berger, L., Speare, R. and Skerratt, L. F. (2005a). Distribution of *Batrachochytrium dendrobatidis* and pathology in the skin of green tree frogs *Litoria caerulea* with severe chytridiomycosis. *Dis. Aquat. Org.* **68**, 65-70.

Berger, L., Hyatt, A. D., Speare, R. and Longcore, J. E. (2005b). Life cycle stages of the amphibian chytrid *Batrachochytrium dendrobatidis. Dis. Aquat. Org.* **68**, 51-63.

Berger, L., Marantelli, G., Skerratt, L. F. and Speare, R. (2005c). Virulence of the amphibian chytrid fungus *Batrachochytrium dendrobatidis* varies with the strain. *Dis. Aquat. Org.* **68**, 47-50.

Berger, L., Speare, R., Daszak, P., Green, D. E., Cunningham, A. A., Goggin, C. L., Slocombe, R., Ragan, M. A., Hyatt, A. D. and McDonald, K. R. (1998). Chytridiomycosis causes amphibian mortality associated with population declines in the rain forests of Australia and Central America. *Proc. Natl. Acad. Sci.* **95**, 9031-9036.

Berger, L., Speare, R., Hines, H., Marantelli, G., Hyatt, A., McDonald, K., Skerratt, L., Olsen, V., Clarke, J. and Gillespie, G. (2004). Effect of season and temperature on mortality in amphibians due to chytridiomycosis. *Aust. Vet. J.* **82**, 434-439.

Blaustein, A. R., Han, B. A., Relyea, R. A., Johnson, P. T., Buck, J. C., Gervasi, S. S. and Kats, L. B. (2011). The complexity of amphibian population declines: understanding the role of cofactors in driving amphibian losses. *Ann. N. Y. Acad. Sci.* **1223**, 108-119.

Bliss, D. E., Wang, S. M. and Martinez, E. A. (1966). Water balance in the land crab, *Gecarcinus lateralis*, during the intermolt cycle. *Am. Zool.* **6**, 197-212.

Booth, D. T., Clayton, D. H. and Block, B. A. (1993). Experimental demonstration of the energetic cost of parasitism in free-ranging hosts. *Proc. R. Soc. Lond. B Biol. Sci.* **253**, 125-129.

Bouhet, S. and Oswald, I. P. (2005). The effects of mycotoxins, fungal food contaminants, on the intestinal epithelial cell-derived innate immune response. *Vet. Immunol. Immunopathol.* **108**, 199-209.

Boutilier, R. G., Stiffler, D. F. and Toews, D. P. (1992). Exchange of respiratory gases, ions, and water in amphibious and aquatic amphibians. In *Environmental physiology of the amphibians*, eds. M. E. Feder and W. W. Burggren). Chicago, USA: University of Chicago Press.

Bouwer, S., Ewer, D. W. and Shiff, C. (1953). Frequency of moulting in Anura. *Nature* **172**, 408.

Bovo, R. P., Andrade, D. V., Toledo, L. F., Longo, A. V., Rodriguez, D., Haddad, C. F., Zamudio, K. R. and Becker, C. G. (2016). Physiological responses of Brazilian amphibians to an enzootic infection of the chytrid fungus *Batrachochytrium dendrobatidis. Dis. Aquat. Org.* **117**, 245-252.

Boyle, D. G., Boyle, D. B., Olsen, V., Morgan, J. A. T. and Hyatt, A. D. (2004). Rapid quantitative detection of chytridiomycosis (*Batrachochytrium dendrobatidis*) in amphibian samples using real-time Taqman PCR assay. *Dis. Aquat. Org.* **60**, 141-148.

Brandner, J. M. (2009). Tight junctions and tight junction proteins in mammalian epidermis. *Eur. J. Pharm. Biopharm.* **72**, 289-294.

Brannelly, L. A., Webb, R. J., Skerratt, L. F. and Berger, L. (2016). Effects of chytridiomycosis on hematopoietic tissue in the spleen, kidney and bone marrow in three diverse amphibian species. *Pathog. Dis.* **74**.

Brannelly, L. A., Roberts, A. A., Skerratt, L. F. and Berger, L. (2017). Epidermal cell death in frogs with chytridiomycosis. *PeerJ* **5**, e2925.

Brucker, R. M., Harris, R. N., Schwantes, C. R., Gallaher, T. N., Flaherty, D. C., Lam, B. A. and Minbiole, K. P. C. (2008). Amphibian chemical defense: antifungal metabolites of the microsymbiont *Janthinobacterium lividum* on the salamander *Plethodon cinereus. J. Chem. Ecol.* **34**, 1422-1429.

Brutyn, M., D'Herde, K., Dhaenens, M., Rooij, P. V., Verbrugghe, E., Hyatt, A. D., Croubels, S., Deforce, D., Ducatelle, R. and Haesebrouck, F. (2012). *Batrachochytrium dendrobatidis* zoospore secretions rapidly disturb intercellular junctions in frog skin. *Fungal Genet. Biol.* **49**, 830-837.

Bruus, K., Kristensen, P. and Larsen, E. H. (1976). Pathways for chloride and sodium transport across toad skin. *Acta Physiol. Scand.* **97**, 31-47.

Budtz, P. E. (1977). Aspects of moulting in anurans and its control. In *Symp. Zool. Soc. Lond.*, vol. 39, pp. 317-334.

Budtz, P. E. and Larsen, L. O. (1973). Structure of the toad epidermis during the moulting cycle. I. Light microscopic observations in *Bufo bufo* (L.). *Z. Zellforsch. Mik. Ana.* **144**, 353-368.

Budtz, P. E. and Larsen, L. O. (1975). Structure of the toad epidermis during the moulting cycle. II. Election microscope observations on *Bufo bufo* (L.). *Cell Tissue Res.* **159**, 459-483.

Burkart, D., Flechas, S. V., Vredenburg, V. T. and Catenazzi, A. (2017). Cutaneous bacteria, but not peptides, are associated with chytridiomycosis resistance in peruvian marsupial frogs. *Anim. Conserv.* **20**, 483-191.

Bustamante, H. M., Livo, L. J. and Carey, C. (2010). Effects of temperature and hydric environment on survival of the panamanian golden frog infected with a pathogenic chytrid fungus. *Intregr. Zool.* **5**, 143-153.

Buttemer, W. A. (1990). Effect of temperature on evaporative water loss of the Australian tree frogs *Litoria caerulea* and *Litoria chloris*. *Physiol. Zool.* **63**, 1043-1057.

Butterworth, M. B., Weisz, O. A. and Johnson, J. P. (2008). Some assembly required: putting the epithelial sodium channel together. *J. Biol. Chem.* **283**, 35305-35309.

Camacho, C., Coulouris, G., Avagyan, V., Ma, N., Papadopoulos, J., Bealer, K. and Madden, T. L. (2009). BLAST+: architecture and applications. *BMC Bioinformatics* **10**, 421.

Campbell, C. R., Voyles, J., Cook, D. I. and Dinudom, A. (2012). Frog skin epithelium: electrolyte transport and chytridiomycosis. *Int. J. Biochem. Cell Biol.* **44**, 431-434.

Canessa, C. M., Merillat, A.-M. and Rossier, B. C. (1994). Membrane topology of the epithelial sodium channel in intact cells. *Am. J. Physiol-Cell Ph.* **267**, C1682-C1690.

Canessa, C. M., Schild, L., Buell, G., Thorens, B., Gautschi, I., Horisberger, J.-D. and Rossier, B. C. (1994). Amiloride-sensitive epithelial Na+ channel is made of three homologous subunits. *Nature* **367**, 463.

Carey, C., Bruzgul, J. E., Livo, L. J., Walling, M. L., Kuehl, K. A., Dixon, B. F., Pessier, A. P., Alford, R. A. and Rogers, K. B. (2006). Experimental exposures of boreal toads (*Bufo boreas*) to a pathogenic chytrid fungus (*Batrachochytrium dendrobatidis*). *EcoHealth* **3**, 5-21.

Carver, S., Bell, B. D. and Waldman, B. (2010). Does chytridiomycosis disrupt amphibian skin function? *Copeia* **2010**, 487-495.

Castanho, L. M. and de Luca, I. M. S. (2001). Moulting behavior in leaf-frogs of the genus *Phyllomedusa* (Anura: Hylidae). *Zool. Anz.* **240**, 3-6.

Castillo, G. A., Coviello, A. and Orce, G. (1991). Effect of theophylline on the electrolyte permeability of the isolated skin of the toad *Bufo arenarum*. *Arch. Int. Physiol. Bio.* **99**, 257-264.

Catterall, W. A. (2000). From ionic currents to molecular mechanisms: the structure and function of voltage-gated sodium channels. *Neuron* **26**, 13-25.

Chammas, S. M., Carneiro, S. M., Ferro, R. S., Antoniazzi, M. M. and Jared, C. (2014). Development of integument and cutaneous glands in larval, juvenile and adult toads (*Rhinella granulosa*): a morphological and morphometric study. *Acta Zoologica*.

Chapman, J. A., Kirkness, E. F., Simakov, O., Hampson, S. E., Mitros, T., Weinmaier, T., Rattei, T., Balasubramanian, P. G., Borman, J. and Busam, D. (2010). The dynamic genome of Hydra. *Nature* **464**, 592.

Chasiotis, H. and Kelly, S. P. (2008). Occludin immunolocalization and protein expression in goldfish. *J. Exp. Biol.* **211**, 1524-1534.

Chasiotis, H. and Kelly, S. P. (2009). Occludin and hydromineral balance in *Xenopus laevis*. *J. Exp. Biol.* **212**, 287-296.

Chasiotis, H. and Kelly, S. P. (2011). Effect of cortisol on permeability and tight junction protein transcript abundance in primary cultured gill epithelia from stenohaline goldfish and euryhaline trout. *Gen. Comp. Endocr.* **172**, 494-504.

Chasiotis, H., Kolosov, D. and Kelly, S. P. (2011). Permeability properties of the teleost gill epithelium under ion-poor conditions. *Am. J. Physiol-Reg. I.* **302**, R727-R739.

Choi, C. Y. and An, K. W. (2008). Cloning and expression of Na+/K+-ATPase and osmotic stress transcription factor 1 mRNA in black porgy, *Acanthopagrus schlegeli* during osmotic stress. *Comp. Biochem. Physiol. Part B Biochem. Mol. Biol.* **149**, 91-100.

Christensen, C. U. (1974). Adaptations in the water economy of some anuran amphibia. *Comp. Biochem. Physiol. Part A Physiol.* **47**, 1035-1049.

Chuong, C., Nickoloff, B., Elias, P., Goldsmith, L., Macher, E., Maderson, P., Sundberg, J., Tagami, H., Plonka, P. and Thestrup-Pederson, K. (2002). What is the 'true' function of skin? *Exp. Dermatol.* **11**, 159-187.

Civan, M. M., Peterson-Yantorno, K., DiBona, D. R., Wilson, D. F. and Erecinska, M. (1983). Bioenergetics of Na+ transport across frog skin: chemical and electrical measurements. *Am. J. Physiol. Renal Physiol.* **245**, F691-F700.

Clarke, A. and Johnston, N. M. (1999). Scaling of metabolic rate with body mass and temperature in teleost fish. *J. Anim. Ecol.* **68**, 893-905.

Clarke, A. and Fraser, K. (2004). Why does metabolism scale with temperature? *Funct. Ecol.* **18**, 243-251.

Cock, P. J., Chilton, J. M., Grüning, B., Johnson, J. E. and Soranzo, N. (2015). NCBI BLAST+ integrated into Galaxy. *Gigascience* **4**, 39.

Cogger, H. G. (2014). Reptiles & Amphibians of Australia. Collingwood, VIC, Australia: CSIRO Publishing.

Cohen, J. M., Civitello, D. J., Venesky, M. D., McMahon, T. A. and Rohr, J. R. (2017a). Thermal mismatches explain how climate change and infectious disease drove widespread amphibian extinctions *bioRxiv*.

Cohen, J. M., Venesky, M. D., Sauer, E. L., Civitello, D. J., McMahon, T. A., Roznik, E. A. and Rohr, J. R. (2017b). The thermal mismatch hypothesis explains host susceptibility to an emerging infectious disease. *Ecol. Lett.* **20**, 184-193.

Collins, J. P. and Crump, M. L. (2009). Extinction in our times: global amphibian decline. New York, USA: Oxford University Press.

Cordenonsi, M., Mazzon, E., De Rigo, L., Baraldo, S., Meggio, F. and Citi, S. (1997). Occludin dephosphorylation in early development of *Xenopus laevis*. *J. Cell Sci.* **110**, 3131-3139.

Cox, T. C. and Alvarado, R. H. (1979). Electrical and transport characteristics of skin of larval *Rana catesbeiana*. *Am. J. Physiol-Reg. I.* **237**, R74-R79.

Crabbé, J. and de Weer, P. (1964). Action of aldosterone on the bladder and skin of the toad. *Nature* **202**, 298-299.

Cramp, R. L., Hudson, N. J. and Franklin, C. E. (2010). Activity, abundance, distribution and expression of Na+/K+-ATPase in the salt glands of *Crocodylus porosus* following chronic saltwater acclimation. *J. Exp. Biol.* **213**, 1301-1308.

Cramp, R. L., Kayes, S. M., Meyer, E. A. and Franklin, C. E. (2009). Ups and downs of intestinal function with prolonged fasting during aestivation in the burrowing frog, *Cyclorana alboguttata*. *J. Exp. Biol.* **212**, 3656-3663.

Cramp, R. L., McPhee, R. K., Meyer, E. A., Ohmer, M. E. and Franklin, C. E. (2014). First line of defence: the role of sloughing in the regulation of cutaneous microbes in frogs. *Conserv. Physiol.* **2**, 1-12.

Cumming, G., Fidler, F. and Vaux, D. L. (2007). Error bars in experimental biology. *J. Cell Biol.* **177**, 7-11.

Cunningham, A., Langton, T., Bennett, P., Lewin, J., Drury, S., Gough, R. and Macgregor, S. (1996). Pathological and microbiological findings from incidents of unusual mortality of the common frog (*Rana temporaria*). *Philos. Trans. R. Soc. B Biol. Sci.* **351**, 1539-1557.

Dall, W. and Smith, D. (1978). Water uptake at ecdysis in the western rock lobster. *J. Exp. Mar. Biol. Ecol.* **35**, 165-176.

Daszak, P., Berger, L., Cunningham, A. A., Hyatt, A. D., Green, D. E. and Speare, R. (1999). Emerging infectious diseases and amphibian population declines. *Emerg. Infect. Dis.* **5**, 735.

Daversa, D. R., Manica, A., Bosch, J., Jolles, J. W. and Garner, T. W. (2018). Routine habitat switching alters the likelihood and persistence of infection with a pathogenic parasite. *Funct. Ecol.* **32**, 1262-1270.

Davidson, E. W., Parris, M., Collins, J. P., Longcore, J. E., Pessier, A. P. and Brunner, J. (2003). Pathogenicity and transmission of chytridiomycosis in tiger salamanders (*Ambystoma tigrinum*). *Copeia* **200**, 601-607.

Davies, S. J., McGeoch, M. A. and Clusella-Trullas, S. (2015). Plasticity of thermal tolerance and metabolism but not water loss in an invasive reed frog. *Comp. Biochem. Physiol. Part A Mol. Integr. Physiol.* **189**, 11-20.

Dawson, D. C. and Liu, X. (2008). Osmoregulation: some principles of water and solute transport. In *Osmotic and ionic regulation: cells and animals*, (ed. D. H. Evans), pp. 1-36. FL, USA: CRC Press.

De Rosario-Martinez, H. (2013). Phia: post-hoc interaction analysis. In *R package version 0.1-3*. Vienna, Austria: R Foundation for Statistical Computing.

Demas, G. E., Greives, T., Chester, E. and French, S. (2011). The energetics of immunity. In *Ecoimmunology*, eds. G. E. Demas and R. J. Nelson). New York, USA: Oxford University Press.

Denèfle, J.-P., Goudeau, H. and Lechaire, J.-P. (1983). Influence of a transepithelial NaCl gradient on the moulting cycle, keratinization and active sodium transport of isolated frog skin cultured with or without aldosterone. *Roux's Arch. Dev. Biol.* **192**, 234-247.

Doody, K. A., Ohmer, M. E., Cramp, R. L. and Franklin, C. E. (In review). Do frogs infected with *Batrachochytrium dendrobatidis* avoid water while sloughing? *Herpetologica*.

Drewes, R. C., Hillman, S. S., Putnam, R. W. and Sokol, O. M. (1977). Water, nitrogen and ion balance in the African treefrog *Chiromantis petersi boulenger* (Anura: Rhacophoridae), with comments on the structure of the integument. *J. Comp. Physiol. (B)* **116**, 257-267.

Duneau, D. and Ebert, D. (2012). The role of moulting in parasite defence. *Proc. R. Soc. B. Biol. Sci.* **279**, 3049-3054.

Eaton, D., Malik, B., Saxena, N., Al-Khalili, O. and Yue, G. (2001). Mechanisms of aldosterone's action on epithelial Na+ transport. *J. Membr. Biol.* **184**, 313-319.

Ehrenfeld, J. and Klein, U. (1997). The key role of the H+ V-ATPase in acid-base balance and Na+ transport processes in frog skin. *J. Exp. Biol.* **200**, 247-256.

Ehrenfeld, J., Masoni, A. and Garcia-Romeu, F. (1976). Mitochondria-rich cells of frog skin in transport mechanisms: morphological and kinetic studies on transepithelial excretion of methylene blue. *Am. J. Physiol.* **231**, 120-126.

Ehrenfeld, J., Lacoste, I. and Harvey, B. (1989). The key role of the mitochondria-rich cell in Na+ and H+ transport across the frog skin epithelium. *Pflügers Archiv* **414**, 59-67.

Elias, H. and Shapiro, J. (1957). Histology of the skin of some toads and frogs. *Am. Mus. Novit.* **1819**, 1-27.

Ellison, A. R., Tunstall, T., DiRenzo, G. V., Hughey, M. C., Rebollar, E. A., Belden, L. K., Harris, R. N., Ibáñez, R., Lips, K. R. and Zamudio, K. R. (2015). More than skin deep: Functional genomic basis for resistance to amphibian chytridiomycosis. *Genome Biol. Evol.* **7**, 286-298.

Emerson, H. and Norris, C. (1905). "Red leg" —An infectious disease of frogs *J. Exp. Med.* **7**, 32-58.

Erlij, D. and Ussing, H. H. (1978). Transport across amphibian skin. In *Membrane transport in biology Vol. 3. Transport across multi-membrane systems*, vol. 3eds. G. Giebisch D. C. Tosteson and H. H. Ussing), pp. 175-208. Berlin: Springer-Verlag.

Ernst, V. V. (1973). The digital pads of the tree frog, *Hyla cinerea*. I. The epidermis. *Tissue Cell* **5**, 83-96.

Eskew, E. A., Worth, S. J., Foley, J. E. and Todd, B. D. (2015). American bullfrogs (*Lithobates catesbeianus*) resist infection by multiple isolates of *Batrachochytrium dendrobatidis*, including one implicated in wild mass mortality. *EcoHealth* **12**, 513-518.

Evans, D. H. (2008). Osmotic and ionic regulation: cells and animals: CRC Press.

Ewer, R. F. (1951). Water uptake and moulting in *Bufo regularis* Reuss. *J. Exp. Biol.* **28**, 369-373.

Farquhar, M. G. and Palade, G. E. (1964). Functional organization of amphibian skin. *Proc. Natl. Acad. Sci. USA* **51**, 569.

Farquhar, M. G. and Palade, G. E. (1965). Cell junctions in amphibian skin. *J. Cell Biol.* **26**, 263-291.

Farrer, R. A., Weinert, L. A., Bielby, J., Garner, T. W., Balloux, F., Clare, F., Bosch, J., Cunningham, A. A., Weldon, C. and du Preez, L. H. (2011). Multiple emergences of genetically diverse amphibian-infecting chytrids include a globalized hypervirulent recombinant lineage. *Proc. Natl. Acad. Sci.* **108**, 18732-18736.

Farrer, R. A., Martel, A., Verbrugghe, E., Abouelleil, A., Ducatelle, R., Longcore, J. E., James, T. Y., Pasmans, F., Fisher, M. C. and Cuomo, C. A. (2017). Genomic innovations linked to infection strategies across emerging pathogenic chytrid fungi. *Nat. Commun.* **8**, 14742.

Feder, M. E. (1976). Lunglessness, body size, and metabolic rate in salamanders. *Physiol. Zool.* **49**, 398-406.

Feder, M. E. and Burggren, W. W. (1992). Environmental physiology of the amphibians. Chicago, USA: University of Chicago Press.

Feldman, G. J., Mullin, J. M. and Ryan, M. P. (2005). Occludin: Structure, function and regulation. *Adv. Drug Delivery. Rev.* **57**, 883-917.

Fellers, G. M., Green, D. E. and Longcore, J. E. (2001). Oral chytridiomycosis in the mountain yellow-legged frog (*Rana muscosa*). *Copeia* **2001**, 945-953.

Finn, R. N., Chauvigné, F., Hlidberg, J. B., Cutler, C. P. and Cerdà, J. (2014). The lineage-specific evolution of aquaporin gene clusters facilitated tetrapod terrestrial adaptation. *PLOS ONE* **9**, e113686.

Fischbarg, J. (2010). Fluid transport across leaky epithelia: central role of the tight junction and supporting role of aquaporins. *Physiol. Rev.* **90**, 1271-1290.

Fisher, M. C., Garner, T. W. and Walker, S. F. (2009). Global emergence of *Batrachochytrium dendrobatidis* and amphibian chytridiomycosis in space, time, and host. *Annu. Rev. Microbiol.* **63**, 291-310.

Foguesatto, K., Boyle, R. T., Rovani, M. T., Freire, C. A. and Souza, M. M. (2017). Aquaporin in different moult stages of a freshwater decapod crustacean: expression and participation in muscle hydration control. *Comp. Biochem. Physiol. Part A Mol. Integr. Physiol.* **208**, 61-69.

Förster, C., Silwedel, C., Golenhofen, N., Burek, M., Kietz, S., Mankertz, J. and Drenckhahn, D. (2005). Occludin as direct target for glucocorticoid-induced improvement of blood–brain barrier properties in a murine in vitro system. *J. Physiol.* **565**, 475-486.

Fujita, K., Katahira, J., Horiguchi, Y., Sonoda, N., Furuse, M. and Tsukita, S. (2000). *Clostridium perfringens* enterotoxin binds to the second extracellular loop of claudin-3, a tight junction integral membrane protein. *FEBS Lett.* **476**, 258-261.

Fukumatsu, M., Ogawa, M., Arakawa, S., Suzuki, M., Nakayama, K., Shimizu, S., Kim, M., Mimuro, H. and Sasakawa, C. (2012). Shigella targets epithelial tricellular junctions and uses a noncanonical clathrin-dependent endocytic pathway to spread between cells. *Cell Host & Microbe* **11**, 325-336.

Furuse, M., Fujita, K., Hiiragi, T., Fujimoto, K. and Tsukita, S. (1998). Claudin-1 and-2: novel integral membrane proteins localizing at tight junctions with no sequence similarity to occludin. *J. Cell Biol.* **141**, 1539-1550.

Furuse, M., Hirase, T., Itoh, M., Nagafuchi, A., Yonemura, S., Tsukita, S. and Tsukita, S. (1993). Occludin: a novel integral membrane protein localizing at tight junctions. *J. Cell Biol.* **123**, 1777-1788.

Furuse, M., Hata, M., Furuse, K., Yoshida, Y., Haratake, A., Sugitani, Y., Noda, T., Kubo, A. and Tsukita, S. (2002). Claudin-based tight junctions are crucial for the mammalian epidermal barrier: a lesson from claudin-1-deficient mice. *J. Cell Biol.* **156**.

Garty, H. (1986). Mechanisms of aldosterone action in tight epithelia. *J. Membr. Biol.* **90**, 193-205.

Gauberg, J., Wu, N. C., Cramp, R. L., Kelly, S. P. and Franklin, C. E. (2019). A lethal fungal pathogen directly alters tight junction proteins in the skin of a susceptible amphibian. *J. Exp. Biol.* **222**, jeb192245.

Giorgi, M. S., Arlettaz, R., Christe, P. and Vogel, P. (2001). The energetic grooming costs imposed by a parasitic mite (*Spinturnix myoti*) upon its bat host (*Myotis myotis*). *Proc. R. Soc. Lond. B Biol. Sci.* **268**, 2071-2075.

Goiran, C., Bustamante, P. and Shine, R. (2017). Industrial melanism in the seasnake *Emydocephalus annulatus*. *Curr. Biol.* **27**, 2510-2513. e2512.

Gonzalez-Mariscal, L., Betanzos, A., Nava, P. and Jaramillo, B. (2003). Tight junction proteins. *Prog. Biophys. Mol. Biol.* **81**, 1-44.

Gray, M. J., Miller, D. L. and Hoverman, J. T. (2009). Ecology and pathology of amphibian ranaviruses. *Dis. Aquat. Org.* **87**, 243-266.

Greenberg, D. A., Palen, W. J. and Mooers, A. Ø. (2017). Amphibian species' traits, evolutionary history, and environment predict *Batrachochytrium dendrobatidis* infection patterns, but not extinction risk. *Evol. Appl.* **10**, 1130-1145.

Greenspan, S. E., Longcore, J. E. and Calhoun, A. J. K. (2012). Host invasion by *Batrachochytrium dendrobatidis*: fungal and epidermal ultrastructure in model anurans. *Dis. Aquat. Org.* **100**, 201-210.

Greenwald, L. (1972). Sodium balance in amphibians from different habitats. *Physiol. Zool.* **45**, 229-237.

Grogan, L. F., Skerratt, L. F., Berger, L., Cashins, S. D., Trengove, R. D. and Gummer, J. P. (2018). Chytridiomycosis causes catastrophic organism-wide metabolic dysregulation including profound failure of cellular energy pathways. *Sci. Rep.* **8**, 1-15.

Gumbiner, B., Stevenson, B. and Grimaldi, A. (1988). The role of the cell adhesion molecule uvomorulin in the formation and maintenance of the epithelial junctional complex. *J. Cell Biol.* **107**, 1575-1587.

Günzel, D. and Fromm, M. (2012). Claudins and other tight junction proteins. *Compr. Physiol.* **2**, 1819-1852.

Günzel, D. and Yu, A. S. L. (2013). Claudins and the modulation of tight junction permeability. *Physiol. Rev.* **93**, 525-569.

Guttman, J. A. and Finlay, B. B. (2009). Tight junctions as targets of infectious agents. *BBA-Biomembranes* **1788**, 832-841.

Guyton, A. C. (1991). Blood pressure control—special role of the kidneys and body fluids. *Science* **252**, 1813-1816.

Hadj-Rabia, S., Baala, L., Vabres, P., Hamel-Teillac, D., Jacquemin, E., Fabre, M., Lyonnet, S., de Prost, Y., Munnich, A. and Hadchouel, M. (2004). Claudin-1 gene mutations in neonatal sclerosing cholangitis associated with ichthyosis: a tight junction disease. *Gastroenterology* **127**, 1386-1390.

Hanukoglu, I. and Hanukoglu, A. (2016). Epithelial sodium channel (ENaC) family: phylogeny, structure–function, tissue distribution, and associated inherited diseases. *Gene* **579**, 95-132.

Harris, R. N., Brucker, R. M., Walke, J. B., Becker, M. H., Schwantes, C. R., Flaherty, D. C., Lam, B. A., Woodhams, D. C., Briggs, C. J. and Vredenburg, V. T. (2009). Skin microbes on frogs prevent morbidity and mortality caused by a lethal skin fungus. *The ISME journal* **3**, 818-824.

Harvey, B. and Kernan, R. (1984). Intracellular ion activities in frog skin in relation to external sodium and effects of amiloride and/or ouabain. *J. Physiol.* **349**, 501-517.

Hasegawa, T., Tanii, H., Suzuki, M. and Tanaka, S. (2003). Regulation of water absorption in the frog skins by two vasotocin-dependent water-channel aquaporins, AQP-h2 and AQP-h3. *Endocrinology* **144**, 4087-4096.

Heatwole, H., Barthalmus, G. T. and Heatwole, A. Y. (1994). Amphibian biology. Vol. 1. The integument. NSW, Australia: Surrey Beatty & Sons.

Hillman, S. S. (1980). Physiological correlates of differential dehydration tolerance in anuran amphibians. *Copeia* **1980**, 125-129.

Hillman, S. S., Hancock, T. V. and Hedrick, M. S. (2013). A comparative meta-analysis of maximal aerobic metabolism of vertebrates: implications for respiratory and cardiovascular limits to gas exchange. *J. Comp. Physiol. B* **183**, 167-179.

Hillman, S. S., Hedrick, M. S., Withers, P. C. and Drewes, R. C. (2004). Lymph pools in the basement, sump pumps in the attic: the anuran dilemma for lymph movement. *Physiol. Biochem. Zool.* **77**, 161-173.

Hillman, S. S., Withers, P. C., Drewes, R. C. and Hillyard, S. D. (2009). Ecological and environmental physiology of amphibians. New York, USA: Oxford University Press

Hillyard, S. D., Viborg, A. and Nagai, T. (2007). Chemosensory function of salt and water transport by the amphibian skin. *Comp. Biochem. Physiol. Part A Mol. Integr. Physiol.* **148**, 44-54.

Hillyard, S. D., Goldstein, J., Tuttle, W. and Hoff, K. (2004). Transcellular and paracellular elements of salt chemosensation in toad skin. *Chem. Senses* **29**, 755-762.

Hillyard, S. D., Møbjerg, N., Tanaka, S. and Larsen, E. H. (2008). Osmotic and ionic regulation in amphibians. In *Osmotic and ionic regulation: cells and animals*, (ed. D. H. Evans), pp. 367-441. FL, USA: CRC Press.

Hothorn, T., Bretz, F. and Westfall, P. (2008). Simultaneous inference in general parametric models. *Biometrical J.* **50**, 346-363.

Houlihan, D. F. (1991). Protein turnover in ectotherms and its relationships to energetics. In *Adv. Comp. Environ. Physiol.*, vol. 7eds. D. F. Houlihan D. R. Livingstone and R. F. Lee), pp. 1-43. Berlin Heidelberg: Springer-Verlag.

Hunter, D. A., Speare, R., Marantelli, G., Mendez, D., Pietsch, R. and Osborne, W. (2010). Presence of the amphibian chytrid fungus *Batrachochytrium dendrobatidis* in threatened corroboree frog populations in the Australian Alps. *Dis. Aquat. Org.* **92**, 209-216.

Ikenouchi, J., Furuse, M., Furuse, K., Sasaki, H., Tsukita, S. and Tsukita, S. (2005). Tricellulin constitutes a novel barrier at tricellular contacts of epithelial cells. *J. Cell Biol.* **171**, 939-945.

IUCN. (2017). The IUCN Red List of Threatened Species. Version 2017.1.

Jaisser, F., Canessa, C. M., Horisberger, J.-D. and Rossier, B. C. (1992). Primary sequence and functional expression of a novel ouabain-resistant Na, K-ATPase. The beta subunit modulates potassium activation of the Na, K-pump. *J. Biol. Chem.* **267**, 16895-16903.

Jones, D. and Holladay, S. (2006). Excretion of three heavy metals in the shed skin of exposed corn snakes (*Elaphe guttata*). *Ecotoxicol. Environ. Saf.* **64**, 221-225.

Jørgensen, C. B. (1949). Permeability of the amphibian skin. II. Effect of moulting of the skin of anurans on the permeability to water and electrolytes. *Acta Physiol. Scand.* **18**, 171-180.

Jørgensen, C. B. (1988). Nature of moulting control in Amphibians: effects of cortisol implants in toads *Bufo bufo. Gen. Comp. Endocr.* **71**, 29-35.

Jørgensen, C. B. and Larsen, L. O. (1961). Molting and its hormonal control in toads. *Gen. Comp. Endocr.* **1**, 145-153.

Katahira, J., Inoue, N., Horiguchi, Y., Matsuda, M. and Sugimoto, N. (1997). Molecular cloning and functional characterization of the receptor for *Clostridium perfringens* enterotoxin. *J. Cell Biol.* **136**, 1239-1247.

Katz, U. (1978). Changes in ionic conductances and in sensitivity to amiloride during the natural moulting cycle of toad skin (*Bufo viridis*, L.). *J. Membr. Biol.* **38**, 1-9.

Kawedia, J. D., Nieman, M. L., Boivin, G. P., Melvin, J. E., Kikuchi, K.-I., Hand, A. R., Lorenz, J. N. and Menon, A. G. (2007). Interaction between transcellular and paracellular water transport pathways through Aquaporin 5 and the tight junction complex. *Proc. Natl. Acad. Sci.* **104**, 3621-3626.

Kelly, S. P. and Wood, C. M. (2001). Effect of cortisol on the physiology of cultured pavement cell epithelia from freshwater trout gills. *Am. J. Physiol-Reg. I.* **281**, R811-R820.

Kilgore, M. W., Stewart, G. L. and Smatresk, N. J. (1988). Oxygen uptake in mice infected with *Trichinella spiralis. J. Parasitol.*, 721-724.

Kilpatrick, A. M., Briggs, C. J. and Daszak, P. (2010). The ecology and impact of chytridiomycosis: an emerging disease of amphibians. *Trends Ecol. Evol.* **25**, 109-118.

Kinney, V. C., Heemeyer, J. L., Pessier, A. P. and Lannoo, M. J. (2011). Seasonal pattern of *Batrachochytrium dendrobatidis* infection and mortality in *Lithobates areolatus*: affirmation of Vredenburg's "10,000 zoospore rule". *PLOS ONE* **6**, e16708.

Kirchmeier, P., Sayar, E., Hotz, A., Hausser, I., Islek, A., Yilmaz, A., Artan, R. and Fischer, J. (2014). Novel mutation in the CLDN 1 gene in a Turkish family with neonatal ichthyosis sclerosing cholangitis (NISCH) syndrome. *Br. J. Dermatol.* **170**, 976-978.

Kirschner, N., Poetzl, C., von den Driesch, P., Wladykowski, E., Moll, I., Behne, M. J. and Brandner, J. M. (2009). Alteration of tight junction proteins is an early event in psoriasis: putative involvement of proinflammatory cytokines. *Am. J. Pathol.* **175**, 1095-1106.

Klein, W., Dabés, L., Bonfim, V. M. G., Magrini, L. and Napoli, M. F. (2016). Allometric relationships between cutaneous surface area and body mass in anuran amphibians. *Zool. Anz.* **263**, 45-54.

Kleyman, T. R. and Cragoe, E. J. (1988). Amiloride and its analogs as tools in the study of ion transport. *J. Membr. Biol.* **105**, 1-21.

Kleyman, T. R., Carattino, M. D. and Hughey, R. P. (2009). ENaC at the cutting edge: Regulation of epithelial sodium channels by proteases. *J. Biol. Chem.* **284**, 20447-20451.

Kobayashi, K., Tsugami, Y., Matsunaga, K., Oyama, S., Kuki, C. and Kumura, H. (2016). Prolactin and glucocorticoid signaling induces lactation-specific tight junctions concurrent with β-casein expression in mammary epithelial cells. *BBA-Mol. Cell Res.* **1863**, 2006-2016.

Koefoed-Johnson, V. and Ussing, H. H. (1958). The nature of the frog skin potential. *Acta Physiol. Scand.* **42**, 298-308.

Köhler, H., Sakaguchi, T., Hurley, B. P., Kase, B. J., Reinecker, H.-C. and McCormick, B. A. (2007). *Salmonella enterica* serovar Typhimurium regulates intercellular junction proteins and facilitates transepithelial neutrophil and bacterial passage. *Am. J. Physiol. Gastrointest. Liver Physiol.* **293**, G178-G187.

Kolosov, D. and Kelly, S. P. (2013). A role for tricellulin in the regulation of gill epithelium permeability. *Am. J. Physiol-Reg. I.* **304**, R1139-R1148.

Kolosov, D. and Kelly, S. P. (2017). Claudin-8d is a cortisol-responsive barrier protein in the gill epithelium of trout. *J. Mol. Endocrinol.* **59**, 299-310.

Kolosov, D., Bui, P., Donini, A., Wilkie, M. P. and Kelly, S. P. (2017). A role for tight junction-associated MARVEL proteins in larval sea lamprey (*Petromyzon marinus*) osmoregulation. *J. Exp. Biol.* **220**, 3657-3670.

Konno, N., Hyodo, S., Yamada, T., Matsuda, K. and Uchiyama, M. (2007). Immunolocalization and mRNA expression of the epithelial Na+ channel α-subunit in the kidney and urinary bladder of the marine toad, *Bufo marinus*, under hyperosmotic conditions. *Cell Tissue Res.* **328**, 583-594.

Kriger, K. and Hero, J. M. (2007). Large-scale seasonal variation in the prevalence and severity of chytridiomycosis. *J. Zool.* **271**, 352-359.

Kriger, K. M., Hines, H. B., Hyatt, A. D., Boyle, D. G. and Hero, J.-M. (2006). Techniques for detecting chytridiomycosis in wild frogs: comparing histology with real-time Taqman PCR. *Dis. Aquat. Org.* **71**, 141.

Krug, S. M., Amasheh, S., Richter, J. F., Milatz, S., Günzel, D., Westphal, J. K., Huber, O., Schulzke, J. D. and Fromm, M. (2009). Tricellulin forms a barrier to macromolecules in tricellular tight junctions without affecting ion permeability. *Mol. Biol. Cell* **20**, 3713-3724.

Krzywinski, M. and Altman, N. (2013). Points of significance: error bars. *Nat. Meth.* **10**, 921-922.

Kuznetsova, A., Brockhoff, P. B. and Christensen, R. H. B. (2015). lmerTest: Tests in linear mixed effects models. In *R package*, vol. 2. Vienn, Austria: R foundation for statistical Computing.

Kwong, R. M., Kumai, Y. and Perry, S. (2013). Evidence for a role of tight junctions in regulating sodium permeability in zebrafish (*Danio rerio*) acclimated to ion-poor water. *J. Comp. Physiol. B* **183**, 203-213.

La Marca, E., Lips, K. R., Lötters, S., Puschendorf, R., Ibáñez, R., Rueda-Almonacid, J. V., Schulte, R., Marty, C., Castro, F. and Manzanilla-Puppo, J. (2005). Catastrophic population declines and extinctions in neotropical harlequin frogs (Bufonidae: Atelopus). *Biotropica* **37**, 190-201.

Laking, A. E., Ngo, H. N., Pasmans, F., Martel, A. and Nguyen, T. T. (2017). *Batrachochytrium salamandrivorans* is the predominant chytrid fungus in Vietnamese salamanders. *Sci. Rep.* **7**.

Lang, M. A., Caplan, S. R. and Essig, A. (1975). Action of aldosterone on frog skin in the presence and absence of *in-vitro* molting effects. *BBA-Biomembranes* **401**, 481-485.

Langhammer, P. F., Burrowes, P. A., Lips, K. R., Bryant, A. B. and Collins, J. P. (2014). Susceptibility to the amphibian chytrid fungus varies with ontogeny in the direct-developing frog, *Eleutherodactylus coqui*. *J. Wildl. Dis.* **50**, 438-446.

Larsen, E. H. (1970). Sodium transport and D.C. resistance in the isolated toad skin in relation to shedding of the *stratum corneum*. *Acta Physiol. Scand.* **79**, 453-461.

Larsen, E. H. (1971a). Effect of aldosterone and oxytocin on the active sodium transport across the isolated toad skin in relation to loosening of *stratum corneum*. *Gen. Comp. Endocr.* **17**, 543-553.

Larsen, E. H. (1971b). The relative contributions of sodium and chloride ions to the conductance of toad skin in relation to shedding of the *stratum corneum*. *Acta Physiol. Scand.* **81**, 254-263.

Larsen, E. H. (1972). Characteristics of aldosterone stimulated transport in isolated skin of the toad, *Bufo bufo* (L.). *J. Steriod Biochem.* **3**, 111-120.

Larsen, E. H. (1991). Chloride transport by high-resistance heterocellular epithelia. *Physiol. Rev.* **71**, 235-283.

Larsen, E. H. and Ramløv, H. (2013). Role of cutaneous surface fluid in frog osmoregulation. *Comp. Biochem. Physiol. Part A Mol. Integr. Physiol.* **165**, 365-370.

Larsen, E. H., Willumsen, N. J., Møbjerg, N. and Sørensen, J. N. (2009). The lateral intercellular space as osmotic coupling compartment in isotonic transport. *Acta Physiologica* **195**, 171-186.

Larsen, E. H., Deaton, L. E., Onken, H., O'Donnell, M., Grosell, M., Dantzler, W. H. and Weihrauch, D. (2014). Osmoregulation and excretion. *Compr. Physiol.* **4**, 405-573.

Larsen, L. O. (1976). Physiology of molting. In *Physiology of the amphibia*, vol. 3(ed. B. Lofts), pp. 53-100. London, UK: Academic Press, Inc.

Leaf, A. and Dempsey, E. (1960). Some effects of mammalian neurohypophyseal hormones on metabolism and active transport of sodium by the isolated toad bladder. *J. Biol. Chem.* **235**, 2160.

Lenth, R. V. (2016). Least-squares means: The R package lsmeans. *J. Stat. Softw.* **69**, 1-33.

Lighton, J. R. (2008). Measuring metabolic rates: a manual for scientists. New York: Oxford University Press.

Lillywhite, H. B. (2006). Water relations of tetrapod integument. *J. Exp. Biol.* **209**, 202-226.

Lillywhite, H. B. and Maderson, P. F. (1988). The structure and permeability of integument. *Am. Zool.* **28**, 945-962.

Lindemann, B. and Voute, C. (1976). Structure and function of the epidermis. In *Frog neurobiology: A handbook*, eds. R. Llinás and P. Wolfgang), pp. 169-210. berlin: Springer-verlag.

Ling, J. K. (1972). Adaptive functions of vertebrate molting cycles. *Am. Zool.* **12**, 77-93.

Lingrel, J. B. and Kuntzweiler, T. (1994). Na+, K+ -ATPase. *J. Biol. Chem.* **269**, 19659-19662.

Lips, K. R. (2016). Overview of chytrid emergence and impacts on amphibians. *Philos. Trans. R. Soc. B Biol. Sci.* **371**, 20150465.

Lips, K. R., Reeve, J. D. and Witters, L. R. (2003). Ecological traits predicting amphibian population declines in Central America. *Conserv. Biol.* **17**, 1078-1088.

Lochmiller, R. L. and Deerenberg, C. (2000). Trade-offs in evolutionary immunology: just what is the cost of immunity? *Oikos* **88**, 87-98.

Longcore, J. E., Pessier, A. P. and Nichols, D. K. (1999). *Batrachochytrium dendrobatidis* gen. et sp. nov., a chytrid pathogenic to amphibians. *Mycologia* **91**, 219-227.

Longo, A. V. and Zamudio, K. R. (2017). Environmental fluctuations and host skin bacteria shift survival advantage between frogs and their fungal pathogen. *The ISME Journal* **11**, 349.

Longo, A. V., Savage, A. E., Hewson, I. and Zamudio, K. R. (2015). Seasonal and ontogenetic variation of skin microbial communities and relationships to natural disease dynamics in declining amphibians. *R. Soc. Open Sci.* **2**, 140377.

MacRobbie, E. A. and Ussing, H. (1961). Osmotic behaviour of the epithelial cells of frog skin. *Acta Physiol. Scand.* **53**, 348-365.

Mandel, L. J. and Curran, P. F. (1972). Chloride flux via a shunt pathway in frog skin: apparent exchange diffusion. *BBA-Biomembranes* **282**, 258-264.

Maniero, G. D. and Carey, C. (1997). Changes in selected aspects of immune function in the leopard frog, *Rana pipiens*, associated with exposure to cold. *J. Comp. Physiol. (B)* **167**, 256-263.

Marcum, R. D., St-Hilaire, S., Murphy, P. J. and Rodnick, K. J. (2010). Effects of *Batrachochytrium dendrobatidis* infection on ion concentrations in the boreal toad *Anaxyrus* (*Bufo*) *boreas boreas*. *Dis. Aquat. Org.* **91**, 17-21.

Mariano, C., Sasaki, H., Brites, D. and Brito, M. A. (2011). A look at tricellulin and its role in tight junction formation and maintenance. *Eur. J. Cell Biol.* **90**, 787-796.

Martel, A., Spitzen-van der Sluijs, A., Blooi, M., Bert, W., Ducatelle, R., Fisher, M. C., Woeltjes, A., Bosman, W., Chiers, K. and Bossuyt, F. (2013). *Batrachochytrium salamandrivorans* sp. nov. causes lethal chytridiomycosis in amphibians. *Proc. Natl. Acad. Sci.* **110**, 15325-15329.

Martel, A., Blooi, M., Adriaensen, C., Van Rooij, P., Beukema, W., Fisher, M. C., Farrer, R. A., Schmidt, B. R., Tobler, U., Goka, K. et al. (2014). Recent introduction of a chytrid fungus endangers Western Palearctic salamanders. *Science* **346**, 630-631.

Martinez-Palomo, A., Erlij, D. and Bracho, H. (1971). Localization of permeability barriers in the frog skin epithelium. *J. Cell Biol.* **50**, 277-287.

McCallum, M. L. (2007). Amphibian decline or extinction? Current declines dwarf background extinction rate. *J. Herpetol.* **41**, 483-491.

McClanahan Jr, L. L. and Baldwin, R. (1969). Rate of water uptake through the integument of the desert toad, *Bufo punctatus*. *Comp. Biochem. Physiol.* **28**, 381-389.

McClanahan Jr, L. L., Stinner, J. N. and Shoemaker, V. H. (1978). Skin lipids, water loss, and energy metabolism in a South American tree frog (*Phyllomedusa sauvagei*). *Physiol. Zool.* **51**, 179-187.

McLaughlin, J., Padfield, P. J., Burt, J. P. and O'Neill, C. A. (2004). Ochratoxin A increases permeability through tight junctions by removal of specific claudin isoforms. *Am. J. Physiol-Cell Ph.* **287**, C1412-C1417.

McLaughlin, J., Lambert, D., Padfield, P. J., Burt, J. P. and O'Neill, C. A. (2009). The mycotoxin patulin, modulates tight junctions in caco-2 cells. *Toxicol. In Vitro* **23**, 83-89.

McMahon, T. A., Brannelly, L. A., Chatfield, M. W., Johnson, P. T., Joseph, M. B., McKenzie, V. J., Richards-Zawacki, C. L., Venesky, M. D. and Rohr, J. R. (2013). Chytrid fungus *Batrachochytrium dendrobatidis* has nonamphibian hosts and releases chemicals that cause pathology in the absence of infection. *Proc. Natl. Acad. Sci.* **110**, 210-215.

McMahon, T. A., Sears, B. F., Venesky, M. D., Bessler, S. M., Brown, J. M., Deutsch, K., Halstead, N. T., Lentz, G., Tenouri, N. and Young, S. (2014). Amphibians acquire resistance to live and dead fungus overcoming fungal immunosuppression. *Nature* **511**, 224-227.

Meyer, E. A., Cramp, R. L. and Franklin, C. E. (2010). Damage to the gills and integument of *Litoria fallax* larvae (Amphibia: Anura) associated with ionoregulatory disturbance at low pH. *Comp. Biochem. Physiol. Part A Mol. Integr. Physiol.* **155**, 164-171.

Meyer, E. A., Cramp, R. L., Bernal, M. H. and Franklin, C. E. (2012). Changes in cutaneous microbial abundance with sloughing: Possible implications for infection and disease in amphibians. *Dis. Aquat. Org.* **101**, 235-242.

Miller, D., Gray, M. and Storfer, A. (2011). Ecopathology of ranaviruses infecting amphibians. *Viruses* **3**, 2351-2373.

Mills, J. W., Ernst, S. A. and Dibona, D. R. (1977). Localization of Na+-pump sites in frog skin. *J. Cell Biol.* **73**, 88-110.

Mullen, T. L. and Alvarado, R. H. (1976). Osmotic and ionic regulation in amphibians. *Physiol. Zool.* **49**, 11-23.

Murphy, M. E. and Taruscio, T. G. (1995). Sparrows increase their rates of tissue and whole-body protein synthesis during the annual molt. *Comp. Biochem. Physiol. Part A Physiol.* **111**, 385-396.

Muza-Moons, M. M., Schneeberger, E. E. and Hecht, G. A. (2004). Enteropathogenic *Escherichia coli* infection leads to appearance of aberrant tight junctions strands in the lateral membrane of intestinal epithelial cells. *Cell. Microbiol.* **6**, 783-793.

Mykles, D. L. (1980). The mechanism of fluid absorption at ecdysis in the American lobster *Homarus americanus. J. Exp. Biol.* **84**, 89-102.

Nichols, D. K., Lamirande, E. W., Pessier, A. P. and Longcore, J. E. (2001). Experimental transmission of cutaneous chytridiomycosis in dendrobatid frogs. *J. Wildl. Dis.* **37**, 1-11.

Nielsen, R. (1969). The effect of aldosterone in vitro on the active sodium transport and moulting of the frog skin. *Acta Physiol. Scand.* **77**, 85-94.

Nielsen, R. (1979). A 3 to 2 coupling of the Na—K pump responsible for the transepithelial Na transport in frog skin disclosed by the effect of Ba. *Acta Physiol. Scand.* **107**, 189-191.

Nielsen, R. and Tomilson, R. (1970). The effect of amiloride on sodium transport in the normal and moulting frog skin. *Acta Physiol. Scand.* **79**, 238-243.

Niessen, C. M. (2007). Tight junctions/adherens junctions: basic structure and function. *J. Invest. Dermatol.* **127**, 2525-2532.

Ogushi, Y., Kitagawa, D., Hasegawa, T., Suzuki, M. and Tanaka, S. (2010a). Correlation between aquaporin and water permeability in response to vasotocin, hydrin and β-adrenergic effectors in the ventral pelvic skin of the tree frog *Hyla japonica. J. Exp. Biol.* **213**, 288-294.

Ogushi, Y., Tsuzuki, A., Sato, M., Mochida, H., Okada, R., Suzuki, M., Hillyard, S. D. and Tanaka, S. (2010b). The water-absorption region of ventral skin of several semiterrestrial and aquatic anuran amphibians identified by aquaporins. *Am. J. Physiol. Regul. Integr. Comp. Physiol.* **299**, R1150-R1162.

Ohmer, M. E., Herbert, S. M., Speare, R. and Bishop, P. J. (2013). Experimental exposure indicates the amphibian chytrid pathogen poses low risk to New Zealand's threatened endemic frogs. *Anim. Conserv.* **16**, 422-429.

Ohmer, M. E., Cramp, R. L., White, C. R. and Franklin, C. E. (2015). Skin sloughing rate increases with chytrid fungus infection load in a susceptible amphibian. *Funct. Ecol.* **29**, 674-682.

Ohmer, M. E., Cramp, R. L., Russo, C. J. M., White, C. R. and Franklin, C. E. (2017). Skin sloughing in susceptible and resistant amphibians regulates infection with a fungal pathogen *Sci. Rep.* **7**, 3592.

Ohmer, M. E., Cramp, R. L., White, C. R., Harlow, P. S., McFadden, M. S., Merino-Viteri, A., Pessier, A. P., Wu, N. C., Bishop, P. J. and Franklin, C. E. (2019). Phylogenetic investigation of skin sloughing rates in frogs: relationships with skin characteristics and disease-driven declines. *Proc. R. Soc. B.* **286**, 20182378.

Olson, D. H., Aanensen, D. M., Ronnenberg, K. L., Powell, C. I., Walker, S. F., Bielby, J., Garner, T. W., Weaver, G. and Fisher, M. C. (2013). Mapping the global emergence of *Batrachochytrium dendrobatidis*, the amphibian chytrid fungus. *PLOS ONE* **8**, e56802.

Orlofske, S., Belden, L. and Hopkins, W. (2013). Larval wood frog (*Rana* [= *Lithobates*] *sylvatica*) development and physiology following infection with the trematode parasite, *Echinostoma trivolvis*. *Comp. Biochem. Physiol. Part A Mol. Integr. Physiol.* **164**, 529-536.

Osborn, C. M. (1936). The inhibition of molting in urodeles following thyroidectomy or hypophysectomy. *Anat. Rec.* **66**, 257-269.

Packard, G. C. and Birchard, G. F. (2008). Traditional allometric analysis fails to provide a valid predictive model for mammalian metabolic rates. *J. Exp. Biol.* **211**, 3581-3587.

Pandey, R. N., Yaganti, S., Coffey, S., Frisbie, J., Alnajjar, K. and Goldstein, D. (2010). Expression and immunolocalization of aquaporins HC-1,-2, and-3 in Cope's gray treefrog, *Hyla chrysoscelis*. *Comp. Biochem. Physiol. Part A Mol. Integr. Physiol.* **157**, 86-94.

Pessier, A. P. (2002). An overview of amphibian skin disease. In *Seminars in avian and exotic pet medicine*, vol. 11, pp. 162-174: Elsevier.

Pessier, A. P., Nichols, D. K., Longcore, J. E. and Fuller, M. S. (1999). Cutaneous chytridiomycosis in poison dart frogs (*Dendrobates spp.*) and White's tree frogs (*Litoria caerulea*). *J. Vet. Diagn. Invest.* **11**, 194-199.

Peterson, J. D., Steffen, J. E., Reinert, L. K., Cobine, P. A., Appel, A., Rollins-Smith, L. and Mendonça, M. T. (2013). Host stress response is important for the pathogenesis of the deadly amphibian disease, chytridiomycosis, in *Litoria caerulea*. *PLOS ONE* **8**, e62146.

Petranka, J. W. (1998). Salamanders of the United States and Canada: Smithsonian Institution Press Washington, DC.

Pfaffl, M. W. (2001). A new mathematical model for relative quantification in real-time RT–PCR. *Nucleic Acids Res.* **29**, e45-e45.

Phillips, B. L., Brown, G. P., Webb, J. K. and Shine, R. (2006). Invasion and the evolution of speed in toads. *Nature* **439**, 803-803.

Pimm, S. L., Jenkins, C. N., Abell, R., Brooks, T. M., Gittleman, J. L., Joppa, L. N., Raven, P. H., Roberts, C. M. and Sexton, J. O. (2014). The biodiversity of species and their rates of extinction, distribution, and protection. *Science* **344**, 1246752.

Pinheiro, J., Bates, D., DebRoy, S., Sarkar, D. and The R Core Team. (2013). nlme: linear and nonlinear mixed effects models. In *R package version 3.1-110*. Vienna, Austria: R Foundation for Statistical Computing.

Pintor, A. F. V., Krockenberger, A. K. and Seymour, J. E. (2010). Costs of venom production in the common death adder (*Acanthophis antarcticus*). *Toxicon* **56**, 1035-1042.

Piotrowski, J. S., Annis, S. L. and Longcore, J. E. (2004). Physiology of *Batrachochytrium dendrobatidis*, a chytrid pathogen of amphibians. *Mycologia* **96**, 9-15.

Pohl, H. R., Wheeler, J. S. and Murray, H. E. (2013). Sodium and potassium in health and disease. In *Interrelations between essential metal ions and human diseases*, eds. A. Sigel H. Sigel and R. K. O. Sigel), pp. 29-47. Netherlands: Springer.

Poorten, T. and Rosenblum, E. (2016). Comparative study of host response to chytridiomycosis in a susceptible and a resistant toad species. *Mol. Ecol.* 25, 5663-5679.

Proksch, E., Brandner, J. M. and Jensen, J. M. (2008). The skin: an indispensable barrier. *Exp. Dermatol.* 17, 1063-1072.

R Core Team. (2018). R: A language and environment for statistical computing. Vienna, Austria: R Foundation for Statistical Computing.

Rachowicz, L. J. and Vredenburg, V. T. (2004). Transmission of *Batrachochytrium dendrobatidis* within and between amphibian life stages. *Dis. Aquat. Org.* 61, 75-83.

Raffel, T., Rohr, J., Kiesecker, J. and Hudson, P. (2006). Negative effects of changing temperature on amphibian immunity under field conditions. *Funct. Ecol.* 20, 819-828.

Raffel, T. R., Romansic, J. M., Halstead, N. T., McMahon, T. A., Venesky, M. D. and Rohr, J. R. (2013). Disease and thermal acclimation in a more variable and unpredictable climate. *Nat. Clim. Change* 3, 146-151.

Raleigh, D. R., Marchiando, A. M., Zhang, Y., Shen, L., Sasaki, H., Wang, Y., Long, M. and Turner, J. R. (2010). Tight junction–associated MARVEL proteins MarvelD3, tricellulin, and occludin have distinct but overlapping functions. *Mol. Biol. Cell* 21, 1200-1213.

Ramsey, J. P., Reinert, L. K., Harper, L. K., Woodhams, D. C. and Rollins-Smith, L. A. (2010). Immune defenses against *Batrachochytrium dendrobatidis*, a fungus linked to global amphibian declines, in the South African clawed frog, *Xenopus laevis*. *Infect. Immun.* 78, 3981-3992.

Rebollar, E. A., Hughey, M. C., Medina, D., Harris, R. N., Ibáñez, R. and Belden, L. K. (2016). Skin bacterial diversity of Panamanian frogs is associated with host susceptibility and presence of *Batrachochytrium dendrobatidis*. *The ISME Journal* 10, 1682-1695.

Reilly, B. D., Cramp, R. L., Wilson, J. M., Campbell, H. A. and Franklin, C. E. (2011). Branchial osmoregulation in the euryhaline bull shark, *Carcharhinus leucas*: a molecular analysis of ion transporters. *J. Exp. Biol.* 214, 2883-2895.

Reynolds, S. J. (2005). Use of tree hollows by the green tree frog *Litoria caerulea* at East Point Reserve, Darwin. *Northern Territory Naturalist* 18, 61-67.

Richards-Zawacki, C. L. (2009). Thermoregulatory behaviour affects prevalence of chytrid fungal infection in a wild population of Panamanian golden frogs. *Proc. R. Soc. Lond. B Biol. Sci.* 277, 519-528.

Robertson, S. L., Smedley, J. G. and McClane, B. A. (2010). Identification of a claudin-4 residue important for mediating the host cell binding and action of *Clostridium perfringens* enterotoxin. *Infect. Immun.* 78, 505-517.

Rohr, J. R. and Raffel, T. R. (2010). Linking global climate and temperature variability to widespread amphibian declines putatively caused by disease. *Proc. Natl. Acad. Sci.* 107, 8269-8274.

Rollins-Smith, L. A. (2017). Amphibian immunity–stress, disease, and climate change. *Dev. Comp. Immunol.* 66, 111-119.

Rollins-Smith, L. A. and Woodhams, D. C. (2012). Amphibian Immunity: Staying in tune with the environment. In *Ecoimmunology*, eds. G. Demas and R. J. Nelson): Oxford University Press.

Rollins-Smith, L. A., Reinert, L. K., O'Leary, C. J., Houston, L. E. and Woodhams, D. C. (2005). Antimicrobial peptide defenses in amphibian skin. *Integr. Comp. Biol.* 45, 137-142.

Rollins-Smith, L. A. (1998). Metamorphosis and the amphibian immune system. *Immunol. Rev.* 166, 221-230.

Rosario-Martinez, H. D., Fox, J. and The R Core Team. (2015). phia: post-hoc interaction analysis. In *R package version 0.2-1*. Vienna, Austria: R Foundation for Statistical Computing.

Rosenblum, E. B., Stajich, J. E., Maddox, N. and Eisen, M. B. (2008). Global gene expression profiles for life stages of the deadly amphibian pathogen *Batrachochytrium dendrobatidis*. *Proc. Natl. Acad. Sci.* **105**, 17034-17039.

Rosenblum, E. B., Poorten, T. J., Settles, M. and Murdoch, G. K. (2012). Only skin deep: shared genetic response to the deadly chytrid fungus in susceptible frog species. *Mol. Ecol.* **21**, 3110-3120.

Rosenthal, R., Milatz, S., Krug, S. M., Oelrich, B., Schulzke, J.-D., Amasheh, S., Günzel, D. and Fromm, M. (2010). Claudin-2, a component of the tight junction, forms a paracellular water channel. *J. Cell Sci.* **123**, 1913-1921.

Rosenzweig, C., Iglesias, A., Yang, X., Epstein, P. R. and Chivian, E. (2001). Climate change and extreme weather events; implications for food production, plant diseases, and pests. *Glob. Change Hum. Health* **2**, 90-104.

Rowley, J. J. and Alford, R. A. (2013). Hot bodies protect amphibians against chytrid infection in nature. *Sci. Rep.* **3**, 1-4.

Ruggeri, J., de Carvalho-e-Silva, S. P., James, T. Y. and Toledo, L. F. (2018). Amphibian chytrid infection is influenced by rainfall seasonality and water availability. *Dis. Aquat. Org.* **127**, 107-115.

Ruhr, I. M., Bodinier, C., Mager, E. M., Esbaugh, A. J., Williams, C., Takei, Y. and Grosell, M. (2014). Guanylin peptides regulate electrolyte and fluid transport in the Gulf toadfish (*Opsanus beta*) posterior intestine. *Am. J. Physiol. Regul. Integr. Comp. Physiol.* **307**, R1167-R1179.

Russo, C. J. M., Ohmer, M. E., Cramp, R. L. and Franklin, C. E. (2018). A pathogenic skin fungus exacerbates cutaneous water loss in amphibians. *J. Exp. Biol.* **221**, jeb167445

Salla, R. F., Rizzi-Possignolo, G. M., Oliveira, C. R., Lambertini, C., Franco-Belussi, L., Leite, D. S., Silva-Zacarin, E. C. M., Abdalla, F. C., Jenkinson, T. S. and Toledo, L. F. (2018). Novel findings on the impact of chytridiomycosis on the cardiac function of anurans: sensitive vs. tolerant species. *PeerJ* **6**, e5891.

Sardella, B. A. and Kültz, D. (2009). Osmo-and ionoregulatory responses of green sturgeon (*Acipenser medirostris*) to salinity acclimation. *J. Comp. Physiol. B* **179**, 383-390.

Sariban-Sohraby, S. and Benos, D. (1986). The amiloride-sensitive sodium channel. *Am. J. Physiol-Cell Ph.* **250**, C175-C190.

Sarnak, M. J., Levey, A. S., Schoolwerth, A. C., Coresh, J., Culleton, B., Hamm, L. L., McCullough, P. A., Kasiske, B. L., Kelepouris, E. and Klag, M. J. (2003). Kidney disease as a risk factor for development of cardiovascular disease. *Circulation* **108**, 2154-2169.

Schild, L. (2004). The epithelial sodium channel: from molecule to disease. In *Reviews of physiology, biochemistry and pharmacology*, eds. S. G. Amara E. Bamberg H. Grunicke R. John W. J. Lederer A. Miyajima H. Murer S. Offermanns G. Schultz and M. Schweiger), pp. 93-107. Berlin Heidelberg: Springer.

Schild, L. (2010). The epithelial sodium channel and the control of sodium balance. *BBA-Mol. Basis Dis.* **1802**, 1159-1165.

Schmid, W. D. (1965). Some aspects of the water economies of nine species of amphibians. *Ecology* **46**, 261-269.

Secor, S. M., Wooten, J. A. and Cox, C. L. (2007). Effects of meal size, meal type, and body temperature on the specific dynamic action of anurans. *J. Comp. Physiol. B* **177**, 165-182.

Seymour, R. S., Withers, P. C. and Weathers, W. W. (1998). Energetics of burrowing, running, and free-living in the Namib Desert golden mole (*Eremitalpa namibensis*). *J. Zool.* **244**, 107-117.

Shahin, S., H. and Blankemeyer, J., T. (1989). Demonstration of gap junctions in frog skin epithelium. *Am. J. Physiol.* **257**, C658-C664.

Shibata, Y., Sano, T., Tsuchiya, N., Okada, R., Mochida, H., Tanaka, S. and Suzuki, M. (2014). Gene expression and localization of two types of AQP5 in *Xenopus tropicalis* under hydration and dehydration. *Am. J. Physiol. Regul. Integr. Comp. Physiol.* **307**, R44-R56.

Shine, R. (2010). The ecological impact of invasive cane toads (*Bufo marinus*) in Australia. *Q. Rev. Biol.* **85**, 253-291.

Shoemaker, V. H., Hillman, S. S., Hillyard, S. D., Jackson, D. C., Mc Clanahan Jr, L. L., Withers, P. C. and Wygoda, M. L. (1992). Exchange of water, ions, and respiratory gases in terrestrial amphibians. In *Environmental physiology of the amphibians*, eds. M. E. Feder and W. W. Burggren). Chicago, USA: University of Chicago Press.

Smith, P. (1975). Aldosterone-induced moulting in amphibian skin and its effect on electrical capacitance. *J. Membr. Biol.* **22**, 165-181.

Sourisseau, M., Michta, M. L., Zony, C., Israelow, B., Hopcraft, S. E., Narbus, C. M., Martín, A. P. and Evans, M. J. (2013). Temporal analysis of hepatitis C virus cell entry with occludin directed blocking antibodies. *PLOS Pathog.* **9**, e1003244.

Spearman, R. I. (1968). Epidermal keratinization in the salamander and a comparison with other amphibia. *J. Morphol.* **125**, 129-143.

Spitzen-van der Sluijs, A., Martel, A., Asselberghs, J., Bales, E. K., Beukema, W., Bletz, M. C., Dalbeck, L., Goverse, E., Kerres, A. and Kinet, T. (2016). Expanding distribution of lethal amphibian fungus *Batrachochytrium salamandrivorans* in Europe. *Emerg. Infect. Dis.* **22**, 1286.

Spotila, J. R. (1972). Role of temperature and water in the ecology of lungless salamanders. *Ecol. Monogr.* **42**, 95-125.

Stefano, F. J. and Donoso, A. O. (1964). Hypophyso-adrenal regulation of moulting in the toad. *Gen. Comp. Endocr.* **4**, 473-480.

Stegen, G., Pasmans, F., Schmidt, B. R., Rouffaer, L. O., Van Praet, S., Schaub, M., Canessa, S., Laudelout, A., Kinet, T. and Adriaensen, C. (2017). Drivers of salamander extirpation mediated by *Batrachochytrium salamandrivorans*. *Nature* **544**, 353-356.

Stuart, S. N., Chanson, J. S., Cox, N. A., Young, B. E., Rodrigues, A. S., Fischman, D. L. and Waller, R. W. (2004). Status and trends of amphibian declines and extinctions worldwide. *Science* **306**, 1783-1786.

Suhail, M. (2010). Na+, K+-ATPase: ubiquitous multifunctional transmembrane protein and its relevance to various pathophysiological conditions. *J. Clin. Med. Res.* **2**, 1.

Suzuki, M. and Tanaka, S. (2009). Molecular and cellular regulation of water homeostasis in anuran amphibians by aquaporins. *Comp. Biochem. Physiol. Part A Mol. Integr. Physiol.* **153**, 231-241.

Suzuki, M., Hasegawa, T., Ogushi, Y. and Tanaka, S. (2007). Amphibian aquaporins and adaptation to terrestrial environments: a review. *Comp. Biochem. Physiol. Part A Mol. Integr. Physiol.* **148**, 72-81.

Symonds, E. P., Trott, D. J., Bird, P. S. and Mills, P. (2008). Growth characteristics and enzyme activity in *Batrachochytrium dendrobatidis* isolates. *Mycopathologia* **166**, 143-147.

Takada, M., Shimomura, T., Hokari, S., Jensik, P. J. and Cox, T. C. (2006). Larval bullfrog skin expresses ENaC despite having no amiloride-blockable transepithelial Na+ transport. *J. Comp. Physiol. B* **176**, 287-293.

Tanii, H., Hasegawa, T., Hirakawa, N., Suzuki, M. and Tanaka, S. (2002). Molecular and cellular characterization of a water-channel protein, AQP-h3, specifically expressed in the frog ventral skin. *J. Membr. Biol.* **188**, 43-53.

Taylor, S. and Ewer, D. W. (1956). Moulting in the Anura: The normal moulting cycle of *Bufo regularis* Reuss. *Proc. Zool. Soc. Lond.* **127**, 461-478.

Thompson, G. G. and Withers, P. C. (1999). Effect of sloughing and digestion on metabolic rate in the Australian carpet python, *Morelia spilota imbricata*. *Aust. J. Zool.* **47**, 605-610.

Thorson, T. B. (1964). The partitioning of body water in amphibia. *Physiol. Zool.* **37**, 395-399.

Tokuda, S., Miyazaki, H., Nakajima, K.-i., Yamada, T. and Marunaka, Y. (2010). NaCl flux between apical and basolateral side recruits claudin-1 to tight junction strands and regulates paracellular transport. *Biochem. Biophys. Res. Commun.* **393**, 390-396.

Towne, J. E., Harrod, K. S., Krane, C. M. and Menon, A. G. (2000). Decreased expression of aquaporin (AQP) 1 and AQP5 in mouse lung after acute viral infection. *Am. J. Respir. Cell Mol. Biol.* **22**, 34-44.

Tracy, C. R., Christian, K. A., Betts, G. and Tracy, C. R. (2008). Body temperature and resistance to evaporative water loss in tropical Australian frogs. *Comp. Biochem. Physiol. Part A Mol. Integr. Physiol.* **150**, 102-108.

Triana, T. M., Henao, L. M. and Bernal, M. H. (2013). Ontogenetic comparison of the molting frequency in *Rhinella marina* (Anura: Bufonidae). *Iheringia. Série Zoologia* **103**, 47-50.

Tsukita, S., Furuse, M. and Itoh, M. (2001). Multifunctional strands in tight junctions. *Nat. Rev. Mol. Cell Biol.* **2**, 285-293.

Uchiyama, M. and Konno, N. (2006). Hormonal regulation of ion and water transport in anuran amphibians. *Gen. Comp. Endocr.* **147**, 54-61.

Ussing, H. H. and Zerahn, K. (1951). Active transport of sodium as the source of electric current in the short-circuited isolated frog skin. *Acta Physiol. Scand.* **23**, 110-127.

Van Rooij, P., Martel, A., Haesebrouck, F. and Pasmans, F. (2015). Amphibian chytridiomycosis: a review with focus on fungus-host interactions. *Vet. Res.* **46**, 137.

Van Rooij, P., Martel, A., D'Herde, K., Brutyn, M., Croubels, S., Ducatelle, R., Haesebrouck, F. and Pasmans, F. (2012). Germ tube mediated invasion of *Batrachochytrium dendrobatidis* in amphibian skin is host dependent. *PLOS ONE* **7**, e41481.

Vander Heiden, M. G., Cantley, L. C. and Thompson, C. B. (2009). Understanding the Warburg effect: the metabolic requirements of cell proliferation. *Science* **324**, 1029-1033.

Volksdorf, T., Heilmann, J., Eming, S. A., Schawjinski, K., Zorn-Kruppa, M., Ueck, C., Vidal-y-Sy, S., Windhorst, S., Jücker, M. and Moll, I. (2017). Tight junction proteins claudin-1 and occludin are important for cutaneous wound healing. *Am. J. Pathol.* **187**, 1301-1312.

Voûte, C. L. and Ussing, H. H. (1968). Some morphological aspects of active sodium transport: the epithelium of the frog skin. *J. Cell Biol.* **36**, 625-638.

Voyles, J., Vredenburg, V. T., Tunstall, T. S., Parker, J. M., Briggs, C. J. and Rosenblum, E. B. (2012a). Pathophysiology in mountain yellow-legged frogs (*Rana muscosa*) during a chytridiomycosis outbreak. *PLOS ONE* **7**, e35374.

Voyles, J., Berger, L., Young, S., Speare, R., Webb, R., Warner, J., Rudd, D., Campbell, R. and Skerratt, L. F. (2007). Electrolyte depletion and osmotic imbalance in amphibians with chytridiomycosis. *Dis. Aquat. Org.* **77**, 113-118.

Voyles, J., Johnson, L. R., Briggs, C. J., Cashins, S. D., Alford, R. A., Berger, L., Skerratt, L. F., Speare, R. and Rosenblum, E. B. (2012b). Temperature alters reproductive life history patterns in *Batrachochytrium dendrobatidis*, a lethal pathogen associated with the global loss of amphibians. *Ecol. Evol.* **2**, 2241-2249.

Voyles, J., Young, S., Berger, L., Campbell, C., Voyles, W. F., Dinudom, A., Cook, D., Webb, R., Alford, R. A. and Skerratt, L. F. (2009). Pathogenesis of chytridiomycosis, a cause of catastrophic amphibian declines. *Science* **326**, 582-585.

Wake, D. B. and Vredenburg, V. T. (2008). Are we in the midst of the sixth mass extinction? A view from the world of amphibians. *Proc. Natl. Acad. Sci.* **105**, 11466-11473.

Walke, J. B., Becker, M. H., Loftus, S. C., House, L. L., Cormier, G., Jensen, R. V. and Belden, L. K. (2014). Amphibian skin may select for rare environmental microbes. *The ISME Journal* **8**, 2207-2217.

Wardziak, T., Luquet, E., Plenet, S., Léna, J.-P., Oxarango, L. and Joly, P. (2013). Impact of both desiccation and exposure to an emergent skin pathogen on transepidermal water exchange in the palmate newt *Lissotriton helveticus*. *Dis. Aquat. Org.* **104**, 215-224.

Weldon, P. J., Demeter, B. J. and Rosscoe, R. (1993). A survey of shed skin-eating (dermatophagy) in amphibians and reptiles. *J. Herpetol.* **27**, 219-228.

Welinder, C. and Ekblad, L. (2011). Coomassie staining as loading control in Western blot analysis. *J. Proteome Res.* **10**, 1416-1419.

White, C. R., Phillips, N. F. and Seymour, R. S. (2006). The scaling and temperature dependence of vertebrate metabolism. *Biology Letters* **2**, 125-127.

Whitear, M. (1975). Flask cells and epidermal dynamics in frog skin. *J. Zool.* **175**, 107-149.

Whittembury, G., De Martínez, C. V., Linares, H. and Paz-Aliga, A. (1980). Solvent drag of large solutes indicates paracellular water flow in leaky epithelia. *Proc. R. Soc. B.* **211**, 63-81.

Willumsen, N. J., Viborg, A. L. and Hillyard, S. D. (2007). Vascular aspects of water uptake mechanisms in the toad skin: perfusion, diffusion, confusion. *Comp. Biochem. Physiol. Part A Mol. Integr. Physiol.* **148**, 55-63.

Withers, P. C. (1992). Comparative animal physiology. New York: Saunders College Publishing.

Wood, C. M. and Grosell, M. (2008). A critical analysis of transepithelial potential in intact killifish (*Fundulus heteroclitus*) subjected to acute and chronic changes in salinity. *J. Comp. Physiol. B* **178**, 713-727.

Wood, C. M. and Grosell, M. (2015). Electrical aspects of the osmorespiratory compromise: TEP responses to hypoxia in the euryhaline killifish (*Fundulus heteroclitus*) in freshwater and seawater. *J. Exp. Biol.* **218**, 2152-2155.

Woodhams, D. C., Brandt, H., Baumgartner, S., Kielgast, J., Küpfer, E., Tobler, U., Davis, L. R., Schmidt, B. R., Bel, C. and Hodel, S. (2014). Interacting symbionts and immunity in the amphibian skin mucosome predict disease risk and probiotic effectiveness. *PLOS ONE* **9**, e96375.

Word, J. M. and Hillman, S. S. (2005). Osmotically absorbed water preferentially enters the cutaneous capillaries of the pelvic patch in the toad *Bufo marinus*. *Physiol. Biochem. Zool.* **78**, 40-47.

Worthy, G. A. J., Morris, P. A., Costa, D. P. and Le Boeuf, B. J. (1992). Moult energetics of the northern elephant seal (*Mirounga angustirostris*). *J. Zool.* **227**, 257-265.

Wu, C. S., Yang, W. K., Lee, T. H., Gomez-Mestre, I. and Kam, Y. C. (2014). Salinity acclimation enhances salinity tolerance in tadpoles living in brackish water through increased Na+, K+-ATPase expression. *J. Exp. Zool. Part A* **321**, 57-64.

Wu, N. C., Cramp, R. L. and Franklin, C. E. (2017). Living with a leaky skin: Upregulation of ion transport proteins during sloughing. *J. Exp. Biol.* **220**, 2026-2035.

Wu, N. C., Cramp, R. L. and Franklin, C. E. (2018). Body size influences energetic and osmoregulatory costs in frogs infected with *Batrachochytrium dendrobatidis*. *Sci. Rep.* **8**, 3739.

Wu, N. C., Cramp, R. L., Ohmer, M. E. B. and Franklin, C. E. (2019). Epidermal epidemic: unravelling the pathogenesis of chytridiomycosis. *J. Exp. Biol.* **222**, jeb191817.

Wu, N. C., Alton, L. A., Clemente, C. J., Kearney, M. R. and White, C. R. (2015). Morphology and burrowing energetics of semi-fossorial skinks (*Liopholis* spp.). *J. Exp. Biol.* **218**, 2416-2426.

Yamagishi, M., Ito, Y., Ariizumi, T., Komazaki, S., Danno, H., Michiue, T. and Asashima, M. (2010). Claudin5 genes encoding tight junction proteins are required for Xenopus heart formation. *Dev. Growth Differ.* **52**, 665-675.

Yokouchi, M., Atsugi, T., Van Logtestijn, M., Tanaka, R. J., Kajimura, M., Suematsu, M., Furuse, M., Amagai, M. and Kubo, A. (2016). Epidermal cell turnover across tight junctions based on Kelvin's tetrakaidecahedron cell shape. *Elife* **5**, e19593.

Yu, A. S., McCarthy, K. M., Francis, S. A., McCormack, J. M., Lai, J., Rogers, R. A., Lynch, R. D. and Schneeberger, E. E. (2005). Knockdown of occludin expression leads to diverse phenotypic alterations in epithelial cells. *Am. J. Physiol-Cell Ph.* **288**, C1231-C1241.

Yuan, J. S., Reed, A., Chen, F. and Stewart, C. N. (2006). Statistical analysis of real-time PCR data. *BMC Bioinformatics* **7**, 85.

Yuki, T., Haratake, A., Koishikawa, H., Morita, K., Miyachi, Y. and Inoue, S. (2007). Tight junction proteins in keratinocytes: localization and contribution to barrier function. *Exp. Dermatol.* **16**, 324-330.

Zanotto, F., Wheatly, M., Reiber, C., Gannon, A. and Jalles-Filho, E. (2004). Allometric relationship of postmolt net ion uptake, ventilation, and circulation in the freshwater crayfish *Procambarus clarkii*: intraspecific scaling. *Physiol. Biochem. Zool.* **77**, 275-284.

Zare, S. and Greenaway, P. (1997). Ion transport and the effects of moulting in the freshwater crayfish *Cherax destructor* (Decapoda: Parastacidae). *Aust. J. Zool.* **45**, 539-551.

Zare, S. and Greenaway, P. (1998). The effect of moulting and sodium depletion on sodium transport and the activities of Na+ K+-ATPase, and V-ATPase in the freshwater crayfish *Cherax destructor* (Crustacea: Parastacidae). *Comp. Biochem. Physiol. Part A Mol. Integr. Physiol.* **119**, 739-745.

Zerahn, K. (1956). Oxygen consumption and active sodium transport in the isolated and short-circuited frog skin. *Acta Physiologica* **36**, 300-318.

8

Appendices

Appendix 1.

A lethal fungal pathogen directly alters tight junction proteins in the skin of a susceptible amphibian

8.1 ABSTRACT

Bacterial and viral pathogens can weaken epithelial barriers by targeting and disrupting tight junction (TJ) proteins. Comparatively, however, little is known about the direct effects of fungal pathogens on TJ proteins and their expression. The disease, chytridiomycosis, caused by the fungal pathogen *Batrachochytrium dendrobatidis* (*Bd*), is threatening amphibian populations worldwide. *Bd* is known to infect amphibian skin and disrupt cutaneous osmoregulation. However, exactly how this occurs is poorly understood. This study considered the impact of Bd infection on the barrier properties of the Australian green tree frog (*Litoria caerulea*) epidermis by examining how inoculation of animals with Bd influenced the paracellular movement of FITC-dextran (4 kDa, FD-4) across the skin in association with alterations in the mRNA and protein abundance of select TJ proteins of the epidermal TJ complex. It was observed that *Bd* infection increased paracellular movement of FD-4 across the skin linearly with fungal infection load. In addition, Bd infection increased transcript abundance of the tricellular TJ (tTJ) protein tricellulin (*tric*) as well as the bicellular TJ (bTJ) proteins occludin (*ocln*), claudin (*cldn*) -1, -4 and the scaffolding TJ protein zonula occludens-1 (*zo-1*). However, while Tric protein abundance increased in accord with changes in transcript abundance, protein abundance of Cldn-1 was significantly reduced and Ocln protein abundance was unchanged. Data indicate that disruption of cutaneous osmoregulation in *L. caerulea* following *Bd* infection occurs, at least in part, by an increase in epidermal paracellular permeability in association with compromised integrity of the epidermal TJ complex.

8.2 INTRODUCTION

Solute movement across epithelial barriers is dictated by (1) the transcellular transport pathway, which moves ions against their concentration gradient across epithelial cells, and (2) the paracellular transport pathway, which regulates the passive movement of solutes down a concentration gradient across tight junctions (TJs) that occlude the juxtaluminal paracellular space between epithelial cells (Martinez-Palomo et al., 1971; Ehrenfeld and Klein, 1997). The TJ complex is composed of cytosolic scaffolding (e.g. zonula occludens-1) and transmembrane (e.g. claudins, occludin, tricellulin) TJ proteins (Günzel and Fromm, 2012; **Fig. 8.1**). Cytosolic scaffolding TJ proteins like zonula occludens-1 (ZO-1) link transmembrane TJ proteins to the cellular cytoskeleton and participate in the dynamic assembly of the TJ complex (Gonzalez-Mariscal et al., 2003). In contrast to scaffolding TJ proteins, transmembrane TJ proteins possess extracellular domains. Transmembrane TJ proteins that link two adjacent cellular membranes are termed bicellular TJ (bTJ) proteins, while those found at tricellular points of contact are referred to as tricellular TJ (tTJ) proteins (Raleigh et al., 2010). Claudins (Cldns) are a large superfamily of bTJ proteins that can influence the paracellular permeability of an epithelium by forming ion-selective barriers or pores (Günzel and Fromm, 2012). The expression of Cldns in cells is sufficient to form TJ strands, and loss of just one Cldn protein may greatly affect the paracellular permeability of an

epithelium (Furuse et al., 1998; Furuse et al., 2002). Other important transmembrane TJ proteins include TJ-associated MARVEL proteins such as the bTJ protein occludin (Ocln) (Furuse et al., 1993) and the tTJ protein tricellulin (Tric) (Ikenouchi et al., 2005). Ocln arose in deuterostomes as an important structural protein for normal barrier function (Chapman et al., 2010) and it has been found in the epithelia and/or endothelia of many terrestrial and aquatic vertebrate groups (Feldman et al., 2005; Chasiotis and Kelly, 2008, 2009). Tric seals the hollow "tube" that is formed perpendicular to the epithelium surface in regions where three epithelial cells meet (Ikenouchi et al., 2005). Tric has been reported to restrict the passage of solutes and contribute to epithelium integrity in mammals and fishes (Krug et al., 2009; Kolosov and Kelly, 2013).
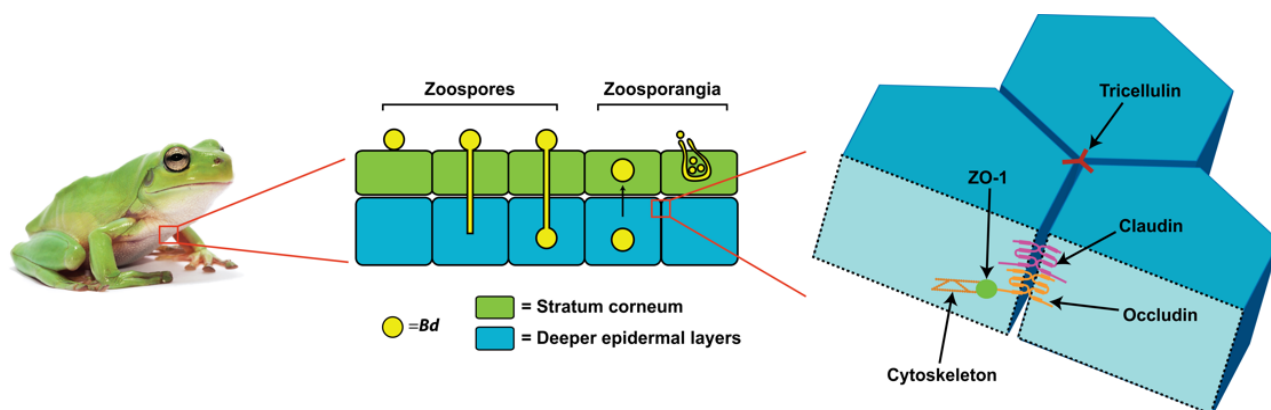
Fig. 8.1 │ Schematic representation of the *Batrachochytrium dendrobatidis* (*Bd*) life cycle in the amphibian epidermis and location of the TJ complex in the epidermis. The stages of *Bd* infection have been summarized by Van Rooij et al. (2015) and are as follows: (1) the fungus encysts on to the outer layer of the skin (the *stratum corneum*), (2) the zoospore sends a germ tube into the deeper layers of the skin, (3) *Bd* injects itself into a living epidermal cell, (4) the zoospore develops into a zoosporangia as the skin cells are pushed upwards and mature, and (5) zoosporangia develop a discharge tube from which new zoospores are released. Photo credit: C. Baker.

Epithelial barriers are generally effective at inhibiting pathogen entry into tissues, however, various bacterial and viral pathogens have been well-known to disrupt and target TJ proteins in order to weaken the epithelial barrier (Guttman and Finlay, 2009). Some bacterial and viral pathogens destroy TJ proteins (Muza-Moons et al., 2004; Köhler et al., 2007), whereas others, such as *Clostridium perfringens* and Hepatitis C virus, target specific TJ proteins as receptors for tissue entry (Katahira et al., 1997; Robertson et al., 2010; Sourisseau et al., 2013). Unlike bacterial and viral pathogens, only a handful of studies have examined the effects of fungal pathogens on TJ proteins (McLaughlin et al., 2004; Yuki et al., 2007; McLaughlin et al., 2009). As a result, we have limited knowledge on the interaction of fungi and fungal toxins with the TJ complex. Understanding the fungus-TJ interaction is especially important in light of an emerging infectious disease that disrupts the skin function of amphibians.

Amphibians are threatened by a disease called chytridiomycosis, a cutaneous infection caused by the pathogenic fungus *Batrachochytrium dendrobatidis* (*Bd*) (Stuart et al., 2004). This fungus has been shown to infect over 500 amphibian species worldwide and has resulted in one of the greatest

disease-driven losses of biodiversity ever recorded (Fisher et al., 2009; Kilpatrick et al., 2010). Although only the superficial layers of the skin are infected by *Bd*, that alone is able to disrupt normal skin function and can lead to death of the infected animal (Voyles et al., 2009). This is because in amphibians, the skin, specifically the ventral skin surface, is a selectively permeable living barrier to the surrounding environment that plays an important (sometimes exclusive) role in gas exchange and is a predominant site for salt and water transport (Boutilier et al., 1992; Hillyard et al., 2008; Campbell et al., 2012).

The mechanism used by *Bd* to infect amphibian skin is still not completely understood (Rosenblum et al., 2008; Fisher et al., 2009). What is known is that the fungus begins its life cycle as a free-living zoospore which encysts onto the surface of the skin (**Fig. 8.1**). The zoospore then develops a germ tube that forces it into the deeper layers of the skin. Finally, *Bd* matures into zoosporangia containing many zoospores that can be shed from the skin via a discharge tube to re-infect the same animal, or infect a new one (Greenspan et al., 2012; Van Rooij et al., 2015). Following infection, *Bd* has been reported to affect active solute transport and transepithelial resistance (TER) across the ventral skin, disrupting cutaneous osmoregulation and causing an imbalance in serum ion levels (Voyles et al., 2007; Voyles et al., 2009; Wu et al., 2018). TER is a measure of transcellular and paracellular transport and, while both pathways contribute to the barrier properties of the amphibian epidermis, the paracellular route heavily influences its permeability properties (Cox and Alvarado, 1979). Although the effects of *Bd* have been examined on active ion transport and TER, the effects of *Bd* on paracellular transport and TJs specifically has not been investigated.

TJs are acknowledged to play a vital role in determining paracellular resistance of terrestrial and aquatic vertebrate epithelia (Günzel and Fromm, 2012; Kolosov et al., 2017; Kolosov and Kelly, 2017), including amphibian skin (Mandel and Curran, 1972; Bruus et al., 1976). Additionally, amphibian TJs, and at least three proteins of the amphibian TJ complex (i.e. Cldn-1, Ocln, ZO-1), have been shown to respond to changes in environmental conditions (Castillo et al., 1991; Chasiotis and Kelly, 2009; Tokuda et al., 2010). Over 30 genes encoding amphibian TJ proteins have now been reported, yet little is known about their contribution to TJ permeability (Cordenonsi et al., 1997; Chasiotis and Kelly, 2009; Yamagishi et al., 2010). In addition, the majority of these genes have been identified in the strictly aquatic anurans *Xenopus laevis* and *Xenopus tropicalis,* thus almost nothing is known about the characteristics of TJ proteins in terrestrial and semi-aquatic amphibians (Günzel and Yu, 2013). There is considerable evidence that a dysregulation of TJ function can deleteriously impact normal solute movement across epithelia that interface directly with the surrounding environment of aquatic vertebrates (Chasiotis et al., 2011; Kolosov and Kelly, 2013, 2017), thus it would seem prudent to carefully consider the effect of *Bd* on epidermal TJs of amphibians. Indeed, it has been demonstrated that *Bd* disrupts junctional components responsible for adhesion

between cells of amphibian skin, resulting in skin lesions (Brutyn et al., 2012). But, unlike TJs, adhesion junctions do not regulate the permeability properties of the skin. Furthermore, several fungi and fungal toxins have been shown to directly target and disrupt various junctional components, including TJs, in the skin of other vertebrates (Bouhet and Oswald, 2005; Yuki et al., 2007). Additionally, *Bd* was found to secrete proteolytic enzymes, which are hypothesized to be linked to its pathogenicity (Rosenblum et al., 2008; Symonds et al., 2008) and may contribute to skin barrier disruption as reported by Brutyn et al. (2012) for the skin of *Xenopus laevis*.

Given that fungal toxins have been shown to target vertebrate TJs and that *Bd* has been found to affect cutaneous osmoregulation as well as disrupt junctional adhesion components in the skin of amphibians, it was hypothesized that the disruption of amphibian cutaneous osmoregulation following *Bd* infection will occur in association with altered epidermal paracellular permeability and TJ protein abundance. To consider this idea further, ventral skin permeability and TJ protein abundance of the Australian green tree frog, *Litoria caerulea,* were examined following experimental infection with *Bd.*

8.3   MATERIALS AND METHODS

8.3.1   Experimental animals

This study was conducted using the Australian green tree frog *Litoria caerulea*, which is susceptible to *Bd* infection and is a model for the study of chytridiomycosis (Pessier et al., 1999; Voyles et al., 2009; Wu et al., 2018). All animals were collected with approval of the Queensland Department of Environment and Heritage Protection (WISP15102214), and all experiments were carried out with the approval of The University of Queensland Animal Welfare Committee (SBS/316/14/URG). Specifically, *L. caerulea* (15–70 g, both sexes) were collected from wet roads in non-protected areas near Fernvale, Southeast Queensland in January 2015. Isolated individual frogs were placed into separate moistened plastic bags and transported to The University of Queensland. Frogs were housed separately in ventilated clear plastic containers (26.2 x 23.7 x 12 cm). Containers were supplied with paper towels saturated with water that was chemically aged (dilution 1:4000; VitaPet, NSW, Australia) and each housing unit contained a half PVC pipe for shelter. Frogs were fed large crickets (5 each week) and the enclosures were cleaned on a weekly basis. Photoperiod was maintained as a 12 h L:12 h D cycle and room temperature was kept constant at $20.5 \pm 0.5°C$. Given that natural *L. caerulea* populations can acquire *Bd* infections, swabs taken from captured frogs were tested for *Bd* using Taqman real-time PCR (qPCR) prior to beginning the experiments and all frogs were confirmed to be uninfected.

8.3.2   Preparation of fungal inoculum and experimental exposure

Batrachochytrium dendrobatidis (*Bd*) strain EPS4, isolated by E.P. Symonds (School of Veterinary Sciences, The University of Queensland) from a *Mixophyes fleayi* tadpole collected from Gap Creek,

Main Range National Park, Queensland, Australia (March 2012), was used for experimental infection. *Bd* cultures were maintained at 4°C until four days before exposure date. The strain was then passaged onto 25 new 1 % agar, 0.5 % tryptone, 0.5 % tryptone-soy plates, and maintained at 20°C for 4–5 days. Immediately prior to infection, zoospores maintained at 20°C were harvested by flooding plates with sterile distilled water for 30 min. The zoospore suspension was collected, and zoospore concentration was calculated using a haemocytometer following Boyle et al. (2004). Frogs were randomly assigned to be either part of the infected ($n = 10$) or control ($n = 10$) groups. All frogs were transferred into 300 ml plastic containers (12.5 x 8.3 x 5 cm) containing 100 ml of aged tap water. Frogs in the infected group were then inoculated with a dose of ~500,000 *Bd* zoospores for 5 h. Control frogs were exposed to identical conditions in the absence of zoospores. After exposure, frogs were returned to their original enclosures. All experiments were conducted when frogs were in the non-sloughing cycle.

8.3.3   Measuring infection load

The swabbing protocol used to determine the presence or absence of *Bd* on collected animals as well as *Bd* infection load on inoculated animals (every two weeks after exposure) involved firmly running a sterile fine-tipped cotton swab (MW100-100; Medical Wire & Equipment, Wiltshire, England) three times over the frog's ventral surface, sides, thighs, feet, webbing and toes. Fungal DNA was isolated using PrepMan Ultra (Applied Biosystems, Foster City, CA, USA) according to manufacturer's instructions (Qiagen Pty Ltd, Australia) and assayed in triplicate via Taqman qPCR (Boyle et al., 2004) using a Mini Opticon qPCR detection system (MJ Mini Cycler, Bio Rad Laboratories Inc). Reactions containing DNA from known (100, 10, 1 and 0.1) *Bd* zoospore equivalent (ZE) standards were prepared, as well as controls with no DNA template. The mean concentration of the test samples was interpolated from the *Bd* standard curve and results were log + 1 transformed to normalise data. All results were expressed as log (ZE+1).

Frogs were monitored daily for pathological or behavioural symptoms of chytridiomycosis, including lethargy, loss of appetite, abnormal posture, areas of sloughed skin not fully removed or visible within the enclosure, loss of righting reflex, discoloured or reddened skin, and weight loss. Only frogs that exhibited these signs of infection were swabbed and consequently sacrificed for tissue sampling.

8.3.4   Tissue sampling

Ventral skin samples (<1 cm^2) from the lower abdominal region were collected. Skin samples for immunohistochemistry were fixed in 10 % neutral buffered formalin at 4°C overnight, after which formalin was replaced with 70 % ethanol and samples were stored at 4°C until use. Skin samples for Western blotting were frozen at -80°C until use and skin samples for RNA extraction were stored in RNA-later (Ambion Inc., TX, USA).

8.3.5   Permeability assays

Ventral skin was collected from control ($n = 7$) and infected ($n = 10$) *L. caerulea* and immediately mounted serosal side up onto the lower chamber of a Franz cell. One ml of 26 mM NaCl was added to the apical chamber and 5 ml of Ringer's solution (in mM: 112 NaCl, 2.5 KCl, 10 D-glucose, 2 Na_2HPO_4, 1 $CaCl_2$, 1 $MgCl_2$, 5 HEPES sodium salt with pH 7.3–7.4 and an osmolality of 230 ± 20 mOsm l^{-1}) was added to the basolateral chamber. To examine the integrity of the paracellular pathway, 0.5 mg of the paracellular permeability fluorescent marker 4 kDa FITC-dextran (FD-4) was added to the basolateral chamber of the Franz cell and its appearance in the apical chamber was monitored. The basolateral solution was mixed continuously with a magnetic stirrer at 600 RPM. 0.25 ml aliquots of both the apical and basolateral solutions were collected immediately and again after 24 h. Sample fluorescence was analyzed using a fluorescent plate reader (DTX880 Multimode Detector, Beckman Coulter Pty Ltd, Australia). The permeability of the skin samples was calculated using a modified equation from Kelly and Wood (2001):

$$P \ (\text{cm s}^{-1}) = \frac{(\Delta FL_{Ap})(\text{Volume}_{Ap})}{(FL_{Bl})(\text{Time})(\text{Area})}$$

where ΔFL_{Ap} is the change in fluorescence on the apical side, Volume_{Ap} is the volume of the apical chamber (1 ml), FL_{Bl} is the fluorescence on the basolateral side, Time is the total flux period (in seconds), and Area defines the area of the Franz cell chamber opening (0.2 cm^2).

8.3.6   RNA extraction and cDNA synthesis

Skin samples were homogenised using a TissueLyser II (Qiagen Pty Ltd, Australia). Total RNA was isolated using an RNeasy Minikit (RNeasy Mini kit, Qiagen Pty Ltd, Australia) as per manufacturer's instructions. RNA purity (absorbance at 260/280) was assayed by spectrometry, and RNA concertation was quantified using a Qubit fluorometer (ThermoFisher Scientific). RNA was then reverse transcribed into cDNA using the QuantiTech Reverse Transcription Kit (Qiagen Pty Ltd, Australia) according to manufacturer's instructions.

8.3.7   Analysis of TJ protein mRNA by PCR and qPCR.

For PCR, the Taq PCR Master Mix Kit (Qiagen Pty Ltd, Australia) was used. The following reaction conditions were utilized: 1 cycle of initial denaturation (95°C, 10 min), then 40 cycles of denaturation (95°C, 30 s), annealing (56–60°C, 30 s) and extension (72°C, 30 s), followed by a final single extension cycle (72°C, 5 min). PCR-generated amplicons were visualized by agarose gel electrophoresis (1.5 %, 120 V separation for 1 h).

Gene specific primers were designed for *L. caerulea* (**Table 8.1**) using the transcriptome of a closely-related species (*Pseudacris regilla*). Primers were confirmed to produce single bands on an agarose gel, the amplicon was sequenced, and primers that did not have 100 % sequence homology were

re-synthesized to be specific to *L. caerulea* genes. TJ protein mRNA abundance was examined by qPCR using a Mini Opticon real-time PCR detection system (MJ Mini Cycler, Bio-Rad Laboratories, Inc.) and using PowerSYBR Supermix (Applied Biosystems, Foster City, CA, USA) under the following conditions: 1 initial cycle of denaturation (95°C, 10 min), followed by 40 cycles of denaturation (95° C, 30 s), annealing (58–61°C, 15 s) and extension (60°C, 45 s). A melting curve was constructed after each qPCR run, ensuring that a single product was synthesized during each reaction. For all qPCR analyses, transcript abundance was normalized to *ef-1α* transcript abundance after determining by statistical analysis that *ef-1α* did not significantly alter ($P = 0.413$) in response to *Bd* infection. *L. caerulea ef-1α* mRNA was amplified using primers reported in Table 7.1.

Table 8.1 │ Primer sets, PCR annealing temperatures, amplicon size, and gene accession numbers for *Litoria caerulea* tight junction proteins and elongation factor-1α.

Tight Junction Protein	Gene	Primers	T_a	Amplicon size (bp)	Accession number
Elongation factor-1a	*ef-1α*	F: GGCAAGTCCACAACAACC	56	229	MH660750
		R: GTCCAGGGGCATCAATAA			
Claudin-1	*cldn-1*	F: GGCTTGTATAGGGTGGATTG	60	316	MH660751
		R: ACCTTGGCCTTCATCACCTC			
Claudin-4	*cldn-4*	F: TGCCTTCATCGGTAACAACA	60	187	MH660752
		R: AACTCCCAGGATAGCCACAA			
Occludin	*ocln*	F: TGCTATTGTTCTGGGGTTCC	60	218	MH660753
		R: CCTTCTCGTTGTATTCGGACA			
Tricellulin	*tric*	F: TAAGCGGATACATTCCAGCA	60	316	MH660754
		R: CAGCGTTCCTTTTTCTCCAA			
Zonula-Occludens 1	*zo-1*	F: GGGATGAGCGAGCAACTCTA	60	265	MH660755
		R: GCACCAGGCTTTGACACTC			

8.3.8   Antibodies

The affinity purified polyclonal antibodies used for western blot and immunohistochemsitry analysis were raised against human Cldn-1 (ThermoFisher Scientific 519000), Ocln (ThermoFisher Scientific 711500), and Tric (EMD Millipore AB2980).

8.3.9   Immunohistochemical analysis

Fixed skin samples were dehydrated and embedded in paraffin wax. Transverse sections (6 μm) of control and infected ventral skin were cut on a rotary microtome (RM2245, Leica Microsystems, Nussloch, Germany) and mounted on glass slides. Additionally, sections along the frontal plane of the skin were obtained to visualize the punctate Tric staining that would be difficult to observe in transverse sections. Sections on slides were first dewaxed in xylene, followed by rehydration using

a graded ethanol series. Subsequently, slides were washed for 10 min in different PBS solutions: 1 % Tween-20 (PBS-T), then in 0.05 % Triton X-100 in PBS (PBS-TX), and finally in 10 % antibody dilution buffer (ADB; 2 % goat serum, 1 % BSA, 0.1 % cold fish skin gelatin, 0.1% Triton X-100, 0.05 % Tween-20, 0.01 PBS) in PBS. Sections were incubated with rabbit polyclonal anti-TJ protein antibodies (1:100 dilution: 2.5 μg ml^{-1} of Cldn-1 and Ocln, 1 μg ml^{-1} of Tric) overnight at room temperature (RT). Slides were then rinsed in PBS-T and incubated with Texas red (TR)-labelled goat anti-rabbit antibody (1:500 in ADB; SC2780, Santa-Cruz Biotechnology) for 1 h at RT. Slides were rinsed and mounted with coverslips using Flouroshield™ DAPI Mounting Medium (Sigma Aldrich, Australia). Fluorescence images were captured using a Leica DMi8 Inverted Confocal microscope and merged using ImageJ software.

8.3.10 Western blot analysis

Frozen skin samples were homogenized using the TissueLyser II (Qiagen Pty Ltd, Australia) in chilled radioimmunoprecipitation assay lysis buffer (RIPA; 0.6 % Tris-HCl, 0.8 % NaCl, 1 % deoxycholic acid, 1 % Triton X-100, 1 % SDS, 1 mM EDTA, 1 mM PMSF, 1 mM DTT) containing 1:20 protease inhibitor cocktail (Sigma-Aldrich, Australia). Protein content was quantified using Bradford reagent (Sigma-Aldrich Canada Ltd) according to the manufacturer's guidelines. Skin protein (25 μg) was electrophoretically separated with NuPAGE™ 10 % Bis-Tris Protein gels and transferred to polyvinylidene difluoride (PVDF) membranes (Immobilon-P PVDF Membrane, Merck, Australia). Following transfer, the membrane was washed in Tris-buffered saline with Tween-20 (TBS-T; TBS (10 mM Tris, 150 mM NaCl, pH 7.4) with 0.05 % Tween-20), and blocked for 1 h at RT in 5 % non-fat dried skimmed milk powder in TBS-T (5 % milk TBS-T). The membrane was then incubated overnight at 4°C with rabbit polyclonal anti-TJ protein antibodies (1:1000 dilution in 5% milk TBS-T). Membranes were incubated with a horseradish peroxidase (HRP)-conjugated goat anti-rabbit secondary antibody (1:5000 in 5 % milk TBS-T) for 1 h at RT. Blots were incubated in 1-Step Ultra TMB Blotting Substrate Solution (Thermo Fisher Scientific, Australia) for 1–15 min at RT and scanned. Following imaging, membranes were incubated with Coomassie Brilliant Blue R-250 staining solution as a modified protocol of that outlined in Welinder and Ekblad (2011) to quantify total protein. Coomassie staining solution was combined with 5 % MeOH and membranes were stained for ~5 min. Membranes were then destained in acetic acid/ethanol/water (1:5:4 ratio respectively), rinsed in water and scanned. TJ protein and total protein abundance were quantified using ImageJ software. Total protein abundance was used for normalizing TJ protein abundance after statistically validating that it did not significantly differ between control and experimental groups.

8.3.11 Statistical analyses

All data were expressed as mean values ± s.e. (*n*), where *n* represents the number of frogs sampled, or as individual data points depending on the nature of the data. Difference between mean skin permeability data were analysed using the Mann-Whitney U test and a linear regression was fitted to individual data points. All other significant differences ($P \leq 0.05$) between groups were determined using the Student's t-test. All statistical analyses were performed using SigmaPlot 12.5 (Systat Software Inc., San Jose, CA, USA) or in RStudio 1.0.136 (RStudio Team, 2016).

8.4 RESULTS

8.4.1 Permeability of FITC-dextran (FD-4) through the skin of Australian green tree frog, *L. caerulea* with *Bd* infection

FD-4 is a fluorescent marker that travels solely through the paracellular pathway. There was little FD-4 permeability through the skin of control frogs after 24 h (**Fig. 8.2**). *Bd* infection had a significant effect on skin paracellular permeability to FD-4 (*P <0.001*), and the skin of infected animals was on average 62 times more permeable that the skin of control animals (**Fig. 8.2**). Additionally, the paracellular permeability significantly increased with infection intensity (*P* = 0.0149, *R²* = 0.3354).
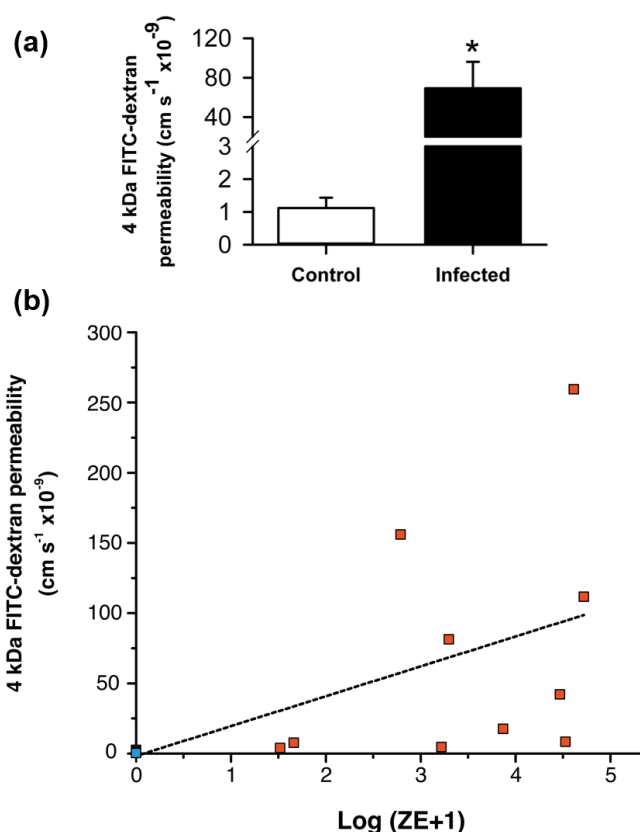
Fig. 8.2 │ Permeability of 4 kDa FITC-dextran (FD-4) through the skin of control and *Bd*-infected, *Litoria caerulea*. Panel **(a)** shows the mean paracellular permeability ± s.e. of FD-4 through control (*n* = 7) and infected (*n* = 10) frog skin. Asterisks indicate significant difference between control and infected frogs as determined by a Mann-Whitney U test. Panel **(b)** shows individual permeability values of control and infected animals over the log zoospore equivalents (ZE) +1.

8.4.2 Effect of *Bd* infection on TJ protein mRNA abundance in the ventral skin of *L. caerulea*

The abundance of *cldn-1, -4, ocln, tric,* and *zo-1* transcripts was examined in the skin of green tree frog. *Cldn-1* was the most highly expressed gene in the skin (**Fig. 8.3A,B**). With *Bd* infection, the abundance of *cldn-1, -4, ocln, tric* and *zo-1* increased by 199 %, 248 %, 255 %, 303 %, and 198 %, respectively (**Fig. 8.3C**).
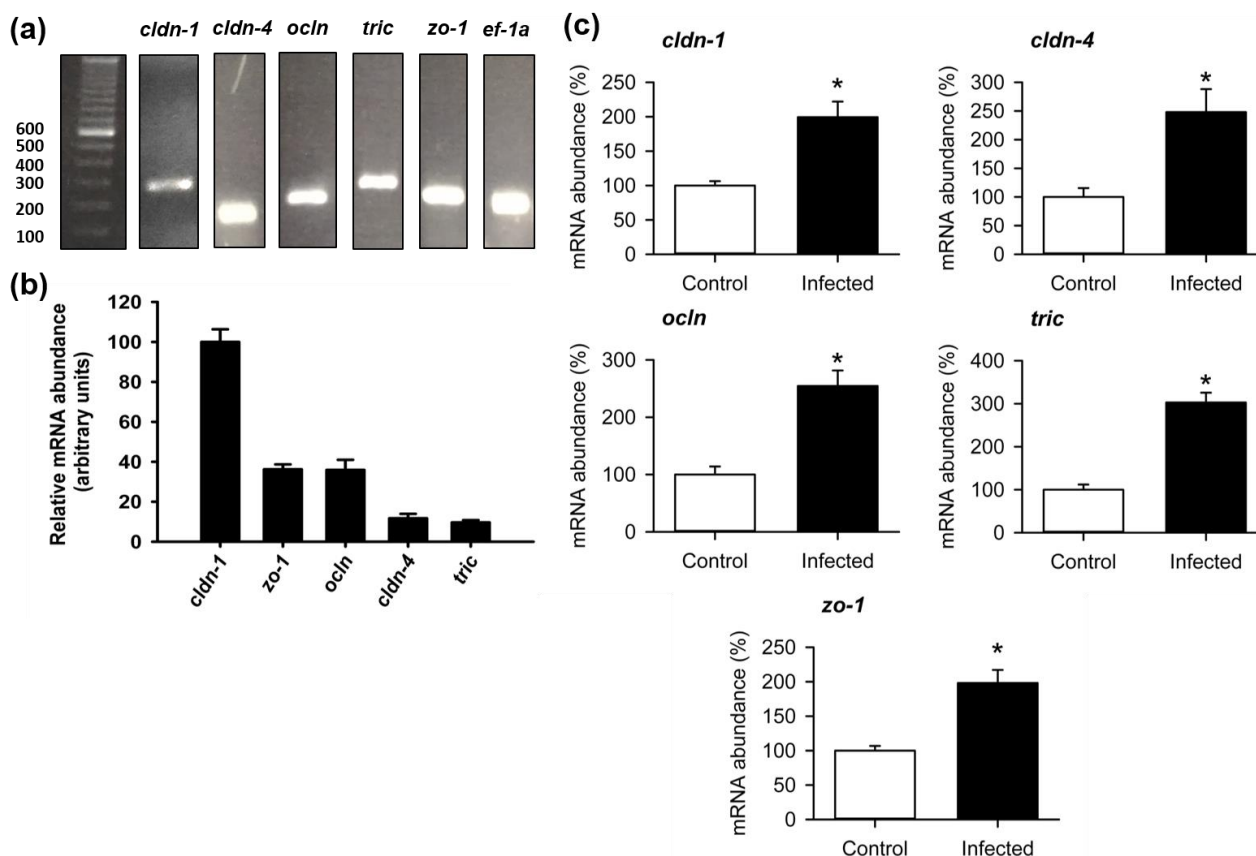
Fig. 8.3 │ **Transcript abundance of control green tree frog (*Litoria caerulea*) claudin (*cldn*)-1, -4, occludin (*ocln*), tricellulin (*tric*), and zonula-occludens 1 (*zo-1*) in the ventral skin.** In panel **(a)** PCR analysis was conducted using ventral skin cDNA and amplicons were visualised by agarose gel electrophoresis. A negative control, which contained sterile water in place of cDNA, was run simultaneously for each target gene (data not shown) and elongation factor 1α (*ef-1α*) was used as a reference gene. Panel **(b)** shows qPCR analysis of the relative abundance of the TJ protein transcripts (*n* = 8). The mRNA abundance of *cldn-1* was set to 100 % and all other transcripts were compared to *cldn-1*. In order to normalize mRNA abundance, *ef-1α* was used as reference gene. Panel **(c)** shows the effect of *Batrachochytrium dendrobatidis* infection on claudin (*cldn*)-1, -4, occludin (*ocln*), tricellulin (*tric*), and zonula occludens 1 (*zo-1*) mRNA abundance in the ventral skin of green tree frog, *Litoria caerulea*. Transcript abundance of tight junction proteins in infected frog skin was expressed relative to abundance in control animals assigned a value of 100 %. All data are expressed as mean values ± s.e. (*n* = 8). Asterisks indicate significant difference between control and infected frogs as determined by a Student's t-test. *ef-1α* was used as a reference gene.

8.4.3 Effect of *Bd* infection on Cldn-1 in the skin of *L. caerulea.*

Cldn-1 immunofluorescence was localized to the epidermis of control frogs and exhibited peri-junctional staining through the basal to upper regions of the epidermis (**Fig. 8.4A**). On a Western blot, the Cldn-1 antibody detected one band of approximately 22 kDa (**Fig. 8.4C**). With *Bd* infection, Cldn-1 protein abundance significantly decreased compared to control frogs (**Fig. 8.4D**). This decrease in protein abundance could also be visualized with immunofluorescence, where Cldn-1

fluorescence decreased in the epidermis (**Fig. 8.4B**). In addition to decreased Cldn-1 fluorescence, the epidermis of infected frogs also appeared thinner than in control animals (**Fig. 8.4B**).

Fig. 8.4 │ **Effect of *Batrachochytrium dendrobatidis* (*Bd*) infection on the localization and abundance of Claudin (Cldn)-1 in the ventral skin of green tree frog, *Litoria caerulea*.** The localization of Cldn-1 (red) in the skin of **(a)** control and **(b)** infected frogs is shown. Panel **(c)** shows a representative Western blot of Cldn-1 in the skin, and panel **(d)** illustrates the effect of *Bd* on skin Cldn-1 abundance. Protein abundance of Cldn-1 in infected frog skin was expressed relative to abundance in control animals assigned a value of 100 % after normalization using total protein. All data are expressed as mean values ± s.e. (*n* = 7). Asterisks indicate a significant difference between control and infected treatments as determined by a Student's t-test. In panel (d) a representative blot is visualized above the graph. L = ladder; T = total protein fraction; ep = epidermis; de = dermis; Scale bar = 20 µm. Nuclear staining is in blue.

8.4.4   Effect of *Bd* infection on Ocln in the skin of *L. caerulea.*

Ocln localized to the basal epidermal layer of control animals (**Fig. 8.5A**). Ocln immunofluorescence could also be seen lining glands in the dermis. Western blotting revealed one band of approximately 62 kDa (**Fig. 8.5C**), and there was no significant decrease in Ocln abundance with *Bd* infection (**Fig. 8.5D**). This could also be observed with immunohistochemistry. That is, there was no qualitative decrease in Ocln fluorescence in the epidermis (**Fig. 8.5B**) and around dermal glands (not shown).
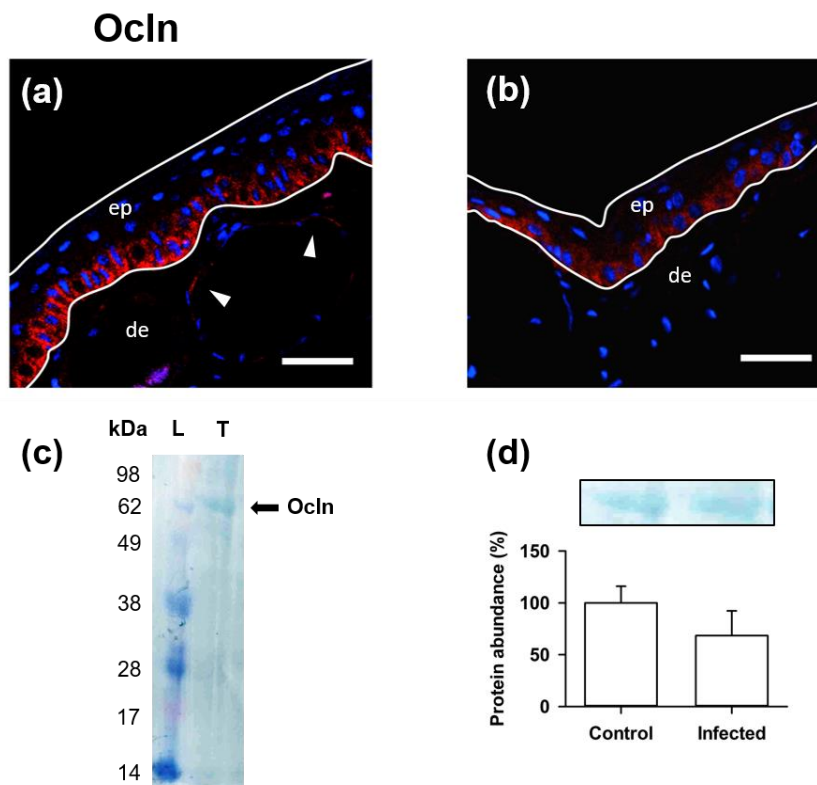
Ocln

Fig. 8.5 │ Effect of *Batrachochytrium dendrobatidis* (*Bd*) infection on Occludin (Ocln) in the ventral skin of green tree frog, *Litoria caerulea*. The localization of Ocln (red) in the skin of **(a)** control and **(b)** infected frogs is shown. Arrowheads point to Ocln fluorescence around dermal glands. Panel **(c)** shows a representative Western blot of Ocln in the skin, and panel **(d)** illustrates the effect of *Bd* on skin Ocln abundance. Protein abundance of Ocln in infected frog skin was expressed relative to abundance in control animals assigned a value of 100 % after normalization using total protein. All data are expressed as mean values ± s.e. (*n* = 7). In panel (d) a representative blot is visualized above the graph. L = ladder; T = total protein fraction; ep = epidermis; de = dermis; Scale bar = 20 µm. Nuclear staining is in blue.

8.4.5   Effect of *Bd* infection on Tric in the skin of *L. caerulea*.

Frontal sections of the skin were taken to visualize Tric staining in the epidermis, and localization was found to be punctate at regions where more than two cells interfaced (**Fig. 8.6A**). Tric fluorescence increased in *Bd*-infected animals and localized to cells that were close to disrupted epidermal margins (**Fig. 8.6B, D**). Western blotting revealed one band of ~55 kDa (**Fig. 8.6E**) and Tric abundance was found to significantly increase with *Bd* infection (**Fig. 8.6F**).
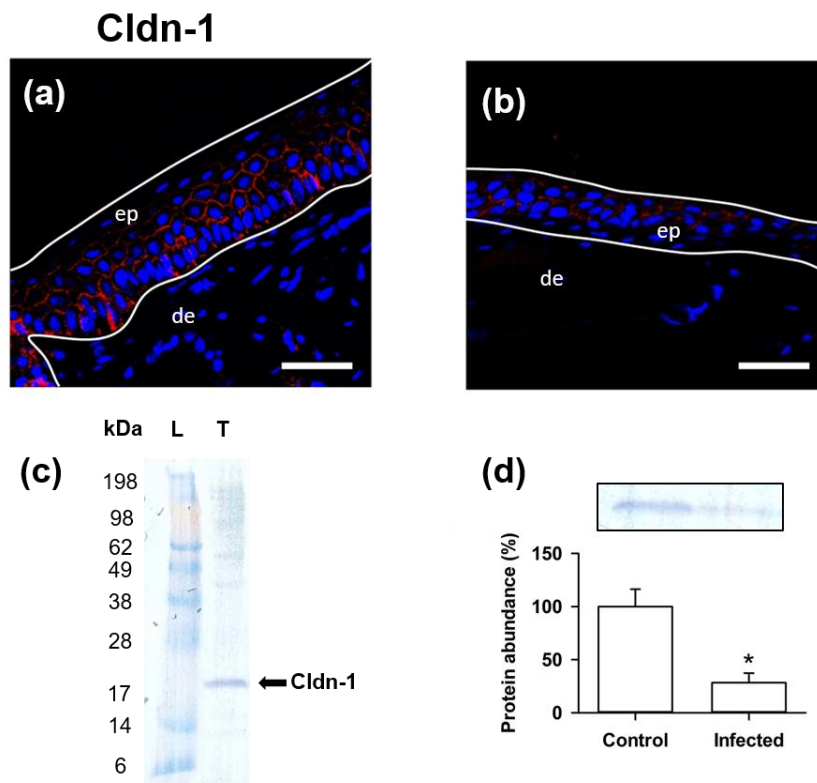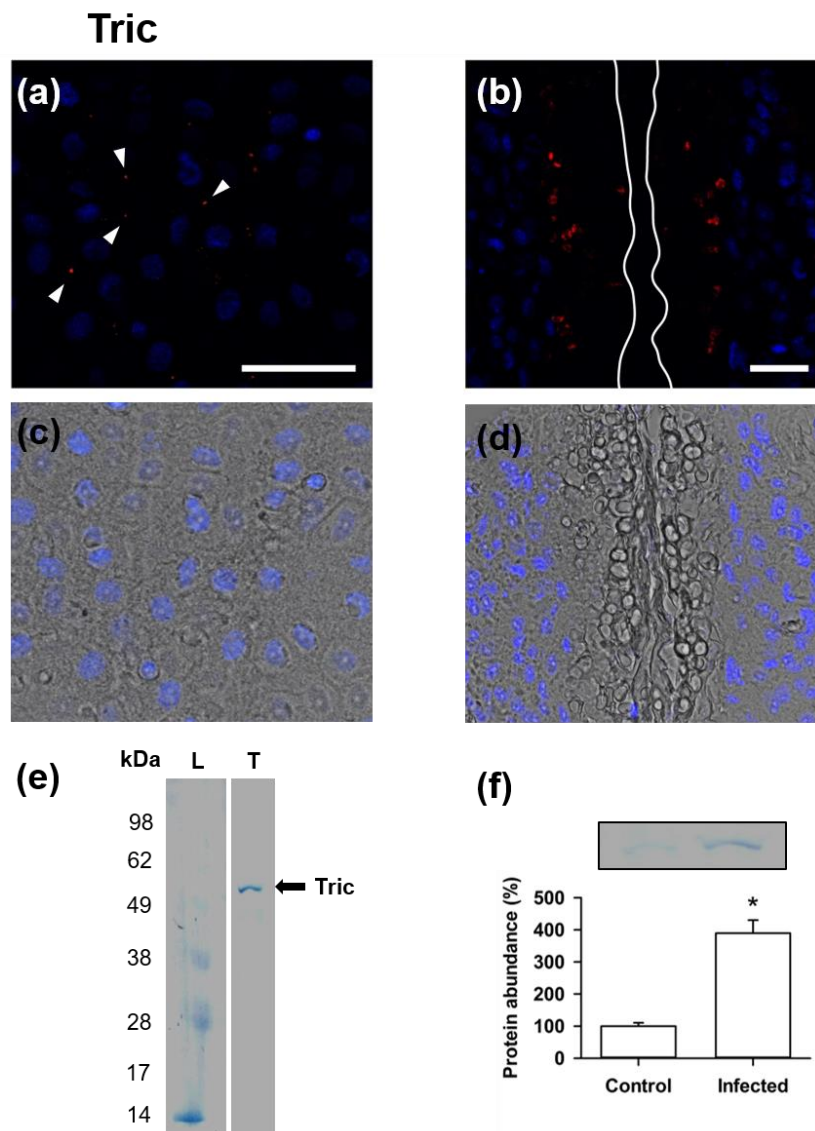
Tric

Fig. 8.6 │ Effect of *Batrachochytrium dendrobatidis* (*Bd*) infection on the localization and abundance of Tricellulin (Tric) in the epidermis of the green tree frog, *Litoria caerulea*. A top down view of the epidermis is pictured. The localization of Tric (red) in the skin of **(a)** control and **(b)** infected frogs is shown. Arrowheads point to Tric staining between three cells and white lines illustrate disrupted epidermal margins. Panels **(c-d)** depict Tric and nuclear staining with brightfield image overlay. Panel **(e)** shows a representative Western blot of Tric in the skin, and panel (f) illustrates the effect of *Bd* on skin Tric abundance. Protein abundance of Tric in infected frog skin was expressed relative to abundance in control animals assigned a value of 100 % after normalization using total protein. All data are expressed as mean values ± s.e. (*n* = 6). Asterisks indicate a significant difference between control and infected treatments as determined by a Student's t-test. In panel **(f)** a representative blot is visualized above the graph. L = ladder; T = total protein fraction. Scale bar = 20 μm. Nuclear staining is in blue.

8.5   DISCUSSION

8.5.1   Overview

This study examined the effects of *Bd* infection on the paracellular permeability of the skin of an amphibian and the associated changes in TJ protein abundance. It was found that *Bd* infection resulted in an increase in paracellular permeability of the skin. This suggests that previously reported disruption of cutaneous osmoregulation with *Bd* infection may be associated with altered paracellular permeability of the epidermis. In addition, changes in TJ protein and transcript

abundance as well as immunohistochemical observations of bicellular and tricellular TJ proteins suggests that alterations in paracellular permeability arose in association with a perturbation of the epidermal TJ complex. This indicates that dysregulation of the TJ complex may contribute to the compromised skin barrier function of *L. caerulea* infected with *Bd.* Together these data support the contention that *Bd* infection directly compromises the amphibian epidermal TJ complex that contributes, at least in part, to previously reported *Bd*-induced disturbances in amphibian salt and water balance (Voyles et al., 2007; Voyles et al., 2009; Wu et al., 2018).

8.5.2   *Bd* infection increased the paracellular permeability of *L. caerulea* skin.

The paracellular permeability of the skin increased significantly in association with *Bd* infection, which was consistent with earlier studies showing that *Bd* decreases the transepithelial resistance (TER) across *L. caerulea* skin leading to a disruption of ionic and osmotic homeostasis (Voyles et al., 2009). The results presented in the current study indicate that the previously reported decrease in TER and disrupted osmoregulatory capacity may have been due, at least in part, to a loss of the paracellular barrier of infected skin and that *Bd* infection influences amphibian skin physiology by directly targeting tight junctions in the outer skin layers.

The effects of *Bd* on skin permeability were dependent on infection load, with increasing *Bd* loads increasing the permeability of the skin. Previous studies using cultured intestinal Caco-2 epithelia and cultured human epidermal keratinocytes have demonstrated that purified fungal toxins increased paracellular permeability in a dose-dependent manner (McLaughlin et al., 2004; Yuki et al., 2007; McLaughlin et al., 2009). This may suggest that the increased paracellular permeability observed in *Bd*-infected frogs in the current study could be partly due to a toxin that *Bd* releases. However, there is additional evidence implicating other pathogenic factors in this process. For example, exposure of *Xenopus laevis* skin to supernatant containing proteases produced by *Bd* resulted in the disruption of adhaerens junction (AJ) components in the skin (Brutyn et al., 2012). Therefore, it is plausible that the same proteases produced by *Bd* can also influence TJs and contribute to an infection load-dependent increase in the paracellular permeability of the skin observed in the current study.

8.5.3   *Bd* infection altered the abundance of TJ proteins and their transcripts.

Protein and mRNA abundance of select components of the TJ complex was examined to determine if the *Bd* infection-induced increase in skin paracellular permeability was linked to the molecular machinery of the TJ. Various infectious agents have been known to target specific TJ proteins in order to disrupt the epithelial barrier and spread within the infected tissue. Notable examples of this are of *Clostridium perfringens* targeting Cldn-3 and -4 proteins in the human intestine (Katahira et al., 1997; Fujita et al., 2000; Robertson et al., 2010), and *Shigella flexneri* targeting Tric in cultured Madin-Darby canine kidney cells (Fukumatsu et al., 2012). Additionally, fungal toxins

have been found to selectively alter the abundance of specific TJ proteins, such as Cldn-1, -4, Ocln, and ZO-1 in cultured Caco-2 cells and human epidermal keratinocytes in conjunction with increased FD-4 permeability (McLaughlin et al., 2004; Yuki et al., 2007; McLaughlin et al., 2009). Therefore, the observed loss of skin barrier properties in this study as a result of *Bd* infection is likely linked, at least in part, to an altered abundance of TJ proteins. As a result, the effect of *Bd* on transcripts encoding *cldn-1, -4, ocln*, *tric*, *ZO-1*, as well as Cldn-1, Ocln and Tric proteins were examined in this study.

8.5.4   Transcript abundance of all examined TJ proteins increased with *Bd* infection.

It was found that *cldn-1* was the most abundant transcript of all of the TJ protein transcripts examined. Cldn-1 has previously been shown to be indispensable for the barrier function of mammalian skin, where mutations in this protein resulted in multiple skin defects and increased epidermal paracellular permeability (Hadj-Rabia et al., 2004; Kirschner et al., 2009; Kirchmeier et al., 2014). Cldn-1 deficient mice died shortly after birth due to evaporative water loss through the skin, implicating that Cldn-1 may act as a water barrier in mammalian skin (Furuse et al., 2002). Therefore, *cldn-1* in the skin of *L. caerulea* is likely important for maintaining the skin barrier properties.

Experimental infection with *Bd* increased the transcript abundance of all TJ protein transcripts examined in this study. If transcriptional changes translated into elevated proteins levels, it would be tempting to speculate that increased mRNA abundance reflects an attempt to increase TJ protein abundance and enhance barrier function in the compromised skin of *Bd*-infected frogs. Alternatively, an across-the-board elevation in mRNA abundance could reflect a tissue response to a systemic stress-induced factor released during *Bd* infection. For example, corticosterone levels are reported to rise during stress and inflammatory responses in amphibians (Rollins-Smith, 2017), and specifically in *L. caerulea* infected with *Bd* (Peterson et al., 2013). Corticosteroids have been shown to alter mRNA and protein abundance of Ocln (Förster et al., 2005; Chasiotis and Kelly, 2011), Tric (Kolosov and Kelly, 2013), Cldns (Kobayashi et al., 2016; Kolosov and Kelly, 2017), and ZO-1 (Chasiotis and Kelly, 2011) in various vertebrate models. Therefore, increased systemic levels of corticosterone in *L. caerulea* that would occur with infection may have triggered an *en masse* increase in TJ protein transcript abundance.

8.5.5   TJ protein abundance altered with *Bd* infection.

In the current study, Cldn-1, Ocln, and Tric proteins immunolocalized to the epidermis of *L. caerulea*, which directly interfaces with the external environment. Therefore, alterations in the abundance of these TJ proteins are likely to have impacted the paracellular permeability of the skin. In addition to alterations in protein abundance, the epidermis of infected animals appeared thinner, which is in accordance with previous observations (Berger et al., 2005a; Greenspan et al., 2012).

This may have also contributed to the increased paracellular permeability of the skin because there were fewer cell layers that could express TJ proteins and act as barriers to solute movement.

Protein abundance of Cldn-1 decreased with *Bd* infection. Cldn-1 is regarded to be a barrier-forming TJ protein in the skin (Brandner, 2009; Günzel and Yu, 2013), important in cutaneous wound healing in humans (Volksdorf et al., 2017). To date, no work has been conducted on Cldn-1 in the skin of amphibians, however, Cldn-1 has been shown to respond to changes in ion concentrations in renal epithelial cells of *Xenopus* (Tokuda et al., 2010). The observed decrease in Cldn-1 protein abundance may have been caused by degradation of Cldn-1 by proteases that were previously reported to be produced by *Bd* (Brutyn et al., 2012) or the direct effect of fungal toxins. In contrast to proteins levels, mRNA levels of *cldn*-1 were elevated. These data suggest that the increase in mRNA abundance was aimed (but not sufficient enough) at compensating for the reduced levels of Cldn-1 protein. Given that Cldn-1 is highly abundant in the skin of *L. caerulea*, the decrease in Cldn-1 protein abundance alone may have contributed heavily to the observed disruption of the skin barrier properties.

Unlike Cldn-1, Ocln protein abundance did not alter with *Bd* infection. Ocln is regarded as an important TJ protein in epithelial barriers (Yu et al., 2005). In *Xenopus*, Ocln has been shown to exhibit spatial differences in tissue localization that relate to the resistance of epithelia, as well as organ-specific alterations in abundance following changes in the salt content of their surroundings (Chasiotis and Kelly, 2009). In the current study, the unperturbed Ocln protein levels in the skin of infected frogs may have been a function of an increase in *ocln* mRNA abundance compensating for the putative proteolytic degradation of Ocln protein. Therefore, although there were no detectable changes in Ocln abundance with *Bd* infection, the Ocln protein may have been degraded in the compromised TJ complex of infected frog skin, which contributed to the increased paracellular permeability.

Finally, Tric protein levels increased following *Bd* infection. Tric is known to be a barrier-forming protein in multiple vertebrates (Günzel and Fromm, 2012; Kolosov and Kelly, 2013) and is concentrated at the tTJ between adjacent epithelial cells, which runs in a basal-to-apical direction, in a plane perpendicular to the bTJ (Ikenouchi et al., 2005). Given its localization, Tric belongs to a different junctional structure and may in part be regulated by different regulatory networks compared to its bTJ counterparts (Mariano et al., 2011). It is possible then, that *Bd* was not able to degrade Tric due to these differences. Furthermore, Tric mRNA and protein abundance are known to be affected by corticosteroids in cultured fish gill epithelia (Kolosov and Kelly, 2013). A corticosterone-based systemic stress response may have upregulated *tric* mRNA abundance and this, in conjunction with the putative inability of *Bd* to degrade Tric protein, resulted in an unperturbed increase in protein levels. Therefore, Tric protein abundance may have increased to

compensate for the loss of paracellular barrier properties that occurred with *Bd* infection. In line with this idea, in the current study Tric fluorescence increased around disrupted epidermal margins in infected frog skin. Previous studies have demonstrated that during epithelial maturation and establishment of resistive properties, Tric is first shuttled to the bTJ (Krug et al., 2009). Following this, after the tricellular contact points are defined, Tric is incorporated into the tTJ (Krug et al., 2009). Therefore, in the current study Tric may be participating in the healing of *Bd* infection-induced epidermal wounds, aimed at re-establishing paracellular barrier properties.

8.5.6   Conclusions and significance

This study directly demonstrates that the paracellular barrier is compromised in the epidermis of amphibians infected with *Bd*. Increased paracellular permeability is correlated with *Bd* infection load and *Bd* infection results in a uniform increase in the abundance of all TJ-related transcripts examined in this study. However, at the protein level, *Bd* infection may target specific bTJ proteins, while the tTJ may not be directly targeted at all. Importantly, a decrease in abundance of a prominent epidermal Cldn in vertebrates, Cldn-1, may contribute significantly to the observed loss of barrier properties. Presently, the deleterious effects of *Bd* infection are broadly accepted but not completely understood, and the current data provide new insight into mechanisms of chytrid fungus action on the skin of amphibians. Future comparative studies examining the effect of *Bd* on TJ proteins in susceptible and resistant animals would be useful for understanding which TJ proteins are impacted by *Bd* infection. It is plausible that frogs with greater resistance to *Bd* may have a larger repertoire of TJ proteins that are not affected by *Bd* infection. Therefore, given the devastating effects of *Bd* on amphibian populations worldwide (Berger et al., 2005a; Fisher et al., 2009; Kilpatrick et al., 2010), understanding its interaction with TJ proteins in the skin will be important for elucidating the mechanism of skin barrier disruption and species susceptibility to *Bd* infection. More generally, examining the fungal-TJ interaction in vertebrate epithelia will allow us to gain insight into mechanisms of fungal pathogenicity that were previously unexplored.

8.5.7   Acknowledgements

Appendix 2.
Animal Ethics and Scientific Permits

Animal Ethics Approval Certificate

Please check all details below and inform the Animal Welfare Unit within 10 working days if anything is incorrect.

Activity Details

Chief Investigator:	Professor Craig Franklin, Biological Sciences
Title:	Skin function during sloughing in amphibians
AEC Approval Number:	SBS/316/14/URG
Previous AEC Number:	
Approval Duration:	24-Sep-2014 to 24-Sep-2017
Funding Body:	URG
Group:	Native and exotic wildlife and marine animals
Other Staff/Students:	Rebecca Cramp, Michel Ohmer, Nicholas Wu
Location(s):	St Lucia Bldg 8 - Goddard

Summary

Subspecies	Strain	Class	Gender	Source	Approved	Remaining
Amphibians	Cane Toad (*Rhinella marina*)	Adults	Unknown	Captured from Natural Habitat	24	24
Amphibians	Green Tree Frog (*Litoria caerulea*)	Adults	Unknown	Captured from Natural Habitat	54	54

Permits

Scientific Purposes Permit WISP15102214   23-Sep-2014 to 31-Dec-2017

Provisos

Approval Details

Description	Amount	Balance
Amphibians (Cane Toad (*Rhinella marina*), Unknown, Adults, Captured from Natural Habitat)		
9 Sep 2014 Initial approval	24	24
Amphibians (Green Tree Frog (*Litoria caerulea*), Unknown, Adults, Captured from Natural Habitat)		
9 Sep 2014 Initial approval	54	54

Animal Welfare Unit   Cumbrae-Stewart Building   +61 7 336 52925 (Enquiries)   animalwelfare@research.uq.edu.au
UQ Research and Innovation   Research Road   +61 7 334 68710 (Enquiries)   uq.edu.au/research
The University of Queensland   Brisbane Qld 4072 Australia   +61 7 336 52713 (Coordinator)

Page 1 of 2

Please note the animal numbers supplied on this certificate are the total allocated for the approval duration

Please use this Approval Number:

1. When ordering animals from Animal Breeding Houses
2. For labelling of all animal cages or holding areas. In addition please include on the label, Chief Investigator's name and contact phone number.
3. When you need to communicate with this office about the project.

It is a condition of this approval that all project animal details be made available to Animal House OIC. (UAEC Ruling 14/12/2001)

The Chief Investigator takes responsibility for ensuring all legislative, regulatory and compliance objectives are satisfied for this project.

This certificate supercedes all preceeding certificates for this project (i.e. those certificates dated before 23-Sep-2014)

Animal Ethics Approval Certificate

20-Nov-2017

Please check all details below and inform the Animal Ethics Unit within 10 working days if anything is incorrect.

Activity Details

Chief Investigator:	Professor Craig Franklin, Biological Sciences
Title:	Chytridiomycosis on skin function during sloughing in amphibians
AEC Approval Number:	SBS/340/17
Previous AEC Number:	SBS/316/14/URG
Approval Duration:	21-Nov-2017 to 21-Nov-2018
Funding Body:	URG
Group:	Native and exotic wildlife and marine animals
Other Staff/Students:	Rebecca Cramp, Nicholas Wu, Callum McKercher
Location(s):	St Lucia Bldg 8 - Goddard

Summary

Subspecies	Strain	Class	GenderSource	Approved	Remaining
Amphibians	Green Tree Frog (*Litoria caerulea*)	Juvenile / Weaners / Pouch animal	Unknown	36	36

Permits

Scientific Purposes Permit WISP15102214   23-Sep-2014 to 31-Dec-2017

Provisos

Approval Details

Description	Amount	Balance
Amphibians (Green Tree Frog (*Litoria caerulea*), Unknown, Juvenile / Weaners / Pouch animal,)		
21 Nov 2017 Initial approval	36	36

Please note the animal numbers supplied on this certificate are the total allocated for the approval duration

Please use this Approval Number:

1. When ordering animals from Animal Breeding Houses
2. For labelling of all animal cages or holding areas. In addition please include on the label, Chief Investigator's name and contact phone number.
3. When you need to communicate with this office about the project.

It is a condition of this approval that all project animal details be made available to Animal House OIC. (UAEC Ruling 14/12/2001)

The Chief Investigator takes responsibility for ensuring all legislative, regulatory and compliance objectives are satisfied for this project.

This certificate supercedes all preceeding certificates for this project (i.e. those certificates dated before 20-Nov-2017)

Animal Ethics Unit   Cumbrae-Stewart Building   +61 7 336 52925 (Enquiries)   animal.ethics@research.uq.edu.au
Office of Research Ethics   Research Road   +61 7 334 68710 (Enquiries)   uq.edu.au/research
The University of Queensland   St Lucia Qld 4072 Australia   +61 7 336 52713 (Coordinator)

Page 1 of 1

Notice of decision - permit[1] application

This notice is issued by the administering authority to advise of a statutory decision on a permit application.

Professor Craig Edwin Franklin
School of Biological Sciences, Goddard Building
Mansfield Place
UNIVERSITY OF QUEENSLAND QLD 4072

Our reference: 279472

Dear Professor Franklin

Re: Decision made in relation to your application

Your application received on 03-SEP-2014 has been assessed and the decision in regard to your application is specified below:

Permit applied for	Permit Number	Decision
Scientific Purposes Permit under Nature Conservation (Administration) Regulation 2006	WISP15102214	Granted

For the permit applied for that has been granted, the conditions of approval are attached. Where applicable, a Statement of Reasons is provided in relation to the decision. Please note that for the approval, this Notice of Decision and the relevant attachments constitute the permit documentation. Please retain this approval documentation for your records.

Included with this notice is advice on review and appeal processes that may be available to you. Should you seek a review or appeal, you are advised to seek independent advice before taking such action.

If you require more information, please contact Jacqui Brock on the telephone number listed below.

Yours sincerely

[signature]

Sally Egan
Department of Environment and Heritage Protection
Date   22/09/2014

Enquiries:
Wildlife - Toowoomba - EHP
PO Box 102
TOOWOOMBA QLD 4350
Phone: (07) 4688 ~~1415~~ 1570
Fax: (07)

Attachment - Permit/Statement of Reasons

---

1 Permit includes licences, approvals, permits, authorisations, certificates, sanctions or equivalent/similar as required by legislation.

Department of Environment and Heritage Protection
www.ehp.qld.gov.au ABN 46 640 294 485

Queensland
Government

Permit[1]

This permit is issued under the following legislation:

S12(F) Nature Conservation (Administration) Regulation 2006

Scientific Purposes Permit

Permit number: WISP15102214

Valid from: 23-SEP-2014 **to** 31-DEC-2017

Parties to the Permit

Role	Name	Address
Principal Holder	Professor Craig Edwin Franklin	211 Birdwood Terrace TOOWONG QLD 4066

Permitted Location Activity Details

Location (s)	Activity (s)
Non Protected Areas - Queensland	Research on non-protected areas for scientific purposes

Permit Details

Species Details

Location	Activity		
Non Protected Areas - Queensland	Research on non-protected areas for scientific purposes		
Common Name	**Scientific Name**	**Category**	**Quantity**
common green treefrog	Litoria caerulea	Live	54 Animal/s

---

[1] Permit includes licences, approvals, permits, authorisations, certificates, sanctions or equivalent/similar as required by legislation.

Queensland Government

Conditions of Approval

Agency Interest: Biodiversity

PB1   AUTHORISATION
This permit authorises the holder to take, use and keep up to 54 of the listed species from non-protected areas for the purpose of a study investigating skin sloughing in amphibians.

No more than four (4) animals may be taken from each location/population.

Animals may be transported to and kept at the University Queensland, School of Biological Sciences, St Lucia.

Animals are to be euthanased at completion of experiments.

This permit is issued subject to the Principal Holder holding the current approval of a registered animal ethics committee.

Unless otherwise specified, all practices and procedures undertaken pursuant to this permit are to be in accordance with those details contained in and attached to the Application for a Scientific Purposes Permit signed by the Principal Holder on 2 September 2014.

PB2   The Principal Holder is to ensure that all the provisions of the (Queensland) Interim Hygiene Protocol for Handling Amphibians are upheld. This document is available on-line at http://www.ehp.qld.gov.au/licences-permits/plants-animals/documents/tm-wl-amphibian-hygiene.pdf

Care must be taken when repositioning logs and rocks to prevent animal injuries and to avoid causing habitat disturbance.

Any accidental mortality during capture or subsequent handling is to be reported immediately to the Project Officer (Scientific Permits), Department of Environment and Heritage Protection, Toowoomba. The Queensland Museum has first refusal of any material resulting from mortality.

PB3   Permission must be obtained from the landholder prior to commencing activities on freehold/leasehold land.

PB4   This permit (or a copy plus proof of identity of the permit holder) must be carried while engaged in any activity authorised by the permit. Additional assistants can be authorised by the permit holder to undertake the listed activities. Additional assistants must carry a copy of the permit endorsed by the Holder with the additional assistants name and residential address and must carry a form of current coloured photographic identification.

Environmental impact is to be kept to a minimum.

All collection and handling equipment, items of clothing (including footwear) and vehicles must be cleaned before and after each separate collection activity.

All equipment (nets, flagging tape, markers etc) and any waste generated during the execution of this research project is to be removed prior to the expiry date of this permit.

All collecting activities are to be effected away from public view.

The Principal Holder must not engage in the activity authorised by this permit for any commercial purpose or for the purpose of bio-prospecting.
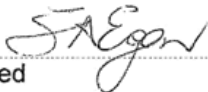
PB5   REPORTING
A Return of Operations and Scientific or Educational Purposes Permit Report must be submitted
on the standard reporting forms:
- within 10 business days of the anniversary date of the permit each year the permit is in force;
and
- within 10 business days of the expiry date.

The return is to show numbers of specimens of each species, the type of habitat and specific
locality or localities where they were collected. This information is to be supplied to the Project
Officer (Scientific Permits), Department of Environment and Heritage Protection, PO Box 102,
Toowoomba or electronically to SPPreport.southern@ehp.qld.gov.au.   Please refer to the Wildlife
Data Return Guidelines available at www.ehp.qld.gov.au for assistance completing the form.

A copy of any resulting publication from this research is to be provided to the Project Officer
(Scientific Permits), Department of Environment and Heritage Protection, PO Box 102,
Toowoomba or electronically to SPPreport.southern@ehp.qld.gov.au.

Signed

Sally Egan
Delegate
Department of Environment and Heritage Protection